Interpreting DGT measurements beyond steady-state and perfect-sink conditions

Martín Emilio Jiménez Piedrahita

http://hdl.handle.net/10803/405372

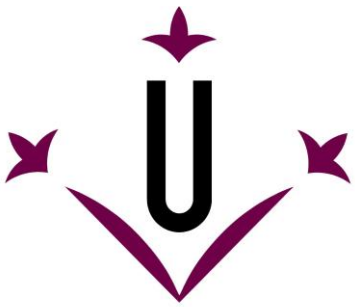

Universitat de Lleida

TESI DOCTORAL

Interpreting DGT measurements beyond steady-state and perfect-sink conditions

Martín Jiménez Piedrahíta

Memòria presentada per optar al grau de Doctor per la Universitat de Lleida
Programa de Doctorat en Enginyeria i tecnologies de la informació

Directors
Dr. Jaume Puy Llorens
Dr. Joan Cecilia Averós

2017

Agradecimientos

La realización de este trabajo de investigación ha sido una experiencia enriquecedora y placentera gracias a las personas que han estado conmigo durante estos años. Son ellas quienes han hecho que me sienta como en casa y me han bridado todo su apoyo para llevar este proyecto a buen término. Quiero dar mis más sinceros agradecimientos:

A mis directores, los Drs. Jaume Puy y Joan Cecilia, por compartir conmigo sus conocimientos, su experiencia, su tiempo y su amistad. Son dos grandes maestros. No podría haber encontrado mejores directores y me siento muy afortunado por eso.

Al Dr. Josep Galceran, porque es un privilegio estar al lado de una persona que siempre te hace crecer.

A los Drs. Carlos Rey, Encarnación Companys, Calin David y José Salvador, quienes me han ofrecido su amistad y su ayuda de manera muy generosa.

A mi compañerita Alexa, por ser la alegría del grupo. Además de su amistad, quiero agradecerle por haber contribuido con gran parte del material presentado en este documento.

A Marjan, Fede y Pepi, con quienes he compartido la mayor parte de mi tiempo dentro y fuera de la Universidad. Ha sido un placer conocer personas tan valiosas y formar parte de este grupo de amigos.

A la gente de orgánica, con quien también compartí muy buenos momentos. Especialmente a Silvia y Olalla.

A los demás miembros del departamento de química de la Universidad de Lleida, porque cada uno de ellos contribuyó de alguna manera a la realización de esta tésis.

A Jordi, un ser humano fantástico y un amigo incomparable.

A Albert, Francesco, María, Pol y Pau, mis compañeros de apartamento, que han hecho muy agradable mi estancia en Lleida.

A Nancy por estar siempre pendiente de mí y regalarme todo su cariño. Una persona que se hace querer con su forma de ser.

A Cathe y Bea, dos personas increíbles cuya amistad espero conservar para el resto de mi vida. Ha sido un placer compartir abrazos, risas, acordes e historias con ellas.

A Merche, por enseñarnos que la vida puede ser fantástica.

A Erika, Mery, Harry, Antonio, Edinson, Karla y Haifa, por los inolvidables momentos que he compartido con cada uno de ellos.

A Nata, porque hay personas que pasan por nuestra vida haciendo de ella algo mejor.

A Marie, Christelle, Fabien y Tristan, por la calidad de personas que son y por hacer que nuestra amistad perdure.

Y del otro lado del Atlántico:

A Ramiro, a quien quiero como a un hermano y quien siempre ha estado ahí para todo lo que he necesitado. Él es, sin duda, una de las mejores personas que he conocido.

A Camilo, Pedro, Sandra y Katerín, por estar siempre cerca, sirviéndome de apoyo o inspiración, a pesar de la distancia.

Y finalmente, al grupo más importante: mi familia. Gracias por estar siempre conmigo. Todo mi amor es para ellos.

Abstract

In the last decades, anthropogenic activities have increased the concentrations of heavy metals in aquatic systems. Since these elements are bio-accumulative and could be toxic, it is important to study their bioavailability in natural media. An analytical technique called **Diffusive Gradients in Thin Films** (DGT) allows studies of the availability of metals in water, based on the deployment of DGT devices, which accumulate the target analytes for a known period of time. Physico-chemical models that consider the reactions and transport of species inside the device and in the solution are required for the interpretation of the accumulations. The commonly used model has shown to be appropiate in many cases, but in some conditions it is not suitable to replicate the experimental results. The main objective of this thesis is to contribute to the study of the bioavailability of metals, through the DGT devices, when the typical model is not adequate.

A starting point was the study of the distribution of binding agent in the resin layer on the accumulation of metal in DGT devices. It was found that this factor is relevant in presence of partially-labile complexes.

The influence of the ionic strength on the DGT measurements was also analysed. It was found that, in systems with only metal, the electrostatic effects can produce nonlinear accumulations with time at some ionic strengths. The main cause of this behavior is the influence of the ionic strength on the affinity between the metal and the resin. A rigorous model based on Nernst-Planck equations and a simplification based on the Donnan model were used to understand this influence and applied to the study of Mg accumulation. The numerical solution was obtained with the Finite Element Method.

Three situations, in which metal accumulations can be nonlinear with time, were analysed: 1) the binding of metal to the resin is kinetically controlled, 2) there are equilibrium effects between free and bound metal and 3) there are other metallic cations competing for the binding sites in the resin. Analytical approximate expressions that improve the standard model in these situations were proposed and applied for the analysis of Mg and Mn accumulations. Their accuracy was checked with the numerical simulation.

Finally, the metal accumulation and lability degree in systems that contain a mixture of complexes were studied under non ligand excess conditions.

Resumen

En las últimas décadas, las actividades antropogénicas han aumentado las concentraciones de metales pesados en los sistemas acuáticos. Dado que estos elementos son bio-acumulativos y podrían ser tóxicos, es importante estudiar su disponibilidad en medios naturales. La técnica analítica llamada **Diffusive Gradients in Thin Films** (DGT) permite estudiar la disponibilidad de los metales en aguas. Los dispositivos DGT se despliegan en el medio para que acumulen el analito durante un período de tiempo determinado. Los análisis de disponibilidad se realizan con base en la masa acumulada y para ello, se requieren modelos fisicoquímicos que consideren las reacciones y el transporte de especies dentro del dispositivo y en la solución. El modelo teórico comúnmente usado para estos análisis funciona en muchos casos, pero en algunas condiciones no es apropiado para explicar los resultados experimentales. El objetivo principal de esta tesis es contribuir al estudio de la disponibilidad de metales, a través de los dispositivos DGT, en situaciones en las que el modelo más utilizado no es el adecuado.

Como punto de partida se estudió la influencia que tiene la distribución de agente extractante en la resina, sobre las medidas realizadas con los dispositivos DGT. Se encontró que este factor es importante en presencia de complejos parcialmente lábiles.

Posteriormente se estudió la influencia que ejerce la fuerza iónica en las medidas realizadas con dispositivos DGT. Se encontró que, en sistemas con sólo metal, los efectos electrostáticos pueden producir acumulaciones no lineales con el tiempo y la causa principal de este comportamiento es la influencia que tiene la fuerza iónica en la constante cinética de asociación entre el metal y la resina. También se propusieron dos modelos para analizar esta influencia y se aplicaron al estudio de la acumulación de Mg. Se proporcionaron soluciones numéricas basadas en el método de los elementos finitos.

Se analizaron tres situaciones en las cuales las acumulaciones de metales pueden no ser lineales con el tiempo: 1) cuando la acumulación de metal en la resina es controlada cinéticamente, 2) cuando hay efectos de equilibrio entre el metal libre y el metal enlazado y 3) cuando hay otros cationes metálicos que compiten por los sitios de enlace de la resina. Se propusieron expresiones analíticas aproximadas que mejoran el modelo típico en estas situaciones y se aplicaron al estudio de las acumulaciones de Mg y Mn. Su exactitud fue contrastada con simulaciones numéricas.

Finalmente, se realizó un primer estudio de la acumulación de metal y del grado de labilidad en sistemas con mezclas de complejos, cuando no hay condiciones de exceso de ligando en la solución.

Resum

En les darreres dècades les activitats antropogèniques han incrementat la concentració de metalls pesants en els ecosistemes aquàtics. Donat que aquests elements són bio-acumulatius i poden ser tòxics, és important estudiar la seva biodisponibilitat en els medis naturals. La tècnica **Diffusive Gradients in Thin Films (DGT)** permet estudiar la disponibilitat d'aquests metalls pesants en les aigües, mitjançant dispositius DGT que s'introdueixen en el medi per a acumular l'analit durant un període de temps determinat. Les anàlisis de disponibilitat es realitzen en funció a la massa acumulada i, per això calen models fisicoquímics que tinguin en compte les reaccions i el transport dels analits dins del dispositiu i en la solució. El model teòric més emprat per efectuar aquestes anàlisis és adequat en la majoria dels casos, però, en determinades condicions, no pot replicar els resultats experimentals. L'objectiu d'aquesta tesis és, doncs, contribuir a l'estudi de la biodisponibilitat de metalls pesants, mitjançant l'ús de dispositius DGT en aquelles situacions en les que el model habitual no resulta òptim.

El punt de partida va ser l'estudi de la influència que té la distribució de l'agent extractant en la resina sobre les mesures realitzades amb els dispositius DGT, un factor especialment rellevant en complexos parcialment làbils.

Es va estudiar la influència que exerceix la força iònica en les mesures realitzades. Els resultats varen mostrar que en sistemes amb presència només de metalls, els efectes electrostàtics poden produir acumulacions no lineals al llarg del temps a determinades forces iòniques. La causa principal d'aquest efecte és la influència de la força iònica en la constant cinètica d'associació entre el metall i la resina. Per analitzar aquesta efecte es va fer servir un model, basat en les equacions de Nernst-Planck i un de simplificat prenent el model de Donnan, els quals van ser aplicat a l'estudi d'acumulació de Mg. Es van proporcionar solucions numèriques basades en el mètode dels elements finits.

Les tres situacions analitzades, en les quals l'acumulació de metalls no va ser lineal al llarg del temps, van ser: 1) l'acumulació de metall en la resina està controlada cinèticament, 2) hi han efectes d'equilibri entre el metall lliure i el metall enllaçat i 3) hi han altres cations metàl·lics competint pels setis d'unió en la resina. Així, es van proposar expressions analítiques aproximades que milloren el model estàndard en aquetes tres situacions i aquestes expressions es van aplicar a l'estudi de l'acumulació de Mg i Mn. La precisió dels models va ser contrastada amb simulacions numèriques.

Finalment, es va estudiar l'acumulació de metalls i el seu grau de labilitat en una barreja de complexos en condicions de no excés de lligand en la solució.

Table of contents

Major Symbols

Symbol	Meaning	Usual units
A	Area	m^2
c_i	Concentration of species *i*	$mol \cdot m^{-3}$
c_i^*	Concentration of species *i* in bulk solution	$mol \cdot m^{-3}$
$c_{\mathbf{TR}}$	Total concentration of free resin sites	$mol \cdot m^{-3}$
D_i	Diffusion coefficient of species *i* common to all phases	$m^2 \cdot s^{-1}$
DBL	Diffusive boundary layer	m
DGT	Diffusive Gradients in Thin films	None
δ^g	Aggregate thickness of the diffusive gel layer +filter + DBL	m
δ^r	Thickness of the resin	m
e	Elementary electric charge	C
ε_0	Permittivity of free space	$F \cdot m^{-1}$
$\varepsilon_{\mathbf{r}}$	Relative permittivity	None
F	Faraday constant	$s \cdot A \cdot mol^{-1}$
FDM	Finite Difference Method	None
FEM	Finite Element Method	None
ϕ	Electric potential	V
I	Ionic strength	$mol \cdot m^{-3}$
J_i	Flux of species *i*	$mol \cdot m^2 \cdot s^{-1}$
κ	Debye-Hückel parameter	m^{-1}
$k_{a,MR}$	Association rate constant of metal with the resin	$m^3 \cdot mol^{-1} \cdot s^{-1}$
$k_{d,MR}$	Dissociation rate constant of metal with the resin	s^{-1}
K_{MR}	Stability constant for the formation of a complex MR	$m^3 \cdot mol^{-1}$
$k_{a,j}$	Association rate constant of metal M with the ligand ^jL	$m^3 \cdot mol^{-1} \cdot s^{-1}$
$k_{d,j}$	Dissociation rate constant of metal M with the ligand ^jL	s^{-1}
K_j	Stability constant for the formation of a complex M ^jL	$m^3 \cdot mol^{-1}$
$k_{\mathbf{B}}$	Boltzmann constant	$m^2 \cdot kg \cdot s^{-2} \cdot K^{-1}$
λ_{ML}	Complex penetration parameter	m
m	Disequilibration parameter	m
n_M	Total accumulation of metal	mol
$N_{\mathbf{R}}$	Concentration of charge in the resin phase	m^{-3}
∇	Spatial gradient operator	None
∇^2	Laplace operator	None
Π_i	Boltzmann factor for species *i*	None
q_i	Normalized concentration of species *i*	None

$\Psi_{\mathbf{D}}$	Donnan Potential	V
$\Psi_{\mathbf{0}}$	Resin–Gel Interface Potential	V
R	Universal gas constant	$J \cdot K^{-1} \cdot mol^{-1}$
T	Temperature	K
ξ	Lability degree	None
z	Charge number (valence) of electrolyte	None
z_i	Charge number (valence) of ionic species *i*	None

CHAPTER 1

OBJECTIVES AND OUTLINE OF THE THESIS

1.1 Significance of the study

Nowadays there is a rising concern on the sustainability of human activities. Sustainability embraces many issues, since a definition generally accepted is that the needs of the present have to be achieved without compromising the resources of future generations. One issue of the sustainability is referred to the environment. Climate change is now recognized as a challenge in the environmental sustainability but contamination has also been a classical problem that has attracted the attention of scientists and of the society. This Thesis develops concepts, methods, techniques and criteria to measure and interpret chemical contamination.

Although most of the concepts, techniques and criteria here developed can be applied to chemicals in general, we restrict ourselves to speak in terms of heavy metals and waters. Many contaminants run into water bodies being, then, the waters the main source of its dissemination. Among contaminants, heavy metals have been studied for long time and they are especially suited to illustrate the concepts here developed.

Even though there is no standard definition for the term "heavy metals", this name is often given to those with higher density.[1,2] Among heavy metals, there is a group known for their tendency to represent serious environmental problems such as mercury, lead, cadmium or copper.[3-5] Sometimes, other light toxic elements are included in this category, such as beryllium or aluminium, or some semimetal like arsenic in the context of contamination. However, not all heavy metals are toxic at low concentrations and some of them are essential for plants and animals.[6,7] Methods developed in this work are intended to be used in dealing with problems of nutrition and contamination.

In industrialized countries, high concentrations of heavy metals dissolved in water or

soil are one of the main sources of pollution for living organisms, whereas, in other parts of the world, these concentrations may be insufficient with respect to nutritional requirements. Metals reach the soil or water from different natural or anthropogenic sources. In the latter sources we find agricultural activities, where fertilizers, animal manures and pesticides containing heavy metals are widely used. Metallurgical activities, processes for the production and transport of energy, microelectronic products and the deposition of waste are also anthropogenic inputs of metal ions in the environment.[8,9]

Heavy metals cannot be degraded (neither chemically nor biologically) and can remain in the environment for hundreds of years, so they can be taken up by plants and animals through absorption processes. For this reason, metals accumulate in living organisms reaching concentrations higher than those achieved in food or in the environment, and these concentrations increase as we ascend the trophic chain, causing toxic effects.

In general, the uptake and toxicity of heavy metals does not only depend on their total concentration, but on other factors such as their speciation,[10-12] the content of organic matter, pH and ionic strength of the medium. Chemical speciation is defined as the distribution of a particular chemical element among the different forms in which it can exist (species), in a given medium. It includes both the free elements (in neutral or ionized form) and the variety of complexes that can be formed with different ligands. Knowledge about the speciation of heavy metals is important because their availability depends on the stability, mobility and kinetic of inter-transformation, under environmental conditions, of the chemical species present.[13]

1.2 DGT devices

One analytical technique increasingly used to determine the availability of trace metals in waters, sediments or soils is **Diffusive Gradients in Thin Films** (DGT).[14] DGT devices are passive samplers and consist of a layer of a strong metal ion-binding agent dispersed in a gel (named resin layer), a diffusive gel and a filter. These layers are housed inside a cylindrical plastic protector (Figure 2.1). The DGT device is introduced

into the soil, sediment or water for a certain time and the metals diffuse from the sample through the filter and the gel to the resin, where the metal is bound. The accumulated masses of the species of interest can be measured for different times. With these data, it is possible to obtain information about average bulk concentrations, mean fluxes, lability of complexes and speciation.[15,16]

Multiple studies have been conducted in order to analyse the relationships between experimental results and factors such as the composition of the system, kinetics of chemical reactions and transport processes.[17-22] Traditional analysis of DGT measurements are based on the following assumptions:

1. All the processes in the DGT device take place essentially in one relevant spatial dimension.
2. A steady-state flux is an accurate approximation for the understanding of the accumulation.
3. The resin acts as a perfect-sink for the metal.
4. There are no saturation effects in the resin layer.
5. Ionic strength in the solution is high enough to screen electrostatic effects between charged species and the resin layer, the diffusive gel or the membrane filter.

The model based in these assumptions has shown to be accurate enough to explain many experimental results. However, there are some cases in which these assumptions are not fulfilled and this approach is not suitable to understand the experimental data.

1.3 Research objectives

The main objective of this work is to contribute to the study of the availability of metals in natural waters, using DGT devices. The particular cases examined in detail in this thesis and the main aims of this work are:

1. To develop a simulation tool based on Finite Element Method (FEM) that allows studying spatio-temporal evolution of the concentrations of chemical species and other relevant state variables inside a DGT device, when it is introduced into a medium with different types of metals, ligands and complexes.

2. To analyse the influence of the distribution of resin beads on the lability of the complexes and the accumulation of metal cations.

3. To develop analytical expressions for the concentration profiles of species in DGT devices with inhomogeneous distribution of binding sites.

4. To study transport and complexation phenomena in devices with two resins, with different distributions of resin sites.

5. To develop theoretical models as well as numerical simulation tools to study the effects of the ionic strength in DGT devices. To apply these models and the simulations tools to study the accumulation of cations that do not bind under perfect-sink conditions or the accumulation in systems where the main species are charged partially labile complexes.

6. To check whether simple models based on Donnan partitioning can describe the behaviour of systems at low ionic strength.

7. To discuss the patterns of DGT accumulations that can arise when there are kinetic limitations in the binding to the resin, saturation or equilibrium effects or non-negligible competitive effects. To check the accuracy of the simple DGT expression and suggest new simplified, approximate expressions to determine the analyte concentration in these situations.

8. To study concentrations of species, lability degree of complexes and accumulation of metals in DGT devices in single ligand and mixed systems, when there are not excess of ligand conditions.

1.4 Outline of the thesis

Chapter 2 is an introduction to the basic concepts of the DGT technique. In this chapter there is a description of the device, the physicochemical phenomena that occur inside the device and the traditional types of analysis of the results.

A discussion on the usefulness of numerical methods in the study of electrochemical systems is presented in **Chapter 3**. We also describe the FEM applied to transient and stationary problems. The final part of this chapter describes the application of the FEM to the construction of a program to simulate the behavior of different species in a DGT sensor. It involves the solution of a system of coupled partial differential equations of diffusion-reaction. The software has been constructed in a one-dimensional scheme, using the FEM for the discretization of the space and a scheme based on Finite Differences Method (FDM) for the solution in time. Input parameters are diffusion coefficients, reaction kinetic constants, type and amount of reactions present, etc. Information about concentrations of species, as well as fluxes and labilities as a function of time can be obtained. Numerical simulation has advantages such as: the possibility of studying systems that are expensive, time consuming or not easily reproducible in labs, contrasting the experimental results with those obtained through simulation or developing analytical expressions based on the data obtained by software. The simulation tool constructed in this chapter was used in the studies presented in the rest of the thesis.

One of the basic assumptions in standard DGT modeling is the homogenous distribution of the binding agent in the resin disc. In **Chapter 4** experimental evidence against this statement is presented and the influence of an inhomogeneous distribution of resin sites on DGT measurements is checked. Systems with one and two resin layers, with different thicknesses and with homogeneous and inhomogeneous distributions of resin

sites were studied. It was found that, for very labile or inert complexes, the distribution of binding beads in the resin layer does not have influence on the total accumulation of metal and in the case of partially labile complexes there is a mild influence that increases with the value of the stability constant.

The influence of electrostatic effects on the accumulation, in systems with only metals, was studied in **Chapter 5**. This was done using numerical and experimental results obtained in devices with two resins. It was found that the main influence on the accumulation comes from the dependence of the kinetic and stability constants of the metal binding to the resin sites on the ionic strength.

Chapter 6 is devoted to study some situations in which the metal accumulations are not linear with time or do not occur under perfect-sink conditions. The first case that was studied is the kinetically controlled binding of metal to the resin. For this case, it was observed a stationary flow, but smaller than expected under perfect-sink conditions. Metal accumulations were also studied when there is a non-negligible influence of equilibrium or competition effects. In these cases, fluxes can decrease along the deployment time. A set of approximate analytical expressions to reproduce the DGT accumulations have been proposed. These expressions have been used to analyse the binding of Mg or Mn as practical examples.

Chapter 7 starts with the study of the dependence of the lability degree and total accumulation on the ligand concentration, in a single ligand system, when there are no excess of ligand conditions. It also studies how the accumulation and lability degree change when more ligands are added into the system (mixture effect). A particular attention was paid to check whether the lability degree determined in single ligand systems can be used to predict the accumulation in mixtures. The accumulation of Ni in the presence of NTA and EtDiam was studied in the final section of this chapter.

The conclusions of the thesis are presented in **Chapter 8**.

1.5 Reference List

1. Duffus, J. H. "Heavy metals" - A meaningless term?. *Pure Appl. Chem.* **2003,** *75* (9), 1357.

2. Morris, C. G. *Academic Press Dictionary of Science and Technology;* San Diego, **1992**.

3. Santala, K. R.; Ryser, P. Influence of heavy-metal contamination on plant response to water availability in white birch, Betula papyrifera. *Environmental and Experimental Botany* **2009,** *66* (2), 334-340.

4. Wang, W. X. Interactions of trace metals and different marine food chains. *Marine Ecology Progress Series* **2002,** *243*, 295-309.

5. Casiot, C.; Egal, M.; Elbaz-Poulichet, F.; Bruneel, O.; Bancon-Montigny, C.; Cordier, M. A.; Gomez, E.; Aliaume, C. Hydrological and geochemical control of metals and arsenic in a Mediterranean river contaminated by acid mine drainage (the Amous River, France); preliminary assessment of impacts on fish (Leuciscus cephalus). *Appl. Geochem.* **2009,** *24* (5), 787-799.

6. Frederickson, C. J.; Suh, S. W.; Silva, D.; Frederickson, C. J.; Thompson, R. B. Importance of zinc in the central nervous system: The zinc-containing neuron. *Journal of Nutrition* **2000,** *130* (5), 1471S-1483S.

7. Altura, B. T.; Brust, M.; Bloom, S.; Barbour, R. L.; Stempak, J. G.; Altura, B. M. Magnesium Dietary-Intake Modulates Blood Lipid-Levels and Atherogenesis. *Proceedings of the National Academy of Sciences of the United States of America* **1990,** *87* (5), 1840-1844.

8. Bradl, H. B. Sources and origins of heavy metals. In *Heavy Metals in the environment*, H. B. Bradl: **2005**.

9. Zhou, Q. F.; Zhang, J. B.; Fu, J. J.; Shi, J. B.; Jiang, G. B. Biomonitoring: An appealing tool for assessment of metal pollution in the aquatic ecosystem. *Anal. Chim. Acta* **2008,** *606* (2), 135-150.

10. Scancar, J.; Milacic, R.; Strazar, M.; Burica, O. Total metal concentrations and partitioning of Cd, Cr, Cu, Fe, Ni and Zn in sewage sludge. *Sci. Total Envir.* **2000,** *250* (1-3), 9-19.

11. Oremland, R. S.; Stolz, J. F. The ecology of arsenic. *Science* **2003,** *300* (5621), 939-944.

12. Gonzalvez, A.; Cervera, M. L.; Armenta, S.; de la Guardia, M. A review of non-chromatographic methods for speciation analysis. *Anal. Chim. Acta* **2009,** *636* (2), 129-157.

13. Alloway, B. J. The origins of heavy metals in soils. In *Heavy metals in soils*,

Alloway, B. J., Ed.; Blackie Academic Professional: Glasgow, **1995**.

14. Davison, W.; Zhang, H. Principles of Measurements in Simple Solutions. In *Diffusive Gradients in Thin-Films for Environmental Measurements.*, Davison, W., Ed.; Cambridge University Press: Cambridge, **2016**; pp 24-27.

15. Galceran, J.; Puy, J. Interpretation of diffusion gradients in thin films (DGT) measurements: a systematic approach. *Environ. Chem.* **2015,** *12* (2), 112-122.

16. Puy, J.; Galceran, J.; Rey-Castro, C. Interpreting the DGT Measurement: Speciation and Dynamics. In *Diffusive Gradients in Thin-Films for Environmental Measurements*, Davison, W., Ed.; Cambridge University Press: Cambridge, **2016**; pp 93-122.

17. Ernstberger, H.; Davison, W.; Zhang, H.; Tye, A.; Young, S. Measurement and dynamic modeling of trace metal mobilization in soils using DGT and DIFS. *Environ. Sci. Technol.* **2002,** *36* (3), 349-354.

18. Mongin, S.; Uribe, R.; Puy, J.; Cecilia, J.; Galceran, J.; Zhang, H.; Davison, W. Key Role of the Resin Layer Thickness in the Lability of Complexes Measured by DGT. *Environ. Sci. Technol.* **2011,** *45* (11), 4869-4875.

19. Tusseau-Vuillemin, M. H.; Gilbin, R.; Taillefert, M. A dynamic numerical model to characterize labile metal complexes collected with diffusion gradient in thin films devices. *Environ. Sci. Technol.* **2003,** *37* (8), 1645-1652.

20. Uribe, R.; Mongin, S.; Puy, J.; Cecilia, J.; Galceran, J.; Zhang, H.; Davison, W. Contribution of Partially Labile Complexes to the DGT Metal Flux. *Environ. Sci. Technol.* **2011,** *45* (12), 5317-5322.

21. Lehto, N. J.; Davison, W.; Zhang, H.; Tych, W. An evaluation of DGT performance using a dynamic numerical model. *Environ. Sci. Technol.* **2006,** *40* (20), 6368-6376.

22. Davison, W.; Lin, C.; Gao, Y.; Zhang, H. Effect of Gel Interactions with Dissolved Organic Matter on DGT Measurements of Trace Metals. *Aquat. Geochem.* **2015,** *21* (2-4), 281-293.

CHAPTER 2

BASIC PRINCIPLES OF DGT TECHNIQUE

2.1 Introduction

Diffusive Gradients in Thin-Films (DGT) devices were invented in 1993 by Bill Davison and Hao Zhang at the University of Lancaster. They were originated due to the need to improve the resolution and to reduce sampling times in the measurements of concentrations of trace metals in soils, which at that time were carried out with techniques such as peepers or Diffusive Equilibrium in Thin-films (DET). Sampling times, which for other techniques were of the order of weeks, with the DGTs were reduced to days and, additionally, it allowed to work at scales of millimeters. However, the technique was initially used in marine waters to measure metal cations.[1,2] The first applications of the technique in soils were carried out in 1998 to measure concentrations of metals in lands treated with sewage sludge.[3] Since that time, the technique has been applied in different media (waters, soils and sediments)[4-6] and in different places around the world.[7-11] In addition, about 40 different types of resins that allow the detection of analytes other than heavy metals, have been developed.[12-14]

Theoretical contributions, numerical simulations and experimental approaches have been developed to interpret the measurements. To carry out these developments, it has been indispensable to study the physical and chemical phenomena that occur in the sensor while it is working. The following is a small review of the main characteristics of the sensor, the phenomena involved in its operation and the way in which the experimental results are interpreted. Much of the topics are discussed for applications in waters, but, in many cases, can be extended to other media.

2.2 Description of DGT devices

The DGT devices consist of a resin layer, a diffusive gel layer and a filter embedded in a plastic holder.[15] Hydrogels are used for both: resin and diffusive gel layers. In general, hydrogels are polymer networks that can absorb large quantity of water, which allows the diffusion of metal cations and complexes of interest. They are normally made of agarose or polyacrylamide. The function of the resin is to bind the analytes of interest, and, for this reason, they contain beads of some binding agent incorporated into the hydrogel. The original DGT devices were developed for detection of trace metals and, in this case, Chelex are used as binding agent. Chelex beads are made of styrene divinylbenzene copolymers containing paired iminodiacetate ions acting as chelating groups in binding metal ions[16]. Other types of binding agents have been developed for the accumulation of anions such as: lanthanides, nanoparticles, antibiotics, phosphate, etc.[12-14]

The diffusive gels were incorporated to the device with the idea of controlling the transport of species to the resin. If the resin were exposed directly to the sample solution, phenomena of convection would have strong influence on the measurements. The presence of the gel, guarantees that there won't be transport of species to the resin by convection. On the other hand, there is a region in solution close to the filter/liquid interface, called the diffusive boundary layer (DBL), where the mass transport occurs only by diffusion. The thickness (δ^{dbl}) of this layer (with typical values in the order of 0.1 to 0.5 mm),[15] will be dependent on both the velocity of the flow and the deployment geometry, but is normally small in comparison with the diffusive gel thickness (usually of the order of 0.8 mm).[15] To reduce the DBL in laboratory measurements, the solution is stirred, producing transport of species by convection. For this reason, the presence of the diffusive gel guarantees that, most of the diffusion will occur in a region of known thickness.

Finally, there is a membrane filter, between the gel and the solution, which can exclude some particles and protects the diffusive gel. The material used for the filter is polyethersulfone due to its resistance to biofouling, but cellulose acetate membranes and nitrate are also used. Their thickness varies from 0.13 to 0.15 mm and the standard pore size is 0.45 microns.[15]

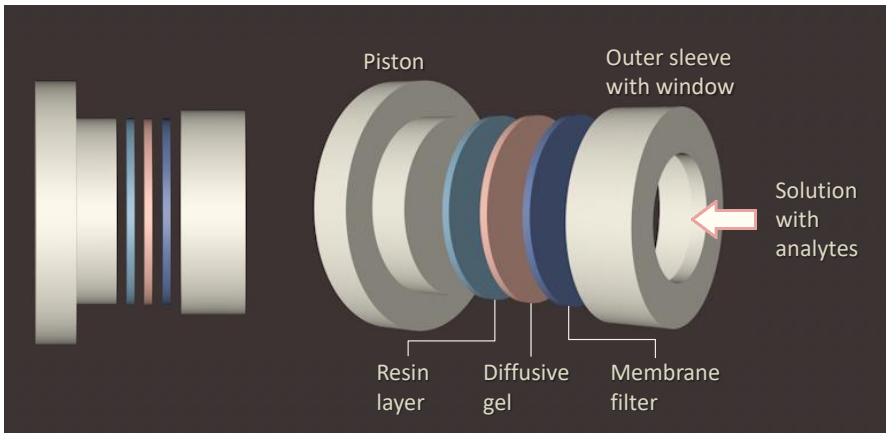

Figure 2.1. DGT device scheme.

2.3 Physicochemical phenomena in DGT sensors

When the DGT device is deposited in a sample solution or in natural waters, some species pass the filter, move through the diffusive gel and reach the resin domain. There are different phenomena occurring in each region of the DGT sensor and in the solution.

2.3.1 Chemical reactions

Species contained in the sample solution can chemically react with each other in all regions of the device. These reactions can have a huge influence on the accumulation or in the bioavailability of the analytes since they modify their transport properties and their uptake characteristics.

Although the processes here outlined can easily be extended to other analytes measured with DGT, we will restrict ourselves in this report to the case of metals which has been the most studied case in DGT using the Chelex resin as binding agent.

Some of the simplest reactions of metal cations, M, in natural samples are the complexation reactions with a ligand L, to form, in the most simple case, a complex ML:

$$\mathrm{M} + \mathrm{L} \underset{k_\mathrm{d}}{\overset{k_\mathrm{a}}{\rightleftharpoons}} \mathrm{ML} \tag{2.1}$$

Let k_a and k_d be the association and the dissociation rate constants between M and L, respectively. It is assumed that species in the bulk solution are in equilibrium, so it is possible to calculate the bulk concentrations of the species using the stability constant *K,* defined as:

$$K = \frac{k_\mathrm{a}}{k_\mathrm{d}} = \frac{c^*_\mathrm{ML}}{c^*_\mathrm{M} c^*_\mathrm{L}} \tag{2.2}$$

where the superscript * represents the concentration in the bulk solution.

Complex processes with other stoichiometric metal-to-ligand ratios may also happen. For instance, a reaction between a species L and ML_{i-1}, to form a complex ML_i:

$$\mathrm{ML}_{i-1} + \mathrm{L} \underset{k_{\mathrm{d},i}}{\overset{k_{\mathrm{a},i}}{\rightleftharpoons}} \mathrm{ML}_i \tag{2.3}$$

With stability constant:

$$K_i = \frac{k_{\mathrm{a},i}}{k_{\mathrm{d},i}} = \frac{c^*_{\mathrm{ML}_i}}{c^*_\mathrm{M} c^*_{\mathrm{L}_{i-1}}} \tag{2.4}$$

It is also usual in natural systems to have mixtures of *n* different metals (^{i}M) and *k* different ligands (^{j}L) that can react according to:

$$^i\mathrm{M} + {}^j\mathrm{L} \underset{k_{\mathrm{d},ij}}{\overset{k_{\mathrm{a},ij}}{\rightleftharpoons}} {}^i\mathrm{M}\,{}^j\mathrm{L} \qquad i = 1 \ldots n \qquad j = 1 \ldots k \tag{2.5}$$

In this complexation process, $k_{\mathrm{a},ij}$ and $k_{\mathrm{d},ij}$ are the association and the dissociation rate constants, respectively. The stability constant for these processes can be written as:

$$K_{ij} = \frac{k_{\mathrm{a},ij}}{k_{\mathrm{d},ij}} = \frac{c^*_{{}^i\mathrm{M}\,{}^j\mathrm{L}}}{c^*_{{}^i\mathrm{M}}\,{}^j c^*_\mathrm{L}} \tag{2.6}$$

Some species in the system can also react with the functional groups R of the resin embedded in the resin layer. For some cases, only metals and protons can react with the

resin sites, a reaction that, in the simplest case, can be written as:

$$\mathrm{M} + \mathrm{R} \underset{k_{\mathrm{d,MR}}}{\overset{k_{\mathrm{a,MR}}}{\rightleftharpoons}} \mathrm{MR} \tag{2.7}$$

Here, $k_{\mathrm{a,MR}}$ and $k_{\mathrm{d,MR}}$ are the association and the dissociation rate constants between M and R, respectively, with stability constant defined as:

$$K_{\mathrm{MR}} = \frac{k_{\mathrm{a,MR}}}{k_{\mathrm{d,MR}}} \tag{2.8}$$

and MR is the metal bounded to the resin.

2.3.2 Transport of species

Mobile species can be subject to a three different transport mechanisms: diffusion, migration and convection[17]. In the DGT device, species diffuse from the bulk solution to the resin disc due to a difference of concentrations and the Brownian motion. According to the first Fick law, this contribution to the total flux (J_i) of species *i* is proportional to the magnitude of the concentration gradient of the diffusing species:

$$J_i(x,t) = -D_i \nabla c_i \tag{2.9}$$

being c_i the concentration and D_i the diffusion coefficient of species *i*, respectively.

Migration is the second possible contribution to transport of species. It is due to an electric force experienced by charged species in presence of an electric field. In the DGT device, this field is produced by fixed charged species in the resin or in the gel, and charged mobile species in the solution. The migrational flux of species *i* will be:

$$J_i(x,t) = -D_i \frac{z_i F c_i}{RT} \nabla \phi \tag{2.10}$$

where $F = 96485.33\ \mathrm{C\ mol^{-1}}$ is the Faraday constant, $R = 8.31\ \mathrm{J\ mol^{-1}\ K^{-1}}$ is the Universal gas constant, T stands for the absolute temperature, z_i is the charge (with sign), ϕ labels the electrostatic potential and $-\nabla\phi$ corresponds to the electric field.

The last contribution to the flux is convection, which consists in a species transport resulting from global motion of the fluid. It is limited inside the device, but may have importance in the deployment solution. The main function of the gel layer is the reduction of the convection influence on the metal accumulation in the resin by allowing the solute species being only transported by diffusion or migration.

Assuming that there is no transport by convection, the total flux can be obtained by the addition of diffusion and migration contributions (Equations (2.9) and (2.10)):

$$J_i(x,t) = -D_i\left(\nabla c_i + \frac{z_i F c_i}{RT}\nabla\phi\right) \tag{2.11}$$

The expression (2.11) is known as the Nernst-Planck Equation.

Applying the law of conservation of mass to species *i*, and assuming that the liquid solution is incompressible

$$\frac{\partial c_i}{\partial t} = -\nabla J_i(x,t) + \left\{\begin{matrix}\text{Rate of}\\ \text{production}\\ \text{of species } i\end{matrix}\right\} - \left\{\begin{matrix}\text{Rate of}\\ \text{consumption}\\ \text{of species } i\end{matrix}\right\} \tag{2.12}$$

Replacing (2.11) in (2.12) we obtain:

$$\frac{\partial c_i}{\partial t} = D_i\nabla^2 c_i + D_i\frac{z_i F}{RT}\nabla\left(c_i\nabla\phi\right) + \left\{\begin{matrix}\text{Rate of}\\ \text{production}\\ \text{of species } i\end{matrix}\right\} - \left\{\begin{matrix}\text{Rate of}\\ \text{consumption}\\ \text{of species } i\end{matrix}\right\} \tag{2.13}$$

Equation (2.13) describes the evolution of the concentration of species *i* in the DGT device, both in time and space.

The solution of the system of partial differential equations described by Equation (2.13) requires a set of initial and boundary conditions. For metals, ligands, metal-ligand complexes and metal-resin complexes it is assumed that there is no species in the resins or in the gel at time $t = 0$:

$$c_i(x,0) = 0 \qquad \text{in} \qquad 0 \le x < \delta^r + \delta^g \tag{2.14}$$

$$c_R(x,0) = c_{T,R} \quad \text{in regions with binding sites} \tag{2.15}$$

With δ^r being the thickness of the resin and δ^g the aggregate thickness of the diffusive gel layer +filter + DBL. Equation (2.15) implies that, initially, all the binding sites are free.

The boundary conditions in $x = 0$ will be:

$$\left.\frac{\partial c_i}{\partial x}\right|_{x=0} = 0 \tag{2.16}$$

Which implies zero flux of species *i* through this boundary. At the diffusive gel/solution interface, mobile species reach the bulk concentrations:

$$c_i(\delta^r + \delta^g, 0) = c_i^* \tag{2.17}$$

In the interface between the resin layer and the diffusive gel, ($x = \delta^r$) there is continuity of the concentration of species *i*:

$$c_i(\delta^{r-}, t) = c_i(\delta^{r+}, t)$$

Were superscripts – and + stand for both sides of the interface. Additionally, there is continuity of flux in the same positions:

$$D_i^R \left.\frac{\partial c_i}{\partial x}\right|_{\delta^{r-}} = D_i \left.\frac{\partial c_i}{\partial x}\right|_{\delta^{r+}} \tag{2.18}$$

It applies to mobile species. In Eqn. (2.18) D_i^R and D_i represent the diffusion coefficient in the resin disc and in the diffusive gel, respectively.

2.4 Regimes in the evolving metal accumulation

Once the DGT sensor is deposited in natural media or in laboratory solutions, species reacting with the resin start to accumulate in the sensor. The device provides the accumulated mass of the species of interest for different times. The time evolution of the metal accumulation (or the analyte of interest) in the DGT devices is shown in Fig.2.2. Four different regimes[18-20] can be recognized during this process:

2.4.1 Transient regime

At short times, there is a transient regime (see inset in Fig.2.2) where the flux, which is proportional to the slope of the accumulation curve, increases as the metal reaches the resin layer and reacts with the resin sites. As indicated in Fig. 2.2, the accumulation, under these conditions bends upwards, this being a practical way to recognize this behavior. Without saturation effects, the time to reach steady-state, t_{ss}, for a single metal can be estimated by the Einstein-Smoluchowski expression,[18]

$$t_{SS} \approx \frac{\left(\delta^g\right)^2}{\pi D_M} \tag{2.19}$$

where δ^g is the thickness of the diffusion domain (also labeled Δg or g in previous works). For standard DGT devices t_{ss} is of the order of 10 min in waters. Since deployment times are of the order of hours, this transient period has usually negligible information in the accumulation and the system can be well understood assuming that quasi steady-state conditions apply during all the deployment time.

2.4.2 Steady-state regime

A second regime corresponds to a linear accumulation of the metal as time increases. In this case, the flux is constant indicating that the system is in quasi steady-state conditions. We refer to this case as a quasi steady-state case to indicate that metals and ligands are in steady-state while the accumulated metal in the resin is monotonously

increasing and the free resin sites monotonously decreasing. Two cases can be recognized. The first one is fulfilled by most of the metals when Chelex is used as a binding layer. In this case, the association rate constant between the metal ion and the resin is so high that the binding is limited by the metal transport to the resin. Accordingly, the metal concentration at the resin-diffusive gel interface during this steady-state regime is zero and the penetration of free metal in the resin domain is negligible (as can be seen in Fig. 2.3). The second case arises when the kinetics of the metal association to the resin is limiting the accumulation. In this case there will be a measurable penetration of the metal in the resin layer and the metal flux will be lower than the one found in perfect-sink conditions. This situation will be discussed in Chapter 6.

2.4.3 Decreasing flux regime

At longer times, the accumulation bends downwards, indicating a decreasing flux as time increases. The decrease of the net rate of metal binding to the resin can be due to a non-negligible decrease of the free sites (due to competition or saturation effects) or to a significant increase of dissociation when equilibrium (of the bound metal with the metal concentration in the bulk solution) is approached. Manifestation of these effects on DGT measurements has been reported in previous development studies,[14,21-23] and this regime, which will be discussed in Section 6, has also been termed "saturable" [24] or “mixed”.[19]

2.4.4 Equilibrium/saturation regime

Finally, at sufficiently long times, the accumulation reaches a plateau, indicating a negligible net metal binding (see the rightmost part of Figure 2.2). Accordingly, there are no metal concentration gradients, the free metal in the resin domain equals the bulk free metal concentration and, in the simplest case, the bound metal is in equilibrium with the free metal concentration in the resin domain.

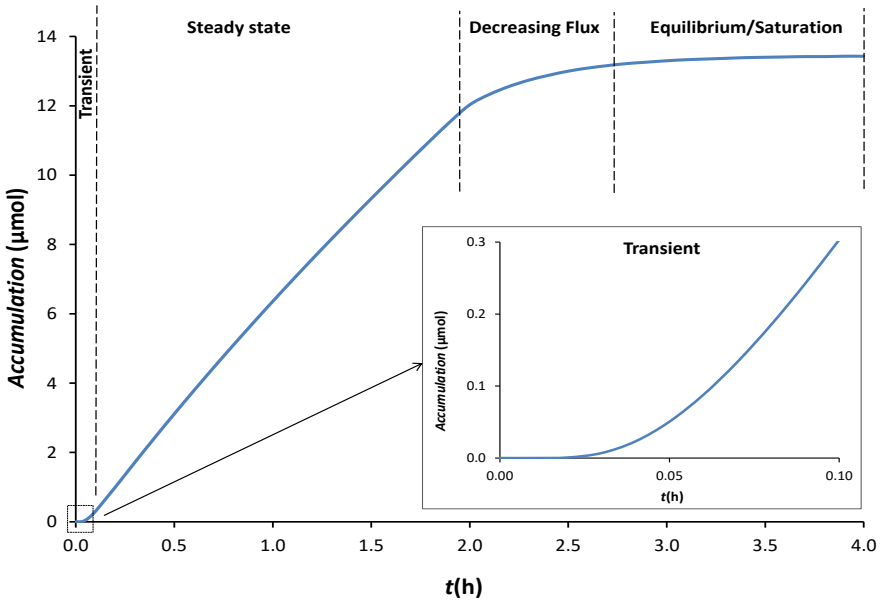

Figure 2.2. Accumulation of metal as a function of time in a DGT device. Different regimes, separated by vertical dashed lines at somewhat arbitrary positions, can be recognized as indicated in the figure. Parameters: $k_{a,R}$ *=1* $m^3 mol^{-1} s^{-1}$, $k_{d,R}$ *=*10^{-3} s^{-1}, D_M *=4.94×*10^{-10} $m^2 s^{-1}$, δ^r *=4×*10^{-4} *m,* δ^g *=1.1×*10^{-3} *m,* $C_{T,R}$ *=28mol* m^{-3}, C_M^* *=10 mol* m^{-3}.

2.5 Interpretation of results

With the experimental data of accumulations obtained with DGT devices it is possible to obtain information about average bulk concentrations, mean fluxes, lability of complexes and speciation. For the interpretation of these measurements, theoretical models that consider transport phenomena and chemical reactions of species on the media and on the device are required. The Mathematical models that describe these processes use systems of partial differential equations (Equation (2.13)). These equations are, in general, coupled and nonlinear and do not admit analytical solutions. For this reason, one manner to face this problem is using computational simulations. In this case, equations are solved using numerical methods. However, making some simplifications it is possible to find analytical solutions in some cases.

2.5.1 Simple systems and perfect-sink approximation

Traditional analyses use a simple approach for the interpretation of the experimental results. This approach is based on the following assumptions:

1. All the processes in the DGT device take place essentially in one relevant spatial dimension.
2. There are steady-state conditions of flux, so the mass accumulated in the initial transient period is negligible compared to the total accumulated mass.
3. There is fast and strong free metal ion binding by the resin, so that the free metal concentration inside the resin layer is negligible.
4. Bound metal is negligible with respect to the concentration of resin sites, so there are not saturation effects.
5. Ionic strength in the solution is high enough to screen electrostatic effects between charged species and the resin layer, the diffusive gel or the membrane filter.
6. The diffusion coefficients are the same in the filter, diffusive gel and the resin disc.

According to condition 5, there will be transport of species only by diffusion. In a system containing only the species M (a metal ion or the analyte of interest), the flux will be done by the first Fick's law:

$$J = D_{\mathrm{M}} \frac{\partial c_{\mathrm{M}}}{\partial x} \tag{2.20}$$

where D_{M} is the diffusion coefficient, c_{M} the concentration and $\frac{\partial c_{\mathrm{M}}}{\partial x}$ the concentration gradient of the metal.

In steady-state, the concentration profile of the metal in the perfect-sink approximation will be:

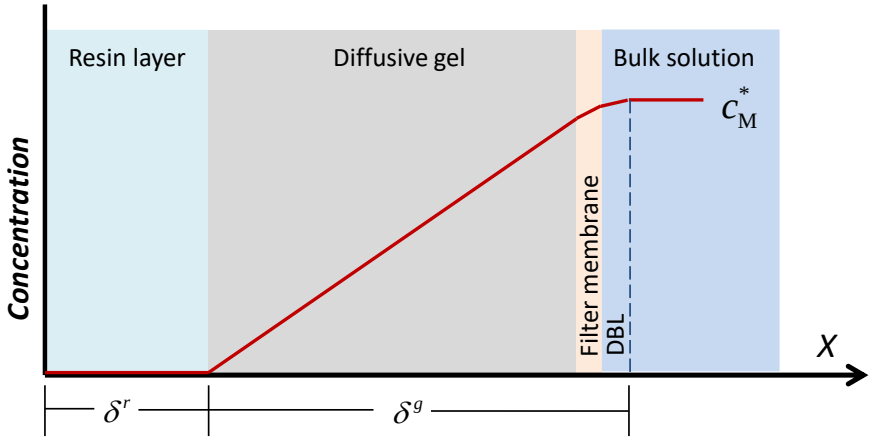

Figure 2.3. Concentration profile in perfect-sink and steady-state conditions.

the flux takes the form:

$$J = D_M \frac{c_M^*}{\delta^g} \tag{2.21}$$

and the accumulation of metal M can be obtained with the expression:

$$n_M = A\int J(t)\,dt = A\left(\frac{D_M c_M^*}{\delta^g}\right)t \tag{2.22}$$

Thus, the concentration of metal in the solution (c_M^*) can be obtained measuring the accumulation at a given time. Eqn. (2.22) is called the "perfect-sink" approximation.

2.5.2 The lability degree

In systems with ligands, the analyte will form complexes and the flux will result from the transport of free M and the contribution by transport and dissociation of complexes containing M. In these situations Eqn. (2.22) turns into:

$$n_M = A\left(\frac{D_M c_{DGT}}{\delta^g}\right)t \tag{2.23}$$

where c_{DGT} represents the metal concentration needed in an only-metal system to obtain the same flux as in the system studied. In general, c_M^* and c_{DGT} are different because the complexes may affect the flux by modifying the mobility of the metal species or kinetically limiting the dissociation process. When complexes containing M have

smaller diffusion coefficients than the one of free metal, it happens that $c_{DGT} < c_M^*$. On the other hand, when the diffusion coefficient of complexes are larger than the coefficient of free metal c_{DGT} could even be higher than c_M^*.

The contribution of a complex to the metal flux (J) is known as lability degree. When the association/dissociation kinetics is very fast (full labile complexes), there is equilibrium between metal and complex at all relevant spatial positions and the resulting flux (J_{lab}) is named fully labile. For extremely slow rate constants (inert complexes), there is not dissociation and the flux is due only to the free metal (J_{free}). For a given complex, the lability can be quantified through a parameter called lability degree of the complex ξ,[25] which compares the actual contribution of the complex to the metal flux with the maximum contribution reached if the complex was labile. It is defined as:

$$\xi \equiv \frac{J - J_{free}}{J_{labile} - J_{free}} \tag{2.24}$$

The lability degree takes values between 0 and 1. For labile systems (ξ=1), the kinetic processes are so fast that the metal and complex are in equilibrium at any relevant spatial position in the gel, except in a layer of negligible thickness at the resin disc-diffusive gel interface (the reaction layer in the diffusive gel). For inert systems (ξ=0), dissociation of the complex is so slow that the complex concentration profile in the gel domain is flat.[18] Partially labile complexes are between these two limits (0<ξ<1).

As shown in references[25,26], for systems with only one ligand and in perfect-sink conditions, the lability degree can be calculated as:

$$\xi = 1 - \frac{c_{ML}^r}{c_{ML}^*} \tag{2.25}$$

where c_{ML}^r indicates the concentration of ML at $x = \delta^r$. According to Eqn. (2.25) the value of c_{ML}^r must increase as the lability degree of the complex decreases, as shown in Figure 2.5. The normalized concentration profile of a labile complex (panel a) is

$\frac{c^r_{ML}}{c^*_{ML}} \approx 0$, which implies $\xi = 1$ in Eqn. (2.25). For inert complexes (panel d) $\frac{c^r_{ML}}{c^*_{ML}} \approx 1$, corresponding to $\xi = 0$.

In measurements of trace metals, the amount of free metal is very low and the lability degree can be estimated as:

$$\xi \approx \frac{J}{J_{\text{labile}}} \approx \frac{n_M / (At)}{\left(\frac{D_{ML}}{D_M}\right) n_M^{no-ligand} / (At)} = \frac{D_M\, n_M}{D_{ML}\, n_M^{no-ligand}} \tag{2.26}$$

where n_M and $n_M^{no-ligand}$ are the accumulations of metal in the same system, with and without ligand respectively. According to Eqn. (2.26), the lability degree can be interpreted as a normalised flux.[20] The labile flux has been estimated from the accumulation of M without ligand and taking into account the different diffusion coefficients of the complex (D_{ML}) and of the metal (D_M).

2.5.3 Penetration of species in the resin volume

Concentration profiles (normalized with respect to the concentration in solution) for different values of $k_{a,R}$ are shown in Figure 2.4 for an only metal system. Panel a) corresponds to a low value of $k_{a,R}$. In this case metal diffuses from the bulk solution through the device until the concentration in all the layers is the same. Profiles show the way the resin is filled. Equilibrium is almost reached at 2h in this example. Panel c) shows the evolution of the concentration profile for a species that binds strongly to the resin. For this kinetic constant a steady-state condition is reached. The concentration profile is a straight line in the gel layer, with zero value in the resin/diffusive gel interface, indicating perfect-sink conditions. In panel b) there is a species that partially binds to the resin. This is an intermediate situation between a) and c). A similar situation to steady-state can be reached, but there will be a penetration of the metal profile inside the resin domain.[27] This case will be discussed in Chapter 6.

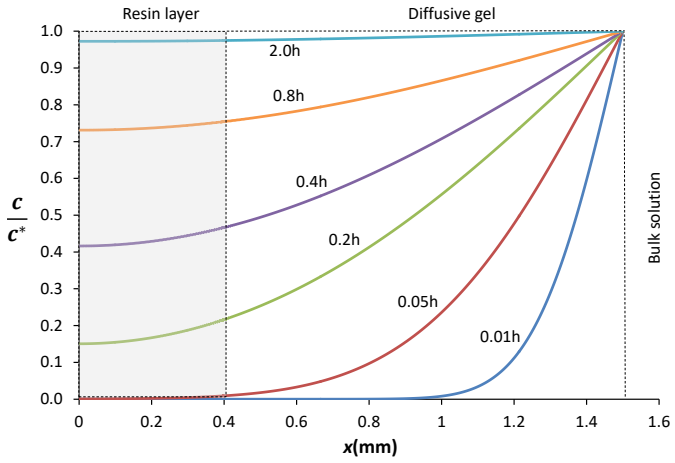

(a)

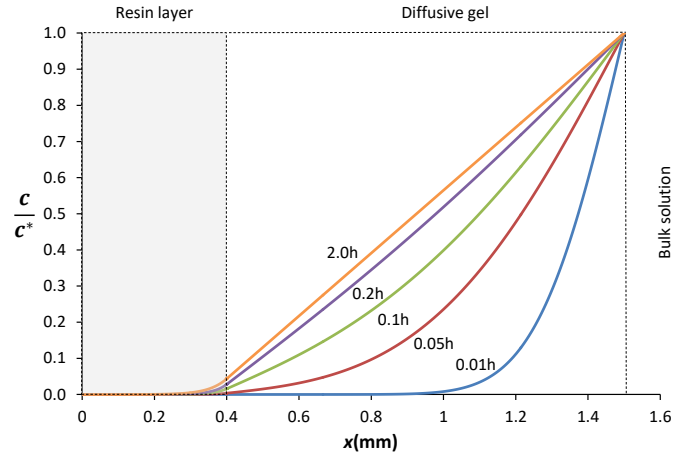

(b)

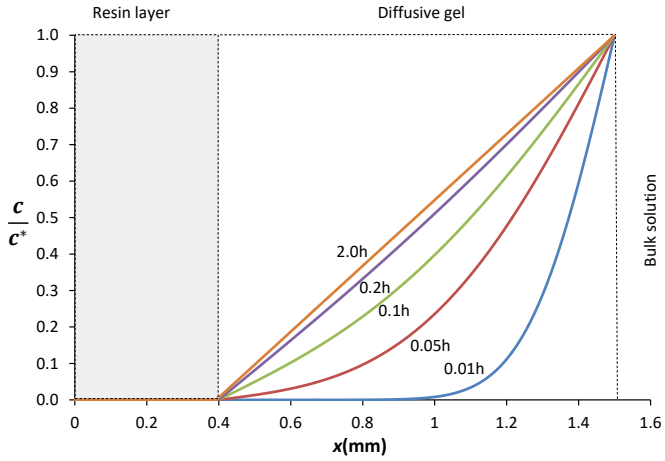

(c)

Figure 2.4. Time-evolution of normalized concentration profiles in a DGT device with only metal. a) $k_{a,R} = 1.7\times10^{-7}\ \mathrm{m^3 mol^{-1} s^{-1}}$, *b)* $k_{a,R} = 1.0\times10^{-2}\ \mathrm{m^3 mol^{-1} s^{-1}}$ *y c)* $k_{a,R} = 44\ \mathrm{m^3 mol^{-1} s^{-1}}$. *In all cases:* $k_{d,R} = 1.0\times10^{-4}\ \mathrm{s^{-1}}$, $D_M = 4.94\times10^{-10}\ \mathrm{m^2 s^{-1}}$ *(common in all layers),* $\delta^r = 4\times10^{-4}\ \mathrm{m}$, $\delta^g = 1.1\times10^{-3}\ \mathrm{m}$.

In presence of complexes, earlier models maintained the perfect-sink hypothesis and also assumed that the complexes did not penetrate the resin domain. These models could accurately reproduce labile complexes, but they could not explain the experimental results for other cases.[28] Improved models include the diffusion of species in the resin domain. As an example, we can analyze the system defined by Eqn. (2.1), constituted by one metal M and a ligand L, forming the complex ML. When the rate constant between M and the resin sites ($k_{a,R}$) is high enough, free metal is negligible in the resin domain although metal complexes can penetrate and dissociate in the resin domain. Fig. 2.5 depicts the M and ML normalized concentration profiles for different lability degrees. The consumption of metal in the resin phase requires in steady-state a decreasing metal concentration profile from the solution to the resin, reaching the metal concentration a null value in the resin/diffusive gel interface due to the high value of $k_{a,R}$. The decrease of the metal concentration induces the dissociation of the complex. If this dissociation is fast enough equilibrium is reached. When the M and ML normalized concentration profiles converge, there is local equilibrium between these species.[18] The thickness of the layer where both profiles diverge is called the reaction layer.[29] The part of the reaction layer in the diffusive gel can be estimated from the disequilibration parameter *m*, which can be calculated as:

$$m = \sqrt{\frac{D_{ML}}{k_d\left(1+c^*_{ML}/c^*_M\right)}} \tag{2.27}$$

The rest of the reaction layer in the resin domain can be estimated through the complex penetration parameter, λ_{ML}, which can be calculated as:

$$\lambda_{ML} = \sqrt{\frac{D_{ML}}{k_d}} \tag{2.28}$$

So the reaction layer is $\lambda_{ML}\coth\left(\frac{\delta^r}{\lambda_{ML}}\right)+m$ for $\lambda_{ML}\coth\left(\frac{\delta^r}{\lambda_{ML}}\right)<\delta^r$. When $\lambda_{ML}\coth\left(\frac{\delta^r}{\lambda_{ML}}\right)>\delta^r$, the reaction layer will be δ^r+m.

Penetration of complexes has an important impact on the reaction layer and therefore, in the lability of the complexes. Figure 2.5 (a) shows the profile of a labile complex (ξ=1). The normalized concentration profiles for both, M and ML, are superimposed all along the diffusive gel, indicating that the dissociation of ML is fast enough to maintain the equilibrium with M. It implies that the entire complex has dissociated when it arrives to the resin (as reflected in the profile) and its contribution to the flux is maximum:

$$J = J_{labile} = \frac{D_{\mathrm{M}} c_{\mathrm{M}}^{*}}{\delta^{g}} + \frac{D_{\mathrm{ML}} c_{\mathrm{ML}}^{*}}{\delta^{g}} \tag{2.29}$$

When the lability of the complex decreases, its contribution to the total flux can be calculated as: [29,30]

$$J = \frac{D_{\mathrm{M}} c_{\mathrm{M}}^{*}}{\delta^{g}} + \frac{D_{\mathrm{ML}} c_{\mathrm{ML}}^{*}}{\delta^{g}} \xi \tag{2.30}$$

Concentration profiles for partially labile complexes (0<ξ<1) are presented in Figs 2.5 (b) and (c). It can be seen that the convergence of both lines is shorter as the lability degree decreases. ML concentration profile penetrates in the resin, being different from 0 at $x = \delta^{r}$.

Finally, inert complexes (ξ=0) don't contributibute to the metal flux (see panel (d) in Fig 2.5). In this case, the flux will be:

$$J = J_{free} = \frac{D_{\mathrm{M}} c_{\mathrm{M}}^{*}}{\delta^{g}} \tag{2.31}$$

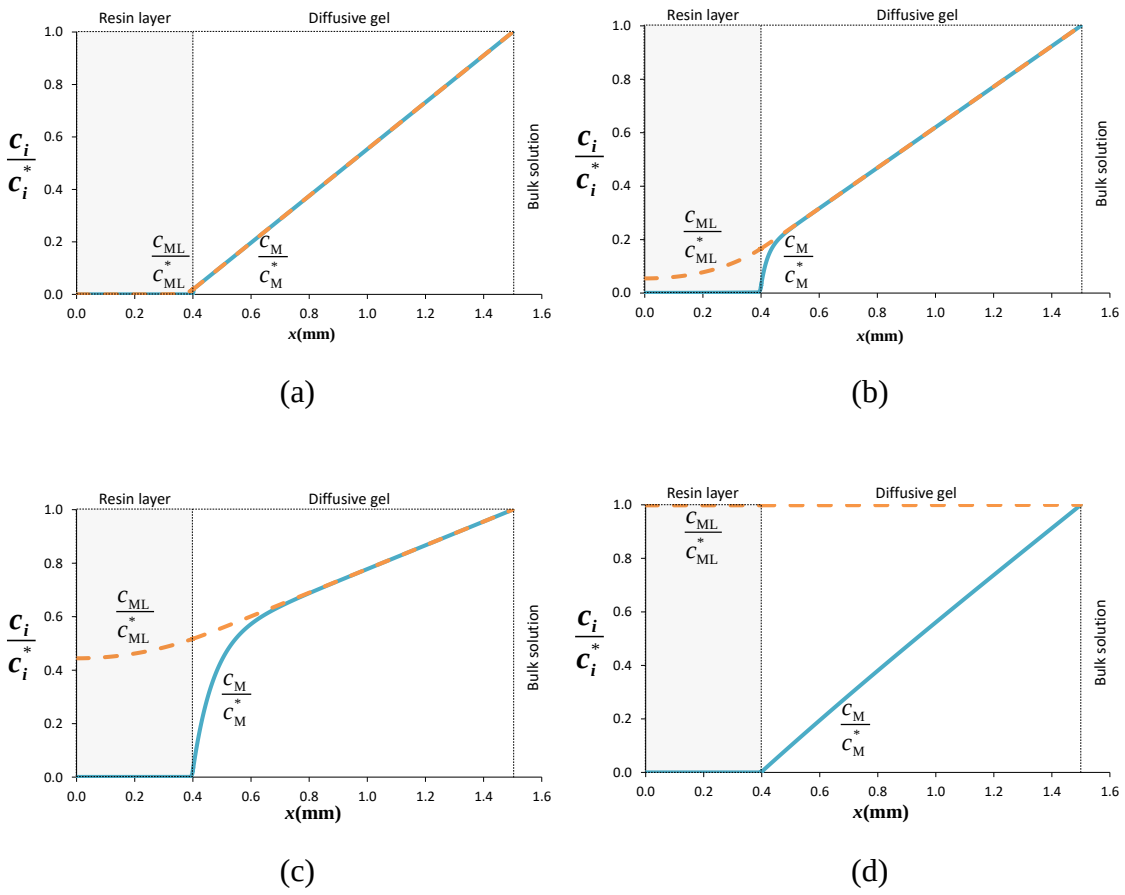

Figure 2.5. Normalized concentration profiles of metal (continuous lines) and complex (dashed lines) species for: (a) ξ=0.98 and $k_a = 10\ \mathrm{m^3 mol^{-1} s^{-1}}$*; (b) ξ=0.83 and* $k_a = 0.1\ \mathrm{m^3 mol^{-1} s^{-1}}$*; (c) ξ=0.48 and* $k_a = 10^{-2}\ \mathrm{m^3 mol^{-1} s^{-1}}$*; (d) ξ=0.0 and* $k_a = 10^{-5}\ \mathrm{m^3 mol^{-1} s^{-1}}$*. In all cases:* $c_{T,M} = 10^{-2}\ \mathrm{mol\ m^{-3}}$, $c_{T,L} = 10^{-1}\ \mathrm{mol\ m^{-3}}$, $c_{T,R} = 28\ \mathrm{mol\ m^{-3}}$, $K = 10\ \mathrm{m^3 mol^{-1}}$, $D_M = D_{ML} = 5.0\times10^{-10}\ \mathrm{m^2 s^{-1}}$ *(common in all layers),* $\delta^r = 4\times10^{-4}\ \mathrm{m}$, $\delta^g = 1.1\times10^{-3}\ \mathrm{m}$.

When the metal flux is time independent, the accumulation is linear with time and Eqn. (2.22) applies. Otherwise the linearity of the metal accumulations with time is distorted and further refinements in the analysis are required. Some of these cases will be discussed in the following chapters.

2.6 Reference List

1. Davison, W.; Zhang, H. In-situ speciation measurements of trace components in natural- waters using thin-film gels. *Nature* **1994,** *367* (6463), 546-548.

2. Zhang, H.; Davison, W. Performance characteristics of diffusion gradients in thin films for the insitu measurement of trace metals in aqueous solution. *Anal. Chem.* **1995,** *67* (19), 3391-3400.

3. Zhang, H.; Davison, W.; Knight, B.; McGrath, S. In situ measurements of solution concentrations and fluxes of trace metals in soils using DGT. *Environ. Sci. Technol.* **1998,** *32* (5), 704-710.

4. Costello, D. M.; Burton, G. A.; Hammerschmidt, C. R.; Taulbee, W. K. Evaluating the Performance of Diffusive Gradients in Thin Films for Predicting Ni Sediment Toxicity. *Environmental Science & Technology* **2012,** *46* (18), 10239-10246.

5. Davison, W.; Fones, G.; Harper, M.; ÿÿ; Zhang, H. Dialysis, DET and DGT: In Situ Diffusional Techniques for Studying Water, Sediments and Soils. In *In Situ Monitoring of Aquatic Systems: Chemical Analysis and Speciation*, Buffle, J., Horvai, G., Eds.; Wiley: Chichester, UK, **2000**; Vol. 6, pp 495-569.

6. Harper, M. P.; Davison, W.; Tych, W. DIFS - a modelling and simulation tool for DGT induced trace metal remobilisation in sediments and soils. *Environmental Modelling & Software* **2000,** *15* (1), 55-66.

7. Six, L.; Pypers, P.; Degryse, F.; Smolders, E.; Merckx, R. The performance of DGT versus conventional soil phosphorus tests in tropical soils - An isotope dilution study. *Plant Soil* **2012,** *359* (1-2), 267-279.

8. Mcbeath, T. M.; McLaughlin, M. J.; Armstrong, R. D.; Bell, M.; Bolland, M. D. A.; Conyers, M. K.; Holloway, R. E.; Mason, S. D. Predicting the response of wheat (Triticum aestivum L.) to liquid and granular phosphorus fertilisers in Australian soils. *Australian Journal of Soil Research* **2007,** *45* (6), 448-458.

9. Leermakers, M.; Gao, Y.; Gabelle, C.; Lojen, S.; Ouddane, B.; Wartel, M.; Baeyens, W. Determination of high resolution pore water profiles of trace metals in sediments of the Rupel River (Belgium) using DET (diffusive equilibrium in thin films) and DGT (diffusive gradients in thin films) techniques. *Water Air Soil Poll.* **2005,** *166* (1-4), 265-286.

10. Pradit, S.; Gao, Y.; Faiboon, A.; De Galan, S.; Baeyens, W.; Leermakers, M. Application of DET (diffusive equilibrium in thin films) and DGT (diffusive gradients in thin films) techniques in the study of the mobility of sediment-bound metals in the outer section of Songkhla Lake, Southern Thailand. *Environmental Monitoring and Assessment* **2013,** *185* (5), 4207-4220.

11. Yabuki, L. N. M.; Colaco, C. D.; Menegario, A. A.; Domingos, R. N.; Kiang, C. H.; Pascoaloto, D. Evaluation of diffusive gradients in thin films technique (DGT) for measuring Al, Cd, Co, Cu, Mn, Ni, and Zn in Amazonian rivers. *Environmental Monitoring and Assessment* **2014,** *186* (2), 961-969.

12. Bennett, W. W.; Teasdale, P. R.; Panther, J. G.; Welsh, D. T.; Jolley, D. F. Speciation of Dissolved Inorganic Arsenic by Diffusive Gradients in Thin Films: Selective Binding of As-III by 3-Mercaptopropyl-Functionalized Silica Gel. *Anal. Chem.* **2011,** *83* (21), 8293-8299.

13. van Leeuwen, H. P. Steady-state DGT fluxes of nanoparticulate metal complexes. *Environ. Chem.* **2011,** *8* (5), 525-528.

14. Panther, J. G.; Teasdale, P. R.; Bennett, W. W.; Welsh, D. T.; Zhao, H. J. Titanium Dioxide-Based DGT Technique for In Situ Measurement of Dissolved Reactive Phosphorus in Fresh and Marine Waters. *Environ. Sci. Technol.* **2010,** *44* (24), 9419-9424.

15. Davison, B.; Zhang, H. Principles of Measurements in Simple Solutions. In *Diffusive Gradients in Thin-Films for Environmental Measurements*, Davison, W., Ed.; Cambridge University Press: Cambridge, **2016**; pp 24-27.

16. Bio-Rad Laboratories . Chelex 100 and Chelex 20 Chelating Ion Exchange Resin Instruction Manual. **2013**.

17. Newman, J.; Thomas-Alyea, K. E. *Electrochemical Systems;* Third ed.; John Wiley & Sons: Hoboken, NJ, **2004**.

18. Puy, J.; Uribe, R.; Mongin, S.; Galceran, J.; Cecilia, J.; Levy, J.; Zhang, H.; Davison, W. Lability Criteria in Diffusive Gradients in Thin Films. *J. Phys. Chem. A* **2012,** *116* (25), 6564-6573.

19. Mongin, S.; Uribe, R.; Rey-Castro, C.; Cecilia, J.; Galceran, J.; Puy, J. Limits of the Linear Accumulation Regime of DGT Sensors. *Environ. Sci. Technol.* **2013,** *47*, 10438-10445.

20. Galceran, J.; Puy, J. Interpretation of diffusion gradients in thin films (DGT) measurements: a systematic approach. *Environ. Chem.* **2015,** *12* (2), 112-122.

21. Mason, S.; Harnon, R.; Zhang, H.; Anderson, J. Investigating chemical constraints to the measurement of phosphorus in soils using diffusive gradients in thin films (DGT) and resin methods. *Talanta* **2008,** *74* (4), 779-787.

22. Panther, J. G.; Bennett, W. W.; Welsh, D. T.; Teasdale, P. R. Simultaneous Measurement of Trace Metal and Oxyanion Concentrations in Water using Diffusive Gradients in Thin Films with a Chelex-Metsorb Mixed Binding Layer. *Anal. Chem.* **2014,** *86* (1), 427-434.

23. Mason, S.; Hamon, R.; Nolan, A.; Zhang, H.; Davison, W. Performance of a mixed binding layer for measuring anions and cations in a single assay

using the diffusive gradients in thin films technique. *Anal. Chem.* **2005,** *77* (19), 6339-6346.

24. Peijnenburg, W. J. G. M.; Teasdale, P. R.; Reible, D.; Mondon, J.; Bennett, W. W.; Campbell, P. G. C. Passive sampling methods for contaminated sediments: State of the science for metals. *Integrated Environmental Assessment and Management* **2014,** *10* (2), 179-196.

25. Galceran, J.; Puy, J.; Salvador, J.; Cecília, J.; van Leeuwen, H. P. Voltammetric lability of metal complexes at spherical microelectrodes with various radii. *J. Electroanal. Chem.* **2001,** *505* (1-2), 85-94.

26. Alemani, D.; Buffle, J.; Zhang, Z.; Galceran, J.; Chopard, B. Metal flux and dynamic speciation at (bio)interfaces. Part III: MHEDYN, a general code for metal flux computation; application to simple and fulvic complexants. *Environ. Sci. Technol.* **2008,** *42*, 2021-2027.

27. Levy, J. L.; Zhang, H.; Davison, W.; Puy, J.; Galceran, J. Assessment of trace metal binding kinetics in the resin phase of diffusive gradients in thin films. *Anal. Chim. Acta* **2012,** *717*, 143-150.

28. Mongin, S.; Uribe, R.; Puy, J.; Cecilia, J.; Galceran, J.; Zhang, H.; Davison, W. Key Role of the Resin Layer Thickness in the Lability of Complexes Measured by DGT. *Environ. Sci. Technol.* **2011,** *45* (11), 4869-4875.

29. Uribe, R.; Mongin, S.; Puy, J.; Cecilia, J.; Galceran, J.; Zhang, H.; Davison, W. Contribution of Partially Labile Complexes to the DGT Metal Flux. *Environ. Sci. Technol.* **2011,** *45* (12), 5317-5322.

30. Puy, J.; Galceran, J.; Rey-Castro, C. Interpreting the DGT Measurement: Speciation and Dynamics. In *Diffusive Gradients in Thin-Films for Environmental Measurements*, Davison, W., Ed.; Cambridge University Press: Cambridge, **2016**; pp 93-122.

CHAPTER 3

NUMERICAL SIMULATION OF DGT DEVICES

3.1 Introduction

Many problems of practical importance, which often appear in engineering, have associated mathematical equations that are in many cases very difficult or impossible to solve analytically. In order to study the properties of the solution or to simply evaluate the solution under some conditions it is then necessary to develop numerical procedures to solve the equations of the system.[1-3] This is the case of the equations corresponding to many electrochemical systems. A pioneering work related to the numerical treatment of electrochemical systems was developed by Feldberg and Auerbach.[4] Since then, many authors have applied different techniques for the numerical solution of these systems. The most widely used approach has been the finite difference method (FDM).[5,6] The original idea was to change the continuous physical space into a set of discrete points, equally spaced, which allows converting a differential problem into an equivalent system of algebraic equations.[7] FDM is very intuitive and easy to implement for simple problems. However, they are not suitable for a great deal of systems, for example with complicated geometries or with moving boundaries. Some variants of the method have been introduced to make it applicable to a wider range of problems, like adaptive intervals, in space or in time.[8-12] This method has been applied to the particular case of DGT devices.[13] Nevertheless, even with the improvements, the application of FDM often leads to very long simulation times.

A more efficient strategy for treating this type of problem is the Finite Element Method that will be discussed in the next section.

3.2 The Finite Element Method

The Finite Element Method (FEM) is a numerical technique to solve problems that are described by partial differential equations. The main idea of this method is to divide the domain, on which the equations are defined, in a set of discrete parts with some privileged points, not necessarily equally spaced, called nodes. The equations governing the behaviour of continuous domain also govern the discrete domain. From a mathematical point of view, the objective is to move from a continuous system with infinite degrees of freedom (governed by a set of differential equations) to a discrete system with a finite number of degrees of freedom (whose behaviour is modelled by a set of algebraic equations). The idea behind this process is that any continuous function of the element can be represented by a linear combination of polynomic functions, which are built in every finite element. The problem is solved on each element to obtain the solution on specific points called nodes. This solution, calculated over the nodes, is combined for building the total solution. Therefore, the objective of the method is to compute an approximate solution rather than an exact solution of the problem.

3.2.1 Application of the FEM

The use of the FEM typically involves the following steps:

a. Definition of the problem
b. Discretization of the domain
c. Construction of the interpolation basis
d. Formulation of the system of equations
e. Solution of the system of equations

a. Definition of the problem

The first step is to define the problem to solve. It implies to make a model of the physical reality. A model is a theoretical construction that reproduces the behaviour of some aspects of a physical system. According to Fritzson[14] a model of a system can also be defined as: “anything an experiment can be applied to in order to answer questions about that system”. The type and complexity of the model depend primarily on the type

of results required. With a model we can obtain information about the system without doing real experiments. The kind of experiments that we develop in the model is what we call simulations.[14]

To perform numerical simulations, mathematical models are required. In this case, the behaviour of the system is represented by a set of equations, and then relationships between variables of the system are expressed in mathematical form.

b. Discretization of the domain

One advantage of FEM is that it can be applied to domains with irregular geometry. In this method we seek to represent a complex domain, where the phenomena to study occur in a collection of subdomains of regular form (let's name them elements for the moment). Depending on the dimension of the problem, these elements can be parts of a line (e.g. truss or beam), an area (e.g. plane stress or membrane) or a volume (e.g. tetrahedral or hexahedral). The process of construction of this discrete space is called: meshing. Due to the importance of this discretization, there have been developed different strategies of meshing such as Delaunay triangulation or Adaptive grids.

The first step is to define the shape of the elements. Then, a certain number of nodes in each of these elements must be defined. The solutions for the equations will be found in these nodes. From a practical point of view, it is convenient to generate a new finite-dimensional space, with a high number of nodes in regions where the solution functions have large gradients and few nodes in regions where these variables show small changes. It is also important to avoid sudden changes in the size of the elements.

The mesh must have sufficient number of nodes to have good results with a computational precision and without excessive investment in resources and computational time. The shape of the elements is often related with the physical characteristics of the problem.[15] For example: in a problem of heat transmission in a bar, a unidimensional treatment can be enough. In this case, one-dimensional elements, with two nodes (one at each end of the element) can be used. If the problem involves two independent spatial coordinates, two-dimensional elements must be used. In this case,

triangles or trapezoids can be used with different possibilities for the nodes placement. In the case of three-dimensional problems, elements like tetrahedron or hexahedron are typically employed. These forms of discretization introduce certain approximations (e.g., curved lines replaced by straight lines or curved elements for flat surfaces). However, using a sufficient number of elements, the domain may be reproduced as well as desired.

Figure 3.1 shows an example of one possible discretization for a given domain. It was discomposed in ten triangles and there are also ten nodes.

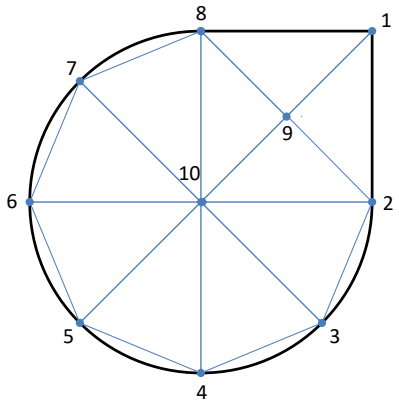

Figure 3.1. Example of discretization for a specific domain.

c. Construction of the interpolation basis

The application of the FEM gives us an approximate solution of the problem in the nodes. But the solution in other points of each element must be interpolated using an appropriate set of functions. Each interpolation function must have a value of 1 in one of the nodes and 0 in the others. Polynomials are typically chosen as interpolation functions over the nodes, mostly because they are easy to differentiate and integrate.

For the one-dimensional problems, the polynomials have the general expression:

$$\omega(x) = \alpha_1 + \alpha_2 x + \alpha_3 x^2 + \cdots + \alpha_m x^m \tag{3.1}$$

In the case of two dimensions:

$$\omega(x, y) = \alpha_1 + \alpha_2 x + \alpha_3 y + \alpha_4 x^2 + \alpha_5 y^2 + \alpha_6 xy + \cdots + \alpha_m y^m \tag{3.2}$$

and in the three-dimensional case:

$$\omega(x,y,z)=\alpha_1+\alpha_2 x+\alpha_3 y+\alpha_4 z+\alpha_5 x^2+\alpha_6 y^2+\alpha_7 z^2+\alpha_8 xy+\alpha_9 yz+\alpha_{10} zx+\cdots+\alpha_m z^n \tag{3.3}$$

Where n is the degree and $\alpha_1, \alpha_2, \ldots \alpha_m$ are the coefficients of the polynomial. In most cases, one-degree polynomials are used.

Figure 3.3 shows two finite elements corresponding to nodes 9 and 10 of the discretization of the domain plotted in Figure 3.1. Each finite element is made up by the polygon, its nodes and the corresponding no null fragments of the ω_i functions.

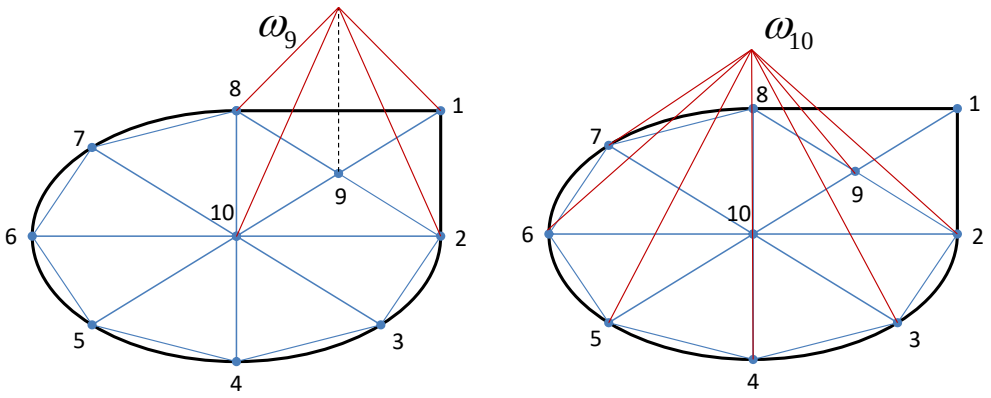

Figure 3.2. Example of two interpolation functions in the domain drawn in Fig 3.1.

d. Formulation of the system of equations

Suppose that we want to find the function u, which is the solution for the following problem:

$$\nabla^2 u + cu = f \qquad \text{in } \Omega \tag{3.4}$$

$$u = g \qquad \text{on } \Gamma_D \tag{3.5}$$

$$\nabla u \cdot \hat{n} = h \qquad \text{on } \Gamma_N \tag{3.6}$$

Where Ω is a domain in $\mathbb{R}^n$ which is limited by a closed curve Γ. This boundary is divided in two sections: Γ_D and Γ_N. The solution is found in a linear space of

functions (i.e. Hilbert or Sobolev spaces). Equations (3.5) and (3.6) are Dirichlet and Neumann boundary conditions, respectively.

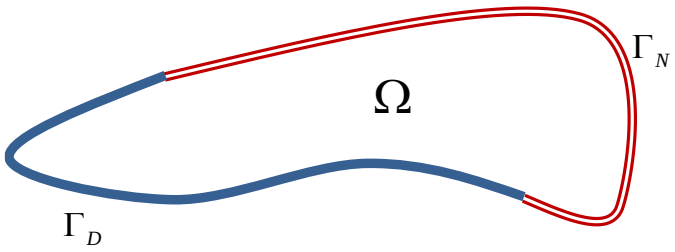

Figure 3.3. The domain Ω with Dirichlet and Neumann boundaries.

The first step consists in expressing the problem in its variational form:

$$\int_{\Omega}\left(\nabla^2 u + cu - f\right)\cdot\omega\,\mathrm{d}\Omega + \int_{\Gamma}\left(\nabla u\cdot\hat{n} - g\right)\cdot\omega'\,\mathrm{d}\Gamma = 0 \qquad \forall\ \omega,\ \omega'\ \in\ V \tag{3.7}$$

Being V the set of functions defined as:

$$V = \left\{\omega \middle|\ \omega \text{ is piecewise } C^2 \text{ and } \omega{=}0 \text{ on } \Gamma_D\right\} \tag{3.8}$$

The next step is the introduction of the weak formulation of the problem. The main advantage of this form is that decreases continuity and differentiability requirements on the potential solutions to the equation. To introduce this formulation, it is necessary to use the divergence theorem, which states:

$$\int_{\Omega}\left(\mathbf{div}\,\vec{A}\right)\mathrm{d}\Omega = \int_{\Gamma}\left(\vec{A}\cdot\hat{n}\right)\mathrm{d}\Gamma \tag{3.9}$$

replacing $A = \vec{\nabla}u\cdot\omega$ in Equation (3.9) we obtain:

$$\int_{\Omega}\left(\nabla^2 u\right)\cdot\omega\,\mathrm{d}\Omega + \int_{\Omega}\left(\nabla u\cdot\nabla\omega\right)\mathrm{d}\Omega = \int_{\Gamma}\left(\nabla u\cdot\hat{n}\right)\cdot\omega\,\mathrm{d}\Gamma \tag{3.10}$$

where we have used:

$$\mathbf{div}\,\left(\vec{\nabla}u\cdot\omega\right) = \left(\nabla^2 u\right)\cdot\omega + \nabla u\cdot\nabla\omega \tag{3.11}$$

Splitting the boundary Γ in two parts, Equation (3.10) takes de form:

$$\int_{\Omega}\left(\nabla^2 u\right)\cdot\omega\,\mathrm{d}\Omega+\int_{\Omega}\left(\nabla u\cdot\nabla\omega\right)\mathrm{d}\Omega=\int_{\Gamma_D}\left(\nabla u\cdot\hat{n}\right)\cdot\omega\,\mathrm{d}\Gamma+\int_{\Gamma_N}\left(\nabla u\cdot\hat{n}\right)\cdot\omega\,\mathrm{d}\Gamma \tag{3.12}$$

In the boundary Γ_N, we are going to impose the condition:

$$\omega=0 \qquad \text{on } \Gamma_D \tag{3.13}$$

Using Equations (3.4), (3.6) and (3.13) in Equation (3.12) we have:

$$\int_{\Omega}\left(\nabla u\cdot\nabla\omega\right)\mathrm{d}\Omega+\int_{\Omega}\left(f\,\omega\right)\mathrm{d}\Omega-c\int_{\Omega}\left(u\,\omega\right)\mathrm{d}\Omega-\int_{\Gamma_N}\left(h\,\omega\right)\mathrm{d}\Gamma=0 \tag{3.14}$$

Expression (3.14) together with the condition (3.5) constitute the **weak formulation** of the problem. [16,17] In this formulation the solution function is not required to be derivable twice.

The solution of the problem is being found in a linear space of functions V. This allows the use of basis (which have an infinite number of functions) of these spaces.

If $B_1=\left\{\omega_1,\omega_2,...,\omega_i,...\right\}$ is a basis of V, the problem can be written as:

$$\int_{\Omega}\left(\nabla u\cdot\nabla\omega_i\right)\mathrm{d}\Omega+\int_{\Omega}\left(f\,\omega_i\right)\mathrm{d}\Omega-c\int_{\Omega}\left(u\,\omega_i\right)\mathrm{d}\Omega-\int_{\Gamma_N}\left(h\,\omega_i\right)\mathrm{d}\Gamma=0 \tag{3.15}$$

On the other hand, each function of the solution can be expressed as a linear combination of elements of another basis $B_2=\left\{\hat{\omega}_1,\hat{\omega}_2,...,\hat{\omega}_j,...\right\}$ as follows:

$$u=\sum_{j=0}^{\infty}u_j\hat{\omega}_j \tag{3.16}$$

Substituting Equation (3.16) in the weak formulation of the problem, Equation (3.14), we obtain:

$$\int_{\Omega} \nabla \left(\sum_{j=0}^{\infty} u_j \hat{\omega}_j(x) \right) \cdot \nabla \omega_i \, \mathrm{d}\Omega + \int_{\Omega} \left(f \, \omega_i \right) \mathrm{d}\Omega - c \int_{\Omega} \left(\sum_{j=0}^{\infty} u_j \hat{\omega}_j(x) \right) \omega_i \, \mathrm{d}\Omega - \int_{\Gamma_N} \left(h \, \omega_i \right) \mathrm{d}\Gamma = 0 \quad (3.17)$$

that turns into:

$$\sum_{j=0}^{\infty} u_j \left(\int_{\Omega} \left(\nabla \hat{\omega}_j \cdot \nabla \omega_i \right) \mathrm{d}\Omega - c \int_{\Omega} \left(\hat{\omega}_j \, \omega_i \right) \mathrm{d}\Omega \right) = \int_{\Gamma_N} \left(h \, \omega_i \right) \mathrm{d}\Gamma - \int_{\Omega} \left(f \, \omega_i \right) \mathrm{d}\Omega \quad (3.18)$$

To solve it numerically, it is useful to write this problem in its matrix form:

$$\mathbf{A} \cdot \vec{\mathbf{u}} = \vec{\mathbf{t}} \quad (3.19)$$

Here, the elements of the matrix **A** can be written as:

$$A_{ij} = \int_{\Omega} \left(\nabla \hat{\omega}_j \cdot \nabla \omega_i \right) \mathrm{d}\Omega - c \int_{\Omega} \left(\hat{\omega}_j \, \omega_i \right) \mathrm{d}\Omega \quad (3.20)$$

Elements of vector $\vec{\mathbf{t}}$ are defined as:

$$t_i = \int_{\Gamma_N} \left(h \, \omega_i \right) \mathrm{d}\Gamma - \int_{\Omega} \left(f \, \omega_i \right) \mathrm{d}\Omega \quad (3.21)$$

Being vector $\vec{\mathbf{u}}$:

$$\vec{\mathbf{u}} = \begin{pmatrix} u_1 \\ u_2 \\ \vdots \\ u_n \\ \vdots \end{pmatrix} \quad (3.22)$$

It is important to clarify that no approximation has been made until now and the formulation remains rigorous. It is at this point when we will actually apply the FEM, passing the weak formulation from a continuous to a discrete form. To do this, the function ω will be selected from a discrete basis B_1 of the space V where the solution is being found. This approach is called the **Petrov-Galerkin method**,[16,17] if the basis of functions B_1 and B_2 are different. When the two basis are taken equal the approach is named **Galerkin method**.

Another important thing is that, in a linear space, the computation $\int_{\Omega} u \, \omega \, \mathrm{d}\Omega$ has

properties of a scalar product: is bilinear, commutative and positive defined. It means that, applying the Galerkin method, matrix **A** will be symmetric and positive defined and accordingly, the problem has only one solution.

As an example let's assume that we want to solve Equation (3.18) in a one-dimensional given domain (see Fig 3.4). Due to the fact that the value of every $\hat{\omega}_j$ function is 1 at nodes, the coefficients u_j correspond to the values of u at these points. Additionally, since each $\hat{\omega}_j$ is a continuous piecewise linear function of x, their linear combination will also be continuous and piecewise linear. Thus, once the values of the u_j have been found, we have an approximation to the analytical function all over the domain of the problem. One possible basis of functions $\hat{\omega}_j$ is:

$$\hat{\omega}_j(x) = \begin{cases} \dfrac{x - x_{j-1}}{x_j - x_{j-1}} & \text{if} \quad x_{j-1} \le x \le x_j \\ \dfrac{x_{j+1} - x}{x_{j+1} - x_j} & \text{if} \quad x_j \le x \le x_{j+1} \\ 0 & \text{otherwise} \end{cases} \tag{3.23}$$

These type of functions are different from zero only in the interval $\left(x_{j-1}, x_{j+1}\right)$, i. e., on the two finite elements containing the node *j*. Figure 3.4 shows the aproximation of a continuous function using this basis. It is easy to see that in the interval $\left(x_{j-1}, x_j\right)$ the aproximate linear piecewise function will be constructed as:

$$u\left(x\right) = u_{j-1}\hat{\omega}_{j-1}(x) + u_j\hat{\omega}_j(x) \tag{3.24}$$

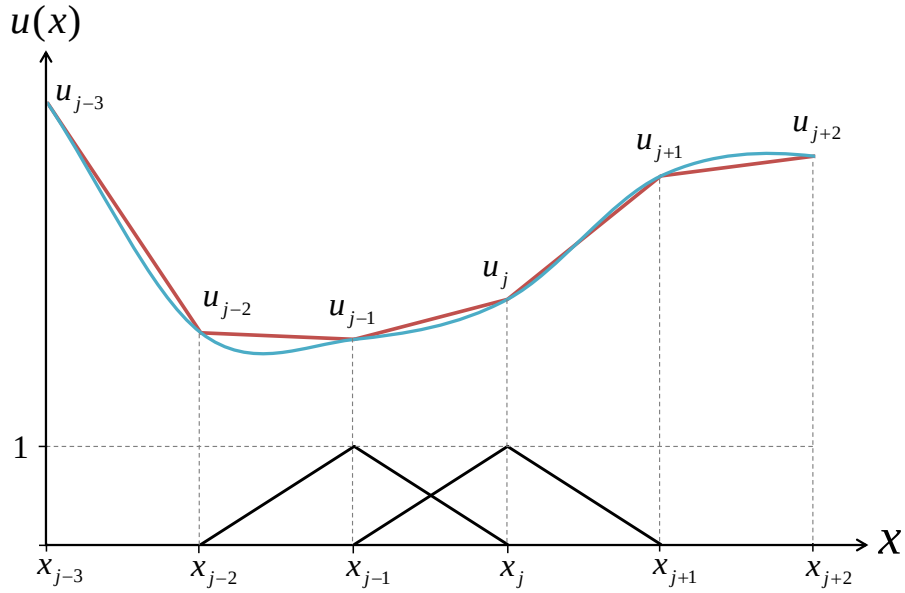

Figure 3.4. Approximation of a continuous function using a basis of linear interpolation functions.

e. Solution of the system of equations

Typically, matrices resulting from the finite element analysis are sparse [18]. Techniques used for solving the system of equations try to take advantage of these characteristics to reduce the required memory and the computational time. These techniques can be separated in two types: direct and iterative.[18] The first group produce the exact solution in a finite number of elementary arithmetic operations. The maximum error, for a given independent matrix and term, is usually associated with the number of operations of each method. Since computers have finite precision, rounding errors are propagated and the numerical solution obtained always differs from the exact solution. Therefore, it is an objective to obtain methods with the minimum number of possible operations. For these reasons, direct methods are usually used for problems of moderate size. Cholesky method and Gaussian elimination are examples of direct methods.

For large systems, iterative methods require less computing time, in part, because they do not require the construction of the matrix. An iterative method progressively calculates approximations to the solution of a problem. They begin with an initial value and then an algorithm is applied to obtain a new approximate solution. It is expected that the new solution obtained is a solution more approximate than the initial one. The process is repeated until the most recent result satisfies certain requirements. The main

advantages of the iterative methods are the simplicity and uniformity of the operations to be done. Examples of them are Gauss-Seidel, Jacobi and Newton-Raphson methods.[18]

3.2.2 Transient problems

Until now, we have been working with stationary problems. But the FEM can also be used in time-dependent problems. In these cases, one useful strategy is to separate the solution function in two parts: one depending on time and the other on the spatial coordinates. Then, we can apply a FDM to the temporal part and the FEM to the spatial part of the problem.

To better explain this strategy, we can use an unidimensional diffusion problem:

$$\frac{\partial u}{\partial t} = D\frac{\partial^2 u}{\partial x^2} \tag{3.25}$$

with the initial condition:

$$u(x,0) = q(x) \tag{3.26}$$

and a boundary value problem:

$$\left.\frac{\partial u}{\partial x}\right|_{x=0} = h \tag{3.27}$$

$$u(L,\mathrm{t}) = g \tag{3.28}$$

This problem can be analysed in similar way to the stationary example defined in Equations (3.4), (3.5) and (3.6) if we replace f by $\frac{\partial u}{\partial t}$ and take $c = 0$. The weak formulation turns into:

$$\int_{\Omega}(\nabla u \cdot \nabla \omega)\,\mathrm{d}\Omega + \int_{\Omega}\left(\frac{\partial u}{\partial t}\omega\right)\mathrm{d}\Omega - \int_{\Gamma_N}(h\,\omega)\mathrm{d}\Gamma = 0 \tag{3.29}$$

Using the same B_1 and B_2 basis to develop the spatial part of the function, the approximate solution function can be expressed as:

$$u = \sum_{j=0}^{N} u_j(t) \cdot \omega_j(x) \tag{3.30}$$

And the weak formulation (3.29) becomes:

$$\int_{\Omega} \frac{\partial}{\partial x}\left(\sum_{j=0}^{N} u_j(t) \cdot \omega_j(x) \right) \cdot \omega_i'(x)\, \mathrm{d}\Omega + \int_{\Omega} \frac{\partial}{\partial t}\left(\sum_{j=0}^{N} u_j(t) \cdot \omega_j(x) \right) \omega_i(x)\, \mathrm{d}\Omega - \int_{\Gamma_N} h\, \omega_i(x)\, \mathrm{d}\Gamma = 0 \tag{3.31}$$

After some reordering:

$$\sum_{j=0}^{N} u_j(t) \int_{\Omega} \left(\hat{\omega}_j'(x) \cdot \omega_i'(x) \right) \mathrm{d}\Omega + \sum_{j=0}^{N} \frac{\partial u_j(t)}{\partial t} \int_{\Omega} \left(\hat{\omega}_j(x) \cdot \omega_i(x) \right) \mathrm{d}\Omega - \int_{\Gamma_N} h\, \omega_i(x)\, \mathrm{d}\Gamma = 0 \tag{3.32}$$

which can be written in matrix form as:

$$\mathbf{B} \cdot \vec{\mathbf{u}}' + \mathbf{A} \cdot \vec{\mathbf{u}} - \vec{\mathbf{t}} = 0 \tag{3.33}$$

where the elements of the matrices are:

$$A_{ij} = \int_{\Omega} \left(\hat{\omega}_j'(x) \cdot \omega_i'(x) \right) \mathrm{d}\Omega \tag{3.34}$$

$$B_{ij} = \int_{\Omega} \left(\hat{\omega}_j(x) \cdot \omega_i(x) \right) \mathrm{d}\Omega \tag{3.35}$$

The elements of the vector $\vec{\mathbf{t}}$ are defined as:

$$t_i = \int_{\Gamma_N} \left(h\, \omega_i \right) \mathrm{d}\Gamma \tag{3.36}$$

and the vectors $\vec{\mathbf{u}}$ and $\vec{\mathbf{u}}'$ are:

$$\vec{\mathbf{u}} = \begin{pmatrix} u_1 \\ u_2 \\ \vdots \\ u_n \\ \vdots \end{pmatrix} \tag{3.37}$$

$$\vec{\mathbf{u}}' = \begin{pmatrix} \frac{\partial u_1}{\partial t} \\ \frac{\partial u_2}{\partial t} \\ \vdots \\ \frac{\partial u_n}{\partial t} \\ \vdots \end{pmatrix} \tag{3.38}$$

The solution of Equation (3.33) requires a time discretization. This can be done using a θ-Scheme[19]:

$$\mathbf{B}\cdot\left(\frac{\vec{\mathbf{u}}(t+\Delta t)-\vec{\mathbf{u}}(t)}{\Delta t}\right)+(1-\theta)\left(\mathbf{A}\cdot\vec{\mathbf{u}}(t)-\vec{\mathbf{t}}(t)\right)+\theta\left(\mathbf{A}\cdot\vec{\mathbf{u}}(t+\Delta t)-\vec{\mathbf{t}}(t+\Delta t)\right)=0 \tag{3.39}$$

which can be written as:

$$\left(\frac{1}{\Delta t}(\mathbf{B})+\theta(\mathbf{A})\right)\vec{\mathbf{u}}(t+\Delta t)=\left(\frac{1}{\Delta t}(\mathbf{B})+(1-\theta)(\mathbf{A})\right)\vec{\mathbf{u}}(t)+(1-\theta)\vec{\mathbf{t}}(t)+\theta\vec{\mathbf{t}}(t+\Delta t) \tag{3.40}$$

That is an expression for the values of u in all the nodes in the time t+Δt, as a function of the values of u at time t. Here, θ is a parameter whose selection originates different methods[19]:

$\theta = 0 \quad \rightarrow$ Euler Explicit

$\theta = 1 \quad \rightarrow$ Euler Implicit

$\theta = 1/2 \quad \rightarrow$ Crank-Nicolson

$0 < \theta < 1 \quad \rightarrow$ Other implicit methods

In explicit methods a direct computation of the dependent variables can be made in terms of known quantities. These methods are of order 1 and have low computation

times, but need smaller time intervals for accuracy and stability.[19]

A numerical method is said to be implicit when the dependent variables are defined by coupled sets of equations and either a matrix or iterative technique is needed to obtain the solution. The matrices originated are normally tridiagonal, which allows solving the system very efficiently. On the other hand, the increase in the number of operations is compensated by the possibility of using larger increments of time in each step. Euler implicit is an unconditional stable method of order 1. Crank-Nicolson is unconditional stable of order 2 and it is the most precise method.[20]

3.3 DGT device with N species

3.3.1 Definition of the problem

Let us describe the simulation tool developed to solve the transport and reaction processes in a DGT device. The model is similar to those used in references [13,21,22] but here, the FEM will be used.

The physical domain has planar symmetry with only one relevant spatial dimension labelled *x*. To be more general, the device was simulated with two resin discs. Additionally, each resin disc is allowed to have a binding agent only in part of the disc. We will call front resin disc the one that is in contact with the gel and back resin disc, the disc located at the bottom as shown in Figure 3.5. The DGT devices are deployed in solutions containing various species, metals, ligands, or combinations of both species. Species diffuse in the sensor both along the diffusive gel and the resin domain. Only free metals can react with the binding agents dispersed in the resin discs. Ligands and complexes do not react with the resin sites.

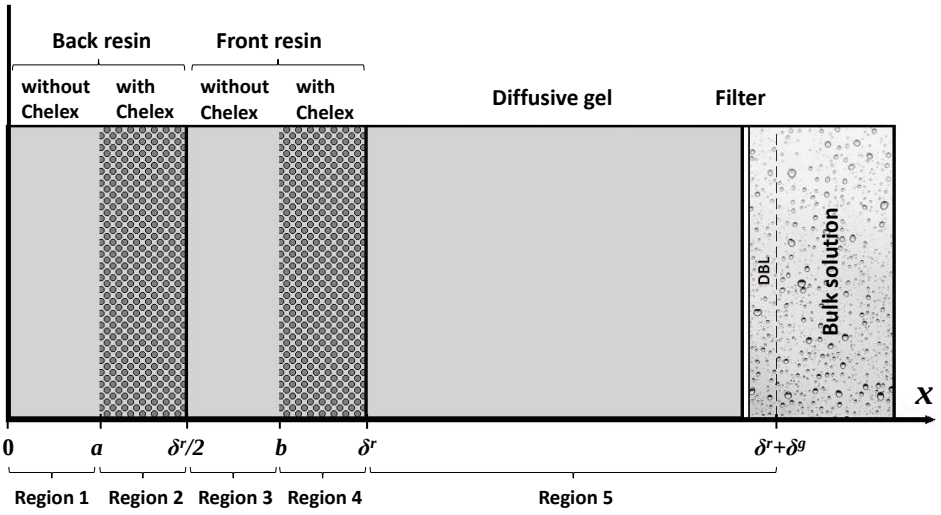

Figure 3.5. Scheme of the DGT device for the simulation

We are going to consider only reactions of the form:

$$\mathrm{A} + \mathrm{B} \rightleftarrows \mathrm{C} \tag{3.41}$$

Any other reaction is essentially composed of reactions of this type.

The balanced equations for species *i* are:

$$\frac{\partial c_i}{\partial t} = D_i^{\mathrm{R}} \frac{\partial^2 c_i}{\partial x^2} + \ll \text{Reaction terms} \gg \quad \text{In regions 2 and 4.} \tag{3.42}$$

$$\frac{\partial c_i}{\partial t} = D_i \frac{\partial^2 c_i}{\partial x^2} + \ll \text{Reaction terms} \gg \quad \text{In regions 1, 3 and 5.} \tag{3.43}$$

The term on the left hand side in both equations represents the change in concentration of species *i* per unit time. The first term on the right hand side describes the change in concentration of the species *i* by diffusion. Source terms describe the variation of the concentration due to homogeneous chemical transformations. These terms are polynomial and depend on the concentration. Diffusion coefficients are labelled as D_i^{R} for species *i* in the regions with binding agent (regions 2 and 4 in Figure 3.5), while D_i labels the corresponding diffusion coefficient in regions without binding agent (regions 1, 3 and 5 in Figure 3.5). Species bound to the resins remain immobile so that the corresponding diffusion coefficient is $D_i^{\mathrm{R}} = 0$.

a. Change of Variables

Some changes of the variables were made in order to obtain more suitable scales. We used the same normalization as in reference [13]. The concentrations of species with a diffusion coefficient different from zero (the species not attached to the resin) are transformed into dimensionless functions by dividing by its bulk concentration:

$$q_i = \frac{c_i}{c_i^*} \tag{3.44}$$

This is done in order to easily compare the values of the concentrations of the different species, even though they take different orders of magnitude. In the case of species with diffusion coefficients equal to zero, concentrations are made dimensionless normalizing by the total concentration of sites on the corresponding resin ($c_{\mathrm{TR},j}$). This normalization applies to resin sites and resin-metal complexes:

$$q_j = \frac{c_j}{c_{\mathrm{T,R},j}} \tag{3.45}$$

The spatial dimensions are divided by the square root of the highest diffusion coefficient:

$$z = \frac{x}{\sqrt{D_{\max}}},\ r^* = \frac{\delta^r}{\sqrt{D_{\max}}},\ g^* = \frac{\delta^g}{\sqrt{D_{\max}}} \tag{3.46}$$

Diffusion coefficients are also normalized relative to the highest diffusion coefficient:

$$d_i = \frac{D_i}{D_{\max}} \tag{3.47}$$

b. Initial conditions

At time $t = 0$ it is assumed that there is no species in the resins or in the gel and all the binding sites are free. The initial conditions are:

$$c_i(x,0) = 0 \qquad \text{in} \qquad 0 \le x < \delta^r + \delta^g \tag{3.48}$$

for metals, ligands, metal-ligand complexes, and metal-resin complexes. For resin sites the initial conditions are:

$$c_{\mathrm{R}}(x,0) = c_{\mathrm{T,R}} \quad \text{in the regions 2 and 4} \tag{3.49}$$

$$c_{\mathrm{R}}(x,0) = 0 \quad \text{in the regions 1, 3 and 5.} \tag{3.50}$$

Initial conditions in terms of the dimensionless variables rewrite

$$q_i(z,0) = 0 \quad \text{in} \quad 0 \le z < r^* + g^* \tag{3.51}$$

for metals, ligands, metal-ligand complexes, and metal-resin complexes.

$$q_{\mathrm{R}}(z,0) = 1 \quad \text{in the regions 2 and 4} \tag{3.52}$$

$$q_{\mathrm{R}}(z,0) = 0 \quad \text{in the regions 1, 3 and 5} \tag{3.53}$$

c. Boundary Conditions

Boundary conditions can be written as:

$$\left.\frac{\partial c_i}{\partial x}\right|_{x=0} = 0 \tag{3.54}$$

because there is no flow of any species through the boundary $x = 0$.

$$c_i(\delta^r + \delta^g, 0) = c_i^* \tag{3.55}$$

which means that, at the gel-solution interface, the species reach the bulk concentrations (only applied to species with $D_i \neq 0$).

In the positions of interfaces between regions with and without binding agent ($x = a$, $x = \frac{\delta^r}{2}$, $x = b$ and $x = \delta^r$) there is continuity of the concentration of species *i*:

$$c_i(x^-,t) = c_i(x^+,t) \tag{3.56}$$

Were superscripts – and + stand for both sides of the interface. Additionally, there is continuity of flux in the same positions:

$$D_i^R \left.\frac{\partial c_i}{\partial x}\right|_{x^-} = D_i \left.\frac{\partial c_i}{\partial x}\right|_{x^+} \tag{3.57}$$

It applies to species that do not involve resins.

In terms of the dimensionless variables, the boundary conditions become:

$$\left.\frac{\partial q_i}{\partial z}\right|_{z=0} = 0 \tag{3.58}$$

$$q_i(r^* + g^*, 0) = 1 \tag{3.59}$$

$$q_i(z^-, t) = q_i(z^+, t) \tag{3.60}$$

$$d_i^R \left.\frac{\partial q_i}{\partial z}\right|_{z^-} = d_i \left.\frac{\partial q_i}{\partial z}\right|_{z^+} \tag{3.61}$$

being $z = a^* = \frac{a}{\sqrt{D_{\max}}}$, $z = \frac{r^*}{2} = \frac{\delta^r}{2\sqrt{D_{\max}}}$, $z = b^* = \frac{b}{\sqrt{D_{\max}}}$ and $z = r^* = \frac{\delta^r}{\sqrt{D_{\max}}}$, dimensionless positions of interfaces.

3.3.2 Discretization of the domain

We expect that the most relevant events happen near the interfaces. For this reason, the density of points on the grid is bigger close to these interfaces. There are five regions. The discretization of every region has been done using the same idea. As an example, let's assume that one of these regions whose boundaries are denoted as $\{l_1, l_2\}$ has a length equal to L (after the change of variables), and we want to discretize the space in N parts. For the discretization of the space we can use the following function:

$$z_k = l_1 + \frac{L}{2}\left[1 - \cos\left(\frac{\pi k}{\mathrm{N}}\right)\right] \tag{3.62}$$

As a particular case we assume two identical resins, with binding agent only in half of their volumes. Figure 3.6 shows the number of divisions of every region. The workspace is divided in N parts, from the point z_1 to the point z_{N+1} (where N=NG1+NR1+ NG2+NR2+NG).

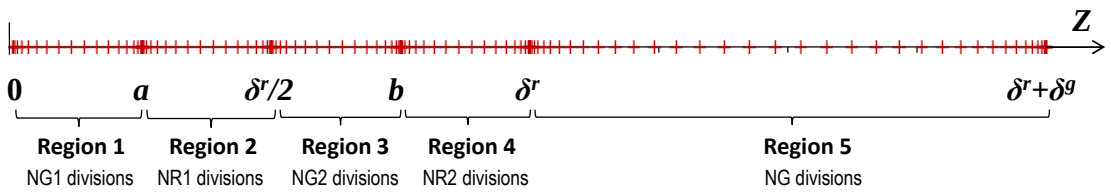

Figure 3.6. Discretization of the domain.

3.3.3 Construction of the interpolation basis

The basis of linear interpolators ω_k is defined as follows:

$$\omega_1(z)=\begin{cases}\dfrac{z_1-z}{z_1} & \text{for } 0<z<z_1\\ 0 & \text{in other points}\end{cases}$$

$$\omega_k(z)=\begin{cases}\dfrac{z-z_{i-1}}{z_i-z_{i-1}} & \text{for } z_{i-1}<z<z_i\\ \dfrac{z_{i+1}-z}{z_{i+1}-z_i} & \text{for } z_i<z<z_{i+1}\\ 0 & \text{in other points}\end{cases} \qquad (3.63)$$

$$\omega_{N+1}=\begin{cases}\dfrac{z-z_N}{z_{N+1}-z_N} & \text{for } z_N<z<z_{N+1}\\ 0 & \text{in other points}\end{cases}$$

is used. In $\omega_k(z)$, k can take values between 1 and N+1, whereas in $\omega_n(z)$, n can take values between 1 and N. A graphic representation of this basis can be seen in Figure 3.7.

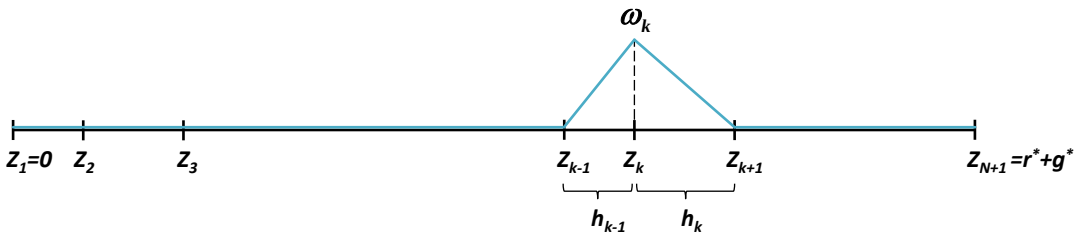

Figure 3.7. Graphical representation for the basis of interpolators.

3.3.4 Formulation of the system of equations

a. Terms of reaction

Equations (3.42) and (3.43) contain a series of terms not explicitly shown, that correspond to the different chemical reactions in which the species *i* is involved. Remembering that only reactions of the type $\mathrm{A+B} \rightleftarrows \mathrm{C}$ are considered in this work, the source terms depend on the role of the species *i* in each reaction, with the following possibilities:

If species *i* correspond to A or B in the reaction (i.e., if species *i* is a reactant), kinetic terms of the form $-k_{\mathrm{a}} c_i c_{\mathrm{B}} + k_{\mathrm{d}} c_{\mathrm{C}}$ or $-k_{\mathrm{a}} c_{\mathrm{A}} c_i + k_{\mathrm{d}} c_{\mathrm{C}}$ will appear in Equations (3.42) and (3.43). If species *i* corresponds to case C of the reaction (i.e., if species *i* is a product), a kinetic term of the form $+k_{\mathrm{a}} c_{\mathrm{A}} c_{\mathrm{B}} - k_{\mathrm{d}} c_i$ will appear.

Equations (3.42) and (3.43) include the sum of all the kinetic terms corresponding to each reaction where the species *i* participates. After changing the variables every term of the form $\pm k_{\mathrm{a}} c_{\mathrm{A}} c_{\mathrm{B}} \mp k_{\mathrm{d}} c_{\mathrm{C}}$ becomes $\pm\left(k_{\mathrm{a}} c_{\mathrm{A}}^{*} c_{\mathrm{B}}^{*}\right) q_{\mathrm{A}} q_{\mathrm{B}} \mp \left(k_{\mathrm{d}} c_{\mathrm{C}}^{*}\right) q_{\mathrm{C}}$.

b. Matrices of equations and the kinetic coefficients

Three matrices are defined: *mreac*, *kreac* and *meq*. The first contains the information of the species involved in every reaction, *kreac* contains the information related to the kinetic association and dissociation constants for all the reactions. Finally *meq* stores information about all reactions where each species is involved.

3.3.5 Solving the equations

The balance equation for each species written in a compact form is:

$$\frac{\partial c_i}{\partial t} = \begin{Bmatrix} D_i^R \\ D_i \end{Bmatrix} \frac{\partial^2 c_i}{\partial x^2} + \sum_j \left(\pm kreac_{(j,1)} c_{mreac(j,1)} c_{mreac(j,2)} \mp kreac_{(j,2)} c_{mreac(j,3)} \right) \tag{3.64}$$

In this equation, the summation scans all the reactions in which species *i* participates,

$c_{mreac(j,1)}$, $c_{mreac(j,2)}$ and $c_{mreac(j,3)}$ are the concentrations of the species involved in the reaction j. $kreac_{(j,1)}$ and $kreac_{(j,2)}$ are the kinetic constants of the reaction j. The signs of reaction terms depend on the role of the species *i* in each reaction. After making the change of variable indicated in Section 3.3.1., these equations become:

$$\frac{\partial q_i}{\partial t} = \begin{Bmatrix} d_i^{\mathrm{R}} \\ d_i \end{Bmatrix} \frac{\partial^2 q_i}{\partial z^2} + \sum_j \left(F_{ij} q_{mreac(j,1)} q_{mreac(j,2)} + G_{ij} q_{mreac(j,3)} \right) \tag{3.65}$$

Where: $F_{ij} = \pm \dfrac{c^*_{mreac(j,1)} c^*_{mreac(j,2)} k_{reac(j,1)}}{c^*_i}$ and $G_{ij} = \mp \dfrac{c^*_{mreac(j,3)} k_{reac(j,2)}}{c^*_i}$

The system will be solved iteratively in time and using the finite element method (FEM) for the spatial dependence. One advantage of the FEM method is that it allows the use of a spatial grid with unequal distribution of the spatial points. Thus, a higher density of points will be used in regions where it is expected a fast change of the physical properties in order to reduce the numerical error, reaching the maximum accuracy with the minimum computational requirements. This procedure also allows a reduction of the CPU time.

The application of the FEM method requires the variational or weak formulation of the problem. In this formulation, it must be satisfied that:

$$\int_0^{r^*+g^*} \left[\frac{\partial q_i}{\partial t} - \sum_j \left(F_{ij} q_{mreac(j,1)} q_{mreac(j,2)} + G_{ij} q_{mreac(j,3)} \right) - \begin{Bmatrix} d_i^R \\ d_i \end{Bmatrix} \frac{\partial^2 q_i}{\partial z^2} \right] \omega_n dz = 0 \tag{3.66}$$

for a complete basis of ω_n functions of the space of solutions. Integration of the previous equation leads to:

$$\begin{aligned} &\int_0^{r^*+g^*} \left[\frac{\partial q_i}{\partial t} - \sum_j \left(F_{ij} q_{mreac(j,1)} q_{mreac(j,2)} + G_{ij} q_{mreac(j,3)} \right) \right] \omega_n dz - \\ &\begin{Bmatrix} d_i^R \\ d_i \end{Bmatrix} \left(\frac{\partial q_i}{\partial z} \right) \omega_n \Bigg|_0^{r^*+g^*} + \begin{Bmatrix} d_i^R \\ d_i \end{Bmatrix} \int_0^{r^*+g^*} \left[\frac{\partial q_i}{\partial z} \right] \omega_n' dz = 0 \end{aligned} \tag{3.67}$$

The second term of the equation (3.67) is zero in $z = 0$ because the flux of all species at this point is zero. Likewise, the second term of the equation (3.67) is also zero in $z = r^* + g^*$ because the solution is already known at this point, then $\omega_n = 0$. Equation (3.67) becomes:

$$\int_0^{r^*+g^*} \left[\frac{\partial q_i}{\partial t} - \sum_j \left(F_{ij} q_{mreac(j,1)} q_{mreac(j,2)} + G_{ij} q_{mreac(j,3)} \right) \right] \omega_n dz + \begin{Bmatrix} d_i^R \\ d_i \end{Bmatrix} \int_0^{r^*+g^*} \left[\frac{\partial q_i}{\partial z} \right] \omega_n' dz = 0 \tag{3.68}$$

In order to discretize the spatial part of the problem, the following approaches are proposed:

$$\begin{aligned} &\frac{\partial q_i}{\partial t} - \sum_j \left(F_{ij} q_{mreac(j,1)} q_{mreac(j,2)} + G_{ij} q_{mreac(j,3)} \right) = \\ &\sum_{k=1}^{N} \left[\frac{\partial q_{ik}}{\partial t} - \sum_j \left(F_{ij} q_{mreac(j,1)k} q_{mreac(j,2)k} + G_{ij} q_{mreac(j,3)k} \right) \right] \omega_k \end{aligned} \tag{3.69}$$

and

$$\frac{\partial q_i}{\partial z} = \sum_{k=1}^{N} q_{ik} \omega_k' \tag{3.70}$$

where $\frac{\partial q_{ik}}{\partial t} - \sum_j \left(F_{ij} q_{mreac(j,1)k} q_{mreac(j,2)k} + G_{ij} q_{mreac(j,3)k} \right)$ and q_{ik} depends only on time, while ω_k depends only on the spatial positions. With these changes, Equation (3.69) becomes:

$$\begin{aligned} &\sum_{k=1}^{N} \left[\frac{\partial q_{ik}}{\partial t} - \sum_j \left(F_{ij} q_{mreac(j,1)k} q_{mreac(j,2)k} + G_{ij} q_{mreac(j,3)k} \right) \right] \int_0^{r^*+g^*} \left[\omega_n \omega_k \right] dz + \\ &\begin{Bmatrix} d_i^R \\ d_i \end{Bmatrix} \sum_{k=1}^{N} q_{ik} \int_0^{r^*+g^*} \left[\omega_n' \omega_k' \right] dz = 0 \end{aligned} \tag{3.71}$$

In Equation (3.71), the integration results depend only on the basis used. Let us define

$A_{nk} = \int_0^{r^*+g^*} [\omega_n \omega_k] dz$ and $B_{nk} = \int_0^{r^*+g^*} \left[\omega_n' \omega_k' \right] dz$ where n and k vary between 1 and N. With the definition of $\omega_n(z)$ given by Equation (3.63), $\mathbf{A}$ and $\mathbf{B}$ become tridiagonal matrices and take the values:

$$\mathbf{A} = \begin{bmatrix} \frac{h_1}{3} & -\frac{h_2}{6} & 0 & \cdots & 0 & 0 \\ -\frac{h_2}{6} & \frac{h_2+h_3}{3} & -\frac{h_3}{6} & \cdots & 0 & 0 \\ \vdots & \vdots & \vdots & & \vdots & \vdots \\ 0 & 0 & 0 & & -\frac{h_{NG-1}}{3} & \frac{h_{NG-1}+h_{NG}}{3} \end{bmatrix} \quad (3.72)$$

$$\mathbf{B} = \begin{bmatrix} \frac{1}{h_1} & -\frac{1}{h_1} & 0 & \cdots & 0 & 0 \\ -\frac{1}{h_1} & \frac{1}{h_1}+\frac{1}{h_2} & -\frac{1}{h_2} & \cdots & 0 & 0 \\ \vdots & \vdots & \vdots & & \vdots & \vdots \\ 0 & 0 & 0 & & -\frac{1}{h_{NG-1}} & \frac{1}{h_{NG-1}}+\frac{1}{h_{NG}} \end{bmatrix} \quad (3.73)$$

where $h_i = z_i - z_{i-1}$, as seen in Figure 3.7. Equations (3.71) for the species i can then be rewritten as:

$$\sum_{k=1}^{N} \left[\left(\frac{\partial q_{ik}}{\partial t} - \sum_j \left(F_{ij} q_{mreac(j,1)k} q_{mreac(j,2)k} + G_{ij} q_{mreac(j,3)k} \right) \right) A_{nk} + \begin{Bmatrix} d_i^R \\ d_i \end{Bmatrix} q_{ik} B_{nk} \right] = 0 \quad (3.74)$$

The system obtained is nonlinear and, depending on the spatial grid used, it can contain a large number of unknowns. Accordingly, the simultaneous solution of all the equations takes prohibitive times. Instead, the system will be solved iteratively, assuming known values for all the concentrations of all the species except one which is solved at this iteration step. This scheme is repeated iteratively until all the concentrations have been calculated up to consistency. In this way, the system is broken down into several smaller systems, each of them easier and faster to solve.[23] This allows the use of tridiagonal matrices, which represent a computational cost of order n.

Time is discretized into equal intervals of value Δt. Using the forward difference method, the unknowns are the values of $q_{ik}(t+\Delta t)$ and to estimate these values, we use the values of the concentrations at time t for all the species still not updated at this iteration time step while provisional estimations at time $t+\Delta t$ are used for those concentrations already updated in the iteration:

$$\sum_{k=1}^{N}\left[\left(\frac{q_{ik}(t+\Delta t)-q_{ik}(t)}{\Delta t}-\sum_{j}\left(F_{ij}q_{mreac(j,1)k}q_{mreac(j,2)k}+G_{ij}q_{mreac(j,3)k}\right)\right)A_{nk}\right]+ \sum_{k=1}^{N}\left[\begin{Bmatrix} d_i^R \\ d_i \end{Bmatrix} q_{ik}(t+\Delta t)B_{nk}\right]=0 \tag{3.75}$$

Iteration proceeds until all concentrations converge at all the spatial positions at the time considered. As a convergence criterion, it is required that the norm of the difference of concentrations between two consecutive iterations is less than a small preset value *ε:*

$$\sqrt{\sum_{i}^{\text{number of species}}\left[\frac{1}{N}\sum_{k=1}^{N}\left(q_{ik}(t+\Delta t)^{\text{mth iteration}}-q_{ik}(t+\Delta t)^{\text{(m-1)th iteration}}\right)^2\right]}\le\varepsilon \tag{3.76}$$

Once this convergence is reached, the next interval of time is considered.

3.4 The Program

3.4.1 General view of the program

The program works using the scheme showed in figure 3.8. Some details of the program are:

1. The program begins with the declaration of the variables used and the reading of the inputs.

2. Then the *mreac*, *meq* and *kreac* matrices are calculated, and with them the problem of equilibrium is solved.

3. The spatial grid and the matrices **A** and **B** are built with a careful selection of the spatial positions so that intervals with lengths shorter than the reaction layer were included in the mesh.

4. The concentrations of all species are stored in two vectors: qact and qsig. In the first vector species concentrations at each point of the grid are stored. The first N values of the vector are the concentrations of the first species at time *t*, the following N values are for species 2 and so on, so that the length of the vector will be N multiplied by the number of species. The values at the position N+1 are already known, so that the concentrations are not calculated at this point. The second vector works with the same way but it stores the concentrations at $t + \Delta t$. The two vectors are initialized in the same way according to the initial conditions discussed above.

5. At each time, the program calculates the concentration of each species at each grid point. Time intervals between the initial and final time are considered.

6. Using the concentrations, the program calculates the accumulation of metal at the resin, the back percentage of accumulation and the lability.

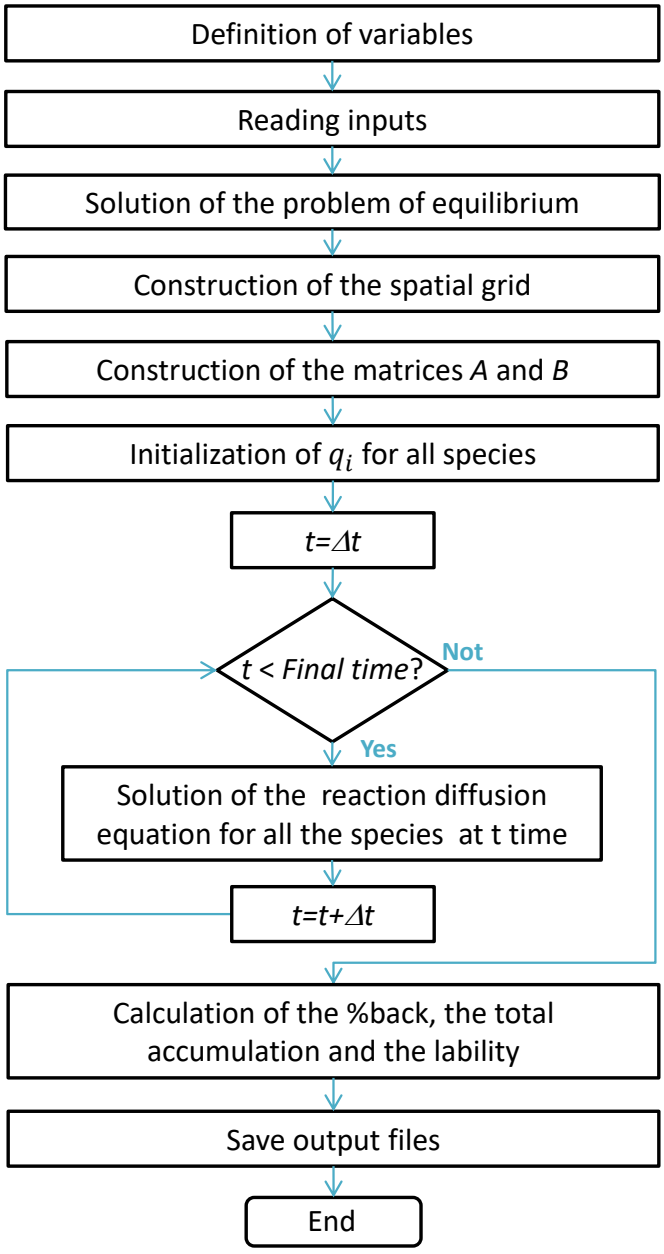

Figure 3.8. General scheme of program operation

3.4.2 Details on the resolution process

Solving the reaction-diffusion equations for a set of species requires the finding of the concentrations at each spatial point at a specific time. For species that diffuse, the concentration at each point depends on its value at $t - \Delta t$ and the concentration of the same species in neighbouring positions. For this case, the FEM is used. In species with diffusion coefficients equal to zero, the concentration at each point only depends on its

previous value and the concentrations of the other species, but not on the concentrations of the same species at neighbouring points. The solution is obtained directly by a simple rearrangement. A solution scheme for all species can be seen in figure 3.9.

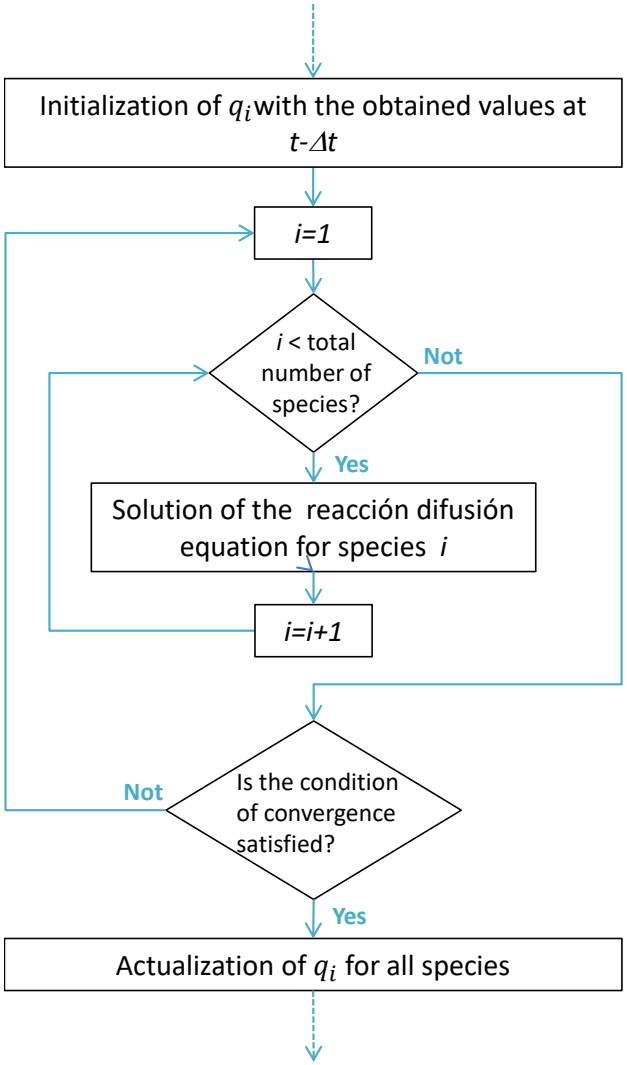

Figure 3.9. Scheme of the solution for all species

The model deals with chemical reactions of the form $A+B \rightleftarrows C$. If only the concentration of one of the species A or B is unknown, the problem becomes linear. For species with $d_i \neq 0$ the finite element method, discussed above, is used. The equation for each point can be represented as follows:

$$\Upsilon q_{ik}(t+\Delta t) = T \tag{3.77}$$

The contribution of each reaction j in Υ and T depends on the role of the species i:

If $i = mreac(j,1)$ the reaction diffusion equation (for position k) becomes:

$$\left[A_{nk} + \Delta t \begin{Bmatrix} d_i^R \\ d_i \end{Bmatrix} B_{nk} + \frac{\Delta t c^*_{mreac(j,1)} c^*_{mreac(j,2)} k_{reac(j,1)} A_{nk} q_{mreac(j,2)k}}{c_i^*} \right] q_{ik}(t+\Delta t) = A_{nk} q_{ik}(t) + \frac{\Delta t c^*_{mreac(j,3)} k_{reac(j,2)} A_{nk} q_{mreac(j,3)k}}{c_i^*} \quad (3.78)$$

If $i = mreac(j,2)$ the reaction diffusion equation becomes:

$$\left[A_{nk} + \Delta t \begin{Bmatrix} d_i^R \\ d_i \end{Bmatrix} B_{nk} + \frac{\Delta t c^*_{mreac(j,1)} c^*_{mreac(j,2)} k_{reac(j,1)} A_{nk} q_{mreac(j,1)k}}{c_i^*} \right] q_{ik}(t+\Delta t) = A_{nk} q_{ik}(t) + \frac{\Delta t c^*_{mreac(j,3)} k_{reac(j,2)} A_{nk} q_{mreac(j,3)k}}{c_i^*} \quad (3.79)$$

If $i = mreac(j,3)$ the reaction diffusion equation becomes:

$$\left[A_{nk} + \Delta t \begin{Bmatrix} d_i^R \\ d_i \end{Bmatrix} B_{nk} + \frac{\Delta t c^*_{mreac(j,3)} k_{reac(j,2)} A_{nk}}{c_i^*} \right] q_{ik}(t+\Delta t) = A_{nk} q_{ik}(t) + \frac{\Delta t c^*_{mreac(j,1)} c^*_{mreac(j,2)} k_{reac(j,1)} A_{nk} q_{mreac(j,1)k} q_{mreac(j,2)k}}{c_i^*} \quad (3.80)$$

The terms are initialized with the common terms for the three options:

$\Upsilon = A_{nk} + \begin{Bmatrix} d_i^R \\ d_i \end{Bmatrix} B_{nk}$ and $T = A_{nk} q_{ik}(t)$

After completing Υ and T the tridiagonal matrix is solved obtaining the values $q_i(t+\Delta t)$ for all grid points in a vector called RES; then, the difference between this vector and q_{sig} values corresponding to the species i is calculated, and this difference is used to analyse the convergence of the solution; RES is finally replaced in the proper positions for q_{sig}.

If $d_i = 0$ the equation for i at every position (Equation (3.75)) becomes:

$$q_{ik}(t+\Delta t)+\Delta t\sum_j\left(F_{ij}q_{mreac(j,1)}q_{mreac(j,2)}+G_{ij}q_{mreac(j,3)}\right)=q_{ik}(t) \tag{3.81}$$

As we have seen before, in this case it is not necessary to apply the FEM. It can be written as:

$$\alpha q_{ik}(t+\Delta t)=\beta \tag{3.82}$$

Since in this case there is no diffusion of the considered species, we only need to evaluate α and β to calculate $q_{ik}(t+\Delta t)$. The contribution of each reaction in these two terms depends on the role of the species *i* in it. If *i=mreac(j,*1*)* the equation becomes:

$$\left[1+\frac{\Delta t c^*_{mreac(j,1)}c^*_{mreac(j,2)}k_{reac(j,1)}q_{mreac(j,2)k}}{c^*_i}\right]q_{ik}(t+\Delta t)=$$
$$q_{ik}(t)+\frac{\Delta t c^*_{mreac(j,3)}k_{reac(j,2)}q_{mreac(j,3)k}}{c^*_i} \tag{3.83}$$

If *i=mreac(j,*2*)* the equation becomes:

$$\left[1+\frac{\Delta t c^*_{mreac(j,1)}c^*_{mreac(j,2)}k_{reac(j,1)}q_{mreac(j,1)k}}{c^*_i}\right]q_{ik}(t+\Delta t)=$$
$$q_{ik}(t)+\frac{\Delta t c^*_{mreac(j,3)}k_{reac(j,2)}q_{mreac(j,3)k}}{c^*_i} \tag{3.84}$$

If *i=mreac(j,*3*)* the equation becomes:

$$\left[1+\frac{\Delta t c^*_{mreac(j,3)}k_{reac(j,2)}}{c^*_i}\right]q_{ik}(t+\Delta t)=$$
$$q_{ik}(t)+\frac{\Delta t c^*_{mreac(j,1)}c^*_{mreac(j,2)}k_{reac(j,1)}q_{mreac(j,1)k}q_{mreac(j,2)k}}{c^*_i} \tag{3.85}$$

α and β will be initialized as $\alpha=1$ and $\beta=q_{ik}(t)$. After completing α and β, the value of $q_{ik}(t+\Delta t)$ is found and stored in q_{sig}. The procedure is repeated for all the grid

points. The convergence criterion is then checked; if the convergence criterion is satisfied these concentrations are taken as the solution at this time. When we have a converged solution the vector q_{sig} is recorded in the vector q_{act}, the time is increased and the procedure is repeated until reach the final time.

3.4.3 Metal accumulation

The total metal flux (as free metal and complexes) entering the resin layer is:

$$J = D_{\mathrm{M}} \left.\frac{\partial c_{\mathrm{M}}}{\partial x}\right|_{x=\delta^r} + \sum_{j=1}^{h} \left(D_{\mathrm{M}^j\mathrm{L}} \left.\frac{\partial c_{\mathrm{M}^j\mathrm{L}}}{\partial x}\right|_{x=\delta^r} \right) \tag{3.86}$$

In transient regime, part of this flow is bound to the resin and another part produces a change in free and complex metal concentrations. The metal flux bound to the resin layer will be:

$$J_{bound} = J - \int_0^{\delta^r} \left(\frac{\partial c_{\mathrm{M}}(x,t)}{\partial t} \right) dx - \sum_{j=1}^{h} \int_0^{\delta^r} \left(\frac{\partial c_{\mathrm{M}^j\mathrm{L}}(x,t)}{\partial t} \right) dx \tag{3.87}$$

Then, the total metal accumulated in the resin, in time t, will be:

$$\begin{aligned} n_{\mathrm{T}}(t) &= A \int_0^t J_{bound}\, dt \\ &= A \int_0^t \left[D_{\mathrm{M}} \left.\frac{\partial c_{\mathrm{M}}(x,t)}{\partial x}\right|_{x=\delta^r} - \int_0^{\delta^r} \frac{\partial c_{\mathrm{M}}(x,t)}{\partial t} dx + \sum_{j=1}^{h} \left(D_{\mathrm{M}^j\mathrm{L}} \left.\frac{\partial c_{\mathrm{M}^j\mathrm{L}}(x,t)}{\partial x}\right|_{x=\delta^r} - \int_0^{\delta^r} \frac{\partial c_{\mathrm{M}^j\mathrm{L}}(x,t)}{\partial t} dx \right) \right] dt \end{aligned} \tag{3.88}$$

In the program, terms with spatial derivatives are evaluated using concentrations at points $z_{\mathrm{NG1+NR1+NG2+NR2}}$ and $z_{\mathrm{NG1+NR1+NG2+NR2+1}}$:

$$\begin{aligned} D_i \left.\frac{\partial c_i}{\partial x}\right|_{x=\delta^r} &= D_{\max} d_i \left.\frac{\partial c_{\mathrm{i}}^* q_i}{\partial \sqrt{D_{\max}}\, z}\right|_{z=r^*} = d_i \sqrt{D_{\max}}\, c_{\mathrm{i}}^* \left.\frac{\partial q_i}{\partial z}\right|_{z=r^*} \\ &= d_i \sqrt{D_{\max}}\, c_{\mathrm{i}}^* \left(\frac{q_{i\ \mathrm{NG1+NR1+NG2+NR2+1}} - q_{i\ \mathrm{NG1+NR1+NG2+NR2}}}{z_{\mathrm{NG1+NR1+NG2+NR2+1}} - z_{\mathrm{NG1+NR1+NG2+NR2}}} \right) \end{aligned} \tag{3.89}$$

Terms with temporal derivatives in Eqn. (3.91) are calculated as:

$$\int_0^{\delta^r} \frac{\partial c_i(x,t)}{\partial t} dx = \int_0^{r^*} \frac{\partial c_i^* q_i}{\partial t} \sqrt{D_{\max}}\, dz = \sqrt{D_{\max}}\, c_i^* \int_0^{r^*} \frac{q_{ik}(t+1) - q_{ik}(t)}{\Delta t} dz$$
$$= \sqrt{D_{\max}}\, c_i^* \sum_{k=1}^{N} \left[\left(\frac{q_{ik}(t+1) - q_{ik}(t)}{\Delta t} + \frac{q_{ik+1}(t+1) - q_{ik+1}(t)}{\Delta t} \right) \left(\frac{z_{k+1} - z_k}{2} \right) \right] \quad (3.90)$$

3.4.4 Lability degree

According to references [24,25], the lability degree of a complex M^jL can be written as:

$$\xi_j = 1 - \frac{c^r_{M^jL}}{c^*_{M^jL}} \quad (3.91)$$

where, $c^r_{M^jL}$ stands for the concentration of M^jL in the resin layer/diffusive gel interface. In the program, $c^r_{M^jL}$ corresponds to the concentration of the complex at the position $z_{NG1+NR1+NG2+NR2}$. The lability degree for species *i* is calculated as:

$$\xi_i = 1 - \frac{c_{i\ NG1+NR1+NG2+NR2}}{c_i^*} = 1 - q_{i\ NG1+NR1+NG2+NR2} \quad (3.92)$$

3.5 Reference List

1. Atkinson, K. E. *An Introduction to Numerical Analysis;* Second ed.; Wiley: New York, **1989**.

2. Deuflhard, P. H. A. *Numerical Analysis in Modern Scientific Computing.;* Second ed.; Springer: Berlin, **2003**.

3. Dahlquist, G.; Björck, A. *Numerical Methods in Scientific Computing;* Society for Industrial and Applied Mathematics: New York, **2008**; Vol. 1.

4. Feldberg, S. W.; Auerbach, C. *Model for current reversal chronopotentiometry with second-order kinetic complications*. *Anal. Chem.* **1964,** *36*, 505-509.

5. Britz, D. *Digital Simulation in Electrochemistry (Lecture Notes in Physics);* Springer: Berlin, **2005**.

6. Newman, J.; Thomas-Alyea, K. E. *Electrochemical Systems;* Third ed.; John Wiley & Sons: Hoboken, NJ, **2004**.

7. Roos, H.; Tobiska, L.; Stynes, M. *Robust Numerical Methods for Singularly Perturbed Differential Equations;* second ed.; Springer-Verlag Berlin and Heidelberg GmbH & Co. KG: Berlin, **2008**.

8. Bieniasz, L. K. Use of Dynamically Adaptive-Grid Techniques for the Solution of Electrochemical Kinetic-Equations .1. Introductory Exploration of the Finite-Difference Adaptive Moving Grid Solution of the One- Dimensional Fast Homogeneous Reaction-Diffusion Problem with a Reaction Layer. *J. Electroanal. Chem.* **1993,** *360* (1-2), 119-138.

9. Bieniasz, L. K. The Von Neumann stability of Finite-difference algorithms for the electrochemical kinetic simulation of diffusion coupled with homogeneous reactions. *J. Electroanal. Chem.* **1993,** *345*, 13-25.

10. Bieniasz, L. K. Use of dynamically adaptive-grid techniques for the solution of electrochemical kinetic-equations .2. An improved finite-difference adaptive moving grid technique for one-dimensional fast homogeneous reaction-diffusion problems with reaction layers at the electrodes. *J. Electroanal. Chem.* **1994,** *374*, 1-22.

11. Bieniasz, L. K. Use of dynamically adaptive-grid techniques for the solution of electrochemical kinetic-equations .3. An adaptive moving grid adaptive time-step strategy for problems with discontinuous boundary- conditions at the electrodes. *J. Electroanal. Chem.* **1994,** *374*, 23-35.

12. Amatore, C.; Klymenko, O.; Svir, I. A new strategy for simulation of electrochemical mechanisms involving acute reaction fronts in solution: Application to model mechanisms. *Electrochem. Commun.* **2010,** *12* (9), 1165-1169.

13. Mongin, S.; Uribe, R.; Puy, J.; Cecilia, J.; Galceran, J.; Zhang, H.; Davison, W. Key Role of the Resin Layer Thickness in the Lability of Complexes Measured by DGT. *Environ. Sci. Technol.* **2011,** *45* (11), 4869-4875.

14. Fritzon, P. *Introduction to Modeling and Simulation of Technical and Physical Systems with Modelica; John Wiley & Sons, Inc., Publication*: New Jersey, **2011**.

15. Rao, S. *The Finite Element Method in Engineering ;* 4th ed.; Butterworth-Heinemann: Saint Louis, Misouri, **2004**.

16. Hughes, T. J. R. *The Finite Element Method: Linear Static and Dynamic Finite Element Analysis; Dover Publications*: Mineola, NY, **2000**.

17. Johnson, C. *Numerical Solution of Partial Differential Equations by the Finite Element Method;* Dover Publications Inc.: New York, **2009**.

18. Stoer, J.; Bulirsch, R. *Introduction to Numerical Analysis;* Springer-Verlag: New York, **2002**.

19. Ames, W. F. *Numerical Methods for Partial Differential Equations;* Academic Press: New York, **1992**.

20. Zarowski, C. *An introduction to numerical analysis for electrical and computer engineers;* John Wiley & sons, Inc.: New Jersey, **2004**.

21. Lehto, N. J.; Davison, W.; Zhang, H.; Tych, W. An evaluation of DGT performance using a dynamic numerical model. *Environ. Sci. Technol.* **2006,** *40* (20), 6368-6376.

22. Tusseau-Vuillemin, M. H.; Gilbin, R.; Taillefert, M. A dynamic numerical model to characterize labile metal complexes collected with diffusion gradient in thin films devices. *Environ. Sci. Technol.* **2003,** *37* (8), 1645-1652.

23. Uribe, R. *Availability of metal cations in aquatic systems from DGT measurements*. PhD thesis. Universitat de Lleida, Oct **2012**.

24. Salvador, J.; Garcés, J. L.; Companys, E.; Cecilia, J.; Galceran, J.; Puy, J.; Town, R. M. Ligand mixture effects in metal complex lability. *J. Phys. Chem. A* **2007,** *111* (20), 4304-4311.

25. Uribe, R.; Puy, J.; Cecilia, J.; Galceran, J. Kinetic Mixture Effects in Diffusion Gradients in Thin Films (DGT). *Phys. Chem. Chem. Phys.* **2013,** *15* (27), 11349-11355.

CHAPTER 4

INFLUENCE OF SETTLING OF THE RESIN BEADS ON DGT MEASUREMENTS

Part of the material of this chapter has been published in:

Jimenez-Piedrahita, M.; Altier, A.; Cecilia, J.; Rey-Castro, C.; Galceran, J.; Puy, J. Influence of the settling of the resin beads on diffusion gradients in thin films measurements. *Anal. Chim. Acta* **2015**, 885, 148-155.

4.1 Introduction

DGT devices were developed for the in situ measurement of trace metals in waters.[1,2] They have two main parts: the resin gel layer (which binds the metal ions) and the diffusive gel (that controls the transport of species). Recently, different publications have highlighted the important role played by the resin disc thickness in determining the metal accumulation in systems with partially labile complexes.[3-8] The argument starts by assuming a fast and strong binding of the metal to the resin sites. Accordingly, the complexation equilibrium shifts towards dissociation, so that complexes release free metal in the gel domain which binds to the resin. In this way, the thickness of the reaction layer (the layer where there is net dissociation, as explained in Chapter 2) extends into both the gel and resin domains. Since the thickness of the resin disc is usually larger than the reaction layer in the gel domain, almost all metal accumulated originates from dissociation of the complex in the resin domain. Dissociation in the resin domain has allowed to justify the labile behaviour of the complex of Cd with nitrilotriacetic acid (NTA) [3] while, without penetration into the resin, it was expected to be only partially labile.

Interesting additional information on the resin role can be gained when DGT devices with two resin discs are used. Thus, the essentially perfect-sink behaviour of the resin was tested in a work with only metals (i.e., in absence of ligands) and DGT devices with

two or three resin discs.[9] This work demonstrated that a kinetic association constant between the metal and the resin sites could, in principle, be obtained from the distribution of the metal bound to two resin discs, whenever this distribution lies within a meaningful sensitive window of kinetic constants. In the presence of complexes, both, the metal accumulation and the distribution of the metal in the stack of resin discs have been used to fit the parameters of the system Ni-NTA.[7,10] Notice that the availability of complementary information to that of the total accumulation in DGT experiments is of high interest, since it helps in fitting the parameters or even allows the direct determination of some of them.

All these works, and the derived analytical expressions, assumed a homogeneous distribution of the resin sites in the resin domain. This assumption can be considered as a first approximation, since the resin beads partially settle during casting of the gel.[7,11] In this chapter, we check the influence of the inhomogeneous distribution of the resin sites in the resin disc on the total accumulation, on the distribution of metal accumulation in a stack of resin discs and on the accuracy of the fitted parameters obtained assuming homogeneous binding site distribution. We compare results for devices with binding beads appearing only in half of the resin disc (Figure 4.1b), denoted as R/2, with devices with homogeneously distributed resin disc (Figure 4.1a), denoted as R. Section 4.2 outlines the mathematical formulation and solution of this problem. Section 4.3 compares the performance of DGT devices containing one R or R/2 resin disc, and Section 4.4 compares the behaviour of DGT devices with a stack of two homogeneous or of two discs containing half-dispersed beads.

4.2 Theoretical model

Let us consider a system containing in solution a metal M and a ligand L which react as

$$\mathrm{M+L} \underset{k_\mathrm{d}}{\overset{k_\mathrm{a}}{\rightleftharpoons}} \mathrm{ML} \tag{4.1}$$

where k_a and k_d are the association and dissociation rate constants, $K = \dfrac{c^*_\mathrm{ML}}{c^*_\mathrm{M} c^*_\mathrm{L}}$ is the

corresponding stability constant, $K' = \frac{c^*_{ML}}{c^*_M}$ is the effective stability constant, and c_i^* is the concentration of species *i* in the bulk solution. When a DGT device is introduced in this solution, all these species diffuse and react through the diffusive gel ($\delta^r < x \leq \delta^r + \delta^g$) until reaching the resin domain ($0 < x \leq \delta^r$) where, due to the presence of the binding beads, another reaction takes place:

$$M + R \underset{k_{d,R}}{\overset{k_{a,R}}{\rightleftharpoons}} MR \tag{4.2}$$

In this chapter we are going to work with DGT devices with two types of resin discs: one with resin beads homogeneously distributed throughout the resin volume (named R resins and showed in Figure 4.1a) and another with beads homogeneously distributed in only half of the resin volume (denoted as R/2 resins and showed in Figure 4.1b).

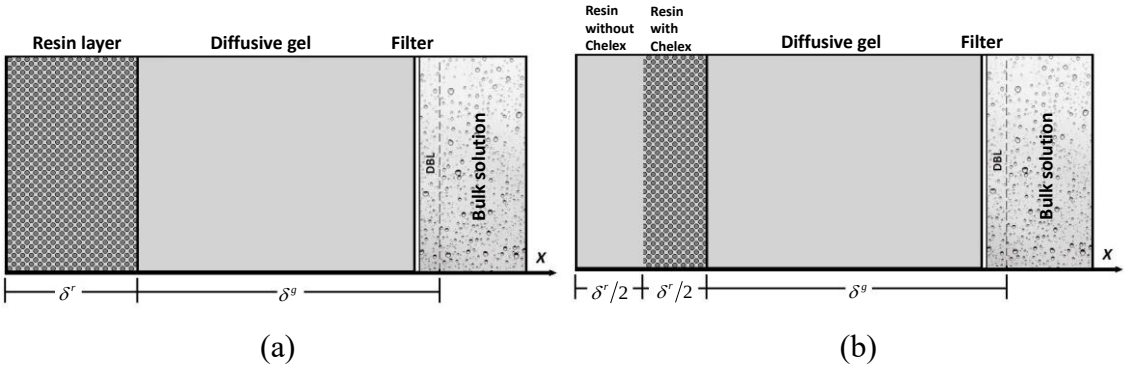

Figure 4.1. Schematic representation of a DGT device with a) one R resin disc and b) one R/2 resin disc.

The mathematical formulation of all these processes is given elsewhere.[3,4,6,12] A simulation code allowing the numerical solution of these equations has been explained in Chapter 3. It has been written using the Finite Element Method which allows the use of a spatial grid with unequal distribution of spatial positions, reducing CPU time and hardware requirements in comparison to algorithms based on Finite Differences. The numerical solution for the concentration profiles can be used to calculate the flux of metal bound to the resin, *J*, as well as the metal accumulation, n_M, both in R and R/2 devices. Details are given in the section 4.6.3.

In practice, the most interesting cases in DGT are those where the association rate constant $k_{a,R}$ between the metal and the resin sites and the stability constant of the metal-resin complex are so high that the resin can be considered as a perfect-sink for the metal. Accordingly, we will consider as a good approximation the existence of zero metal concentration in the resin domain, whenever the accumulation is far from saturation, while L and ML undergo diffusion and reaction along both gels. The restriction to perfect-sink, together with the assumption of ligand excess conditions leads to an approximate analytical solution for the concentration profiles of metal and complex.

4.2.1 Analytical expressions for concentration profiles of metal and single ligand complexes in homogeneous (R) DGT devices

Analytical expressions for the free metal and the complex in DGT devices with homogeneous distribution of binding agent are deduced in references [4,5]. In the resin disc, $0 < x \le \delta^r$ (see Figure 4.1a), the concentration profiles of metal (c_M) and complex (c_{ML}) can be written as:

$$c_M(x) = 0 \tag{4.3}$$

$$c_{ML}(x) = \frac{c_{ML}^{*}\left(1+\varepsilon K'\right)}{\varepsilon K' + \frac{\delta^g}{m}\cot\left(\frac{\delta^g}{m}\right) + \frac{\delta^g\left(1+\varepsilon K'\right)}{\lambda_{ML}}\tanh\left(\frac{\delta^r}{\lambda_{ML}}\right)} \cdot \frac{\cosh\left(\frac{x}{\lambda_{ML}}\right)}{\cosh\left(\frac{\delta^r}{\lambda_{ML}}\right)} \tag{4.4}$$

And in the diffusive gel (of thickness δ^g which also includes the filter and the DBL), $\delta^r < x \le \delta^r + \delta^g$:

$$c_M(x) = \frac{\varepsilon c_{ML}^{r}}{1+\varepsilon K'} + \left(\frac{c_M^{*} + \varepsilon c_{ML}^{*} - \varepsilon c_{ML}^{r}}{\delta^g\left(1+\varepsilon K'\right)}\right)\left(x-\delta^r\right) - \frac{\varepsilon c_{ML}^{r}\sinh\left(\frac{\delta^r+\delta^g-x}{m}\right)}{\left(1+\varepsilon K'\right)\sinh\left(\frac{\delta^g}{m}\right)} \tag{4.5}$$

$$c_{ML}(x) = \frac{\varepsilon K' c_{ML}^{r}}{1+\varepsilon K'} + \left(\frac{c_M^{*} + \varepsilon c_{ML}^{*} - \varepsilon c_{ML}^{r}}{\delta^g\left(1+\varepsilon K'\right)}\right)K'\left(x-\delta^r\right) + \frac{c_{ML}^{r}\sinh\left(\frac{\delta^r+\delta^g-x}{m}\right)}{\left(1+\varepsilon K'\right)\sinh\left(\frac{\delta^g}{m}\right)} \tag{4.6}$$

where the value for the concentration of the complex at $x = \delta^r$ can be computed as:

$$c_{\mathrm{ML}}^r = \frac{c_{\mathrm{ML}}^* \left(1+\varepsilon K'\right)}{\varepsilon K' + \frac{\delta^g}{m}\coth\left(\frac{\delta^g}{m}\right) + \frac{\delta^g \left(1+\varepsilon K'\right)}{m\lambda_{\mathrm{ML}}}\tanh\left(\frac{\delta^r}{\lambda_{\mathrm{ML}}}\right)} \tag{4.7}$$

ε is the normalized diffusion coefficient:

$$\varepsilon = \frac{D_{\mathrm{ML}}}{D_{\mathrm{M}}} \tag{4.8}$$

m is a distance related to the thickness of the layer in the gel where the metal and the complex are not in equilibrium:

$$m = \sqrt{\frac{D_{\mathrm{ML}}}{k_{\mathrm{d}}\left(1+\varepsilon K'\right)}} \tag{4.9}$$

and the penetration parameter λ_{ML}, can be calculated as:

$$\lambda_{\mathrm{ML}} = \sqrt{\frac{D_{\mathrm{ML}}}{k_{\mathrm{d}}}} \tag{4.10}$$

4.2.2 Analytical expressions for concentration profiles of metal and single ligand complexes in (R/2) DGT devices

In this section, DGT devices with an inhomogeneous distribution of the binding beads on the resin disc will be studied. Due to the settle of the binding beads during casting, it will be assumed that they are present only on half of the resin thickness. This inhomogeneous resin disc will be labelled as R/2 from now on. In this case there are two regions in the resin: the first one without binding agent ($0 < x \le \delta^r/2$) and another with this agent ($\delta^r/2 < x \le \delta^r$). Notice that all the processes in the DGT device take place essentially in one relevant spatial dimension, quoted here as *x* axis, since there is planar symmetry. If diffusion coefficients of the species are not far different in the DBL, the filter and the diffusive gel, these three layers can be treated as a region of the device ($\delta^r < x \le \delta^r + \delta^g$) so that Figure 4.1b shows the scheme DGT device used in simulation.

Two main assumptions are made to deduce an analytical expression for the concentrations of the species:

1. There is excess of ligand (L), so that the ligand concentration profile (c_L) can be assumed constant along all the DGT device;
2. The layer of the resin containing the binding agent acts as a perfect-sink for free metal and other species do not bind to it.

The system is solved for three regions:

Region I ($0 < x \leq \delta^r/2$)

It is the part of the resin without binding beads. Since there is excess of ligand we define $k'_a = k_a c_L^*$, in order to have linear equations. The transport equations at steady-state are:

For the free metal:

$$0 = D_M \frac{d^2 c_M}{dx^2} - k'_a c_M + k_d c_{ML} \tag{4.11}$$

For the complex:

$$0 = D_{ML} \frac{d^2 c_{ML}}{dx^2} + k'_a c_M - k_d c_{ML} \tag{4.12}$$

The boundary conditions in this region are:

$$\left.\frac{dc_M}{dx}\right|_{x=0} = 0 \qquad \left.\frac{dc_{ML}}{dx}\right|_{x=0} = 0$$
$$c_M\left(\tfrac{\delta^r}{2}\right) = 0 \qquad c_{ML}\left(\tfrac{\delta^{r\,-}}{2}\right) = c_{ML}\left(\tfrac{\delta^{r\,+}}{2}\right) \tag{4.13}$$

The first two conditions are due to no flux of any species at $x = 0$. Due to the perfect-sink behaviour of the layer where there is binding agent, at $x = \delta^r / 2$ the metal concentration falls to zero. The last boundary condition is the continuity of $c_{ML}(x)$ at $x = \delta^r / 2$.

Combining Equations (4.11) and (4.12) an uncoupled system of equations is obtained:

$$0 = \frac{d^2}{dx^2}\left(D_M c_M + D_{ML} c_{ML}\right) \tag{4.14}$$

$$0 = \frac{d^2}{dx^2}\left(c_{\mathrm{ML}} - K' c_{\mathrm{M}}\right) - \left(\frac{k_{\mathrm{d}}}{D_{\mathrm{ML}}} + \frac{k_{\mathrm{a}} c_{\mathrm{L}}^{*}}{D_{\mathrm{M}}}\right)\left(c_{\mathrm{ML}} - K' c_{\mathrm{M}}\right) \tag{4.15}$$

Integration of Equation (4.14) leads to:

$$D_{\mathrm{M}} c_{\mathrm{M}}(x) + D_{\mathrm{ML}} c_{\mathrm{ML}}(x) = Ax + B \tag{4.16}$$

and applying the boundary conditions at $x = \delta^r / 2$:

$$D_{\mathrm{ML}} c_{\mathrm{ML}}^{r/2} = A\left(\frac{\delta^r}{2}\right) + B \tag{4.17}$$

Where $c_{\mathrm{ML}}^{r/2}$ is the complex concentration at $x = \delta^r / 2$.

Using the boundary conditions at $x = 0$:

$$\frac{d}{dx}\left(D_{\mathrm{M}} c_{\mathrm{M}}\right)\Big|_{x=0} + \frac{d}{dx}\left(D_{\mathrm{ML}} c_{\mathrm{ML}}\right)\Big|_{x=0} = A = 0 \tag{4.18}$$

Being A=0, a solution for B follows from equation (4.17). Equation (4.16) becomes:

$$D_{\mathrm{M}} c_{\mathrm{M}}(x) + D_{\mathrm{ML}} c_{\mathrm{ML}}(x) = D_{\mathrm{ML}} c_{\mathrm{ML}}^{r/2} \tag{4.19}$$

The solution of the Equation (4.15) is:

$$c_{\mathrm{ML}}(x) - K' c_{\mathrm{M}}(x) = A\sinh\left(\frac{\delta^r + \delta^g - x}{m}\right) + B\cosh\left(\frac{\delta^r + \delta^g - x}{m}\right) \tag{4.20}$$

With the boundary conditions at $x = \delta^r / 2$:

$$c_{\mathrm{ML}}^{r/2} = A\sinh\left(\frac{\delta^g + \delta^r/2}{m}\right) + B\cosh\left(\frac{\delta^g + \delta^r/2}{m}\right) \tag{4.21}$$

and at $x = 0$:

$$\frac{d}{dx}\left(c_{\mathrm{ML}}\right)\Big|_{x=0} - \frac{d}{dx}\left(K' c_{\mathrm{M}}\right)\Big|_{x=0} = A\sinh\left(\frac{\delta^r + \delta^g}{m}\right) + B\cosh\left(\frac{\delta^r + \delta^g}{m}\right) = 0 \tag{4.22}$$

we obtain:

$$A = \frac{-\tanh\left(\frac{\delta^r + \delta^g}{m}\right) c_{\mathrm{ML}}^{r/2}}{\cosh\left(\frac{\delta^g + \delta^r/2}{m}\right) - \sinh\left(\frac{\delta^g + \delta^r/2}{m}\right)\tanh\left(\frac{\delta^r + \delta^g}{m}\right)} \tag{4.23}$$

$$B = \frac{c_{\mathrm{ML}}^{r/2}}{\cosh\left(\frac{\delta^g + \delta^r/2}{m}\right) - \sinh\left(\frac{\delta^g + \delta^r/2}{m}\right)\tanh\left(\frac{\delta^r + \delta^g}{m}\right)} \tag{4.24}$$

and replacing A and B in Equation (4.20) we obtain:

$$c_{\mathrm{ML}}(x) - K' c_{\mathrm{M}}(x) = \frac{c_{\mathrm{ML}}^{r/2}\cosh\left(\frac{\delta^r + \delta^g - x}{m}\right) - c_{\mathrm{ML}}^{r/2}\tanh\left(\frac{\delta^r + \delta^g}{m}\right)\sinh\left(\frac{\delta^r + \delta^g - x}{m}\right)}{\cosh\left(\frac{\delta^g + \delta^r/2}{m}\right) - \sinh\left(\frac{\delta^g + \delta^r/2}{m}\right)\tanh\left(\frac{\delta^r + \delta^g}{m}\right)} \tag{4.25}$$

Using equations (4.19) and (4.25) we have:

$$c_{\mathrm{M}}(x) = \frac{\varepsilon}{1 + \varepsilon K'}\left(1 - \frac{\cosh\left(\frac{x}{m}\right)}{\cosh\left(\frac{\delta^r}{2m}\right)}\right) c_{\mathrm{ML}}^{r/2} \tag{4.26}$$

$$c_{\mathrm{ML}}(x) = \frac{1}{1 + \varepsilon K'}\left(\varepsilon K' + \frac{\cosh\left(\frac{x}{m}\right)}{\cosh\left(\frac{\delta^r}{2m}\right)}\right) c_{\mathrm{ML}}^{r/2} \tag{4.27}$$

Where ε by Eqn. (4.8) and m is given by Eqn. (4.9). $c_{\mathrm{ML}}^{r/2}$ and c_{ML}^{r} are the values of the complex concentration at $x = \delta^r/2$ and $x = \delta^r$ respectively. Analytical expressions for these concentrations are reported below.

Region II ($\delta^r/2 < x \le \delta^r$)

In this region, all the free metal is bound to the resin, so for the free metal concentration is zero:

$$c_{\mathrm{M}}(x) = 0 \tag{4.28}$$

The transport equation for the complex is:

$$0 = D_{\mathrm{ML}} \frac{d^2 c_{\mathrm{ML}}}{dx^2} - k_{\mathrm{d}} c_{\mathrm{ML}} \tag{4.29}$$

At $x = \delta^r / 2$ and $x = \delta^r$ the boundary conditions for the complex concentration are:

$$\begin{aligned} c_{\mathrm{ML}}(\tfrac{\delta^{r}}{2}^{-}) &= c_{\mathrm{ML}}(\tfrac{\delta^{r}}{2}^{+}) \qquad \left.\frac{dc_{\mathrm{ML}}}{dx}\right|_{x=\frac{\delta^{r}}{2}^{-}} = \left.\frac{dc_{\mathrm{ML}}}{dx}\right|_{x=\frac{\delta^{r}}{2}^{+}} \\ c_{\mathrm{ML}}(\delta^{r-}) &= c_{\mathrm{ML}}(\delta^{r+}) \qquad \left.\frac{dc_{\mathrm{ML}}}{dx}\right|_{x=\delta^{r-}} = \left.\frac{dc_{\mathrm{ML}}}{dx}\right|_{x=\delta^{r+}} \end{aligned} \tag{4.30}$$

These boundary conditions follow from the continuity of the function $c_{\mathrm{ML}}(x)$ and its derivative at $x = \delta^r / 2$ and $x = \delta^r$ (we are assuming that the diffusion coefficient of ML do not change at $x = \delta^r / 2$).

A general solution of Equation (4.29) is:

$$c_{\mathrm{ML}}(x) = Ae^{x/\lambda_{\mathrm{ML}}} + Be^{-x/\lambda_{\mathrm{ML}}} \tag{4.31}$$

Applying the continuity of the function at $x = \delta^r / 2$:

$$c_{\mathrm{ML}}^{r/2} = Ae^{\delta^r/2\lambda_{\mathrm{ML}}} + Be^{-\delta^r/2\lambda_{\mathrm{ML}}} \tag{4.32}$$

and using the continuity of the derivative at the same point:

$$\frac{c_{\mathrm{ML}}^{r/2} \tanh\left(\dfrac{\delta^r}{2m}\right)}{m\left(1+\varepsilon K'\right)} = \frac{Ae^{\delta^r/2\lambda_{\mathrm{ML}}} - Be^{-\delta^r/2\lambda_{\mathrm{ML}}}}{\lambda_{\mathrm{ML}}} \tag{4.33}$$

Finally, using the condition of continuity of the function at $x = \delta^r$:

$$c_{\mathrm{ML}}^{r} = Ae^{\delta^r/\lambda_{\mathrm{ML}}} + Be^{-\delta^r/\lambda_{\mathrm{ML}}} \tag{4.34}$$

Equations (4.32), (4.33) and (4.34) determine A, B and $c_{\mathrm{ML}}^{r/2}$ which become:

$$A = \frac{\left(m + m\varepsilon K' + \lambda_{\mathrm{ML}} \tanh\left(\frac{\delta^r}{2m}\right)\right) c^r_{\mathrm{ML}}}{m\left(e^{\delta^r/\lambda_{\mathrm{ML}}} + 1\right)\left(1 + \varepsilon K'\right) + \left(e^{\delta^r/\lambda_{\mathrm{ML}}} - 1\right)\lambda_{\mathrm{ML}} \tanh\left(\frac{\delta^r}{2m}\right)} \tag{4.35}$$

$$B = \frac{\left(m + m\varepsilon K' + \lambda_{\mathrm{ML}} \tanh\left(\frac{\delta^r}{2m}\right)\right) e^{\delta^r/\lambda_{\mathrm{ML}}} c^r_{\mathrm{ML}}}{m\left(e^{\delta^r/\lambda_{\mathrm{ML}}} + 1\right)\left(1 + \varepsilon K'\right) + \left(e^{\delta^r/\lambda_{\mathrm{ML}}} - 1\right)\lambda_{\mathrm{ML}} \tanh\left(\frac{\delta^r}{2m}\right)} \tag{4.36}$$

$$c^{r/2}_{\mathrm{ML}} = \frac{2m\left(1 + \varepsilon K'\right) e^{\delta^r/2\lambda_{\mathrm{ML}}} c^r_{\mathrm{ML}}}{m\left(e^{\delta^r/\lambda_{\mathrm{ML}}} + 1\right)\left(1 + \varepsilon K'\right) + \left(e^{\delta^r/\lambda_{\mathrm{ML}}} - 1\right)\lambda_{\mathrm{ML}} \tanh\left(\frac{\delta^r}{2m}\right)} \tag{4.37}$$

The complex concentration, Equation (4.31), becomes:

$$c_{\mathrm{ML}}(x) = \left(\frac{\left(m + m\varepsilon K' + \lambda_{\mathrm{ML}} \tanh\left(\frac{\delta^r}{2m}\right)\right) e^{x/\lambda_{\mathrm{ML}}} + e^{\delta^r/\lambda_{\mathrm{ML}}} \left(m + m\varepsilon K' - \lambda_{\mathrm{ML}} \tanh\left(\frac{\delta^r}{2m}\right)\right) e^{-x/\lambda_{\mathrm{ML}}}}{m\left(e^{\delta^r/\lambda_{\mathrm{ML}}} + 1\right)\left(1 + \varepsilon K'\right) + \left(e^{\delta^r/\lambda_{\mathrm{ML}}} - 1\right)\lambda_{\mathrm{ML}} \tanh\left(\frac{\delta^r}{2m}\right)} \right) c^r_{\mathrm{ML}} \tag{4.38}$$

Region III ($\delta^r < x \leq \delta^r + \delta^g$)

for the free metal, the transport equations can be written as:

$$0 = D_{\mathrm{M}} \frac{d^2 c_{\mathrm{M}}}{dx^2} - k'_{\mathrm{a}} c_{\mathrm{M}} + k_{\mathrm{d}} c_{\mathrm{ML}} \tag{4.39}$$

and for the complex:

$$0 = D_{\mathrm{ML}} \frac{d^2 c_{\mathrm{ML}}}{dx^2} + k'_{\mathrm{a}} c_{\mathrm{M}} - k_{\mathrm{d}} c_{\mathrm{ML}} \tag{4.40}$$

The boundary conditions in this case are:

$$c_{\mathrm{M}}(\delta^r) = 0 \qquad c_{\mathrm{ML}}(\delta^{r-}) = c_{\mathrm{ML}}(\delta^{r+}) \qquad \left.\frac{dc_{\mathrm{ML}}}{dx}\right|_{x=\delta^{r-}} = \left.\frac{dc_{\mathrm{ML}}}{dx}\right|_{x=\delta^{r+}}$$
$$c_{\mathrm{M}}(\delta^r + \delta^g) = c^*_{\mathrm{M}} \qquad c_{\mathrm{ML}}(\delta^r + \delta^g) = c^*_{\mathrm{ML}} \tag{4.41}$$

The first three conditions were already discussed in the previous region. The last two conditions follow from considering bulk concentrations at $x = \delta^r + \delta^g$.

As in the region I, Equations (4.39) and (4.40) can be combined to obtain a new set of uncoupled equations:

$$0 = \frac{d^2}{dx^2}\left(D_{\mathrm{M}} c_{\mathrm{M}} + D_{\mathrm{ML}} c_{\mathrm{ML}}\right) \tag{4.42}$$

$$0 = \frac{d^2}{dx^2}\left(c_{\mathrm{ML}} - K' c_{\mathrm{M}}\right) - \left(\frac{k_{\mathrm{d}}}{D_{\mathrm{ML}}} + \frac{k_{\mathrm{a}} c_{\mathrm{L}}^*}{D_{\mathrm{M}}}\right)\left(c_{\mathrm{ML}} - K' c_{\mathrm{M}}\right) \tag{4.43}$$

Integration of Equation (4.42) leads to:

$$D_{\mathrm{M}} c_{\mathrm{M}}(x) + D_{\mathrm{ML}} c_{\mathrm{ML}}(x) = Ax + B \tag{4.44}$$

Applying the boundary conditions at $x = \delta^r$:

$$D_{\mathrm{ML}} c_{\mathrm{ML}}^r = A\delta^r + B \tag{4.45}$$

and at $x = \delta^r + \delta^g$

$$D_{\mathrm{M}} c_{\mathrm{M}}^* + D_{\mathrm{ML}} c_{\mathrm{ML}}^* = A\left(\delta^r + \delta^g\right) + B \tag{4.46}$$

and solving for A and B, Equation (4.44) becomes:

$$D_{\mathrm{M}} c_{\mathrm{M}} + D_{\mathrm{ML}} c_{\mathrm{ML}} = D_{\mathrm{ML}} c_{\mathrm{ML}}^r + \frac{\left(D_{\mathrm{M}} c_{\mathrm{M}}^* + D_{\mathrm{ML}} c_{\mathrm{ML}}^*\right) - D_{\mathrm{ML}} c_{\mathrm{ML}}^r}{\delta^g}\left(x - \delta^r\right) \tag{4.47}$$

The general solution of equation (4.43) can be written as:

$$c_{\mathrm{ML}}(x) - K' c_{\mathrm{M}}(x) = A\sinh\left(\frac{\delta^g + \delta^r - x}{m}\right) + B\cosh\left(\frac{\delta^g + \delta^r - x}{m}\right) \tag{4.48}$$

Using the boundary conditions at $x = \delta^r$:

$$c_{\mathrm{ML}}^{r} = A\sinh\left(\frac{\delta^{g}}{m}\right) + B\cosh\left(\frac{\delta^{g}}{m}\right) \tag{4.49}$$

and at $x = \delta^{r} + \delta^{g}$:

$$c_{\mathrm{ML}}^{*} - K'c_{\mathrm{M}}^{*} = A\sinh(0) + B\cosh(0) \tag{4.50}$$

we have:

$$B = 0 \tag{4.51}$$

$$A = \frac{c_{\mathrm{ML}}^{r}}{\sinh\left(\frac{\delta^{g}}{m}\right)} \tag{4.52}$$

Accordingly:

$$c_{\mathrm{ML}}(x) - K'c_{\mathrm{M}}(x) = \frac{c_{\mathrm{ML}}^{r}\sinh\left(\frac{\delta^{g} + \delta^{r} - x}{m}\right)}{\sinh\left(\frac{\delta^{g}}{m}\right)} \tag{4.53}$$

and using Equations (4.47) and (4.53) we obtain:

$$c_{\mathrm{M}}(x) = \frac{\varepsilon c_{\mathrm{ML}}^{r}}{1+\varepsilon K'} + \left(\frac{c_{\mathrm{M}}^{*} + \varepsilon c_{\mathrm{ML}}^{*} - \varepsilon c_{\mathrm{ML}}^{r}}{\delta^{g}\left(1+\varepsilon K'\right)}\right)\left(x - \delta^{r}\right) - \frac{\varepsilon c_{\mathrm{ML}}^{r}\sinh\left(\frac{\delta^{g} + \delta^{r} - x}{m}\right)}{\left(1+\varepsilon K'\right)\sinh\left(\frac{\delta^{g}}{m}\right)} \tag{4.54}$$

$$c_{\mathrm{ML}}(x) = \frac{\varepsilon K' c_{\mathrm{ML}}^{r}}{1+\varepsilon K'} + \left(\frac{c_{\mathrm{M}}^{*} + \varepsilon c_{\mathrm{ML}}^{*} - \varepsilon c_{\mathrm{ML}}^{r}}{\delta^{g}\left(1+\varepsilon K'\right)}\right)K'\left(x - \delta^{r}\right) + \frac{c_{\mathrm{ML}}^{r}\sinh\left(\frac{\delta^{g} + \delta^{r} - x}{m}\right)}{\left(1+\varepsilon K'\right)\sinh\left(\frac{\delta^{g}}{m}\right)} \tag{4.55}$$

where:

$$c_{\mathrm{ML}}^{r} = \frac{K'\left(c_{\mathrm{M}}^{*} + \varepsilon c_{\mathrm{ML}}^{*}\right)}{\varepsilon K' + \left(\frac{\delta^{g}}{m}\right)\coth\left(\frac{\delta^{g}}{m}\right) + \frac{\delta^{g}\left(1+\varepsilon K'\right)\left(m\left(e^{\delta^{r}/\lambda_{\mathrm{ML}}} - 1\right)\left(1+\varepsilon K'\right) + \left(e^{\delta^{r}/\lambda_{\mathrm{ML}}} + 1\right)\lambda_{\mathrm{ML}}\tanh\left(\frac{\delta^{r}}{2m}\right)\right)}{\lambda_{\mathrm{ML}}\left(m\left(e^{\delta^{r}/\lambda_{\mathrm{ML}}} + 1\right)\left(1+\varepsilon K'\right) + \left(e^{\delta^{r}/\lambda_{\mathrm{ML}}} - 1\right)\lambda_{\mathrm{ML}}\tanh\left(\frac{\delta^{r}}{2m}\right)\right)}} \tag{4.56}$$

4.2.3 Metal accumulation and % back

To obtain the flux of metal bound to the resin, *J*, and the metal accumulation, n_M, the numerical solution for the concentration profiles can be used, both in R and R/2 devices:

$$J = D_M \left(\frac{dc_M(x,t)}{dx} \right)\Bigg|_{x=\delta^r} + D_{ML} \left(\frac{dc_{ML}(x,t)}{dx} \right)\Bigg|_{x=\delta^r} - \int_0^{\delta^r} \frac{\partial c_M(x,t)}{\partial t} dx - \int_0^{\delta^r} \frac{\partial c_{ML}(x,t)}{\partial t} dx \quad (4.57)$$

$$n_M = A \int_0^t J dt \quad (4.58)$$

Alternatively, assuming instantaneously reached steady-state conditions, the analytical solutions for the concentration profiles can be used to calculate n_M as:

$$n_M = tA \left(D_M \left(\frac{dc_M(x)}{dx} \right)\Bigg|_{x=\delta^r} + D_{ML} \left(\frac{dc_{ML}(x)}{dx} \right)\Bigg|_{x=\delta^r} \right) \quad (4.59)$$

or

$$n_M = tA \int_0^{\delta^r} k_d c_{ML}(x) dx + tAD_M \left(\frac{dc_M(x)}{dx} \right)\Bigg|_{x=\delta^r} \quad (4.60)$$

Expressions (4.59) and (4.60) can be used for both the R and R/2 devices. In the case of R devices, using Equations (4.4), (4.5) and (4.7), the total accumulation becomes:

$$n_M = tAk_d \lambda_{ML} \tanh\left(\frac{\delta^r}{\lambda_{ML}} \right) c_{ML}^r + tAD_M \left(\frac{c_M^* + \varepsilon c_{ML}^* - \varepsilon c_{ML}^r}{\delta^g (1 + \varepsilon K')} + \frac{\varepsilon c_{ML}^r \coth\left(\frac{\delta^g}{m} \right)}{m(1 + \varepsilon K')} \right) \quad (4.61)$$

In systems with two resin discs, the accumulation in moles on the back resin (at a given time *t*) can be calculated as: [13]

$$n_M^{Back} = tA \int_0^{\delta^r/2} k_d c_{ML}(x) dx \quad (4.62)$$

where *A* is the effective area of the gel-solution interface.

For homogeneous resins (R), the concentration profiles given by Equations (4.4) and (4.5) can be used in Equations (4.60) and (4.62) to obtain the back and total accumulations.

Complementary information can be gained when DGT devices with two resin discs are used. Metal accumulation in the back resin disc will indicate the presence of partially labile complexes that penetrate into the resin by diffusion. The percentage of the total mass that is accumulated in the back resin disc (for 2 disc stacks of R devices)[13] are:

$$\%back = \frac{n_{\mathrm{M}}^{\mathrm{Back}}}{n_{\mathrm{M}}} = \frac{m\epsilon K'}{2m(1+\epsilon K')\cosh\left(\frac{\delta^r}{2\lambda_{\mathrm{ML}}}\right) + \lambda_{\mathrm{ML}}\cosh\left(\frac{\delta^r}{\lambda_{\mathrm{ML}}}\right)\coth\left(\frac{\delta^g}{m}\right)\mathrm{csch}\left(\frac{\delta^r}{2\lambda_{\mathrm{ML}}}\right)} \tag{4.63}$$

The first term of the right side of Equation (4.60) corresponds to the metal released from dissociation inside the resin layer. The second term is the free metal arriving from the gel. The contribution of this second term is negligible for typical cases. Using only the first term in Equation (4.60), Equation (4.63) can be simplified as:

$$\%back = \frac{1}{2}\mathrm{Sech}\left(\frac{\delta^r}{2\lambda_{\mathrm{ML}}}\right) \tag{4.64}$$

4.3 DGT devices with one resin disc

4.3.1 Concentration profiles

Normalized concentration profiles ($c_i(x)/c_i^*$) for M, L and ML computed from numerical simulation and analytical solutions (as described in sections 4.6.1 and 4.6.2) are shown in Figures 4.2, 4.3 and 4.4 for cases where the complexation equilibrium constant takes the values K = 10 m^3 mol^{-1}, K = 10^2 m^3 mol^{-1} and K = 10^3 m^3 mol^{-1}, respectively. The agreement between the analytical and numerical concentration profiles for these parameters is excellent and the curves are almost identical. For this reason only one single line for M and one for ML are shown in Figures 4.2 to 4.4. Free metal concentration profiles are almost zero along the resin domain for the R devices (see Figures 4.2a, 4.3a and 4.4a), in agreement with the fast and strong metal binding to the resin sites considered. Recalling that, when the total concentration of M is negligible in front of the total concentration of L (*i.e.*: excess of ligand conditions), the divergence of the normalized metal and complex concentration profiles indicates disequilibrium between both species, i.e., net dissociation, Figures 4.2a, 4.3a and 4.4a indicate that the reaction layer in the R devices extends along the resin domain plus an extra layer in the gel domain whose thickness m can be computed with Equation (4.9). In the R/2 devices, the metal concentration is non-negligible in the volume region without binding sites (see Figures 4.2b, 4.3b and 4.4b), as a consequence of the release of M by complex dissociation and the absence of binding agent in those regions. Under some conditions, this dissociation can be fast enough for the system M+L to reach equilibrium, as shown in the leftmost part of Figure 4.4b.

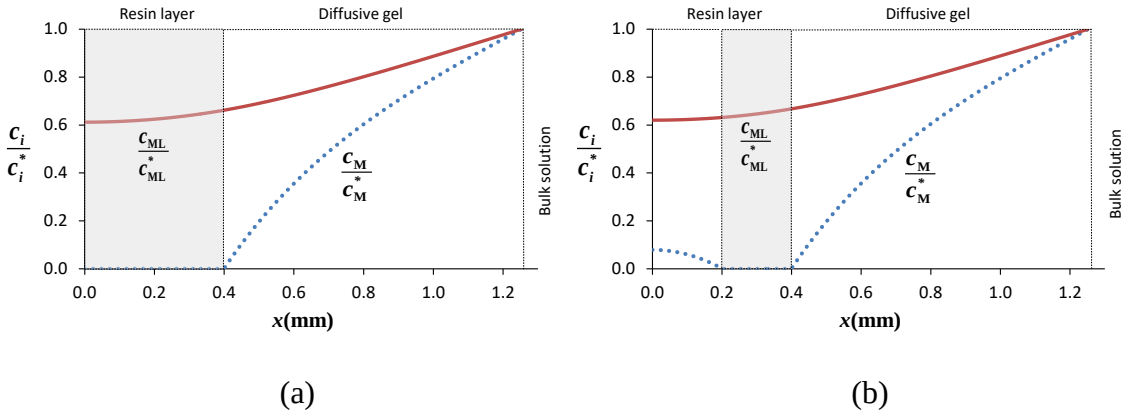

Figure 4.2. Normalized concentration profiles of metal and complex species for (a) R resin (beads homogeneously distributed) and (b) R/2 resin (beads in one half of the resin disc), with K=10m³ mol⁻¹, k_d = 5×10⁻⁴ s⁻¹, $c_{T,M}$ =0.01mol m⁻³, $c_{T,L}$ =1.0 mol m⁻³, D_M =7.07×10⁻¹⁰ m² s⁻¹, D_{ML} =4.95×10⁻¹⁰ m² s⁻¹, δ^r =4×10⁻⁴ m, δ^g =8.52×10⁻³ m and t=24h.

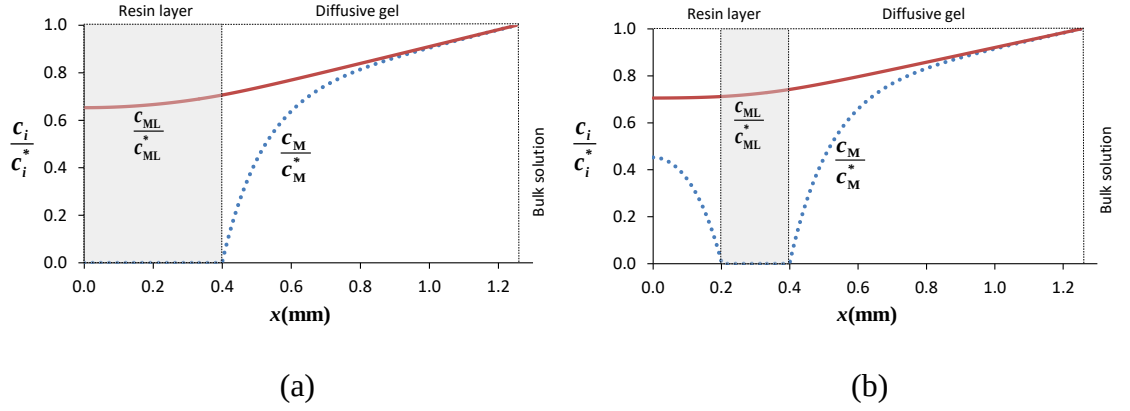

Figure 4.3. Normalized concentration profiles of metal and complex species for (a) R resin and (b) R/2 resin, with K=10² m³ mol⁻¹. The rest of parameters as in figure 4.2.

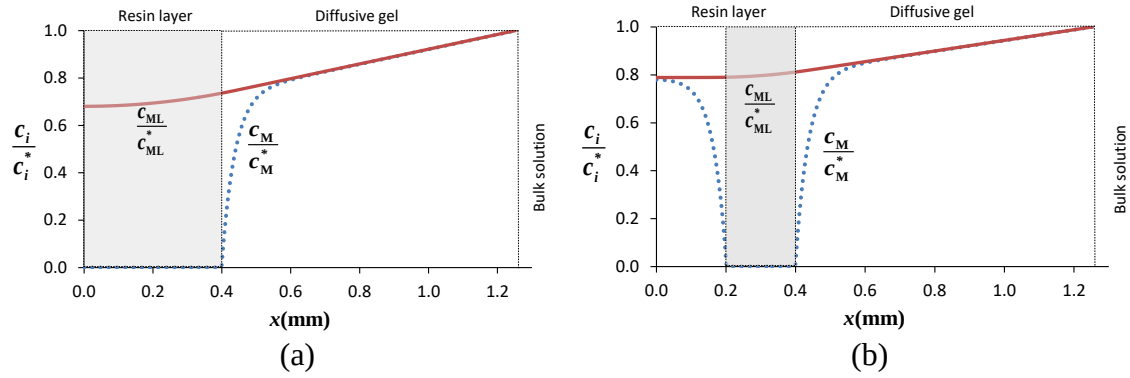

Figure 4.4. Normalized concentration profiles of metal and complex species for (a) R resin and (b) R/2 resin, with K=10³ m³ mol⁻¹. The rest of parameters as in figure 4.2.

There is an important influence of K' ($K' = Kc_L^* = c_{ML}^* / c_M^*$) on the metal profiles (compare Figures 4.2b, 4.3b and 4.4b), even when a fixed value of k_d is used. The expression for *m* helps in justifying this influence. Equation (4.9) indicates that when K' increases, thinner reaction layers are obtained, so that $m < \delta^r$ in Figure 4.4b, while $m > \delta^r$ in Figure 4.2b. In other words, small values of m indicate that the dissociation of the complex is quite effective in buffering the metal consumption at $x = \delta^r/2$. For instance, the normalized metal concentration increases and merges with the normalized complex concentration profile in a part of the layer without binding agent ($0 < x \le \delta^r/2$) in Figure 4.4b ($K'=10^3$) and thus, very little dissociation is expected in this volume.

4.3.2 Influence of the inhomogeneous binding site distribution on the total metal accumulation

Since larger differences in the concentration profiles were found for high values of K', $K'=10^3$ was used in Figure 4.5 to analyse the influence of the homogeneity of the resin site distribution on the accumulation and lability degree of complexes measured in the DGT devices. As expected, the total accumulations in both DGT devices increase as the dissociation constants of the complexes increase. It also indicates that the accumulation for R/2 device is always less than for R device.

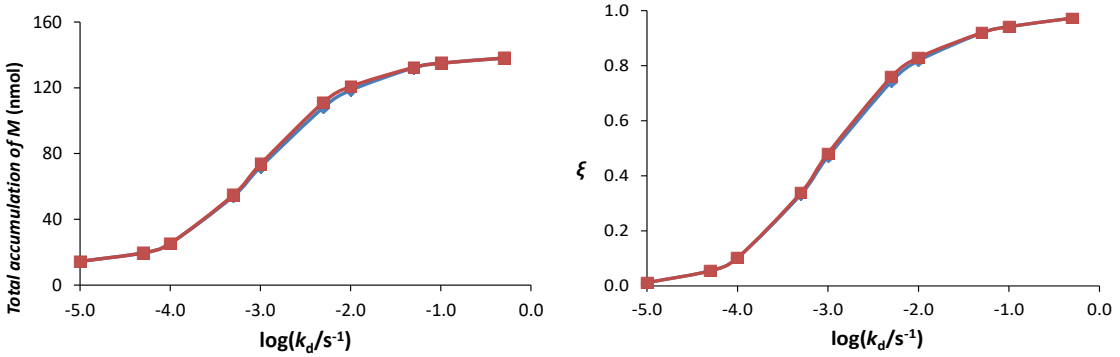

(a)

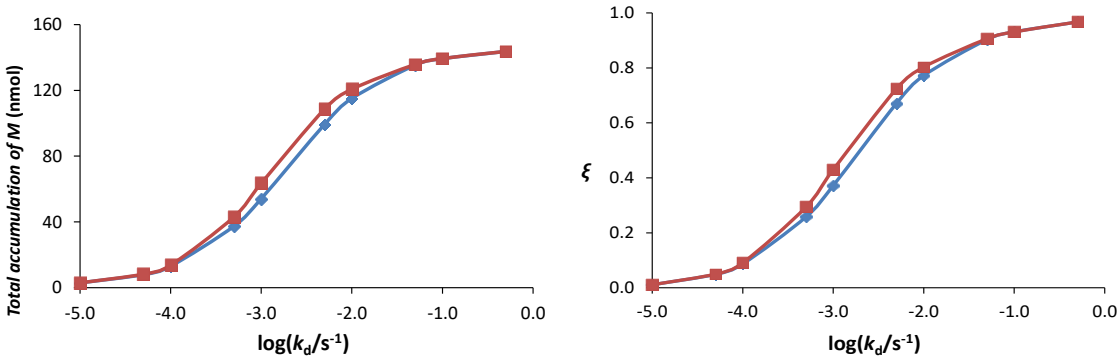

(b)

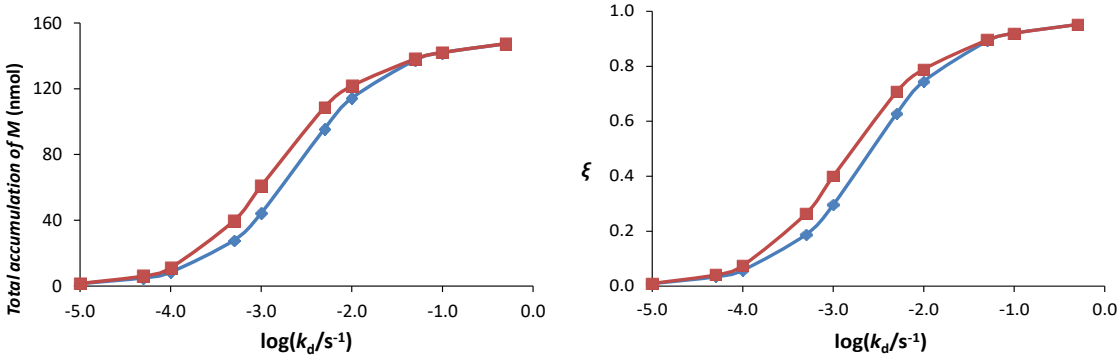

(c)

Figure 4.5. Total accumulation of metal and Lability degree of the complex (ξ) as functions of k_d *for: (a) K=10 m³ mol⁻¹, (b) K=10² m³ mol⁻¹ and (c) K=10³ m³ mol⁻¹. The rest of parameters as in figure 4.2. Markers: Red square for R device, blue diamond for R/2 device. Lines represent a guide to the eye.*

Moreover, the total accumulations in R and R/2 devices are very close for low or high enough values of k_d, while they diverge for intermediate k_d values. As noted above, when the complex is very labile, the entire complex dissociates at the resin disc-diffusive gel interface ($x = \delta^r$) so that the absence of reactive sites at the bottom of the resin layer is irrelevant with respect to the accumulation. A similar situation arises for inert complexes: dissociation is negligible (both in the gel or the resin layers) and the inhomogeneity of the binding bead distribution has no impact on the metal accumulation.

For intermediate values of k_d, dissociation inside the resin disc is the main mechanism of metal accumulation. In this situation the inhomogeneous resin site distribution has the highest influence on metal accumulation. A similar behaviour is observed for the lability degree in Figure 4.5b, which can also be understood using the same arguments as for the accumulation. In order to assess an extreme situation with a large discrepancy between results of R and those of R/2, calculations for a set of *K* values by changing k_a and k_d were done. Table 4.1 shows the percentages of largest discrepancy between the accumulation and lability in R and R/2 devices. The maximum influence of the inhomogeneity of the resin disc increases as *K* increases until the lability reaches an almost fixed value close to 0.25. Notice that this lability degree corresponds to a fixed k_d of the complex (see column 3 in Table 4.1) which indicates that, for $\delta^g > \delta^r$, the lability degree essentially depends on k_d but not on k_a and *K,* as stated in reference [4]. Although the decrease of accumulation in the R/2 devices increases as *K* increases, it remains below 13% for $K = 10^2$ m^3 mol^{-1} (i.e. $K = 10^5$ L mol^{-1}) in the worst scenario (Table 4.1). Notice that stronger complexes could increase this error, but it should also be taken into account that such strong complexes will distort the linear accumulation in the DGT due to their similar (or higher) affinity for the metal to that of the resin.[14]

Table 4.1. Discrepancies in lability degree (ξ) and total accumulation (n_M) between a DGT device with a homogeneous resin (R) and another DGT device with an inhomogeneous disc where resin beads are in just in one half of the volume (R/2). Parameters: $c_{T,M}$=0.01mol m^{-3}, $c_{T,L}$=1.0 mol m^{-3}, D_M=7.07×10^{-10} m^2s^{-1}, D_{ML}=4.95×10^{-10} m^2s^{-1} and t=24h.

K (m^3mol^{-1})	k_a ($m^3mol^{-1}s^{-1}$)	k_d (s^{-1})	ξ (R)	n_M (R) (nmol)	Discrepancy ξ (%)	Discrepancy n_M (%)
10	5×10^{-3}	5×10^{-4}	0.34	54.8	1.8	1.5
10^2	5×10^{-2}	5×10^{-4}	0.29	43.0	12.2	13.1
10^3	5×10^{-1}	5×10^{-4}	0.26	39.7	28.8	29.9
10^4	5	5×10^{-4}	0.25	38.4	41.1	41.2

(Discrepancy ξ*)* $= \frac{\xi(R)-\xi(R/2)}{\xi(R)}$; *(Discrepancy* n_M *)* $= \frac{n_M(R)-n_M(R/2)}{n_M(R)}$

4.3.3 Influence of the system parameters on the measurements made with R and R/2 DGT devices

Metal complexes with simple ligands have diffusion coefficients close to those of the hydrated metal ions, since the sizes of both species are not very different. For macromolecular metal complexes like those with humic matter, the diffusion coefficients can be one order of magnitude smaller than the diffusion coefficient of the free metal ion.[15]

Figure 4.7 shows the influence of the diffusion coefficient of the complex on the metal accumulation in R and R/2 devices. The accumulation decreases as D_{ML} decreases, since the transport of M from the solution to the resin domain decreases. The system is not fully labile since both, the R and R/2 curves are not linear as it would be expected for a labile system ($n_{M,labile} = At\frac{D_{ML}c^*_{ML}}{\delta^g}$ whenever $\varepsilon K' >> 1$). For fixed values of K and k_d, Figure 4.7 shows a decreasing divergence of the accumulation in the R and R/2 devices as the diffusion coefficient of the complex decreases, a result of interest when complexes with natural macromolecular ligands are present in the system. Actually, the increase of D_{ML} in Figure 4.7 is concomitant to an increase of the lability degree which approaches 0.25, the value corresponding to the maximum influence of the inhomogeneous distribution of the reactive sites (see Table 4.1).

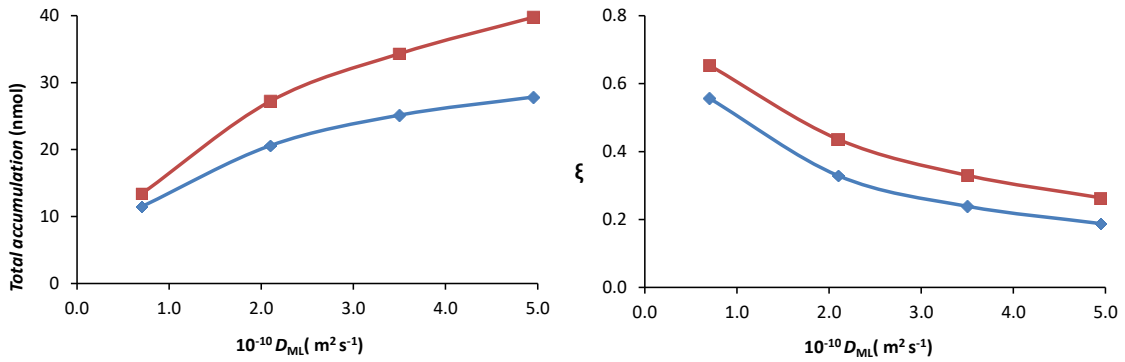

(a) (b)

Figure 4.6. (a)Total accumulation and (b) lability degree as functions of the diffusion coefficient of the complex. $D_{ML}=0.7\times D_M$. $K=10^3$ m^3 mol^{-1}. The rest of parameters as in figure 4.2. Markers: Red square for R device, blue diamond for R/2 device. Lines represent a guide to the eye.

Increasing the resin layer thickness increases both the metal accumulation and the lability degree (data not shown). As explained elsewhere [4,5], an increase of the resin thickness increases the volume where there is net dissociation. This is true whenever partially labile complexes are present in the system, can penetrate in the resin domain and they do not reach full dissociation in the resin domain. Divergences between R and R/2 devices decrease as the thickness of the resin layer decreases (e.g. in ultra-thin DGT),[16] until convergence to a common value for devices with negligible resin thickness, or whenever penetration of complexes was prevented. In the other limit, reduction of the differences between R and R/2 devices is also expected when the resin is thick enough to reach full dissociation of complexes in the layer $\delta^r/2 < x \leq \delta^r$.

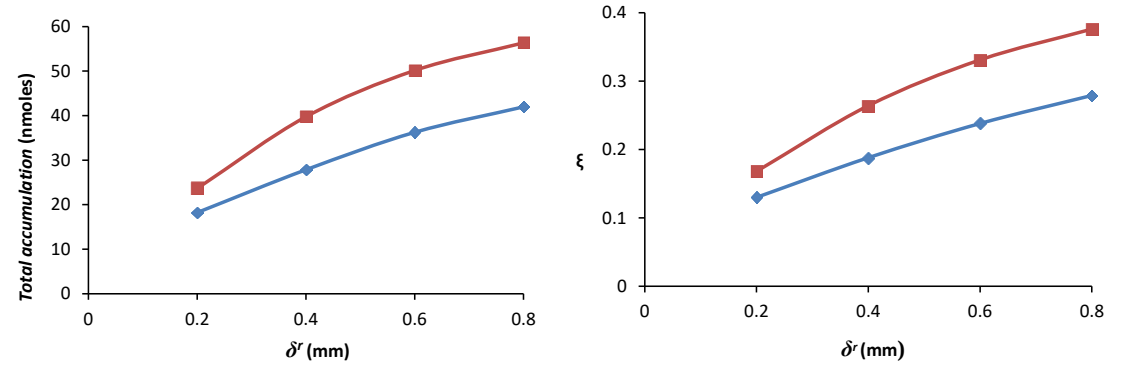

(a) (b)

Figure 4.7. (a)Total accumulation and (b) lability degree as a function of the thickness of the resin disc. Parameters as in figure 4.2. Markers: Red square for R device, blue diamond for R/2 device. Lines represent a guide to the eye

4.3.4 Inhomogeneity effects in commercial DGT devices when sampling metal availability in natural waters

Commercial DGT devices use a binding-bead concentration in large excess to avoid saturation effects under typical working conditions. Thus, small fluctuations in the resin distribution do not influence the accumulation. However, it is well known that the resin beads of Chelex 100 tend to settle to one side of the resin disc while casting. The average diameter of these beads is 100 μm. The amount of resin beads used per disc is close to that corresponding to a packed single layer of beads at the surface of the resin disc, as schematically depicted in reference [11]. If the settling was total, only ¼ of the resin volume would contain resin beads. An imperfect settling renders reasonable that around half of the volume of the resin disc may contain Chelex beads in a standard resin disc (thickness 400 μm). Thus, results reported in this work can be straightforwardly applied to commercial DGT devices.

Table 4.1 indicates the highest percentage of decrease in the accumulation due to settling for different values of the stability constant. Notice that this percentage applies only to the contribution of partially labile complexes, while free metal and labile complexes are not influenced by the settling of the resin. Assuming Eigen ideas (i.e. a fixed k_a), the lability decreases as the stability of the complex increases. As a rule of thumb, inorganic complexes tend to be labile in DGT so that the main influence of the resin settling is mostly linked to complexes with organic ligands. Some strong organic metal complexes, partially labile in DGT, have stabilities in the range of the values reported in Tables 1 and 2. For instance, Visual MINTEQ uses a stability constant for Ni-NTA at 25ºC of log K=9.39 and DGT experiments in systems with $c_{T,Ni}$ = 0.01mol m^{-3} and $c_{T,NTA}$ =1.0 mol m^{-3} indicate that Ni-NTA behaves as partially labile with log K' =6,3. NTA can be found in natural waters due to anthropogenic activities,[17] and it is also studied as model of natural organic matter. Thus, metal accumulation from such complexes could also be influenced by the settling of the resin in the DGT although other phenomena like accumulation of humic acid on the diffusive gel have also been described.[18] In any case, the reduction of accumulated mass due to the resin settling is always below the percentage of volume of the resin domain without resin beads (50%), since part of the metal released there still binds to the resin after travelling back by

diffusion.

4.4 Study of DGT devices with two resin discs

The use of DGT devices with a stack of resin discs has been suggested as a way of obtaining complementary information on the behaviour of the system.[7,9,10] By eluting and analysing each resin disc separately, these devices allow assessing whether the resin acts as a perfect-sink for the free metal. The condition of perfect-sink is necessary to support the application of the simplest formula to describe the metal accumulation in DGT, i.e.:

$$c_{\mathrm{DGT}} = \frac{n_{\mathrm{M}}\delta^{g}}{AtD_{\mathrm{M}}} \tag{4.65}$$

The use of disc stacks can also help to elucidate if complexes are partially labile and can penetrate into the resin domain. Recently, it has been highlighted that the knowledge of the metal distribution in the front and back resin discs can be used to fit the kinetic dissociation constant of the complex in the resin domain.[10,13] For all these reasons, it is of interest to assess the influence of the inhomogeneity of the binding sites within the resin disc on the accumulation, lability degree of the complex, distribution of the accumulated mass (between front and back resin discs) and the retrieval of the kinetic dissociation constant from this distribution.

DGT devices with two homogeneous (R) or two half occupied resin discs (R/2) were studied by numerical simulation. Standard resin discs of 4×10^{-4}m thickness and diffusive gel of 8.52×10^{-4} m thickness were considered. Figure 4.8 shows very different concentration profiles of metal for both types of resin discs. The physical explanation outlined in Section 4.3.1 can be extended here to rationalize this behaviour.

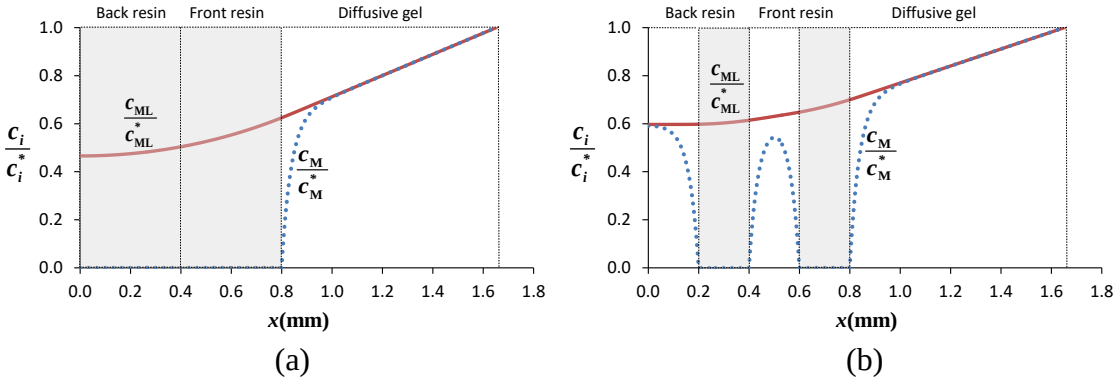

Figure 4.8. Normalized concentration profiles of metal and complex species for (a) two R resins and (b) two R/2 resins, with $K=10 m^3 mol^{-1}$, $k_d = 5\times10^{-4} s^{-1}$, $c_{T,M}=0.01 mol\ m^{-3}$, $c_{T,L}=1.0\ mol\ m^{-3}$, $D_M=7.07\times10^{-10} m^2 s^{-1}$, $D_{ML}=4.95\times10^{-10} m^2 s^{-1}$, $\delta^r =4\times10^{-4} m$ for each resin, $\delta^g =8.52\times10^{-3} m$ and t=24h

Parallel to Table 4.1, Table 4.2 reports (for each K value) the metal accumulations in DGT devices that accommodate two R or two R/2 resin discs. Only data corresponding to the kinetic constants that lead to the maximum discrepancies between both devices are reported. The lability degree of complexes obtained in Table 4.2 is quite constant, but higher than the lability degree of the complexes reported in Table 4.1 for just one resin disc. The maximum discrepancy between both types of resins (Table 4.2) arises for complexes with lability degree below 0.5. As in the case with only one resin device, the maximum discrepancy increases as K increases, but the relative difference remains lower than the fraction of volume without binding agent.

Table 4.2. Lability degree (ξ) and total accumulation (n_M) in DGT devices with two R or two R/2 resin discs. Parameters as in Table 4.1.

K ($m^3 mol^{-1}$)	k_a ($m^3 mol^{-1} s^{-1}$)	k_d (s^{-1})	ξ (R)	n_M (R) (nmol)	% back (R)	ξ (R/2)	n_M (R/2) (nmol)	% back (R/2)
10	5×10^{-3}	5×10^{-4}	0.44	72.0	33.3	0.43	70.2	40.1
10^2	5×10^{-2}	5×10^{-4}	0.40	64.0	40.8	0.38	55.4	49.2
10^3	5×10^{-1}	5×10^{-4}	0.38	62.2	44.1	0.31	48.4	47.7
10^7	5×10^{3}	5×10^{-4}	0.36	56.2	46.1	0.24	37.4	47.9
10^9	5×10^{5}	5×10^{-4}	0.36	56.2	46.1	0.24	37.4	47.9

DGT devices with two resin discs can be used to find k_d of the complex by fitting the % of back accumulation using the analytical expression (4.63) or, alternatively, by fitting the total accumulation with the analytical expression (4.61). In order to check the influence of the inhomogeneous distribution of the binding beads on the recovered k_d

values, numerical simulations of DGT devices with two R/2 resin discs with partially labile complex in excess of ligand were conducted. These were used to compute the % back and total accumulation. Subsequently these values were used to recover k_d using the analytical expressions (4.61) or (4.63). The results are reported in Table 4.3. k_d values fitted from %back are of the same order of magnitude than the one used in the simulation (10^{-2} s^{-1}), but systematically modified by a factor close to 1/2 (*i. e.*, recovered values tend to be half of the correct ones). The agreement of the values recovered from the total accumulation is better, with relative errors around 25%. The consistency of these errors for all the *K* values examined suggests the use of this empirical factor as a way to improve the estimation.

Table 4.3. Recovered kinetic dissociation constant of a complex species when data from two R/2 devices are interpreted with the analytical expressions for homogeneous resins (equations (4.61) and (4.63)). Simulations run with k_d =10^{-2} s^{-1}. The rest of parameters as in Table 4.1.

K ($m^3 mol^{-1}$)	% back	n_M (mol)	k_d (s^{-1}) Fitted from % back	k_d (s^{-1}) Fitted from n_M
10^2	26.2%	1.20×10^{-7}	4.80×10^{-3}	6.85×10^{-3}
10^3	26.3%	1.21×10^{-7}	4.85×10^{-3}	7.46×10^{-3}
10^4	26.3%	1.21×10^{-7}	4.83×10^{-3}	7.50×10^{-3}
10^5	26.3%	1.21×10^{-7}	4.83×10^{-3}	7.46×10^{-3}

To check the applicability of this correction factor, new simulations in DGT devices with two R/2 resin discs were conducted for systems with a fixed equilibrium constant (K=10^4 m^3/mol) and with values of k_d scanning the range of lability degrees from inert complexes to labile complexes. Results are listed in Table 4.4, which confirms that the errors in recovering k_d from the %back data assuming a homogeneous distribution of the resin beads are also quite independent of the actual k_d. The simulated values indicate that a factor of 2 is suitable to improve the value of k_d (assuming homogeneous distributions of the binding agent) estimated from %back measurement. For other fractions (*f*) of volume in the resin disc being occupied by the binding agent, a better estimate of k_d is f^{-1} $k_{d,Recovered}$, when data from %back is used (data not shown). In the case of the values recovered using the total accumulation as input information, the error depends on k_d, so one cannot suggest a general correction factor.

Table 4.4. Recovered kinetic dissociation constants from simulated data of two R/2 resin discs, with K=10^{4}m^{3}mol^{-1}. The rest of parameters as in Table 4.1.

k_d (s^{-1})	% back	n_M (mol)	k_d (s^{-1}) Recovered from % back	k_d (s^{-1}) Recovered from n_M
5.0×10^{-4}	47.9	3.76×10^{-8}	2.45×10^{-4}	2.51×10^{-4}
1.0×10^{-3}	46.1	5.84×10^{-8}	4.99×10^{-4}	5.18×10^{-4}
5.0×10^{-3}	35.0	1.07×10^{-7}	2.47×10^{-3}	3.25×10^{-3}
1.0×10^{-2}	26.4	1.21×10^{-7}	4.83×10^{-3}	7.50×10^{-3}
5.0×10^{-2}	6.7	1.40×10^{-7}	2.26×10^{-2}	4.31×10^{-2}
1.0×10^{-1}	2.4	1.45×10^{-7}	4.25×10^{-2}	9.03×10^{-2}
3.0×10^{-1}	0.2	1.51×10^{-7}	1.18×10^{-1}	3.57×10^{-1}

Notice, however, that the accuracy decreases for both low and high % back, especially if we also include the experimental measurement uncertainty, which is not considered here. Actually, for a given thickness of the resin disc there is a window of sensitive k_d values.[13] Too high k_d values lead to negligible accumulation in the back resin disc, since the complex has been fully dissociated in the diffusive gel and the adjacent resin disc. Conversely, k_d values below a given threshold lead to a % back close to 50% and thus no information on the decrease of the complex concentration along the resin domain is obtained. Therefore, only intermediate values of %back contain significant information on the complex dissociation.[13]

4.5 Conclusions

It has been studied the influence of the distribution of resin beads on the concentration profiles of the species, the total metal accumulation and the lability of the complexes in DGT devices. For very labile or inert complexes, this distribution does not show influence on the concentration profiles, on the total accumulation of metal and on the lability degree of complexes. For partially labile complexes, the influence of this distribution increases with the value of the equilibrium constant K and the diffusion coefficient of the complex. In these cases, the assumption of binding site homogeneity always leads to underestimation of both c_{DGT} and the accumulation, but the present

results indicate that only 13% decrease of accumulation arises in both i) inhomogeneous devices where resin beads are only dispersed in half of the resin volume and ii) complexes with stability constant $K < 10^2$ m^3 mol^{-1} dominating the metal speciation.

Analytical expressions for the concentration profiles in an inhomogeneous resin layer have been derived. It was assumed excess of ligand and perfect-sink conditions in the layer of the resin containing the binding. Predictions obtained with the analytical expresions agree with the rigorous numerical simulations.

The complex dissociation rate constant, k_d, can be determined from the percentage of back accumulation in a DGT with a stack of two resin discs. This determination is a direct measurement of the kinetic dissociation constant in the resin domain, which can differ from the value in the diffusive gel or bulk solution as has recently been suggested.[10] However, the application of this procedure is restricted to a meaningful window of kinetic constants values.[13] The relative error values (due to inhomogeneity of the resin layer) found in recovering k_d from the %back are quite independent of *K* and k_d. In R/2 devices, there is a ratio of 2 between the real value and the recovered one assuming homogeneous distributions of binding resin beads.

Finally, tests were performed with different thickness of resin. Differences in accumulations and lability degrees between devices with resins R and R/2 are very small, when δ^r tends to zero. Differences in these magnitudes increase when δ^r increases, but it is expected to decrease again when δ^r is so large that the complexes reach full dissociation in the layer $\delta^r/2 < x \leq \delta^r$.

4.6 Reference List

1. Davison, W.; Zhang, H. In-situ speciation measurements of trace components in natural- waters using thin-film gels. *Nature* **1994,** *367* (6463), 546-548.

2. Davison, W.; Zhang, H. Progress in understanding the use of diffusive gradients in thin films (DGT) – back to basics. *Environ. Chem.* **2012,** *9*, 1-13.

3. Mongin, S.; Uribe, R.; Puy, J.; Cecilia, J.; Galceran, J.; Zhang, H.; Davison, W. Key Role of the Resin Layer Thickness in the Lability of Complexes Measured by DGT. *Environ. Sci. Technol.* **2011,** *45* (11), 4869-4875.

4. Uribe, R.; Mongin, S.; Puy, J.; Cecilia, J.; Galceran, J.; Zhang, H.; Davison, W. Contribution of Partially Labile Complexes to the DGT Metal Flux. *Environ. Sci. Technol.* **2011,** *45* (12), 5317-5322.

5. Puy, J.; Uribe, R.; Mongin, S.; Galceran, J.; Cecilia, J.; Levy, J.; Zhang, H.; Davison, W. Lability Criteria in Diffusive Gradients in Thin Films. *J. Phys. Chem. A* **2012,** *116* (25), 6564-6573.

6. Lehto, N. J.; Davison, W.; Zhang, H.; Tych, W. An evaluation of DGT performance using a dynamic numerical model. *Environ. Sci. Technol.* **2006,** *40* (20), 6368-6376.

7. Shafaei-Arvajeh, M. R.; Lehto, N.; Garmo, O. A.; Zhang, H. Kinetic Studies of Ni Organic Complexes Using Diffusive Gradients in Thin Films (DGT) with Double Binding Layers and a Dynamic Numerical Model. *Environ. Sci. Technol.* **2013,** *47* (1), 463-470.

8. Uribe, R.; Puy, J.; Cecilia, J.; Galceran, J. Kinetic Mixture Effects in Diffusion Gradients in Thin Films (DGT). *Phys. Chem. Chem. Phys.* **2013,** *15* (27), 11349-11355.

9. Levy, J. L.; Zhang, H.; Davison, W.; Puy, J.; Galceran, J. Assessment of trace metal binding kinetics in the resin phase of diffusive gradients in thin films. *Anal. Chim. Acta* **2012,** *717*, 143-150.

10. Puy, J.; Galceran, J.; Cruz-Gonzalez, S.; David, C. A.; Uribe, R.; Lin, C.; Zhang, H.; Davison, W. Metal accumulation in DGT: Impact of ionic strength and kinetics of dissociation of complexes in the resin domain. *Anal. Chem.* **2014,** *86*, 7740-7748.

11. Zhang, H.; Davison, W. Performance-characteristics of diffusion gradients in thin-films for the in-situ measurement of trace-metals in aqueous- solution. *Anal. Chem.* **1995,** *67* (19), 3391-3400.

12. Tusseau-Vuillemin, M. H.; Gilbin, R.; Taillefert, M. A dynamic numerical model to characterize labile metal complexes collected with diffusion gradient in thin films devices. *Environ. Sci. Technol.* **2003,** *37* (8), 1645-1652.

13. Galceran, J.; Puy, J. Interpretation of diffusion gradients in thin films (DGT) measurements: a systematic approach. *Environ. Chem.* **2015,** *12* (2), 112-122.

14. Mongin, S.; Uribe, R.; Rey-Castro, C.; Cecilia, J.; Galceran, J.; Puy, J. Limits of the Linear Accumulation Regime of DGT Sensors. *Environ. Sci. Technol.* **2013,** *47*, 10438-10445.

15. Balch, J.; Gueguen, C. Effects of molecular weight on the diffusion coefficient of aquatic dissolved organic matter and humic substances. *Chemosphere* **2015,** *119*, 498-503.

16. Lehto, N. J.; Davison, W.; Zhang, H. The use of ultra-thin diffusive gradients in thin-films (DGT) devices for the analysis of trace metal dynamics in soils and sediments: a measurement and modelling approach. *Environ. Chem.* **2012,** *9* (4), 415-423.

17. Schmidt, C. K.; Fleig, M.; Sacher, F.; Brauch, H. E. Occurrence of aminopolycarboxylates in the aquatic environment of Germany. *Environ. Pollut* **2004,** *131* (1), 107-124.

18. van der Veeken, P. L. R.; van Leeuwen, H. P. DGT/DET Gel Partition Features of Humic Acid/Metal Species. *Environ. Sci. Technol.* **2010,** *44* (14), 5523-5527.

CHAPTER 5

KINETIC AND THERMODYNAMIC EFFECTS OF THE IONIC STRENGTH IN ONLY-METAL SYSTEMS

Part of the material of this chapter has been published in:

Altier, A.; Jimenez-Piedrahita, M.; Rey-Castro, C.; Cecilia, J.; Galceran, J.; Puy, J. Accumulation of Mg to Diffusive Gradients in Thin Films (DGT) Devices: Kinetic and Thermodynamic Effects of the Ionic Strength. *Anal. Chem*. **2016**, 88 (20), 10245-10251

5.1 Introduction

In the last years many studies have been devoted to analyse both the theoretical basis and the applications of the DGT devices. However, there are still many issues that need clarification for a proper interpretation of the DGT data. As an example we can mention the influence on the measurements of the electric interactions between charged species inside the sensor. When we are interested in measuring species that are electrically charged in solution, electrical interactions between them and the charges of the active groups in the resin layer, or the interactions with residuals charges in the gel layer can affect the transport and the kinetics of the chemical reactions inside the sensor. In laboratory measurements a supporting electrolyte is sometimes used to reduce the electrical influence of the resin sites over the ions in the solution. The ions of the salt background screen the electrical field produced by the charges of the resin beads by creating an opposite field.

As a measurement of the concentration of electrical charges in a solution it is used the Ionic strength (I), which is defined as:

$$I = \frac{1}{2}\sum_i c_i z_i^2 \qquad (5.1)$$

Where c_i and z_i are the concentration and the electrical charge of species i. The bigger

the Ionic strength the lower the electrical forces between the reacting ions of the solution and the resin sites.

There are controversial results in previous studies of the electrostatic effects in DGT. Some authors have reported no influence of the ionic strength on the metal accumulation in simple systems with only metal or in systems in presence of complexes.[1-3] In other cases, an increase or a decrease of the metal accumulation has been reported.[4] The effects of the ionic strength on the accumulation have been explained by different authors through a varying "effective" diffusion coefficient that includes ion migration phenomena,[5] by the use of an electrostatic partitioning at the gel−solution interface,[6-8] or by the combination of electrostatic partitioning and changes on the resin−metal binding rate constants.[9] To clarify the influence of the ionic strength it seems convenient to start with the simplest systems made up by metal cations without any ligand being present in the system. The standard treatment of DGT considers that the metal ions bind immediately and irreversible to the Chelex as soon as they contact the front of the resin layer. This approximation is referred to as perfect-sink and it corresponds to the limiting case where the metal association with the resin is so fast that the accumulation is limited by the transport. By using DGT devices with a stack of two resin discs, this approximation has proved to be useful for many cations for which the accumulated mass in the back resin disc is negligible.[10] However, other cations diverge from this behaviour due to slow binding. In these cases, a steady-state is also reached but there is a non-null metal profile in the resin domain and the metal accumulation flux is not the maximum possible. These are the cases of interest to look at the effect of the ionic strength on the kinetics of reactions, since any change in the kinetic constants will be reflected in the accumulation.

In this chapter we are going to discuss theoretical models that allow to study the effects of the ionic strength in DGT devices. Additionally, numerical tools based in these models are discussed and compared. Mg accumulations are used as a particular example of these electrical effects.

5.2 Theoretical models

Two theoretical models to analyse the DGT metal accumulation in a simple system will be discussed. The system contains the target metal cation in a solution with a low concentration of supporting electrolyte. The first model explicitly takes into account the migration term in the transport equation, considering that the electrical field is determined by the supporting electrolyte, i. e., the concentration of the target metal cation is still negligible in comparison to the supporting electrolyte even at low ionic strength. An analytical approximate expression for the electrical field produced by the resin charges and the background electrolyte will be used. In the second one, the electrical effect is restricted to a plane at the interfaces of regions with and without resin beads and is modelled as a discontinuity in the concentrations according to a partitioning Boltzmann factor.

5.2.1 A model based on the Nernst-Planck equations

Let us consider a DGT device with two resin discs immersed in an electrolyte solution. It is assumed that both resin gels can be seen as a continuous ion-penetrable region, with a homogeneous distribution of immobile charged resin sites, under planar symmetry with only one relevant spatial dimension labelled *x (i.e.,* neglecting edge effects).[11] We are not going to take into account the settling of the Chelex beads during casting, because this effect is almost negligible in our system as commented elsewhere.[12] This model neglects, then, the effects of the particulate nature of the resin beads, an approximation that can be justified when the diffusion layers around the beads overlap. Fig. 5.1 is a magnification picture of a resin disc where we can see the Chelex beads as a collection of small spherical drops. As seen in the picture, the distance between the resin beads and their radius are of the same order. As the radius of the bead equals the thickness of the diffusion layer, the picture suggests that there is superposition of the diffusion layer around each individual bead so that the diffusive problem approaches planar geometry towards the whole resin disc. The main advantage of this model is a reduced computational cost, since it allows a 1-D simulation while the explicit consideration of the beads would require a 3-D simulation as well as a large set of parameters describing the position and structure of the beads and diffusion inside them.

A more detailed treatment of the electrostatic influence of the bead charges, modelled as soft particles, on the kinetics of the reaction with cations is given in references [13] and [14]. However, such treatment, for a dispersion of beads, requires 3-D mapping of the domain, as indicated above. As a first approximation, we restrict ourselves here to a mean field approximation. The kinetic constants $k_{a,R}$ and $k_{d,R}$ of this work can be regarded as effective values that include the influence of diffusion and spatial heterogeneity of the binding sites on the rate of reaction with the Chelex particles. A detailed discussion of this effect to only one particle is given in. [15]

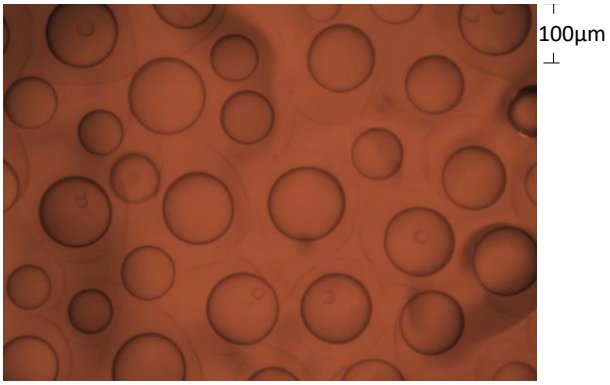

Figure 5.1. Imagen of Chelex beads in the resin gel taken with an optical microscope (magnification: 100x).

Let us consider that metal cations (M) diffuse along the gel domain and penetrate into the resin where they bind to free resin sites (R) to form occupied sites (MR) according to:

$$\mathrm{M} + \mathrm{R} \underset{k_{d,R}}{\overset{k_{a,R}}{\rightleftharpoons}} \mathrm{MR} \tag{5.2}$$

where charges are omitted for simplicity, and $k_{a,R}$ and $k_{d,R}$ are the association and dissociation rate constants of the binding process, respectively. Since we could find cases where the accumulation approaches equilibrium, the kinetics of both association and dissociation processes from the resin sites have to be considered in the model.

Additionally, since we are interested in analysing data corresponding to different ionic strengths, electrostatic effects due to the poor screening of the resin sites have also to be considered. To model the transport by migration, we will assume that there is an electric potential produced by the fixed charges of the resin sites and the background electrolyte.

It is also assumed that M does not modifies this potential (it's concentration is in general negligible in comparison with the background electrolyte or the concentration of resin sites)[16]. The potential can be calculated using the Poisson-Boltzmann equation:

$$\frac{\partial^2 \phi}{\partial x^2} = -\frac{F}{\varepsilon}\sum_j z_j c_j(x,t) \tag{5.3}$$

Where c_j and z_j are concentration and charge of species *j*, *F* is the Faraday constant and ε is the permittivity of the medium.

An analytical solution for Eqn. (5.3) (when the fixed charges of the resin follow a Heaviside step function) was given by Ohshima.[17] As the charge of the functional groups of Chelex is negative, cations of the background electrolyte tend to accumulate while the concentration of anions tends to decrease. The electric potential in the resin layer ($0 \le x \le \delta^r$) becomes:

$$\Psi(x) = \Psi_D + (\Psi_0 - \Psi_D)\mathrm{e}^{-k_m|x|} \tag{5.4}$$

and in the gel layer ($\delta^r < x \le \delta^r + \delta^g$)

$$\Psi(x) = \frac{2k_B T}{e}\ln\left(\frac{1+\gamma \mathrm{e}^{-\kappa x}}{1-\gamma \mathrm{e}^{-\kappa x}}\right) \tag{5.5}$$

where

$$\Psi_D = \left(\frac{k_B T}{ze}\right)\mathrm{ArcSinh}\left(\frac{z_R c_{TR}}{2zn}\right) \tag{5.6}$$

and

$$\Psi_0 = \Psi_D - \left(\frac{k_B T}{ze}\right)\mathrm{Tanh}\left(\frac{ze\Psi_D}{2k_B T}\right) \tag{5.7}$$

stand for the Donnan potential and the resin-gel interface potential respectively, with:

$$\kappa = \sqrt{\frac{2ne^2}{\varepsilon_0 \varepsilon_r k_B T}} \tag{5.8}$$

$$k_m = \kappa \left(1 + \left(\frac{Z_R c_{TR}}{2zn} \right)^2 \right)^{1/4} \tag{5.9}$$

and

$$\gamma = \mathrm{Tanh}\left(\frac{e\Psi_0}{4k_B T} \right) \tag{5.10}$$

In these equations k_B is the Boltzmann constant, e is the elementary electric charge, ε_0 is the permittivity of free space, ε_r is the relative permittivity, T is the absolute temperature, n is the concentration of electrolyte, z is electric charge of the symmetric background electrolyte, c_{TR} is the total concentration of free resin sites and Z_R is the electric charge of free resin sites.

The Debye-Hückel parameter κ in Eqn. (5.8) is the reciprocal of the Debye length ($1/\kappa$), which is directly related with the thickness of the layer where the potential changes. A representation of this potential is given in Figure 5.2.

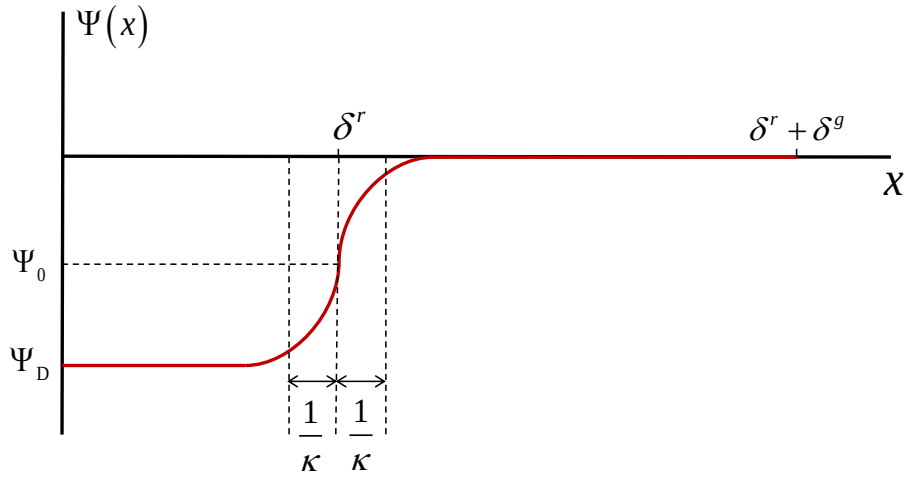

Figure 5.2. Ohshima electric potential for a negatively charged resin disc in presence of an electrolyte solution.

This expression indicates that the potential is almost constant in both phases: resin and diffusive gels. Since the transient regime is short in comparison to the deployment time

(the electrolyte rapidly reaches equilibrium with the resin), Eqns. (5.4) and (5.5) will be used to describe the electrostatic potential independent of time. The potential drop, given by Eqn. (5.6), takes place in a layer of thickness of the order of the Debye length located at the interface resin-gel. M is subjected to diffusion, migration and reaction with the resin sites.

The transport equations for the free metal (M), the bound metal (MR), and free resin sites (R) in the resin layer ($0 \le x \le \delta^r$) can be written as:

$$\frac{\partial c_{\mathrm{M}}}{\partial t} = D_{\mathrm{M}} \frac{\partial^2 c_{\mathrm{M}}}{\partial x^2} + D_{\mathrm{M}} \frac{z_{\mathrm{M}} F}{RT} \frac{\partial}{\partial x}\left(c_{\mathrm{M}} \frac{\partial \Psi(x)}{\partial x} \right) + k_{\mathrm{d,R}} c_{\mathrm{MR}} - k_{\mathrm{a,R}} c_{\mathrm{M}} c_{\mathrm{R}} \tag{5.11}$$

$$\frac{\partial c_{\mathrm{MR}}}{\partial t} = -k_{\mathrm{d,R}} c_{\mathrm{MR}} + k_{\mathrm{a,R}} c_{\mathrm{M}} c_{\mathrm{R}} \tag{5.12}$$

$$\frac{\partial c_{\mathrm{R}}}{\partial t} = k_{\mathrm{d,R}} c_{\mathrm{MR}} - k_{\mathrm{a,R}} c_{\mathrm{M}} c_{\mathrm{R}} \tag{5.13}$$

and in the gel layer ($\delta^r < x \le \delta^r + \delta^g$)

$$\frac{\partial c_{\mathrm{M}}}{\partial t} = D_{\mathrm{M}} \frac{\partial^2 c_{\mathrm{M}}}{\partial x^2} + D_{\mathrm{M}} \frac{z_{\mathrm{M}} F}{RT} \frac{\partial}{\partial x}\left(c_{\mathrm{M}} \frac{\partial \Psi(x)}{\partial x} \right) \tag{5.14}$$

where the first term in the r.h.s. of Eqns. (5.11) and (5.14) corresponds to the diffusive transport, the second term corresponds to migration and the third and fourth ones in Eqn. (5.11) to the reaction of M with the resin sites in the resin domain.

The boundary conditions for M (the mobile species) will be:

$$\left(\frac{\partial c_{\mathrm{M}}}{\partial x} \right)_{x=0} = 0 \tag{5.15}$$

for x = 0, indicating absence of flux and negligible migration effects. For $x = \delta^r$ we have:

$$D_{\mathrm{M}} \left(\frac{\partial c_{\mathrm{M}}}{\partial x} \right)_{x=\delta^{r-}} + D_{\mathrm{M}} \frac{z_{\mathrm{M}} F}{RT} \left(c_{\mathrm{M}} \frac{\partial \Psi}{\partial x} \right)_{x=\delta^{r-}} = D_{\mathrm{M}} \left(\frac{\partial c_{\mathrm{M}}}{\partial x} \right)_{x=\delta^{r+}} + D_{\mathrm{M}} \frac{z_{\mathrm{M}} F}{RT} \left(c_{\mathrm{M}} \frac{\partial \Psi}{\partial x} \right)_{x=\delta^{r+}} \tag{5.16}$$

$$c_{\mathrm{M}}\left(\delta^{r-},t\right)=c_{\mathrm{M}}\left(\delta^{r+},t\right) \tag{5.17}$$

indicating continuity in the flux of metal and in the concentration profile.

For $x=\delta^{r}+\delta^{g}$

$$c_{\mathrm{M}}(\delta^{r}+\delta^{g},t)=c_{\mathrm{M}}^{*} \tag{5.18}$$

Here, Ψ is given by Eqns. (5.4) and (5.5).

The initial conditions will be:

for $x<\delta^{r}+\delta^{g}$

$$c_{\mathrm{M}}(x,t=0)=0 \tag{5.19}$$

for $x=\delta^{r}+\delta^{g}$

$$c_{\mathrm{M}}(\delta^{r}+\delta^{g},t=0)=c_{\mathrm{M}}^{*} \tag{5.20}$$

This formulation holds independently of the ratio of the pertinent time scales of both steps, the transport to the resin domain given by $\left(\delta^{g}\right)^{2}/\pi D_{\mathrm{M}}$ and the association reaction given by $\left(k_{\mathrm{a,R}}c_{\mathrm{R}}\right)^{-1}$.

The system of Eqns. (5.11) – (5.20) has been numerically solved using a simulation code based on the PDEPE function in MATLAB.[18] Details of the implementation are explained in section 5.5.1.

Simulations were run to check the influence of the thickness of the layer along which the potential changes ($\approx 2/\kappa$ in Figure 5.2) on the accumulation of metal. The results are shown in table 5.1. Since the thickness of the resin is of the order of 10^{-4} m, higher values of κ are not of interest.

Table 5.1. Total metal accumulation and %back accumulation obtained by simulation for different values of the potential transition layer ($1/\kappa$). Parameters used: c_M^* = 10^{-2} mol m^{-3}, Ψ_D=44,3 mV, $k_{a,R}$ = 10^{-3} m^3 $mol^{-1}s^{-1}$, $k_{d,R}$ = 10^{-4} s^{-1}, D_M = 6.0 × 10^{-10} m^2 s^{-1}, A=3.8× 10^{-4} m^2, δ^g =1.1× 10^{-3} m and two resin discs with δ^r =4.0× 10^{-4} m.

	$\frac{1}{\kappa}=10^{-5}$m		$\frac{1}{\kappa}=10^{-7}$m		$\frac{1}{\kappa}=10^{-10}$m	
***t*(h)**	**n_T (nmol)**	***%back***	**n_T (nmol)**	***%back***	**n_T (nmol)**	***%back***
4	28	14.6	28	15.2	27	15.5
8	56	19.5	55	20.2	55	20.4
12	83	23.3	83	23.9	83	24.3
16	111	26.7	110	27.3	110	27.7
20	138	29.6	137	30.2	137	30.6
24	164	32.1	164	32.7	163	33.1
28	191	34.2	190	34.7	189	35.2
32	217	36.0	216	36.5	216	37.0
36	243	37.5	242	38.0	241	38.5
40	269	38.7	268	39.2	267	39.7
44	294	39.8	293	40.3	292	40.8
48	320	40.7	319	41.2	317	41.7

As seen in Table 5.1, the thickness of the potential transition layer (whenever it is lower than 10^{-5}m) has small impact on the accumulations of metal calculated with the fitted kinetic constants. However, the concentration profile of free M ions does actually depend on the thickness of this layer and the slope of the potential at the resin-gel interface, as seen in Fig 5.3 for three different values of $1/\kappa$. This can be explained as follows: in steady-state conditions, the metal profile is linear in the diffusive gel region away from the transition layer. But close to the gel-resin interface, where migration effects take place, the electrical influence is compensated by a reduction in the slope of the concentration profile (as can be seen in the insert of Fig 5.3) to keep the flux constant. When the electrical influence is high enough (the electrical force is proportional to the slope of the electrostatic potential) the slope of the M concentration profile reverses its sign. The limiting case is the electrostatic potential discontinuity (Donnan model).

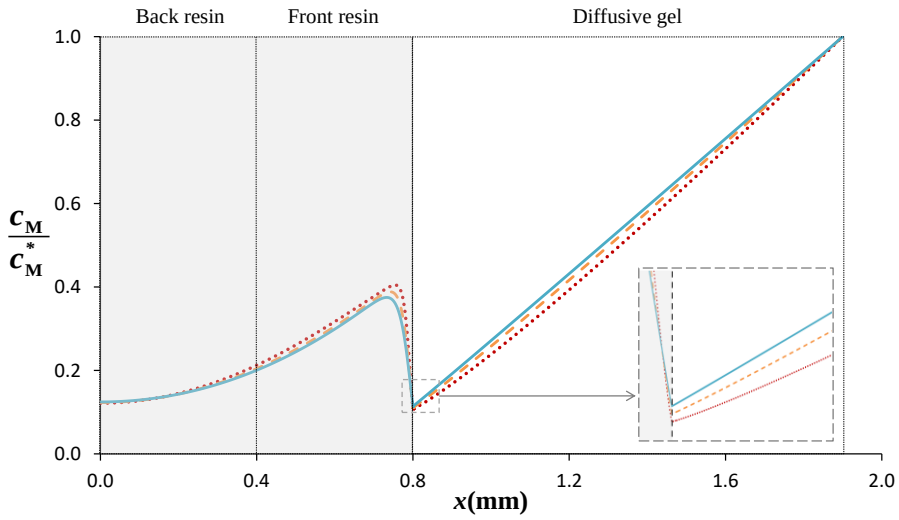

Figure 5.3. Concentration profiles of metal for different thickness of the potential transition layer (1/κ). Red dotted line corresponds to 1/κ=1×10^{-5} m, orange dashed line to 1/κ=2×10^{-5} m and blue continuous line to 1/κ=3×10^{-5} m. t=24h. Other parameters as in table 5.1.

5.2.2 The Partition model

Since the thickness of the region where the potential changes is well below the thickness of the resin domain ($1/\kappa \ll \delta^r$), and since this thickness does not affect the accumulations once it is below a certain threshold (see Table 5.1), a model that reduces the electrostatic effects to a partitioning factor at the resin-gel interface is also used. In this model the change of the electrostatic potential between the gel and resin phases is just given by a step function instead of being described by the continuous function defined in Eqns. (5.4) and (5.5). Notice that this approximation has an important impact on the transport equations since it reduces the migration effects to take place only in a plane. The electrostatic potential is then given by:

$$\Psi(x) = \Psi_D\left[1 - H\left(x - \delta^r\right)\right] \tag{5.21}$$

where Ψ_D is given by Eqn. (5.6) and $H\left(x-\delta^r\right)$ is the Heaviside function centered in $x = \delta^r$.

The system of equations to be solved in this case can be written as:

in the resin layer ($0 \le x \le \delta^r$)

$$\frac{\partial c_{\mathrm{M}}}{\partial t} = D_{\mathrm{M}} \frac{\partial^2 c_{\mathrm{M}}}{\partial x^2} + k_{\mathrm{d,R}} c_{\mathrm{MR}} - k_{\mathrm{a,R}} c_{\mathrm{M}} c_{\mathrm{R}} \tag{5.22}$$

$$\frac{\partial c_{\mathrm{MR}}}{\partial t} = -k_{\mathrm{d,R}} c_{\mathrm{MR}} + k_{\mathrm{a,R}} c_{\mathrm{M}} c_{\mathrm{R}} \tag{5.23}$$

$$\frac{\partial c_{\mathrm{R}}}{\partial t} = k_{\mathrm{d,R}} c_{\mathrm{MR}} - k_{\mathrm{a,R}} c_{\mathrm{M}} c_{\mathrm{R}} \tag{5.24}$$

in the gel layer ($\delta^r < x \le \delta^r + \delta^g$)

$$\frac{\partial c_{\mathrm{M}}}{\partial t} = D_{\mathrm{M}} \frac{\partial^2 c_{\mathrm{M}}}{\partial x^2} \tag{5.25}$$

with the same initial conditions (Eqns. (5.19) - (5.20)) than the Nernst- Planck model and the following boundary conditions:

for $x = 0$

$$\left(\frac{\partial c_{\mathrm{M}}}{\partial x} \right)_{x=0} = 0 \tag{5.26}$$

for $x = \delta^r$ (see Fig. 5.4)

$$D_{\mathrm{M}} \left(\frac{\partial c_{\mathrm{M}}}{\partial x} \right)_{x=\delta^{r-}} = D_{\mathrm{M}} \left(\frac{\partial c_{\mathrm{M}}}{\partial x} \right)_{x=\delta^{r+}} \tag{5.27}$$

$$c_{\mathrm{M}} \left(\delta^{r-}, t \right) = \Pi_{\mathrm{M}} \; c_{\mathrm{M}} \left(\delta^{r+}, t \right) \tag{5.28}$$

for $x = \delta^r + \delta^g$

$$c_{\mathrm{M}}(\delta^r + \delta^g, t) = c_{\mathrm{M}}^{*} \tag{5.29}$$

Notice that the new boundary condition at the resin-gel interface, Eqn. (5.28), has been introduced to model the effects of migration. This condition implies a discontinuity in the metal concentration at $x=\delta^r$ which is given by the Boltzmann factor:

$$\Pi_M = \exp\left(-\frac{z_M F \Psi_D}{RT}\right) \tag{5.30}$$

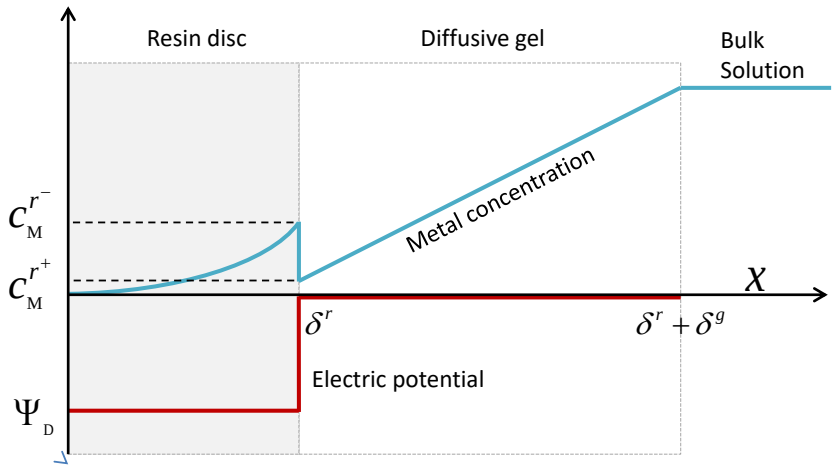

Figure 5.4. Concentration profile of metal and electric potential in the partition model.

This assumption is an approximation, since Donnan conditions can only be fulfilled by species whose flux is null.[19] Indeed, the condition of null flux of a species *i* can be written as

$$D_i\left(\frac{\partial c_i}{\partial x}\right)_x + D_i \frac{z_i F}{RT}\left(c_i \frac{\partial \Psi}{\partial x}\right)_x = 0 \tag{5.31}$$

so that

$$\frac{d}{dx}\ln c_i = -\frac{z_i F}{RT}\frac{d\Psi}{dx} \tag{5.32}$$

Integration of eqn. (5.32) in an infinitesimal region that includes $x=\delta^r$ leads to

$$c_i^{r-} = c_i^{r+} \exp\left(-\frac{z_M F \Psi_D}{RT}\right) \tag{5.33}$$

as assumed in the Eqn.(5.28) for the metal, with the Boltzmann factor defined in Eqn. (5.30).

The numerical solution of this model has been carried out in FORTRAN as explained in section 5.5.2.

Ions not consumed at the resin domain can be considered in equilibrium with the electrostatic potential along the time of measurement, because they reach the equilibrium partitioning between the solution and the resin domain in a short transient time in comparison to the deployment time. Accordingly, their concentration profile will show a discontinuity determined by the Boltzmann factor at the resin-gel interface. On the other hand, for the cations consumed at the resin domain, the binding process competes with the free metal accumulation required for the equilibrium partitioning. In this case, the Boltzmann conditions are just limiting conditions corresponding to equilibrium which might not be reached during the deployment, especially when the kinetic binding process becomes fast enough for the metal accumulation being determined by the transport. Despite Donnan partitioning is strictly applicable to species with a null flux, in many cases it is possible to obtain accurate results with this model.

5.3 Study of the influence of the Ionic Strength on accumulation of Magnesium in DGT devices

Availability of Mg is a subject of environmental concern, where topics like interactions with DOM [22] as well as uptake mechanisms [23] have received attention recently. In terms of environmental aquatic toxicology, the bioavailability and the affinity of metals to accumulate on surfaces of organisms depend on the site-specific water quality including parameters such as pH, hardness and DOM concentration. DGT data reported in literature for Mg^2 in an only metal system show linear accumulations with time, indicating that the process happened in conditions of perfect-sink. However, these measurements were made at low ionic strength and, the behaviour at other salt concentrations is explored in this work. Measurements of accumulations of Mg are shown in this section to check the suitability of perfect-sink approximation at different

Ionic strengths. The model based on the Nernst-Planck equations and the partition model discussed in the previous section will be applied to analyse the Mg binding.

5.3.1 Experimental details

Accumulations of Mg reported in reference [20] are used below. Briefly, Mg accumulations were measured at four different Ionic strength (in the range from 0.01 to 0.5 $mol \cdot L^{-1}$) and at different times (Figs 5.6 and 5.7). A solution containing 9×10^{-5} $mol \cdot L^{-1}$ Mg and at pH= 7.5 was employed. The DGT sensors consisted of DGT holders (piston type, 2 cm diameter window), polyacrylamide gel discs (diffusive disc, 0.8 mm thick, and Chelex resin disc, 0.4 mm thick). To obtain additional information on the spatial distribution of the accumulated metals, DGT devices with 2 resin discs were used [21]. Rubidium (2.5×10^{-4} $mol \cdot L^{-1}$) was added to the deployment solutions to measure the Boltzmann factors at different ionic strengths.

5.3.2 Boltzmann factors

Rb and Na (the last one already present in the supporting electrolyte) were assumed to show a negligible chemical binding with the resin sites, so that their accumulation in the resin domain with respect to bulk concentration in the solution can be understood as due to the electrostatic partitioning. For this reason they were employed to measure the Boltzmann factor at different ionic strength. The concentration profiles for these ions will be homogeneous in both resin and gel phases. An example of these profiles is shown in Fig 5.5.

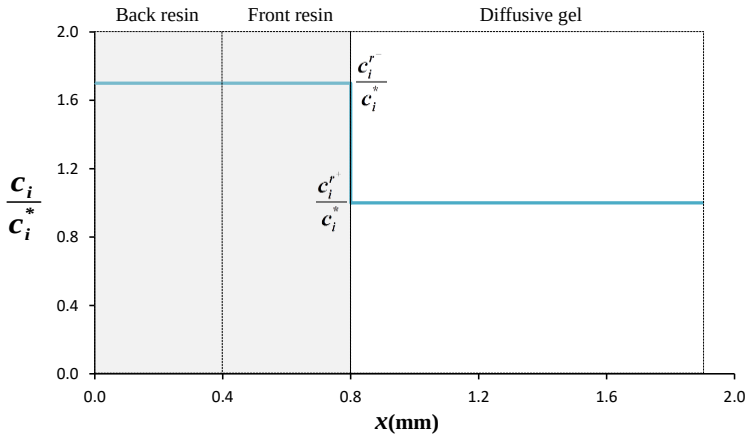

Figure 5.5. Concentration profile of no reacting species in the partition model for a specific value of ionic strength.

It is possible to obtain Π_i from the accumulation of species *i* using the expression:

$$n_i = Arc_i^{r-} = Ar\Pi_i c_i^* \tag{5.34}$$

Experimental values (obtained with Eqn. (5.34)) and theoretical values of Π (obtained with Eqns. (5.6) and (5.30)) are reported in Table 5.2. A noticeable good agreement between theoretical and experimental values is deduced from the values reported in Table 5.2.

Table 5.2 Boltzmann factor values, Π, estimated from Eqns. (5.6) and (5.30), and from the experimental accumulations (with Eqn. (5.34)) of Rb or Na at pH= 7.5.

I (mM)	Π	Π_{Rb}	Π_{Na}
10	5.77	5.84	5.71
50	1.71	1.89	2.07
100	1.32	1.27	1.36
500	1.06	1.06	1.08

5.3.3 Accumulation of Mg

Results for the accumulation of Mg at different times and ionic strengths are shown in Fig. 5.6. It can be seen that accumulations as a function of time gradually approximate the perfect-sink behaviour. It can also be seen a decrease in the %back as *I* decreases. It shows that perfect-sink conditions only apply for the Mg binding at low enough ionic strength ($I < 10^{-2}$ mol L^{-1}). Additionally, at short times the slope of the accumulation

depends on *I*, which also means that the accumulation does not follow perfect-sink conditions since this would imply a common slope for all ionic strengths. The different slopes point towards a dependence of the association rate constant on the ionic strength, but they could also reflect a faster accumulation due to an increasing partitioning of the metal at the resin-diffusive gel interface as the ionic strength decreases.

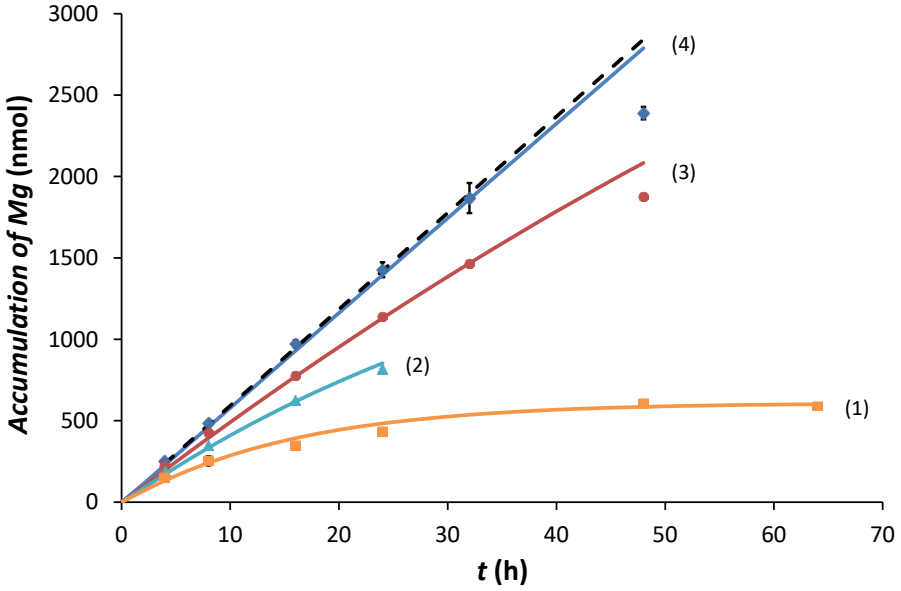

Figure 5.6. Time evolution of the total accumulation of Mg in DGT devices with two resin discs. Markers correspond to experimental accumulations at salt background concentrations of 0.5 mol·L⁻¹ (1, orange square), 0.1 mol·L⁻¹ (2 green triangle), 0.05 mol·L⁻¹ (3, red bullet) and 0.01 mol·L⁻¹ (4, blue diamond). Continuous lines correspond to the numerical simulations at pH = 7.5 and the corresponding ionic strengths. Other parameters for the numerical simulations are listed in Table 5.3. Dashed black line corresponds to Mg accumulation assuming perfect-sink conditions.

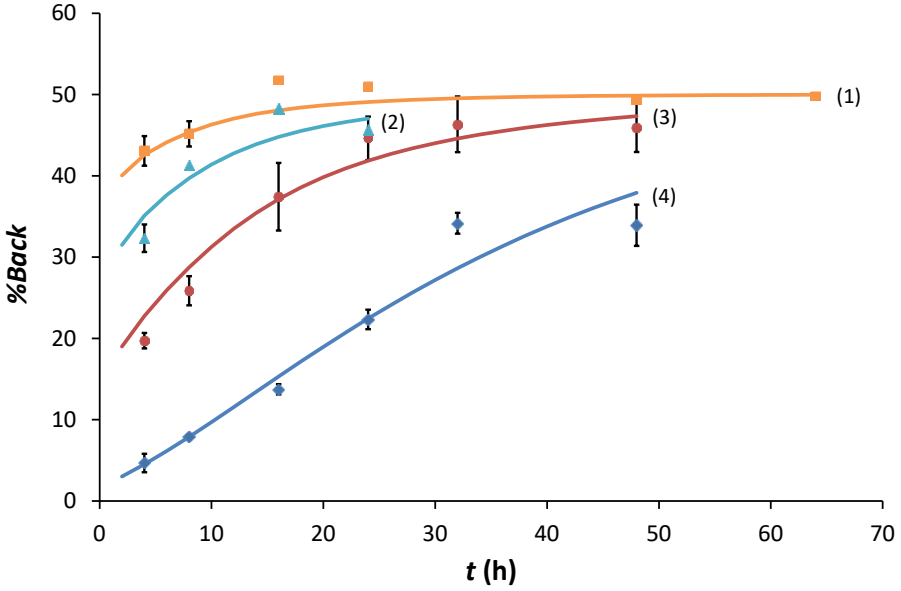

Figure 5.7. Percentage of Mg accumulated in the back resin disc. Markers and experimental conditions as in Fig.5.. Continuous lines correspond to results obtained by numerical simulations.

The non-linearity of accumulation with time, at high ionic strength, indicates the absence of steady-state conditions due to the approaching to saturation or equilibrium conditions. For I= 0.5 mol·L^{-1} the accumulation approach a value around 500 nmol (the capacity of the resin is bigger that this value) so that the distortion of the linearity at high ionic strength is not due to saturation of the resin disc. Instead, we can say that the accumulations are arriving to an equilibrium value. We refer to this accumulation as thermodynamically limited. Under these conditions, the concentration of bound Mg is homogeneous all along the resin domain (which justifies that %back has raised up to 50%) while the free Mg concentration in the resin domain reaches equilibrium with that in the bulk solution.

The dependence of the stability constant of the Mg binding to the resin on the ionic strength is also clear in Fig. 5.6. That influence is responsible of the increase of the limiting bound Mg that would be obtained at long times for each ionic strength.

5.3.4 Dependence of kinetic and thermodynamic constants on the ionic strength

Numerical simulations based on the models explained in section 5.2 were used to estimate the values of the kinetic constants for the chemical reaction of Mg with the resin sites. They were found from the simultaneous fitting of the numerical models to both sets of experimental measurements (Mg accumulation and %back) shown in Fig. 5.6 and Fig. 5.7. As both, metal cation and resin sites, have charges of opposite sign, increasingly attractive forces will arise between Mg and the resin sites, so that the kinetic association constant will increase as I decreases. Thus, a fitted value of $k_{a,R}$ for each ionic strength has to be considered. As seen in Fig. 5.6, the bending of the accumulation line is especially important at I=0.5M, this indicating that the accumulation is close to the equilibrium value, so that this curve is the most sensitive to $k_{d,R}$. According to Eigen approach,[24,25] the influence of the ionic strength only applies to the association kinetic constant, so that the value of $k_{d,R}$ fitted at I=0.5M will be used for all ionic strengths considered. The increase of the association rate constant as I decreases is then parallel to the increase of the stability constant since $K = k_{a,R} / k_{d,R}$.

The values of the kinetic constants fitted with the Nernst–Planck model are reported in Table 5.3 and the agreement between predicted and measured accumulations can be seen in Fig. 5.6. The agreement is also quite reasonable in Fig. 5.7, especially if we consider the moderate reproducibility of the experimental %back measurements.

Table 5.3. Recovering of the kinetic association constant $k_{a,R}$ using a numerical simulation with experimental values of Boltzmann factor and $k_{d,R}$ = 1.0×10^{-4} s^{-1}.

I (mM)	I_R (mM)	c^*_{Mg} (mol m^{-3})	K (m^3 mol^{-1})	$k_{a,R}$ (m^3 mol^{-1}s^{-1})
10	30	9.2×10^{-2}	20.5	2.0×10^{-3}
50	62	9.0×10^{-2}	4.4	4.4×10^{-4}
100	108	9.0×10^{-2}	1.7	1.7×10^{-4}
500	500	9.3×10^{-2}	0.7	7.0×10^{-5}

The values of the kinetic constants reported in Table 5.2 are used in the simulation tool developed with the Partition model. In that case, partition factors $\Pi_{Mg} = \Pi^2_{Rb}$ are used according to the values reported in Table 5.2. The accumulation and %back merge perfectly with those reported in Figs. 5.6 and 5.7.

It is possible to see that Π_{Mg} increases with decreasing *I*, indicating a tendency of the free Mg concentration to the territorial binding in the resin domain to achieve electrostatic equilibrium consistent with the potential drop at the resin-gel interface. This effect has a negligible influence on the %back, as supported by the numerical simulation (Table 5.4). Thus, the decrease of the %back as the ionic strength decreases is an evidence of the increase of the kinetic association and accordingly, the increase of the stability constant, which reduces the penetration of the Mg in the resin domain.

Table 5.4. Time dependence of percentages of accumulations of metal in the back resin obtained by simulation for different values of the Boltzmann factor. Conditions for the numerical simulation: c_M^* = 10^{-2} mol m^{-3}, $k_{a,R}$ = 5 × 10^{-4} m^3 $mol^{-1}s^{-1}$, $k_{d,R}$ = 1.0 × 10^{-4} s^{-1}, D_M = 4.94 × 10^{-10} m^2 s^{-1}.

***t*(h)**	$\Pi_M = 1.0$	$\Pi_M = 2.3$	$\Pi_M = 4.0$	$\Pi_M = 6.3$
1.0	13.2%	13.2%	13.2%	13.2%
2.0	15.4%	15.4%	15.4%	15.4%
3.0	17.3%	17.3%	17.3%	17.3%
4.0	19.1%	19.1%	19.1%	19.1%
5.0	20.8%	20.8%	20.8%	20.8%
6.0	22.4%	22.4%	22.3%	22.3%
7.0	23.9%	23.8%	23.8%	23.8%
8.0	25.3%	25.2%	25.1%	25.1%
9.0	26.6%	26.5%	26.4%	26.4%
10.0	27.8%	27.7%	27.6%	27.6%

5.3.5 Corresponding concentration profiles of Mg

Although the experimental setup only allows the measurement of the mass accumulated in the back and front resin discs, an estimation of the metal concentration profile in the whole resin domain can be obtained taking advantage of the numerical simulation tools developed in this work. Figure 5.8 depicts the Mg concentration profiles expected at a deployment time of 8 h corresponding to the measurements presented in figures 5.6 and 5.7. Values of partition coefficients and kinetic constants were taken from tables 5.2 and 5.3. The software based on the partition model (explained in section 5.5.2) was used for simulations.

Notice the jump of the metal concentration at the resin-diffusive gel interface and how this jump increases as the ionic strength decreases, in agreement with the Π values reported in Table 5.2. Moreover, the slope of the metal concentration profile in the resin domain at the interface grows as *I* decreases indicating an increase in the association rate constant and a larger metal accumulation.

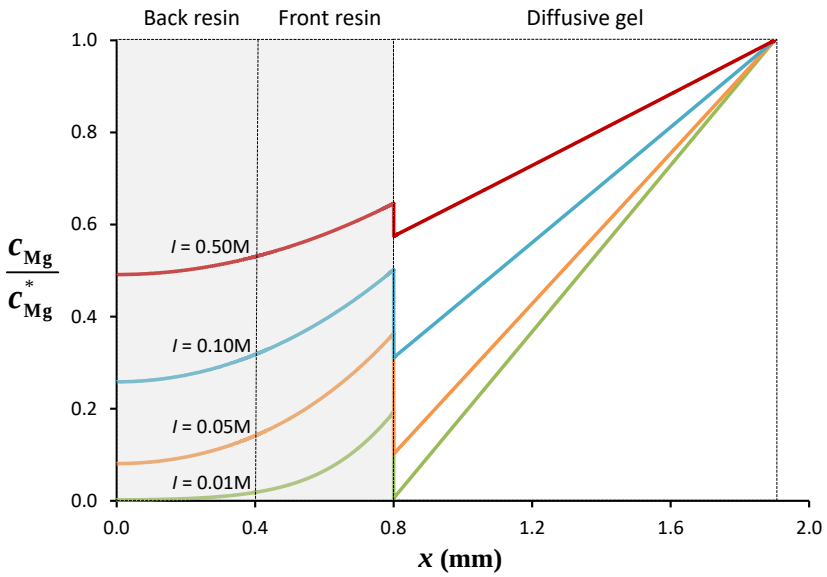

Figure 5.8 Concentration profiles of Mg at different values of ionic strength. Time of deployment 8h. Other parameters for the numerical simulations are listed in Table 5.3.

5.3.6 Influence of the Donnan factor on the metal accumulation

It seems also interesting to discuss the relative importance of the "territorial" (i.e., purely electrostatic) and specific binding mechanisms in the overall metal accumulation. Accumulations depicted in Fig 5.6 are split in Table 5.5 into two fractions, namely: the moles of free Mg^{2+} ions within the resin volume (column 8 in Table 5.5) and the moles of Mg chemically bound (column 9 in Table 5.5). As can be seen, the amount of free Mg is, at any *I*, negligible in comparison to the amount of Mg specifically bound to the resin groups. Notice also that, in contrast to what is expected from equilibrium arguments, the amount of free Mg accumulated in the resin disc decreases as ionic strength decreases, indicating that equilibrium conditions with the bulk Mg concentration are far to be reached since the system has approached perfect-sink conditions. However, the electrostatic effects are not only responsible for the territorial accumulation, but also for an increase of the accumulation due to a faster transport. This influence can be estimated by just comparing the total accumulation with the hypothetical accumulation calculated with $\Pi_M = 1.0$ (i.e., without electrostatic partitioning), as reported in Table 5.5, column 5.

For a 24 h deployment, the influence of the electrostatic partitioning is similar in all the range of ionic strengths and remains around 22% at the lowest *I* (see column 7 in Table 5.5 which reports the percentage with respect to column 6 of the differences between column 6 and 5 in Table 5.5). Under the conditions of this work, the increase of the association rate constant (and that of the corresponding equilibrium value) is, then, the most relevant phenomena responsible for the increase of Mg accumulation as *I* decreases.

Table 5.5. Comparison of total metal accumulation with and without the Donnan factor. Values obtained by simulation. Deployment time =24h.

I (mM)	Π	$k_{a,R}$ ($m^3\ mol^{-1}s^{-1}$)	$k_{d,R}$ (s^{-1})	n_T (nmol) with $\Pi = 1$	n_T (nmol) with Π_{Mg}	Percentage of the Influence of Π_{Mg}	n_M (nmol) Free metal in the resin domain	n_{MR} (nmol) Bound metal in the resin domain
0.01	34.1	2.05×10^{-3}	1.0×10^{-4}	1093	1395	21.6%	3	1392
0.05	3.6	4.4×10^{-4}	1.0×10^{-4}	880	1129	22.1%	12	1117
0.10	1.6	1.7×10^{-4}	1.0×10^{-4}	672	853	21.2%	21	832
0.50	1.1	7.0×10^{-5}	1.0×10^{-4}	446	483	7.6%	27	456

5.4 Conclusions

Two theoretical models for the interpretation of metal accumulations at different ionic strengths have been studied. Both models consider the transport and complexation reactions of the metallic cations in the gel and the resin domain. Electrostatic effects due the resin charges and the background electrolyte are also included. Numerical simulation tools for the previous models have been implemented.

The models and numerical tools developed in this work have been used to analyse the experimental results for Mg accumulations. It has been found that, the main phenomenon that increases the Mg availability is the dependence of the kinetic association constant and the stability constant between the cation and the resin sites on the ionic strength. The accumulation of Mg at high ionic strength is thermodynamically limited by Mg binding to the resin at pH 7.5. However, as ionic strength decreases, the thermodynamic limitation is lower due to the increase of the stability and kinetic association constants.

The electrostatic effects on DGT devices can be approximated using a partition factor at the resin-gel interface. This factor was here determined experimentally for different values ionic strength by adding a small concentration of Rb to the system and has a smaller influence on Mg accumulation.

Using numerical simulation has been shown that the thickness of the potential transition layer ($1/\kappa$) has an impact on the concentration profiles, but its influence on the total accumulation and percentage of accumulation in the back resin is negligible, in the range of values here studied.

5.5 Supporting Information

5.5.1 Numerical solution for the model based on the Nernst-Planck equations

The numerical solution of this model, described by Eqns. (5.11) – (5.20), has been done using the solver *pdepe* in MATLAB 5. The spatial domain was meshed with a logarithmic grid in both resin and gel phases, with a fine grid (one tenth of the Debye length) only near the resin-gel interface to improve computational efficiency.

We can see an outline of the program in Figure 5.9 which contains the following general elements:

1. The program begins with the declaration of the variables used and the reading of the inputs.

2. Construction of the spatial grid with a careful selection of the spatial positions so that intervals with lengths shorter than the reaction layer were included in the mesh.

3. *pdepe* function of Matlab has one input named options. It is used to set some parameters of the simulation as error tolerance or step size in time. This is important for the convergence of the solution and must be settled before calling pdepe function.

4. *pdepe* function is used to solve the system of equations (5.11) – (5.14) on a 1-dimensional domain. Details of this function will be discussed below.

5. Results for concentrations of different species are obtained.

6. Using the concentrations, the program calculates the total accumulation and the percentage of accumulation on the back resin disc.

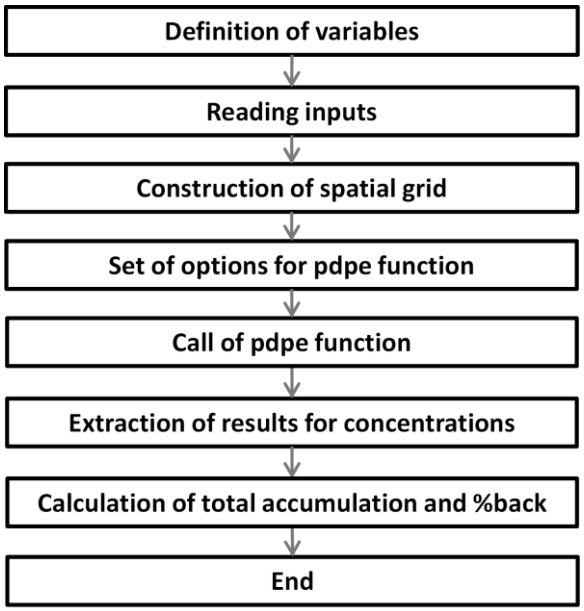

Figure 5.9. General scheme of the simulation tool in Matlab.

pdepe function allows us to solve a system of partial differential equations (PDE) in one Space variable x and a time variable t. The standard form of the equations that can be solved is:

$$c\left(x,t,u,\frac{\partial u}{\partial x}\right)\frac{\partial u}{\partial t}=x^{-m}\frac{\partial}{\partial x}\left(x^{m}f\left(x,t,u,\frac{\partial u}{\partial x}\right)\right)+s\left(x,t,u,\frac{\partial u}{\partial x}\right) \tag{5.35}$$

for $t_0 \leq t \leq t_f$ and $a \leq x \leq b$, being the interval $[a,b]$ finite.

In Eqn. (5.35) the coefficient c is a diagonal matrix (which is specified as a vector) that multiplies the derivative with respect to t. The parameter m is associated with the geometry of the problem: m = 0, 1,2 corresponds to corresponding to slab, cylindrical, or spherical symmetry, respectively. The term $f\left(x,t,u,\frac{\partial u}{\partial x}\right)$ is a flux and $s\left(x,t,u,\frac{\partial u}{\partial x}\right)$ is a source term.

Initial conditions for this problem have the form:

$$u\left(x,t_0\right)=u_0\left(x\right) \tag{5.36}$$

and boundary conditions at $x = a$ and $x = b$ have the form of the expression:

$$p(x,t,u)+q(x,t)\,f\left(x,t,u,\frac{\partial u}{\partial x}\right)=0 \tag{5.37}$$

The function is called and the solutions saved in a matrix *u*:

u = pdepe(m,pdefun,icfun,bcfun,xmesh,tspan,options) (5.38)

where:

- xmesh defines the spatial mesh and the special boundaries a and b.

- tspan is a vector that defines the interval of simulation time, i.e. t0 and tf.

- m is the parameter of symmetry previously discussed.

- *pdfun* is a function that computes the terms *c, f,* and *s* in Eqn. (5.35). It has the form:

[c,f,s] = pdefun(x,t,u,dudx) (5.39)

where x and t are scalars, and u and dudx are vectors with np dimension. This function returns three vectors *c*, *f*, *s* with np dimension, corresponding to the diagonals elements of the matrix $c\left(x,t,u,\frac{\partial u}{\partial x}\right)$, the flux $f\left(x,t,u,\frac{\partial u}{\partial x}\right)$ and the source $s\left(x,t,u,\frac{\partial u}{\partial x}\right)$.

- *icfun* is a function which evaluates the initial conditions. It has the form:

ui = icfun(x) (5.40)

with *x* being a scalar and u_i being a np dimension vector.

- *bcfun* is a function which evaluates the boundary conditions and is expressed as:

[pl,ql,pr,qr] = bcfun(xl,ul,xr,ur,t) (5.41)

where u_l is the approximate solution at p_l, q_l are np dimension column vectors corresponding to functions $p(x,t,u)$ and $q(x,t)$ in Eqn. (5.37) evaluated in x=x_l. The same for p_r and q_r in x=x_r. u_l and u_r are the approximate solution at x=x_l and x=x_r respectively.

In the particular case of the system described by Eqns. (5.11) – (5.20) we have:

The parameter m=0 in Eqn. (5.38), corresponding to a flat symmetry.

$$c\left(x,t,u,\frac{\partial u}{\partial x}\right)=1 \tag{5.42}$$

for all the species.

$$f\left(x,t,u,\frac{\partial u}{\partial x}\right)=D_{\mathrm{M}}\left(\frac{\partial c_{\mathrm{M}}}{\partial x}\right)+D_{\mathrm{M}}\frac{z_{\mathrm{M}}F}{RT}\left(c_{\mathrm{M}}\frac{\partial \Psi}{\partial x}\right) \tag{5.43}$$

for the metal and

$$f\left(x,t,u,\frac{\partial u}{\partial x}\right)=0 \tag{5.44}$$

for R and MR

$$s\left(x,t,u,\frac{\partial u}{\partial x}\right)=k_{\mathrm{d,R}}c_{\mathrm{MR}}-k_{\mathrm{a,R}}c_{\mathrm{M}}c_{\mathrm{R}} \tag{5.45}$$

for M and R.

$$s\left(x,t,u,\frac{\partial u}{\partial x}\right)=-k_{\mathrm{d,R}}c_{\mathrm{MR}}+k_{\mathrm{a,R}}c_{\mathrm{M}}c_{\mathrm{R}} \tag{5.46}$$

for MR.

5.5.2 Implementation of a numerical tool based on the partition model

A numerical tool based on the Finite Element Method has been described in Chapter 3. The partition model allows us to adapt this program easily to take into account effects of migration. To adapt the program to this model, it is only necessary to make some modifications in the interfaces between regions with and without resin beads. In these points there will be discontinuities in the concentration profiles (as seen in Fig *5.10*), but continuity of flux is still a condition at these points.

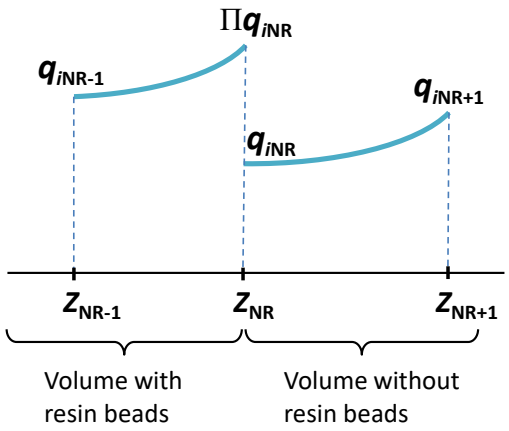

Figure 5.10. Discontinuity in the concentration profile of species i

Boundary conditions at this point ($x=\delta^r$) can be written as:

$$c_i\left(\delta^{r-},t\right)=\Pi c_i\left(\delta^{r+},t\right) \tag{5.47}$$

which relates the concentration of species *i* at both sides of the interface. This condition works at the interfaces connecting regions with and without binding agent.

$$D_i^R\left(\frac{\partial c_i}{\partial x}\right)_{x=\delta^{r-}}=D_i\left(\frac{\partial c_i}{\partial x}\right)_{x=\delta^{r+}} \tag{5.48}$$

describes the continuity of the flow at the interface located at spatial position $x=\delta^r$. It applies to mobile species.

In terms of the dimensionless variables, the boundary conditions become:

$$q_i\left(\delta^{r-},t\right)=\Pi q_i\left(\delta^{r+},t\right) \tag{5.49}$$

$$d_i^R\left.\frac{\partial q_i}{\partial z}\right|_{z^-}=d_i\left.\frac{\partial q_i}{\partial z}\right|_{z^+} \tag{5.50}$$

The discretization of Eqn. (5.51) in the point *k*=NR of the mesh, which coincides with x=δ^r, needs to incorporate some changes:

$$d_i^R\left(\frac{\Pi q_{i\mathrm{NR}}-q_{i\mathrm{NR\text{-}1}}}{h_{\mathrm{NR\text{-}1}}}\right)=d_i\left(\frac{q_{i\mathrm{NR+1}}-q_{i\mathrm{NR}}}{h_{\mathrm{NR}}}\right) \tag{5.51}$$

A Π has been introduced in Eqn (5.51), to fulfil Eqn. (5.49). Then, Eqn. (5.51) can be rewritten as:

$$-\left(\frac{d_i^R h_{\mathrm{NR}}}{d_i h_{\mathrm{NR\text{-}1}}}\right)q_{i\mathrm{NR\text{-}1}}+\left(\frac{\Pi d_i^R h_{\mathrm{NR}}}{d_i h_{\mathrm{NR\text{-}1}}}+1\right)q_{i\mathrm{NR}}-q_{i\mathrm{NR+1}}=0 \tag{5.52}$$

Which indicates that, at the point NR, the system equation that defines q_i is tridiagonal (See Chapter 3, section 3.4.2)

In the equation corresponding to the point NR-1, it is necessary to change the value $q_{i\mathrm{NR}}$ for the value $\Pi q_{i\mathrm{NR}}$ to take into account the discontinuity in the concentration of q_i at point NR (see Fig 5.10).

Finally, in the matrix α (Chapter 3, Eqn. (3.80)) it is necessary to change the term:

$$\alpha_{\mathrm{sup}}(NR-1)=\Pi\alpha_{\mathrm{sup}}(NR-1) \tag{5.53}$$

For the rest of points the program remains as described in Chapter 3.

5.6 Reference List

1. Warnken, K. W.; Zhang, H.; Davison, W. Trace metal measurements in low ionic strength synthetic solutions by diffusive gradients in thin films. *Anal. Chem.* **2005,** *77* (17), 5440-5446.

2. Dahlqvist, R.; Zhang, H.; Ingri, J.; Davison, W. Performance of the diffusive gradients in thin films technique for measuring Ca and Mg in freshwater. *Analytica Chimica Acta* **2002,** *460* (2), 247-256.

3. Peters, A. J.; Zhang, H.; Davison, W. Performance of the diffusive gradients in thin films technique for measurement of trace metals in low ionic strength freshwaters. *Anal. Chim. Acta* **2003,** *478* (2), 237-244.

4. Garmo, O. A.; Royset, O.; Steinnes, E.; Flaten, T. P. Performance study of diffusive gradients in thin films for 55 elements. *Anal. Chem.* **2003,** *75* (14), 3573-3580.

5. Alfaro-De la Torre, M.; Beaulieu, P. Y.; Tessier, A. In situ measurement of trace metals in lakewater using the dialysis and DGT techniques. *Anal. Chim. Acta* **2000,** *418* (1), 53-68.

6. Yezek, L. P.; Duval, J. F. L.; van Leeuwen, H. P. Electrokinetics of diffuse soft interfaces. III. Interpretation of data on the polyacrylamide/water interface. *Langmuir* **2005,** *21* (14), 6220-6227.

7. Yezek, L. P.; van der Veeken, P. L. R.; van Leeuwen, H. P. Donnan Effects in Metal Speciation Analysis by DET/DGT. *Environ. Sci. Technol.* **2008,** *42* (24), 9250-9254.

8. van der Veeken, P. L. R.; Pinheiro, J. P.; van Leeuwen, H. P. Metal Speciation by DGT/DET in Colloidal Complex Systems. *Environ. Sci. Technol.* **2008,** *42* (23), 8835-8840.

9. Puy, J.; Galceran, J.; Cruz-Gonzalez, S.; David, C. A.; Uribe, R.; Lin, C.; Zhang, H.; Davison, W. Metal accumulation in DGT: Impact of ionic strength and kinetics of dissociation of complexes in the resin domain. *Anal. Chem.* **2014,** *86*, 7740-7748.

10. Levy, J. L.; Zhang, H.; Davison, W.; Puy, J.; Galceran, J. Assessment of trace metal binding kinetics in the resin phase of diffusive gradients in thin films. *Anal. Chim. Acta* **2012,** *717*, 143-150.

11. Santner, J.; Kreuzeder, A.; Schnepf, A.; Wenzel, W. W. Numerical Evaluation of Lateral Diffusion Inside Diffusive Gradients in Thin Films Samplers. *Environ. Sci. Technol.* **2015,** *49* (10), 6109-6116.

12. Jimenez-Piedrahita, M.; Altier, A.; Cecilia, J.; Rey-Castro, C.; Galceran, J.; Puy, J. Influence of the settling of the resin beads on diffusion gradients in thin films measurements. *Anal. Chim. Acta* **2015,** *885*, 148-155.

13. Duval, J. F. L.; van Leeuwen, H. P. Rates of Ionic Reactions With Charged Nanoparticles In Aqueous Media. *J. Phys. Chem. A* **2012,** *116* (25), 6443-6451.

14. Town, R. M.; Buffle, J.; Duval, J. F. L.; van Leeuwen, H. P. Chemodynamics of Soft Charged Nanoparticles in Aquatic Media: Fundamental Concepts. *J. Phys. Chem. A* **2013,** *117* (33), 7643-7654.

15. Pinheiro, J. P.; Minor, M.; van Leeuwen, H. P. Metal speciation dynamics in colloidal ligand dispersions. *Langmuir* **2005,** *21* (19), 8635-8642.

16. Puy, J.; Galceran, J.; Cruz-Gonzalez, S.; David, C. A.; Uribe, R.; Lin, C.; Zhang, H.; Davison, W. Measurement of Metals Using DGT: Impact of Ionic Strength and Kinetics of Dissociation of Complexes in the Resin Domain. *Analytical Chemistry* **2014,** *86* (15), 7740-7748.

17. Ohshima, H.; Ohki, S. Donnan potential and surface-potential of a charged membrane. *Biophys. J.* **1985,** *47* (5), 673-678.

18. *MATLAB, Release 2012b;* MathWorks Inc: Natick: Massachusetts, **2012**.

19. Aguilella, V.; Belaya, M.; Levadny, V. A perturbed electric double layer near a soft polar interface. *J. Colloid. Interf. Sci.* **1997,** *186* (1), 212-214.

20. Altier, A.; Jimenez-Piedrahita, M.; Rey-Castro, C.; Cecilia, J.; Galceran, J.; Puy, J. Accumulation of Mg to Diffusive Gradients in Thin Films (DGT) Devices: Kinetic and Thermodynamic Effects of the Ionic Strength. *Anal. Chem.* **2016,** *88* (20), 10245-10251.

21. Galceran, J.; Puy, J. Interpretation of diffusion gradients in thin films (DGT) measurements: a systematic approach. *Environ. Chem.* **2015,** *12* (2), 112-122.

22. Yan, M. Q.; Lu, Y. J.; Gao, Y.; Benedetti, M. F.; Korshin, G. V. In-Situ Investigation of Interactions between Magnesium Ion and Natural Organic Matter. *Environmental Science & Technology* **2015,** *49* (14), 8323-8329.

23. Guskov, A.; Nordin, N.; Reynaud, A.; Engman, H.; Lundback, A. K.; Jong, A. J. O.; Cornvik, T.; Phua, T.; Eshaghi, S. Structural insights into the mechanisms of Mg2+ uptake, transport, and gating by CorA. *Proceedings of the National Academy of Sciences of the United States of America* **2012,** *109* (45), 18459-18464.

24. Eigen, M.; Wilkins, R. *The Kinetics and Mechanism of Formation of Metal Complexes;* 49 ed.; American Chemical Society: Washington, **1965**; Vol. 6;.pp. 55-80.

25. Morel, F. M. M.; Hering, J. G. In *Principles and Applications of Aquatic Chemistry*, John Wiley: New York, **1993**.

CHAPTER 6

COMPETITION, SATURATION AND KINETIC EFFECTS IN DGT DEVICES

Part of the material of this chapter has been published in:

Jiménez-Piedrahita, M; Altier, A; Cecilia, J; Puy, J; Galceran, J; Rey-Castro, C; Zhang, H; Davison, W. Extending the Use of Diffusive Gradients in Thin Films (DGT) to Solutions Where Competition, Saturation, and Kinetic Effects Are Not Negligible. *Anal. Chem*. Publication Date (Web): May 16, **2017**. DOI: 10.1021/acs.analchem.7b00704.

6.1 Introduction

The original idea of DGT devices was a time-averaged measurement of trace metals in soils and waters.[1-5] The set-up and the experimental deployment conditions were established to allow interpretation of a linear accumulation of metal with time using a simple expression based on a steady-state flux under perfect-sink conditions. However, the extension of DGT to a wide range of analytes [6-11] and its use in varied conditions [6,12-14] has shown that, in some situations, accumulations with time are non-linear. There are different causes for this type of accumulations. In the perfect-sink regime, the association rate constant between the resin and the analyte, is assumed to be very high, but: what happens this is not true? Analogously, in perfect-sink conditions saturation or equilibrium effects are neglected, but what happens when the amount of bound metal is not negligible? There have been examples of linear accumulations with time, but with less than theoretical slopes [15] and of the accumulation rate declining with time.[16-18] Some competition effects are observed when the effective capacity of the binding layer is approached, as in the case of Fe competing with the measurement of Mn [19] and Ca competing with the measurement of Sr.[20] For ions at high concentrations, such as the major cations Ca and Mg, the capacity issue may become a problem [21] especially when the ionic strength reduces noticeably the affinity of the binding to the Chelex.

This chapter aims to discuss the patterns of DGT accumulations that can arise, to provide a check of the accuracy of the simple DGT expression and to suggest new simplified, approximate expressions to determine the solution concentration for three situations: i) kinetic limitations in the binding to the resin, ii) saturation or equilibrium effects or iii) non-negligible competitive effects. We show how the accumulations can be quantified in terms of the required kinetic and thermodynamic constants and provide practical guidance for their use to obtain reliable estimates of solution concentrations. We focus on systems where the analyte does not react with other dissolved species (e.g. a metal in a solution without ligand). Solutions containing Mg or Mn, where all three situations can prevail, are used as examples.

The numerical simulation code explained in Chapter 3 is used to illustrate the processes that take place in the DGT device. This code is also used to check the accuracy of the analytical approximate expressions reported and the agreement of all these results with the experimental ones.

6.2 Kinetic limitations in the metal accumulation in simple metal systems

It is usually assumed that the reaction of trace metals with the binding phase is so fast and strong that the resin acts as a perfect-sink whenever saturation or equilibrium effects are negligible. Under these conditions, the accumulation can be calculated using:

$$n_{\mathrm{M}} = A\left(\frac{D_{\mathrm{M}}\, c_{\mathrm{M}}^{*}}{\delta^{g}}\right)t \qquad (6.1)$$

This model was already discussed in Chapter 2. Eqn. (6.1) has been tested using stacks of two different binding layers in DGT devices. The separate analysis of the two binding layers [22] indicate that, in simple metal solutions at pH 7, metal penetration to the back layer was very low and similar for many metals (Mn, Co, Ni, Cu, Cd, Pb). However, as pH decreases, the percentage of Mn, Cd and Co accumulated in the back resin layer (%back) increases up to 34.2%, 10.9% and 25.4%, respectively at pH 4. These results suggest that the binding of metals to Chelex-type resins may sometimes be kinetically

or thermodynamically limited as was also observed elsewhere.[17,23]

6.2.1 An approximate analytical expression for the DGT accumulation of a metal when there is penetration of the metal into the resin layer

We aim to find an approximate analytical expression for the accumulation when the association kinetic constant between the metal and the resin sites is not high enough to assume perfect-sink conditions. In this situation the metal can penetrate into the resin layer, and the metal concentration profile inside the resin will be different from zero.

Let us adhere to the following assumptions:

1. Only a metal M is present in the solution (i.e. complexation with ligands or competition effects with other cations are negligible) that is strongly bound to the resin sites

2. There is a large excess of resin sites (R) with respect to the metal bound (MR) during the deployment time of interest so that saturation effects and dissociation of MR are negligible in comparison with the metal association to the resin.

3. There are steady-state conditions (i.e. transient effects are neglected).

4. Electrostatic effects across the resin /diffusive gel interface located at $x = \delta^r$, if present, can be described by a partition factor. Let Π_M be the Boltzmann factor that relates the metal concentration at both sides of the resin-diffusive gel interface:

$$\Pi_M = \frac{c_M\left(x = \delta^{r-}\right)}{c_M\left(x = \delta^{r+}\right)} \tag{6.2}$$

The balance equation of M in the resin layer can be written as:

$$\frac{\partial c_M}{\partial t} = 0 = D_{M,R}\frac{\partial^2 c_M}{\partial x^2} - k_{a,R}c_M c_R + k_{d,R}c_{MR} \tag{6.3}$$

where $D_{M,R}$ stands for the metal diffusion coefficient in the resin layer.

According to assumption 2, there is an excess of resin sites with respect to the metal bound for all deployment times, so that c_R is essentially constant in space and time and:

$$k_{\mathrm{d,R}}\, c_{\mathrm{MR}} \ll k_{\mathrm{a,R}} c_{\mathrm{M}} c_{\mathrm{R}} \tag{6.4}$$

In these conditions, Eqn. (6.3) reduces to

$$\frac{d^2 c_{\mathrm{M}}}{dx^2} = \frac{k'_{\mathrm{a,R}}}{D_{\mathrm{M}}} c_{\mathrm{M}} = \frac{c_{\mathrm{M}}}{\lambda_{\mathrm{M}}^{\ 2}} \tag{6.5}$$

with $k'_{\mathrm{a,R}} = k_{\mathrm{a,R}} c_{\mathrm{R}}$ and

$$\lambda_{\mathrm{M}} = \sqrt{\frac{D_{\mathrm{M,R}}}{k'_{\mathrm{a,R}}}} \tag{6.6}$$

The boundary conditions for Eqn. (6.5) are

$$\left(\frac{\partial c_{\mathrm{M}}}{\partial x} \right)\Bigg|_{x=0} = 0 \tag{6.7}$$

and

$$c_{\mathrm{M}}(x = \delta^{r-}) = c_{\mathrm{M}}^{r-} \tag{6.8}$$

Solving Eqn. (6.5) and applying the boundary conditions:

$$c_{\mathrm{M}}(x) = c_{\mathrm{M}}^{r-} \frac{\cosh\left(\frac{x}{\lambda_{\mathrm{M}}} \right)}{\cosh\left(\frac{r}{\lambda_{\mathrm{M}}} \right)} \tag{6.9}$$

In steady-state, the concentration profile of MR is given by

$$c_{\mathrm{MR}}(x,t) = k'_{\mathrm{a,R}} c_{\mathrm{M}}(x) t = k'_{\mathrm{a,R}} c_{\mathrm{M}}^{r-} \frac{\cosh\left(\frac{x}{\lambda_{\mathrm{M}}} \right)}{\cosh\left(\frac{r}{\lambda_{\mathrm{M}}} \right)} t \tag{6.10}$$

And neglecting the transient, the metal accumulation can be found by integration:

$$n(t) = \int_0^{\delta^r} A c_{\mathrm{MR}}(t)\, dx = tA k'_{\mathrm{a,r}} c_{\mathrm{M}}^{r-} \lambda_{\mathrm{M}} \tanh\left(\frac{\delta^r}{\lambda_{\mathrm{M}}} \right) \tag{6.11}$$

In steady-state, the metal profile in the gel domain is linear and:

$$n(t) = \frac{D_{\mathrm{M}}(c_{\mathrm{M}}^{*} - c_{\mathrm{M}}^{r+})}{g} At \tag{6.12}$$

Being D_{M} the diffusion coefficient in the gel layer and:

$$c_{\mathrm{M}}^{r+} = \frac{c_{\mathrm{M}}^{r-}}{\Pi_{\mathrm{M}}} \tag{6.13}$$

Since in steady-state, the metal arriving to the resin (Equation (6.12)) must be equal to the metal bound (Equation (6.11)):

$$tAk_{\mathrm{a,r}}^{'} c_{\mathrm{M}}^{r-} \lambda_{\mathrm{M}} \tanh\left(\frac{\delta^{r}}{\lambda_{\mathrm{M}}}\right) = \frac{D_{\mathrm{M}}(c_{\mathrm{M}}^{*} - c_{\mathrm{M}}^{r-}/\Pi_{\mathrm{M}})}{g} At \tag{6.14}$$

And solving for c_{M}^{r-}:

$$c_{\mathrm{M}}^{r-} = \frac{c_{\mathrm{M}}^{*}}{\frac{1}{\Pi_{\mathrm{M}}} + \left(\frac{g}{\lambda_{\mathrm{M}}}\right)\left(\frac{D_{\mathrm{M,R}}}{D_{\mathrm{M}}}\right)\tanh\left(\frac{r}{\lambda_{\mathrm{M}}}\right)} \tag{6.15}$$

Replacing Eqn. (6.15) in Eqn. (6.11) we have an expression for the accumulation of metal:

$$n(t) = \frac{D_{\mathrm{M,R}} c_{\mathrm{M}}^{*}}{\delta^{g}\left(\frac{D_{\mathrm{M,R}}}{D_{\mathrm{M}}}\right) + \frac{\lambda_{\mathrm{M}}}{\Pi_{\mathrm{M}}}\coth\left(\frac{\delta^{r}}{\lambda_{\mathrm{M}}}\right)} At \tag{6.16}$$

When $D_{\mathrm{M,R}} = D_{\mathrm{M}}$, equation (6.16) reduces to

$$n(t) = \frac{D_{\mathrm{M}} c_{\mathrm{M}}^{*}}{\delta^{g} + \frac{\lambda_{\mathrm{M}}}{\Pi_{\mathrm{M}}}\coth\left(\frac{\delta^{r}}{\lambda_{\mathrm{M}}}\right)} At \tag{6.17}$$

The term $\frac{\lambda_{\mathrm{M}}}{\Pi_{\mathrm{M}}}\coth\left(\frac{\delta^{r}}{\lambda_{\mathrm{M}}}\right)$ is just a measure of the effective distance of penetration of M corresponding to the distance necessary for the metal concentration to drop to zero in the resin domain by linear extrapolation of the metal profile at the resin/diffusive gel interface. Accordingly, Eqn. (6.17) is parallel to Eqn. (6.1) when δ^{g} is replaced with

$\frac{\lambda_M}{\Pi_M}\coth\left(\frac{\delta^r}{\lambda_M}\right)$, Eqn. (6.17) can be used to determine the metal concentration in solution whenever λ_M or $k'_{a,R}$ are known.

6.2.2 Accumulation of Mg with thermodynamic limitations

Experimental accumulation of Mg in DGT devices, with a stack of two resin discs deployed in a solution at pH 7.5 and ionic strength 100mM, serves as an example of accumulation under kinetic limiting conditions. Indeed, as can be seen in Fig. 6.1, the accumulation in a solution with c^*_{Mg} = 0.09 mol m^{-3} is almost linear for times smaller than 10 h, with a slope smaller than that of the perfect-sink case (dotted line). For longer deployment times, the accumulation bends downwards, indicating that equilibrium effects are non-negligible and steady-state conditions are lost.

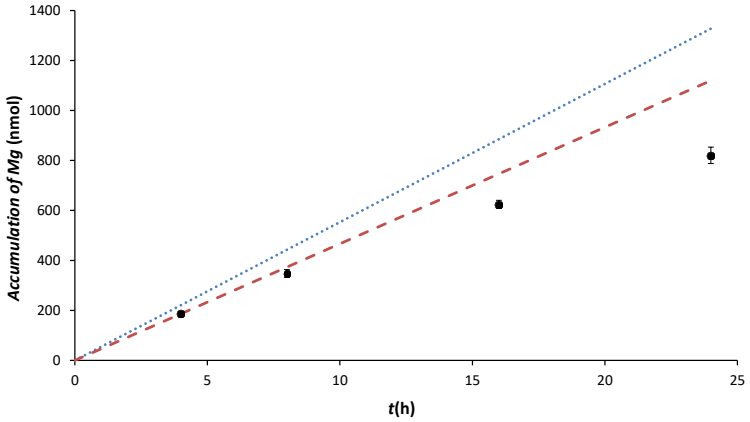

Figure 6.1. Time evolution of the total accumulation of Mg in DGT devices with two resin discs. Markers correspond to experimental accumulations at salt background concentrations of 100 mol·m^{-3} at pH 7.5. Dashed line corresponds to results obtained with Eqn.(6.17) when $k_{a,R}$=1.7×10^{-4} m^3 mol^{-1} s^{-1} and $k_{d,R}$=10^{-4} s^{-1}. Dotted line corresponds to accumulation of Mg obtained with Eqn. (6.1). Other parameters: Π_M=1.7, D_M=4.94×10^{-10} m^{2}s^{-1}, δ^r=8×10^{-4} m (corresponding to two resin discs), δ^g=1.1×10^{-3} m, $C_{T,R}$=28mol m^{-3} and c^*_{Mg}=0.09 mol m^{-3}.

The use of Eqn. (6.17) to calculate $k_{a,R}$ requires the determination of the slope at short times before downward bending starts. Using the first data point, we obtained $k_{a,R}$ =1.7×10^{-4} m^3 mol^{-1}s^{-1}, which introduced in Eqn. (6.17) yields the dashed line in Fig. 6.1.

Normalized concentration profiles for Mg obtained by simulation (with the conditions

of Fig. 6.1) are presented in Fig. 6.2. It is possible to see a jump in the concentration of Mg at the resin layer/diffusive gel interface. This effect was studied in Chapter 5, and is produced by electrostatic interactions between the metal cation and the charges in the resin and the supporting electrolyte. The effect of electrical migration on the concentration of metal can be approximated using a partition factor at the resin-gel interface. For the ionic strength of this experiment (100mM), a partition factor Π_M =1.6, was used. This value was experimentally measured as explained in Chapter 5. Fig. 6.2 also shows the penetration of free Mg in the resin domain, which means that accumulation is kinetically controlled for this ionic strength. Finally, changes on the concentration profiles with time are further evidence that metal accumulation does not occur under steady-state conditions.

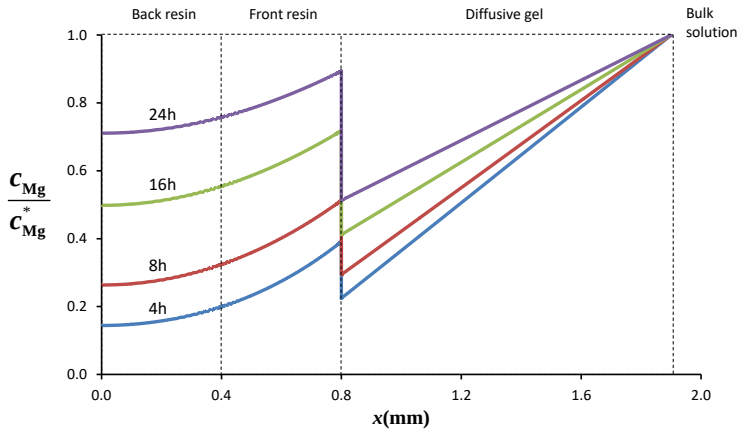

Figure 6.2. Normalized Mg concentration profiles at different times for the conditions of Fig. 6.1. Vertical dashed lines indicate the frontiers of each resin gel disc.

6.3 Saturation and equilibrium effects

The net binding rate of metal to the resin can be written as:

$$\frac{\partial c_{MR}}{\partial t} = k_{a,R} c_M c_R - k_{d,R} c_{MR} \tag{6.18}$$

where c_M and c_R are the local concentrations of free M and free resin sites at the spatial position considered and $k_{d,R}$ is the kinetic dissociation rate constant. The first term in the right hand side of Eqn. (6.18) stands for the association rate, while the

second one quantifies the dissociation. For a sufficiently large amount of bound metal, the net metal binding rate decreases as time increases. This decrease arises from both the increase of the rate of dissociation and the decrease of the association rate, as Eqn. (6.18) indicates. Dissociation becomes non-negligible when equilibrium (or "effective capacity") between bound and bulk free metal is approached and the decrease of the association term becomes non-negligible when equilibrium is closely approached or when competitive effects are relevant as will be commented in the next Section.

6.3.1 An approximate analytical expression for the DGT accumulation of a metal when saturation or equilibrium effects are non-negligible

An approximate analytical expression able to reproduce the data when equilibrium between the bound metal and the bulk metal is approached requires that both the association and dissociation processes of metal to the resin sites have to be considered.

Let us derive an approximate analytical expression for the accumulation in DGT devices when equilibrium effects between free and bound metal to the resin sites are non-negligible. Let us assume:

1. A metal concentration profile homogeneous (flat) in the resin domain and linear in the diffusive disc. Disregarding the diffusion of free M in the resin (by assuming a flat profile of free metal) is equivalent to assuming an infinite D_{M} value in the resin, while a finite value of D_{M} is used in the gel domain

2. A homogeneous concentration profile (flat) of the bound metal in the resin disc.

3. A concentration of free resin sites homogeneous and time independent as a first approximation which will be later refined.

4. Electrostatic effects across the resin /diffusive gel interface located at $x = \delta^r$, if present, can be described by a partition factor. Let Π_{M} be the Boltzmann factor that relates the metal concentration at both sides of the resin-diffusive gel interface:

$$\Pi_{\mathrm{M}} = \frac{c_{\mathrm{M}}\left(x=\delta^{r-}\right)}{c_{\mathrm{M}}\left(x=\delta^{r+}\right)} \tag{6.19}$$

Let us denote as c_{M}^{r} and c_{MR}^{r} the concentrations of free and bound metal in the resin domain ($c_{\mathrm{M}}^{r} = c_{\mathrm{M}}\left(x=\delta^{r-}\right)$). The flux of metal through the plane $x=\delta^{r}$ can be written as:

$$J = D_{\mathrm{M}}\left(\frac{dc_{\mathrm{M}}}{dx}\right)\Bigg|_{x=\delta^{r}} = \frac{1}{A}\frac{dn_{\mathrm{M}}}{dt} = D_{\mathrm{M}}\left(\frac{c_{\mathrm{M}}^{*} - c_{\mathrm{M}}^{r}/\Pi_{\mathrm{M}}}{\delta^{g}}\right) \tag{6.20}$$

Where n_{M} stands for the total accumulation of metal, c_{M}^{*} is the concentration of metal in the bulk solution, $c_{\mathrm{M}}^{r}/\Pi_{\mathrm{M}}$ the free metal concentration in the gel side of the resin-diffusive gel interface, δ^{g} represents the thickness of the diffusive gel, D_{M} is the diffusion coefficient of metal ion (common to all phases) and A and δ^{r} are the effective area and the thickness of the resin disc, respectively.

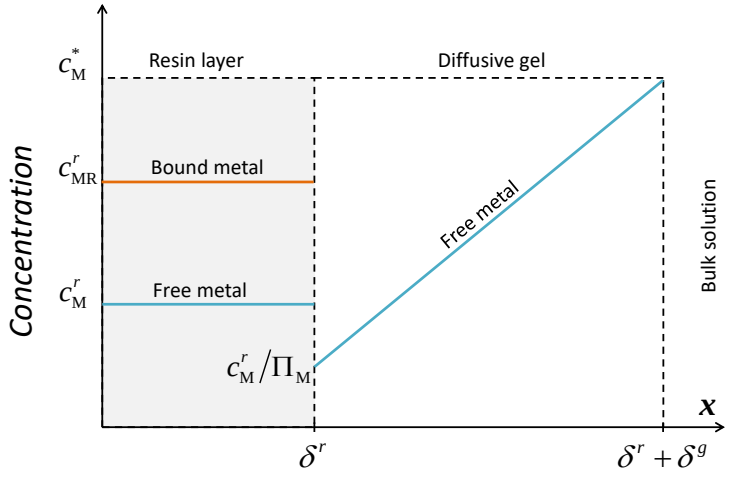

Figure 6.3. Schematic representation of the concentration profiles of free and bound metal.

The balance equation for free metal inside the resin ($0 \le x \le \delta^{r}$) can be written as:

$$A\delta^{r}\frac{dc_{\mathrm{M}}^{r}}{dt} = AD_{\mathrm{M}}\left(\frac{c_{\mathrm{M}}^{*} - c_{\mathrm{M}}^{r}/\Pi_{\mathrm{M}}}{\delta^{g}}\right) - A\delta^{r}k'_{\mathrm{a,R}}c_{\mathrm{M}}^{r} + A\delta^{r}k_{\mathrm{d,R}}c_{\mathrm{MR}}^{r} \tag{6.21}$$

where:

$$k'_{\mathrm{a,R}} = k_{\mathrm{a,R}}c_{\mathrm{R}} \tag{6.22}$$

$k_{\mathrm{a,R}}$ and $k_{\mathrm{d,R}}$ stand for the association and dissociation rate constants of metal with the

resin sites, respectively. Eqn. (6.21) indicates that the time variation of the free metal in the resin domain is equal to the entering metal through the diffusive flux minus the free metal that gets complexed during the time unit and plus the free metal that appears by dissociation.

Likewise, for the bound metal:

$$A\delta^r \frac{dc^r_{\mathrm{MR}}}{dt} = A\delta^r k'_{\mathrm{a,R}} c^r_{\mathrm{M}} - A\delta^r k_{\mathrm{d,R}} c^r_{\mathrm{MR}} \tag{6.23}$$

The initial conditions are:

$$c^r_{\mathrm{M}}(0) = 0 \text{ and } c^r_{\mathrm{MR}}(0) = 0 \tag{6.24}$$

If we provisionally assume, according to hypothesis 3, that c_{R} is time independent (i.e. excess of resin sites), $k'_{\mathrm{a,R}}$ is a constant and Eqns. (6.21) - (6.23) form a system of coupled ordinary differential equations of first order with constant coefficients that allow to determine $c^r_{\mathrm{M}}(t)$ and $c^r_{\mathrm{MR}}(t)$ with the help of the initial conditions (6.36). A general solution of this system can be obtained by uncoupling the system defining an appropriate combination of the unknowns.

The solutions are given by

$$c^r_{\mathrm{M}}(t) = \frac{\Pi_{\mathrm{M}} c^*_{\mathrm{M}}}{2H}\left(2H + \left(-H + F + 2k'_{\mathrm{a,R}} + k_{\mathrm{d,R}}\right)\mathrm{e}^{\frac{1}{2}\left(F - H - k_{\mathrm{d,R}}\right)t} - \left(H + F + 2k'_{\mathrm{a,R}} + k_{\mathrm{d,R}}\right)\mathrm{e}^{\frac{1}{2}\left(F + H - k_{\mathrm{d,R}}\right)t}\right) \tag{6.25}$$

and

$$c^r_{\mathrm{MR}}(t) = \frac{K_{\mathrm{MR}} c_{\mathrm{R}} \Pi_{\mathrm{M}} c^*_{\mathrm{M}}}{2H}\left(-2H + \left(F + H - k_{\mathrm{d,R}}\right)\mathrm{e}^{\frac{1}{2}\left(F - H - k_{\mathrm{d,R}}\right)t} + \left(-F + H + k_{\mathrm{d,R}}\right)\mathrm{e}^{\frac{1}{2}\left(F + H - k_{\mathrm{d,R}}\right)t}\right) \tag{6.26}$$

where:

$$F = -\left(\frac{D_{\mathrm{M}}}{\Pi_{\mathrm{M}} \delta^r \delta^g} + k'_{\mathrm{a,R}}\right) \tag{6.27}$$

$$H = \sqrt{F^2 + 2Fk_{\mathrm{d,R}} + 4k'_{\mathrm{a,R}} k_{\mathrm{d,R}} + k^2_{\mathrm{d,R}}} \tag{6.28}$$

and K_{MR} is the stability constant between the metal and the resin sites:

$$K_{MR} = \frac{k_{a,R}}{k_{d,R}} \tag{6.29}$$

The term $\left(H - F - 2k'_{a,R} - k_{d,R}\right)e^{\frac{1}{2}\left(F-H-k_{d,R}\right)t}$ in Eqn. (6.25) and the term $\left(F + H - k_{d,R}\right)e^{\frac{1}{2}\left(F-H-k_{d,R}\right)t}$ in Eqn. (6.26) are negligible for almost all the deployment time in comparison to the terms $\left(H + F + 2k'_{a,R} + k_{d,R}\right)e^{\frac{1}{2}(F+H-k_{d,R})t}$ and $\left(-F + H + k_{d,R}\right)e^{\frac{1}{2}\left(F+H-k_{d,R}\right)t}$. Indeed, assuming $k'_{a,R} \gg k_{d,R}$ for the cases of interest ($K'_{MR} >> 1$), we have $H \approx -F \approx k'_{a,R}$, so that $F + H - k_{d,R} << F - H - k_{d,R}$. The exponential terms with the highest exponent suffer a faster decay with time so that they can be neglected for most of the deployment time. Neglecting the corresponding exponential terms and assuming $H \approx -F \approx k'_{a,R}$ in Eqns. (6.25) and (6.26) (except in the exponential term) the concentrations of free and bound metal in the resin domain become:

$$c^r_M(t) \approx \Pi_M c^*_M\left(1 - e^{-bt}\right) \tag{6.30}$$

and

$$c^r_{MR}(t) \approx \frac{\Pi_M c^*_M k'_{a,R}}{k_{d,R}}\left(1 - e^{-bt}\right) = K_{MR}\Pi_M c^*_M c_R\left(1 - e^{-bt}\right) \tag{6.31}$$

with

$$b = \left(k_{d,R} - F - H\right)/2 \tag{6.32}$$

As saturation could be approached for high metal concentrations, it would be convenient to overcome the condition that c_R remains time-independent during the accumulation. A rough estimate of a time dependent expression for c_R, can be derived assuming local equilibrium between M, R and MR,

$$k_{a,R} c_M c_R = k_{d,R} c_{MR} \tag{6.33}$$

Using Eqn. (6.29), Eqn. (6.30) and $c_{MR} + c_R = c_{TR}$, Eqn. (6.33) turns into:

$$c_{\mathrm{R}}(t)=\frac{c_{\mathrm{TR}}}{1+K_{\mathrm{MR}}c_{\mathrm{M}}(t)}=\frac{c_{\mathrm{TR}}}{1+K_{\mathrm{MR}}\Pi_{\mathrm{M}}c_{\mathrm{M}}^{*}\left(1-\mathrm{e}^{-bt}\right)} \tag{6.34}$$

Replacing Eqn. (6.34) in Eqn. (6.31), the concentration of bound metal becomes

$$c_{\mathrm{MR}}^{r}(t)=\frac{\Pi_{\mathrm{M}}K_{\mathrm{MR}}c_{\mathrm{TR}}c_{\mathrm{M}}^{*}\left(1-\mathrm{e}^{-bt}\right)}{1+\Pi_{\mathrm{M}}K_{\mathrm{MR}}c_{\mathrm{M}}^{*}\left(1-\mathrm{e}^{-bt}\right)} \tag{6.35}$$

Finally, the total accumulation of metal can be written as

$$n_{\mathrm{T}}(t)=A\delta^{r}c_{\mathrm{MR}}^{r}(t)=\frac{A\delta^{r}\Pi_{\mathrm{M}}K_{\mathrm{MR}}c_{\mathrm{TR}}c_{\mathrm{M}}^{*}\left(1-\mathrm{e}^{-bt}\right)}{1+\Pi_{\mathrm{M}}K_{\mathrm{MR}}c_{\mathrm{M}}^{*}\left(1-\mathrm{e}^{-bt}\right)} \tag{6.36}$$

Figures 6.4 and 6.5 show a comparison between the accumulations of metal calculated using numerical simulation (continuous lines) with those predicted with Eqn. (6.36) (dotted lines), for different values of the stability and the association rate constant between the metal and the resin sites. The agreement of both curves for all evaluated cases suggests that Eqn. (6.36) can replace numerical simulation in approaching non-linear accumulations in DGT.

As Figure 6.4 shows, the accumulation is thermodynamically limited, as the bending indicates. When the stability constant increases, the thermodynamic limitation is less severe and the equilibrium concentration of bound metal increases which leads to the increase of the plateau in the accumulation plot.

The increase of the kinetic constants, instead, does not modify the plateau, whenever the stability constant is fixed, see Fig. 6.5, but the plateau is reached at shorter times until convergence to a limiting curve were kinetic constants cease to have an impact, indicating that the accumulation is controlled by transport or equilibrium.

A simple equation for the limiting curve can be obtained if c_{MR}^{r} in Eqn (6.21) is replaced with $c_{\mathrm{MR}}^{r}=K_{\mathrm{MR}}c_{\mathrm{R}}c_{\mathrm{M}}^{r}$, which indicates that the metal binding has proceed in the resin domain until equilibrium is reached. Eqn (6.21) becomes then an equation to determine

c_M^r and the accumulation can be written as:

$$n_T(t) = A\delta^r c_{MR}^r(t) = \frac{A\delta^r \Pi_M K_{MR} c_{TR} c_M^*}{1+\Pi_M K_{MR} c_M^*}\left(1-e^{-\frac{D_M}{\delta^r \delta^g \Pi(1+K_{MR}c_{TR})}t}\right) \quad (6.37)$$

Eqn. (6.37), plotted in Fig. 6.5 as dashed red line, shows good agreement with numerical simulation results obtained for high enough kinetic constants.

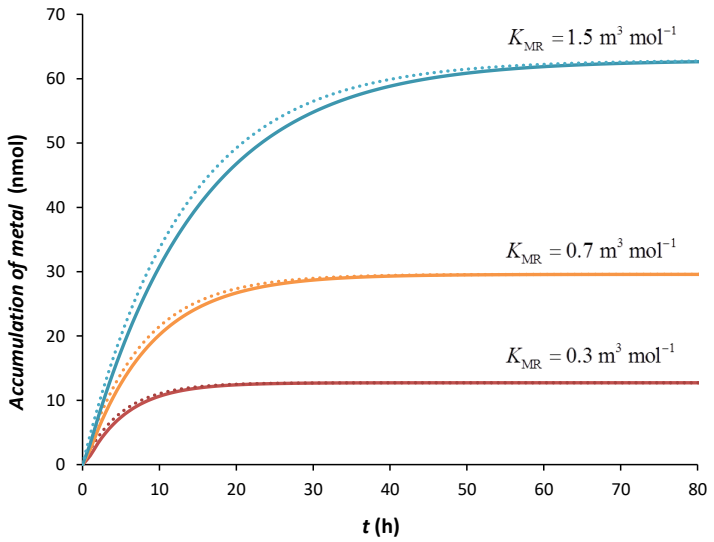

Figure 6.4. Accumulation of metal in a standard DGT device from a solution with c_M^* = 0.01 mol m^{-3} for different values of K_{MR} (see label above the lines). Continuous lines correspond to numerical simulation and dotted lines correspond to Eqn. (6.36.) Parameters used: $k_{d,R}$ =1×10^{-4} s^{-1}, D_M =4.94 ×10^{-10} m^2 s^{-1} , c_{TR} =28, Π =1.0, effective area of the sensor 3.80×10^{-4} m^2, thickness (δ^r) of the resin disc equal to 4.0×10^{-4}m and aggregated thickness (δ^g) of the gel, filter and DBL, 1.1×10^{-3}m.

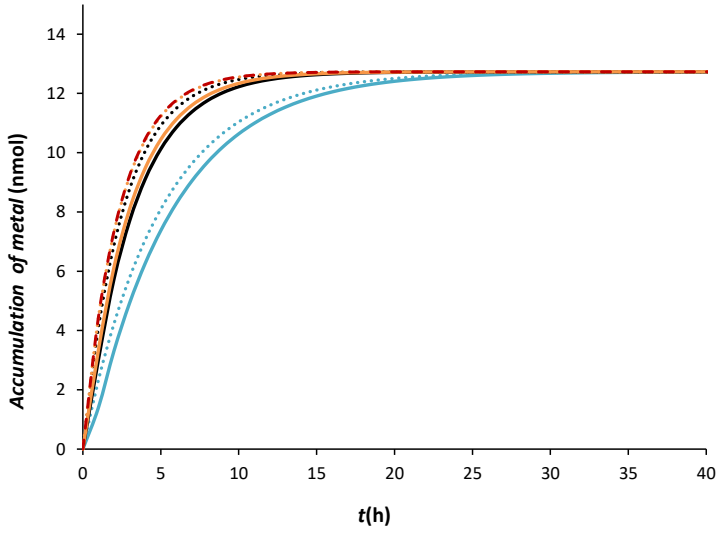

Figure 6.5. Accumulation of metal in a standard DGT device from a solution with $c_M^* = 0.01$ *mol* m^{-3}, $K_{MR} = 0.3$ m^3 mol^{-1} *and* $k_{a,R} = 3\times10^{-5}$ m^3 mol^{-1} s^{-1} *(blue lines),* $k_{a,R} = 3\times10^{-4}$ m^3 mol^{-1} s^{-1} *(black lines) and* $k_{a,R} = 3\times10^{-3}$ m^3 mol^{-1} s^{-1} *(orange lines) . Continuous lines correspond to numerical simulation, dotted lines correspond to Eqn. (6.36.) and dashed red line was obtained with Eqn. (6.37). Other parameters as in Fig 6.4.*

A final comment can be devoted to the initial slope of the accumulation plot. When the binding to the resin is fast enough to reach local equilibrium, Eqn. (6.37) indicates that the initial slope is

$$slope_{t\to 0} = \left(\frac{AD_M c_M^*}{\delta^g}\right)\left(\frac{K_{MR}c_{TR}}{1+K_{MR}c_{TR}}\right) \tag{6.38}$$

For $K_{MR}c_{TR} >> 1$, the binding is fast and complete and Eqn. (6.38) reduces to

$$slope_{t\to 0} = \frac{AD_M c_M^*}{\delta^g} \tag{6.39}$$

which corresponds to the perfect-sink behaviour.

If the kinetics of the metal binding is not fast enough to reach equilibrium in the resin domain, the initial slope of the accumulation plot has to be obtained from Eqn. (6.26). Eqn. (6.36) could not be a good approximation due to the cancellation of the first exponential term in Eqn. (6.26) according to the faster decay of this term in comparison to the second exponential one.

Alternatively, a simpler way to obtain an analytical expression for the initial slope of the accumulation plot under kinetic influence consists in considering Eqn. (6.17). This equation has been obtained neglecting the dissociation term in the balance equation of the metal which could be a reasonable approximation for $t \to 0$. Using Eqn. (6.17), the initial slope of the accumulation plot can be written as:

$$slope_{t\to 0} = \frac{AD_{\mathrm{M}}c_{\mathrm{M}}^{*}}{\delta^{g} + \frac{\lambda_{\mathrm{M}}}{\Pi_{\mathrm{M}}}\coth\left(\frac{\delta^{r}}{\lambda_{\mathrm{M}}}\right)} \tag{6.40}$$

For $\lambda_{\mathrm{M}} << \delta^{r}$, $\coth\left(\delta^{r}/\lambda_{\mathrm{M}}\right) \to 1$ and the slope becomes

$$slope_{t\to 0} = \frac{AD_{\mathrm{M}}c_{\mathrm{M}}^{*}}{\delta^{g} + \lambda_{\mathrm{M}}/\Pi_{\mathrm{M}}} \tag{6.41}$$

which is a very simple approximate expression for the initial slope.

Conversely, when $\lambda_{\mathrm{M}} >> \delta^{r}$, $\coth\left(\delta^{r}/\lambda_{\mathrm{M}}\right) \to \infty$ and the slope tends to zero indicating that there is no accumulation in agreement with the fact that $k_{\mathrm{a,R}} \to 0$ when $\lambda_{\mathrm{M}} >> \delta^{r}$. Eqn. (6.41) indicates that the slope is mainly dependent on the kinetic association constant while the dissociation constant plays the main role in the bending of the accumulation curve and in the plateau which is determined by the affinity.

The initial slope of the accumulation plot can, then, be helpful in assessing if there is kinetic or thermodynamic influence in the accumulation. The largest slope that could be reached is proportional to D_{M} and corresponds to the perfect-sink expression. If the slope is smaller, the accumulation is thermodynamically limited and given by Eqn. (6.38). If the slope is smaller than predicted by Eqn. (6.38), the accumulation is kinetically limited and given by Eqn. (6.41).

6.3.2 Accumulation of Mg with thermodynamic limitations

Fig. 6.6 shows a clear case where thermodynamic limitations due to equilibrium have been observed. It corresponds to the Mg binding to DGT devices with a stack of two

resin discs in a solution at pH 7.5 and ionic strength of 500 mM. (Details of the experimental setup can be found in Chapter 5, section 5.3.1).

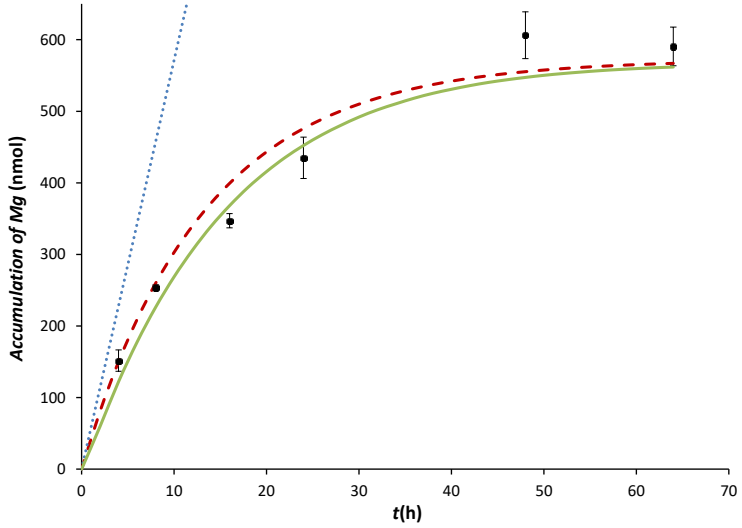

Figure 6.6. Evolution of Mg accumulation at salt background concentration ($NaNO_3$)= 500 mol m^{-3}. Markers: experimental accumulations (both discs) in DGT devices with a stack of two resin discs at pH=7.5. Continuous line stands for numerical simulation, dashed lines for results obtained with Eqn. (6.36) and dotted line for results obtained with Eqn. (6.1), i.e. corresponding to perfect-sink conditions. $k_{a,R}$ *=7.0×10^{-5} m^3 mol^{-1} s^{-1},* K_{MR} *=0.7 m^3 mol^{-1},* Π_M *=1.1,* c_M^* *=0.093 mol m^{-3}. Other parameters as in Figure 6.1.*

As explained in Chapter 5, the Mg accumulation is kinetically controlled for ionic strength above 10 mM. The influence of the ionic strength can be explained by a salt effect on the kinetic association constant of Mg, which increases as ionic strength decreases due to the increase of the electrostatic attraction between positive Mg cations and negative resin sites. This explanation is also consistent with the decrease of the %back as ionic strength decreases, since a faster metal binding reduces the penetration of the free Mg in the resin disc. Concomitant to the dependence of the kinetic association constant on ionic strength, there is an influence on the stability constant of the Mg binding to the Chelex beads. Indeed, within the Eigen model, the kinetic dissociation constant will be independent of ionic strength, so that the dependence of $k_{a,R}$ of Mg on ionic strength is the same as that of the stability constant. At high ionic strength, the stability constant of the Mg binding to the Chelex beads takes the smallest value and, accordingly, equilibrium phenomena can easily be seen at earlier accumulation times since the bound metal in equilibrium with the bulk concentration takes lower values.

Fig. 6.6 shows the bending of the experimental values for metal accumulation (see markers) approaching equilibrium conditions for long times (notice the decrease of the slope of the accumulation). Fig. 6.6 also shows, in continuous line, the accumulation calculated with numerical simulation after fitting the equilibrium and kinetic association constants to the experimentally obtained total accumulation and to the percentage in the back resin disc [24]. These results have been used to plot concentration profiles corresponding to different times in Fig. 6.7. The approach to equilibrium is confirmed by the increase of the average free metal concentration in the resin domain as time increases as Fig. 6.7 indicates. When the concentration of unbound metal in the resin approaches the bulk solution concentration, at t>40h (See Fig. 6.7), there is almost no net accumulation (the rate of association is close to that of dissociation) as seen at the rightmost part of Fig. 6.6.

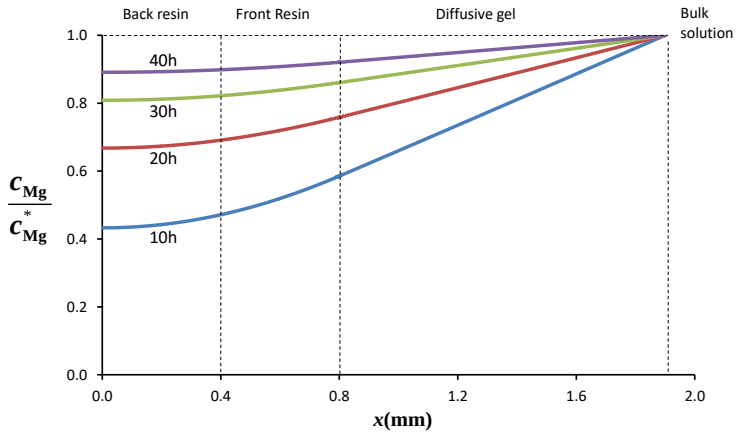

Figure 6.7. Normalized Mg concentration profiles at time 10, 20, 30 and 40 h for the conditions of Fig. 6.6. Vertical dashed lines indicate the frontiers of each resin gel disc.

A good agreement between Eqn. (6.36), plotted with dashed line, with numerical simulation results and experimental accumulations can be seen in Fig. 6.6 using the Mg binding parameters estimated in [24] and reported in the caption of Fig. 6.6. Experimental values of the Boltzmann factor Π reported in Chapter 5, Table 5.2, were used.

6.4 Competition effects

Now we are going to study the influence of other metal cations on the accumulation evolution of a metal cation of interest. This influence can also lead to a departure of the linear accumulation regime and to an underestimation of the actual species concentration in solution if Eqn. (6.1) is used.

6.4.1 Competition between two metals

In general, in probing metals with DGT, competition effects will arise between a major concentration cation and a trace metal. No competition effects are expected between trace metals themselves given the large amount of Chelex used per disc. As an example we can study the total accumulation of a trace metal (^{1}M) in presence of a second metal (^{2}M) at a higher concentration than that of ^{1}M, for different values of the association rate constant of ^{2}M, $k_{a,^2\mathrm{MR}}$. Both metals compete to bind to the resin sites. The reactions for these metals with resin sites will be:

$$^1\mathrm{M} + \mathrm{R} \rightleftarrows {}^1\mathrm{MR} \tag{6.42}$$

$$^2\mathrm{M} + \mathrm{R} \rightleftarrows {}^2\mathrm{MR} \tag{6.43}$$

Using the numerical simulation program described in Chapter 3, and assuming that the interaction between metals is only through the occupation of the resin sites, we can obtain the accumulation for both metals at different times. Accumulations of ^{1}M and ^{2}M, for different values of $k_{a,^2\mathrm{MR}}$ can be seen in Figure 6.8. In panel (a), the accumulation of ^{1}M in absence of ^{2}M (line 1) does not correspond to perfect-sink conditions (dotted line), but is very close. The addition of a big concentration of ^{2}M to the sample causes a decreasing on the accumulation of ^{1}M. The influence of ^{2}M on the accumulation of ^{1}M increases as the value of $k_{a,^2\mathrm{MR}}$ increases, because the occupation of the resin sites by ^{2}M is faster.

Panel (b) of Figure 6.8 depicts the accumulation of ^{2}M. Since $c^{*}_{1_M} \ll c^{*}_{2_M}$, ^{2}M requires less time to reach the binding equilibrium than ^{1}M. Comparing both panels of Figure 6.8 it is clear that as bigger is the accumulation of ^{2}M, lower is the accumulation of ^{1}M, for a constant value of $c^{*}_{1_M}$. This is an evident case of competition.

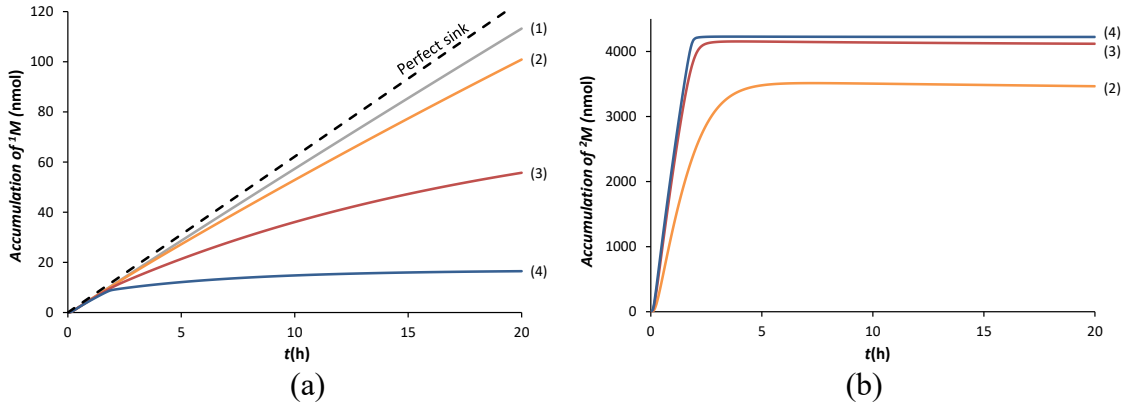

Figure 6.8. Accumulations of ^{1}M panel (a) and ^{2}M panel (b), in a standard DGT device using numerical simulations. (1) is the accumulation of ^{1}M without ^{2}M. In both panels: (2) $k_{a,^{2}MR}$ =1.0×10^{-4} m^{3}mol^{-1}s^{-1}, (3) $k_{a,^{2}MR}$ =1.0×10^{-3} m^{3}mol^{-1}s^{-1}and (4) $k_{a,^{2}MR}$ =5.0×10^{-3} m^{3}mol^{-1}s^{-1}. Other parameters used: $c^{*}_{1_M}$ =0.01 mol m^{-3}, $c^{*}_{2_M}$ =5.0 mol m^{-3}, c_{TR} =28 mol m^{-3}, Π =1.0, $k_{a,^{1}MR}$ =1.0×10^{-2} m^{3}mol^{-1}s^{-1}, $k_{d,^{1}MR}$ =1.0×10^{-4} s^{-1}, $k_{d,^{2}MR}$ =1.0×10^{-4} s^{-1}, D_{1_M} =5.0×10^{-10} m^{2} s^{-1}, D_{2_M} =5.0×10^{-10} m^{2} s^{-1}, δ^{r} =4×10^{-4} m, δ^{g} =1.1×10^{-3} m. Dashed line stands for accumulation in perfect-sink conditions.

6.4.2 Analytical approximate expression for the DGT accumulation of a metal when competitive effects are non-negligible

We aim at finding an approximate analytical expression for the accumulation of a trace metal (^{1}M) in presence of a second metal (^{2}M) at a higher concentration than that of ^{1}M. Both metals compete to bind to the resin sites in a set of parallel reactions:

$$^{1}\mathrm{M} + \mathrm{R} \rightleftarrows {}^{1}\mathrm{MR} \qquad (6.44)$$

$$^{2}\mathrm{M} + \mathrm{R} \rightleftarrows {}^{2}\mathrm{MR} \qquad (6.45)$$

Assumptions:

1. The concentration profiles of the free and bound metal for both ^{1}M and ^{2}M are homogeneous in the resin domain and the concentration profiles of both free metals are linear in the diffusive gel.
2. The interaction between metals is only through the occupation of the resin sites.
3. Electrostatic effects derived by low ionic strength can be described by a partitioning of the charged species at the resin-diffusive gel interface.

An equation parallel to (6.21) can be written for each metal ^{1}M and ^{2}M which indicates that interaction effects are just due to the free resin sites. With assumptions 1, 2 and 3, and a time independent concentration of free resin sites, Eqns. (6.30) and (6.31) hold for each metal.

The concentrations of bound ^{1}M or ^{2}M can then be written as

$$c^r_{i\,\mathrm{MR}}(t) = \Pi_\mathrm{M} K_{i\,\mathrm{MR}} c_\mathrm{R} c^*_{i\,\mathrm{MR}} \left(1 - \mathrm{e}^{-b_i t}\right) \tag{6.46}$$

and the accumulation of ^{1}M

$$n_{\mathrm{T},^1\mathrm{M}}(t) = A\delta^r c^r_{^1\mathrm{MR}}(t) = A\delta^r \Pi_\mathrm{M} K_{^1\mathrm{MR}} c_\mathrm{R} c^*_{^1\mathrm{M}} \left(1 - \mathrm{e}^{-b_1 t}\right) \tag{6.47}$$

where $c^*_{^1\mathrm{MR}}$ and $c^*_{^2\mathrm{MR}}$ are the bulk concentrations of the metals, b_1 and b_2 are given by Eqn. (6.32), and $K_{^1\mathrm{MR}}$ and $K_{^2\mathrm{MR}}$ are the respective stability constants between ^{1}M or ^{2}M and R.

Due to the high concentration of ^{2}M, its time to reach equilibrium can be much shorter than the deployment time. The metal concentration in the resin domain can then be approximated by $c^r_{^2\mathrm{M}} \approx c^*_{^2\mathrm{M}}$ and since $K_{^2\mathrm{MR}} c^*_{^2\mathrm{M}} >> K_{^1\mathrm{MR}} c^*_{^1\mathrm{MR}}$, c_R can be written as

$$c_\mathrm{R} = \frac{c_\mathrm{TR}}{1 + K_{^2\mathrm{MR}} \Pi_\mathrm{M} c^*_{^2\mathrm{MR}}} \tag{6.48}$$

Finally, if $K_{^2\mathrm{MR}}c^*_{^2\mathrm{M}} \ll 1$ and $k'_{\mathrm{a},^2\mathrm{MR}} \gg \frac{D_{^1\mathrm{M}}}{\Pi_\mathrm{M}\delta^r\delta^g}$, the approximation (6.47) becomes

$$n_{\mathrm{T},^1\mathrm{M}}(t) = A\delta^r c_\mathrm{R}\Pi_\mathrm{M}K_{^1\mathrm{MR}}c^*_{^1\mathrm{M}}\left(1-\mathrm{e}^{-k_{\mathrm{d},^1\mathrm{MR}}t/2}\right) \tag{6.49}$$

Alternatively, when a time independent c_R is not a good approximation during the accumulation of ^{1}M, c_R could be written as

$$c_\mathrm{R}(t) = \frac{c_\mathrm{TR}}{1+K_{^1\mathrm{MR}}\Pi_\mathrm{M}c^*_{^1\mathrm{MR}}\left(1-\mathrm{e}^{-b_1t}\right)+K_{^2\mathrm{MR}}\Pi_\mathrm{M}c^*_{^2\mathrm{M}}\left(1-\mathrm{e}^{-b_2t}\right)} \tag{6.50}$$

Which considers that the occupied sites decrease as time increases due to the accumulation of both ^{1}M and ^{2}M.

To check the accuracy of the analytical expressions deduced in section 2.1, comparisons between accumulations of metal ^{1}M obtained using numerical simulations (continuous blue line) and using Eqns. (6.47)-(6.48) (dashed green line), Eqns. (6.48)-(6.49) (dotted black line) and Eqns. (6.47)-(6.50) (dashed dotted red line) have been done. Different values of the stability constant between ^{1}M and the resin sites have been used in the different panels. The stability constant of ^{1}M in Panel a) corresponds to the Mn stability constant under the conditions of Fig. 6.10.

The accuracy of Eqns. (6.49)-(6.48) (dotted black line) with respect to values computed with numerical simulation is quite good, justifying its use from now on. Increasing the stability constant, panels b) and c), the accuracy of Eqns. (6.48)-(6.49) decreases, but the approximation based on the use of (6.47)-(6.48) (dashed green line) maintains a good agreement with the numerical simulation results. This suggests that a good approximation for a general case could be based on Eqns. (6.47)-(6.48).

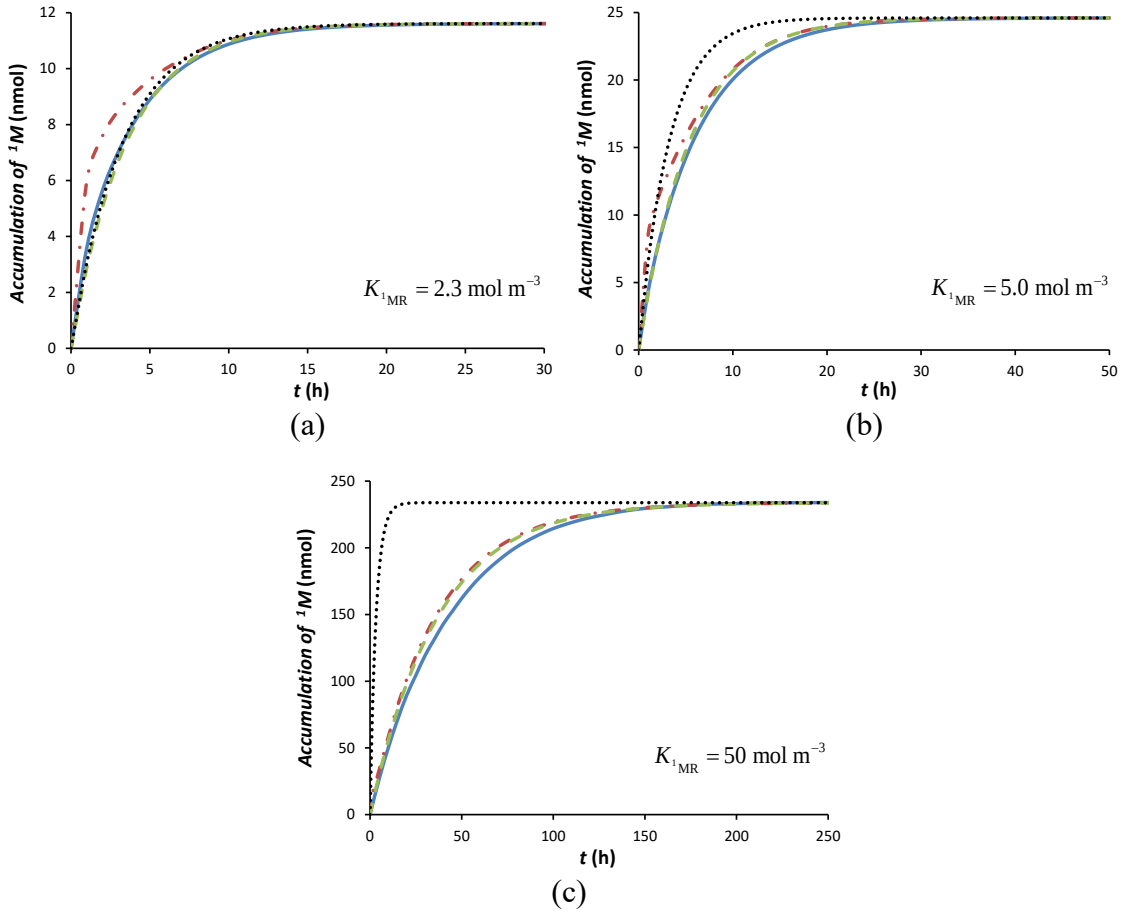

Figure 6.9. Accumulation of trace metal (^{1}M) in presence of a second metal (^{2}M) in a standard DGT device using numerical simulations (continuous blue line), Eqns. (6.47)-(6.48) (dashed green line), Eqns. (6.48)-(6.49) (dotted black line) and Eqns. (6.47)-(6.50) (dashed dotted red line). Values used for the stability constant were: Panel (a) $K_{^1MR}$ =2.3 mol m^{-3}, panel (b) $K_{^1MR}$ =5.0 mol m^{-3} and panel (c) $K_{^1MR}$ =50.0 mol m^{-3}. Other parameters used: $c^*_{^1M}$ =0.01 mol m^{-3}, $c^*_{^2M}$ =60.0 mol m^{-3}, c_{TR} =28 mol m^{-3}, Π_M =1.0, $k_{d,^1MR}$ =1.7×10^{-4} s^{-1}, $k_{d,^2MR}$ =1.5×10^{-4} s^{-1}, $K_{^2MR}$ =0.13 mol m^{-3}, $D_{^1M}$ =5.39×10^{-10} m^2 s^{-1}, $D_{^2M}$ =4.94×10^{-10} m^2 s^{-1}. Rest of parameters as in Fig 6.4.

6.4.3 Accumulation of Mn in presence of Mg

Markers in Fig. 6.10 correspond to the DGT accumulation of Mn in presence of different concentrations of Mg at fixed ionic strength, 155 mol m^{-3}, and pH 5.5. In data reported in reference [15], Mn accumulation follows the trend of perfect-sink conditions when the ionic strength in the system is 10 mol m^{-3}. The experimental accumulation of Mn when Mg is absent (square markers in Fig. 6.10) is lower than the perfect-sink expectation. This is an effect of the ionic strength which has been increased from 10 to 155 mol m^{-3}. Thus, the decrease and the bending of the Mn accumulation reflect the

decrease of the stability constant of the Mn binding to the Chelex due to the screening of the electric charge by the salt background.

Fig. 6.10 also shows that, when the concentration of Mg increases keeping fixed the ionic strength, the accumulation of Mn decreases, which is an evidence of the competing effects between Mg and Mn. As in the previous case (Fig. 6.8) the binding of Mg reduces c_R and, the association rate of Mn (first term in Eqn. (6.18)) decreases. Accordingly, both the slope of the Mn accumulation at short times and the plateau reached by the Mn accumulation decrease as the Mg concentration increases.

The simulation tool described in Chapter 3 was used to fit the kinetic and stability constants of Mn and Mg. In order to reduce the numbers of unknowns to be simultaneously fitted, in a first step, the Mn kinetic constants ($k_{a,MnR}$ and $k_{d,MnR}$) were fitted using the accumulation data for only Mn (red markers in Fig. 6.10). These parameters were then kept fixed and ($k_{a,MgR}$ and $k_{d,MgR}$) were obtained by fitting the Mn accumulations in the presence of Mg. The values of these constants are reported in Table 6.1 while continuous lines in Figure 6.10 show the accumulation predicted by numerical simulation with these values.

Table 6.1. Kinetic parameters of Mn and Mg obtain by numerical simulation fitting accumulations of Mn (in presence of different concentrations of Mg) to experimental results. Experimental details in Figure 6.10.

	$k_{a,MR}$ ($m^3\ mol^{-1}\cdot s^{-1}$)	$k_{d,MR}$ (s^{-1})	K_{MR} ($m^3\ mol^{-1}$)
Mn	4.0×10^{-4}	1.7×10^{-4}	2.35
Mg	1.9×10^{-5}	1.5×10^{-4}	0.13

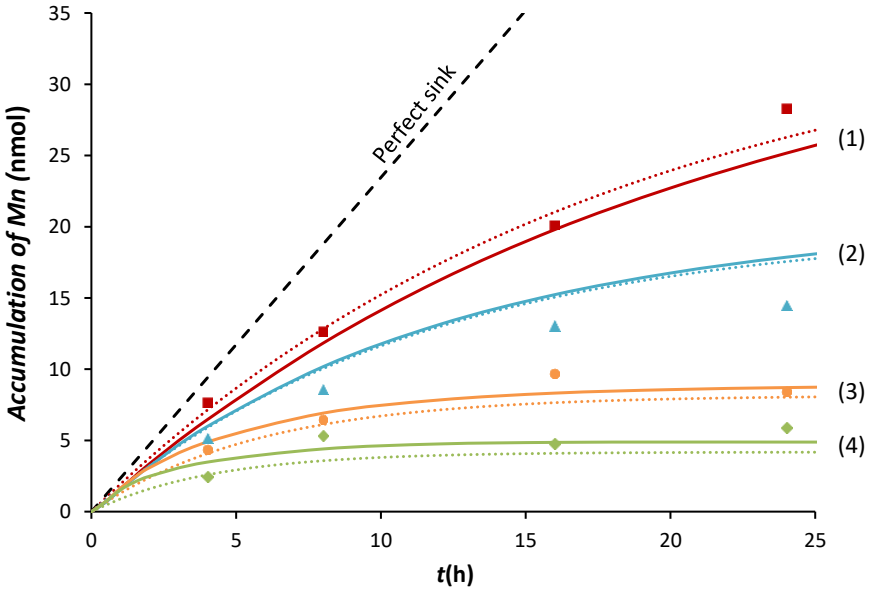

Figure 6.10. Mn accumulation in a standard DGT device from a solution with c^*_{Mn} *= 3.64×10⁻³ mol m⁻³ in the presence of different concentrations of Mg. Dashed line corresponds to perfect-sink approximation. Markers correspond to experimental values for: only Mn (squares),* c^*_{Mg} *=5.5 mol m⁻³ (triangles),* c^*_{Mg} *=27.7 mol m⁻³ (circles) and* c^*_{Mg} *=60.8 mol m⁻³ (diamonds). Continuous lines were obtained with numerical simulation and parameters of table 6.1. Dotted lines were calculated with Eqn. (6.51) and kinetic constants of table 6.2. Labels stand for: only Mn (label 1),* c^*_{Mg} *=5.5 mol m⁻³ (label 2),* c^*_{Mg} *=27.7 mol m⁻³ (label 3) and* c^*_{Mg} *=60.8 mol m⁻³ (label 4). Other parameters used: ionic strength 155 mol m⁻³,* Π_M *=1.1,* $k_{a,MnR}$ *=4.0×10⁻⁴ m³ mol⁻¹ s⁻¹,* K_{MnR} *= 2.35 m³ mol⁻¹,* $k_{a,MgR}$ *=1.9×10⁻⁵ m³ mol⁻¹ s⁻¹,* K_{MgR} *=0.13 m³ mol⁻¹,* D_{Mn} *=5.39×10⁻¹⁰ m² s⁻¹and* D_{Mg} *=4.94 ×10⁻¹⁰ m² s⁻¹.*

The above obtained analytical expressions (6.47)-(6.50) can also be used to fit the Mn accumulations in presence of Mg. Assuming that the Mg occupation is in equilibrium along the binding of Mn, the number of free sites that the Mn can occupy is given by Eqn.(6.48) so that Eqn. (6.47) becomes:

$$n_{T,Mn}(t) = \frac{A\delta^r c_{TR}}{1+\Pi_M K_{MgR} c^*_{Mg}} \Pi_M K_{MnR} c^*_{Mn} \left(1-e^{-b_1 t}\right) \qquad (6.51)$$

where b_1 is given by Eqn. (6.32) with the parameters corresponding to Mn.

As done above in fitting the experimental data with the numerical simulation code, in order to reduce the number of unknowns to be simultaneously fitted with Eqn. (6.51), the kinetic parameters of Mn can be determined from the Mn accumulation in absence

of Mg, while the stability constant of Mg is then obtained from the accumulations in presence of Mg in the system. The results are reported in Table 6.2, while Fig. 6.10 depicts in dotted line the corresponding calculated accumulations. The agreement with experimental data is quite reasonable and similar to that of the numerical simulation reported in the same figure. It could, then, be concluded that for this system, the simple Eqn. (6.51) is able to reach a good agreement with the experimental data using kinetic and thermodynamic values in the order of those obtained by using more sophisticated numerical methods.

Table 6.2. Kinetic parameters of Mn and stability constant of Mg derived using Eqn (6.51) to fit the accumulation data at ionic strength 155 mol m^{-3} and pH 5.5 reported in Fig. 6.10. Parameters used are those reported in the caption of Fig. 6.10.

	$k_{a,R}$ (m^3 mol^{-1} s^{-1})	$k_{d,R}$ (s^{-1})	K_{MR} (m^3 mol^{-1})
Mn	7.0×10^{-5}	3.0×10^{-5}	2.19
Mg	-	-	0.07

The application of Eqn. (6.51) to determine c^*_{Mn}, requires the knowledge of c^*_{Mg}, K_{MgR}, K_{MnR}, $k_{d,Mn}$, Π and the geometrical parameters of the DGT device.. These parameters have to be determined in dedicated experiments at the pH, temperature and ionic strength of the sample. In the present case, it has been quite simple, since Mn and Mg parameters could be determined in separate experiments with only one metal in the system. Once these parameters are known, c^*_{Mn} can be calculated from the accumulation. Applying this process to the accumulations shown in Fig 6.10, one obtains the c^*_{Mn} values reported in Table 6.3, which are in reasonable agreement with the experimental ones, significantly improving the estimations based on perfect-sink conditions. The highest error arises for the highest Mg concentration since the accumulation is, then, the lowest one, this increasing the relative error of Eqn. (6.51).

Table 6.3. Calculation of c^*_{Mn} using the perfect-sink approximation (Eqn. (6.1)) or the competition approximation, Eqn. (6.51), in the Mg/Mn competing system with parameters and Mn experimental accumulations reported in Fig. 6.10 at 24 h.

Experimental bulk concentrations (mol m^{-3})		c^*_{Mn} calculated (mol m^{-3})	
c^*_{Mn}	c^*_{Mg}	From Eqn. (6.1) (Perf. Sink)	From Eqn. (6.51) (competition explicitly included)
3.64×10^{-3}	5.3	9.02×10^{-4}	2.49×10^{-3}
	25	5.22×10^{-4}	3.87×10^{-3}
	53	3.68×10^{-4}	5.27×10^{-3}

6.5 Conclusions

There are some situations in which steady-state and perfect-sink conditions are not fulfilled in DGT deployments. Equilibrium or competition effects may produce non-linear accumulations with time. These situations have been analysed in this chapter.

There have been developed a set of analytical approximate expressions to reproduce the DGT accumulations when there are kinetic limitations in the metal binding to the resin, saturation or equilibrium influence or non-negligible competition effects. The binding of Mg or Mn have been used to exemplify the use of these expressions.

Values of concentrations obtained with the simple approximate expressions reported in this work significantly improve the estimations based on perfect-sink conditions. Such an approach opens up the possibility of using DGT more widely in challenging systems and allows DGT data to be interpreted more fully.

For the studied conditions, accumulations of Mg or Mn in single metal systems have provided examples of equilibrium effects.

In a mixed system, the accumulation of Mg reduces the accumulation rate of Mn, due to competition between Mg and Mn for the resin sites.

6.6 Reference List

1. Davison, W.; Zhang, H. In-situ speciation measurements of trace components in natural- waters using thin-film gels. *Nature* **1994,** *367* (6463), 546-548.

2. Garmo, O. A.; Royset, O.; Steinnes, E.; Flaten, T. P. Performance study of diffusive gradients in thin films for 55 elements. *Anal. Chem.* **2003,** *75* (14), 3573-3580.

3. Davison, W.; Zhang, H. Progress in understanding the use of diffusive gradients in thin films (DGT) – back to basics. *Environ. Chem.* **2012,** *9*, 1-13.

4. Warnken, K. W.; Zhang, H.; Davison, W. Accuracy of the diffusive gradients in thin-films technique: Diffusive boundary layer and effective sampling area considerations. *Anal. Chem.* **2006,** *78* (11), 3780-3787.

5. Zhang, H.; Davison, W. Performance characteristics of diffusion gradients in thin films for the insitu measurement of trace metals in aqueous solution. *Anal. Chem.* **1995,** *67* (19), 3391-3400.

6. Panther, J. G.; Teasdale, P. R.; Bennett, W. W.; Welsh, D. T.; Zhao, H. J. Titanium Dioxide-Based DGT Technique for In Situ Measurement of Dissolved Reactive Phosphorus in Fresh and Marine Waters. *Environ. Sci. Technol.* **2010,** *44* (24), 9419-9424.

7. Zhang, Y. L.; Mason, S.; McNeill, A.; McLaughlin, M. J. Optimization of the diffusive gradients in thin films (DGT) method for simultaneous assay of potassium and plant-available phosphorus in soils. *Talanta* **2013,** *113*, 123-129.

8. Panther, J. G.; Stewart, R. R.; Teasdale, P. R.; Bennett, W. W.; Welsh, D. T.; Zhao, H. J. Titanium dioxide-based DGT for measuring dissolved As(V), V(V), Sb(V), Mo(VI) and W(VI) in water. *Talanta* **2013,** *105*, 80-86.

9. Chen, C. E.; Zhang, H.; Ying, G. G.; Jones, K. C. Evidence and Recommendations to Support the Use of a Novel Passive Water Sampler to Quantify Antibiotics in Wastewaters. *Environ. Sci. Technol.* **2013,** *47* (23), 13587-13593.

10. Challis, J. K.; Hanson, M. L.; Wong, C. S. Development and Calibration of an Organic-Diffusive Gradients in Thin Films Aquatic Passive Sampler for a Diverse Suite of Polar Organic Contaminants. *Anal. Chem.* **2016,** *88* (21), 10583-10591.

11. Navarro, E.; Piccapietra, F.; Wagner, B.; Marconi, F.; Kaegi, R.; Odzak, N.; Sigg, L.; Behra, R. Toxicity of Silver Nanoparticles to Chlamydomonas reinhardtii. *Environ. Sci. Technol.* **2008,** *42* (23), 8959-8964.

12. Bennett, W. W.; Teasdale, P. R.; Welsh, D. T.; Panther, J. G.; Stewart, R. R.; Price, H. L.; Jolley, D. F. Inorganic arsenic and iron(II) distributions in sediment

porewaters investigated by a combined DGT-colourimetric DET technique. *Environ. Chem.* **2012,** *9* (1), 31-40.

13. Bennett, W. W.; Teasdale, P. R.; Panther, J. G.; Welsh, D. T.; Jolley, D. F. New Diffusive Gradients in a Thin Film Technique for Measuring Inorganic Arsenic and Selenium(IV) Using a Titanium Dioxide Based Adsorbent. *Anal. Chem.* **2010,** *82* (17), 7401-7407.

14. Mason, S.; Hamon, R.; Nolan, A.; Zhang, H.; Davison, W. Performance of a mixed binding layer for measuring anions and cations in a single assay using the diffusive gradients in thin films technique. *Anal. Chem.* **2005,** *77* (19), 6339-6346.

15. Tankere-Muller, S.; Davison, W.; Zhang, H. Effect of competitive cation binding on the measurement of Mn in marine waters and sediments by diffusive gradients in thin films. *Analytica Chimica Acta* **2012,** *716*, 138-144.

16. Panther, J. G.; Teasdale, P. R.; Bennett, W. W.; Welsh, D. T.; Zhao, H. J. Titanium Dioxide-Based DGT Technique for In Situ Measurement of Dissolved Reactive Phosphorus in Fresh and Marine Waters. *Environmental Science & Technology* **2010,** *44* (24), 9419-9424.

17. Panther, J. G.; Bennett, W. W.; Welsh, D. T.; Teasdale, P. R. Simultaneous Measurement of Trace Metal and Oxyanion Concentrations in Water using Diffusive Gradients in Thin Films with a Chelex-Metsorb Mixed Binding Layer. *Anal. Chem.* **2014,** *86* (1), 427-434.

18. Mason, S.; Hamon, R.; Nolan, A.; Zhang, H.; Davison, W. Performance of a mixed binding layer for measuring anions and cations in a single assay using the diffusive gradients in thin films technique. *Analytical Chemistry* **2005,** *77* (19), 6339-6346.

19. Tankere-Muller, S.; Zhang, H.; Davison, W.; Finke, N.; Larsen, O.; Stahl, H.; Glud, R. N. Fine scale remobilisation of Fe, Mn, Co, Ni, Cu and Cd in contaminated marine sediment. *Mar. Chem.* **2007,** *106* (1-2), 192-207.

20. Chang, L. Y.; Davison, W.; Zhang, H.; Kelly, M. Performance characteristics for the measurement of Cs and Sr by diffusive gradients in thin films (DGT). *Anal. Chim. Acta* **1998,** *368* (3), 243-253.

21. Dahlqvist, R.; Zhang, H.; Ingri, J.; Davison, W. Performance of the diffusive gradients in thin films technique for measuring Ca and Mg in freshwater. *Analytica Chimica Acta* **2002,** *460* (2), 247-256.

22. Levy, J. L.; Zhang, H.; Davison, W.; Puy, J.; Galceran, J. Assessment of trace metal binding kinetics in the resin phase of diffusive gradients in thin films. *Anal. Chim. Acta* **2012,** *717*, 143-150.

23. Tankere-Muller, S.; Davison, W.; Zhang, H. Effect of competitive cation binding on the measurement of Mn in marine waters and sediments by diffusive gradients in thin films. *Anal. Chim. Acta* **2012,** *716*, 138-144.

24. Altier, A.; Jimenez-Piedrahita, M.; Rey-Castro, C.; Cecilia, J.; Galceran, J.; Puy, J. Accumulation of Mg to Diffusive Gradients in Thin Films (DGT) Devices: Kinetic and Thermodynamic Effects of the Ionic Strength. *Anal. Chem.* **2016,** *88* (20), 10245-10251.

CHAPTER 7

MIXED LIGAND SYSTEMS

7.1 Introduction

The knowledge of the lability degree of the complexes in natural systems is a key issue to know which species contribute to the metal flux and, in this way, to improve our knowledge of the functioning of the natural systems. The lability degree quantifies the contribution of a complex to the metal flux arising in a consuming limiting surface, [1]

$$\xi \equiv \frac{J - J_{free}}{J_{\text{labile}} - J_{free}} \tag{7.1}$$

In this definition, J is the current flux, $J_{free} = D_{\text{M}} \frac{c_{\text{M}}^{*}}{g}$ is the flux in the system if the complex was inert and J_{labile} labels the flux in the system if the complex was labile, i. e., if dissociation was fast enough to reach equilibrium with the metal at any relevant position of the diffusion domain.

For single ligand systems (SLS), the lability degree can be experimentally measured as a normalized flux. If the speciation is known, J_{free} can be computed, but for the case where almost all the metal is complexed, the determination of ξ is still simpler since

$$\xi \approx \frac{J}{J_{\text{labile}}} = \frac{n_{\text{M}}}{\left(\frac{D_{\text{ML}}}{D_{\text{M}}}\right) n_{\text{M}}^{no-ligand}} \tag{7.2}$$

where n_{M} is the current accumulation and $n_{\text{M}}^{no-ligand}$ is the accumulation in absence of ligand. However, it should be recalled that the lability degree is not a characteristic of a complex since it depends on the sensor as well as on the composition of the system. The analysis of this dependence is of special interest when the system contains a mixtue of ligands.

In mixed ligand systems, complexes can mutually influence their lability degrees.[2-4] The difference between the measured metal flux in a system that contains a mixture of ligands and the value predicted using the lability degree of each complex in a SLS is called the mixture effect.[4] This effect has been studied previously in conditions of excess of ligand.[4,5] In these cases it has been found that the addition of a complex in the solution tends to increase the lability of complexes more inert than the added one and to decrease the lability of those more labile than the added one. However, the assumption of ligand excess could be unrealistic since strong ligands can exhibit low concentrations in natural systems or, alternatively, the complex with the strongest ligand can dominate the speciation reducing the mixture to a single complex.

It seems then timely to examine the mixture effect in non-ligand excess conditions, and this will be the subject of this chapter.

7.2 Dependence of the total accumulation and the lability degree on the ligand concentration in a single ligand system

Let us consider a system with a metal M and a ligand L, which react according to the simplest reaction:

$$\mathrm{M} + \mathrm{L} \underset{k_d}{\overset{k_a}{\rightleftharpoons}} \mathrm{ML} \tag{7.3}$$

The metal can also be accumulated in the resin domain according to the reaction:

$$\mathrm{M} + \mathrm{R} \underset{k_{d,MR}}{\overset{k_{a,MR}}{\rightleftharpoons}} \mathrm{MR} \tag{7.4}$$

As starting point, the dependence of the lability degree on the concentration of ligand is studied using numerical simulations. For systems with only one ligand and where the metal profile falls to zero at the resin layer/diffusive gel interface, the lability degree can be calculated as: [1,6,7]

$$\xi = 1 - \frac{c_{\mathrm{ML}}^{r}}{c_{\mathrm{ML}}^{*}} \tag{7.5}$$

where, c_{ML}^{r} labels the concentration of ML in the resin layer/diffusive gel interface.

For $c_{TL} > c_{TM}$ it is expected that, in DGT, labilities are almost independent of the ligand concentration. In references [1,5,8], an analytical expression for the lability under excess of ligand conditions is reported:

$$\xi = 1 - \frac{\left(1+\varepsilon K^{'}\right)}{\varepsilon K^{'} + \frac{g}{m}\coth\left(\frac{g}{m}\right) + \frac{g}{\lambda_{ML}}\left(1+\varepsilon K^{'}\right)\tanh\left(\frac{r}{\lambda_{ML}}\right)} \tag{7.6}$$

which can approximately be reduced to:

$$\xi = 1 - \frac{1}{1 + \frac{g}{\lambda_{ML}}\tanh\left(\frac{r}{\lambda_{ML}}\right)} \tag{7.7}$$

a value independent of the ligand concentration and only dependent on the parameters characterizing the dissociation in the resin domain since λ_{ML}, the complex penetration parameter, can be calculated as:

$$\lambda_{ML} = \sqrt{\frac{D_{ML}}{k_d}} \tag{7.8}$$

Eqn. (7.7) was obtained assuming that almost all the metal accumulation comes from dissociation of the complex in the resin domain whenever $\varepsilon K' >> 1$ as in the cases of interest.

According to Eqn. (7.7), the lability degree of a complex in a SLS is almost independent of the ligand concentration. Thus, the measurement of the lability degree in these systems can be done at any ligand concentration without influence of these conditions on the mixture effect, when this lability degree is used to predict the accumulation in a mixture.

Figure 7.1a shows the lability degree obtained with numerical simulation, for complexes with different stabilities. As shown at the rightmost part of the figure, when $c_{TL} > c_{TM}$, the lability degree tends to a constant that coincides with the result obtained with Eqn. (7.7) (see Table 7.1). The almost independence of the lability degree on c_{TL} supports that almost all the metal accumulated in the device comes from dissociation of the

complex inside the resin layer. In this layer there is not free metal concentration when the resin acts as a perfect-sink and then, the ligand concentration is useless for shifting the dissociation process.

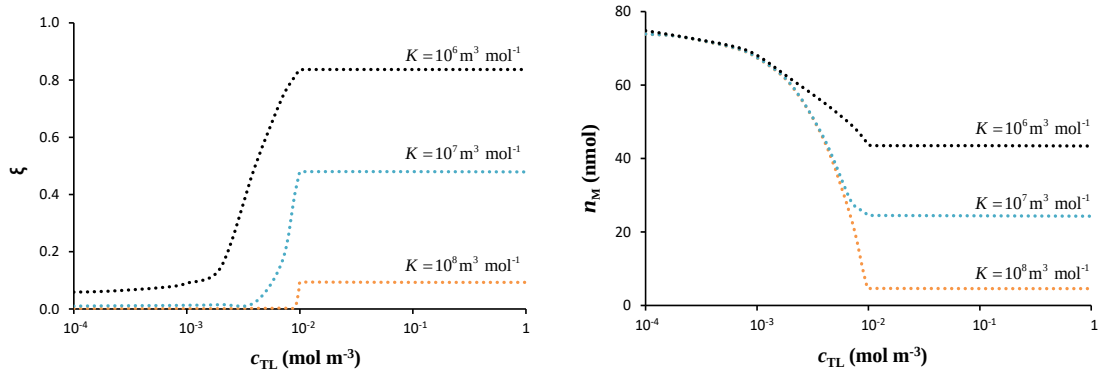

(a) (b)

Figure 7.1. Lability degree of the complex (ξ) and total accumulation of metal (n_M) as functions of c_{TL} in a single ligand system. Results obtained using numerical simulation for different values of stability constant. Parameters used: c_{TM} = 10^{-2} mol m^{-3}, D_M = 6.09 × 10^{-10} m^2 s^{-1}, D_L = 4.26 × 10^{-10} m^2 s^{-1}, D_{ML} = 4.26 × 10^{-10} m^2 s^{-1}, δ^r=4×10^{-4} m, δ^g =1.1×10^{-3} m, $c_{T,R}$ =28 mol m^{-3}, k_a =10^4 m^3 mol^{-1} s^{-1}, t=10h. Perfect-sink conditions between M and the resin sites have been used.

Table 7.1. Lability degree of the complex (ξ) (calculated with Eqn. (7.7)) and total accumulation of metal (calculated with Eqn. (7.14)) for different values of stability constant. Parameters used as in Figure 7.1.

K (m^3 mol^{-1})	10^6	10^7	10^8
ξ	0.09	0.48	0.84
n_T (nmol)	4.9	25.4	44.3

However, for $c_{TL} < c_{TM}$, the lability degree decreases as c_{TL} decreases. When ligand excess conditions are not valid, the ligand concentration profile is not flat. Instead, the free ligand concentration is higher inside the resin than in the diffusive gel, as shown in Fig. 7.2b since there is a net flux of free ligand from the resin to the diffusive gel, in order to reach steady-state conditions. The increasing ligand concentration that finds the free metal and the complex in their diffusion towards the resin disc, leads to a shift of the complexation process towards association. Accordingly, the lability degree of the complex and the concentration of free metal (Fig. 7.2a) decrease. Notice that, the lability degree tends to a constant value, when c_{TL} tends to zero.

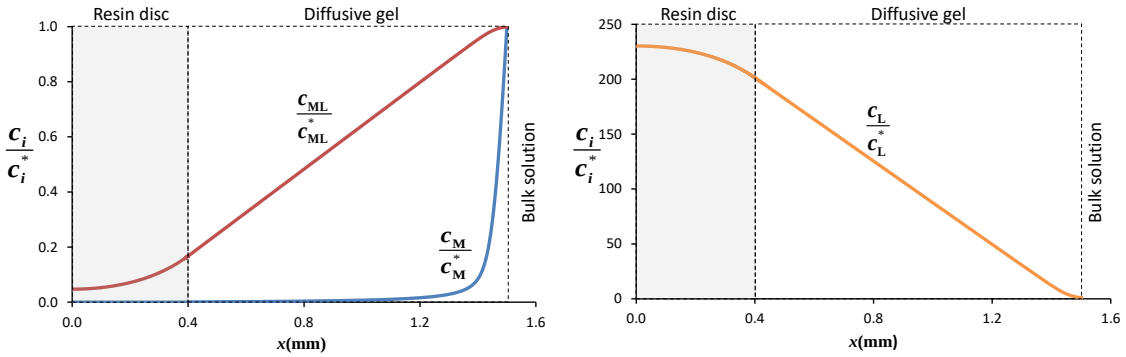

(a) (b)

Figure 7.2. Normalized concentration profiles of species in a single ligand system. Panel (a) metal and complex. Panel (b) ligand. Parameters used: $c_{TM} = 10^{-2}$ *mol* m^{-3}, $c_{TL} = 9.8\times10^{-2}$ *mol* m^{-3}, $k_a = 10^4$ $m^3 mol^{-1} s^{-1}$ *and* $K = 10^6$ $m^3 mol^{-1}$. *Other parameters as in Fig. 7.1.*

Conversely, the accumulation increases as c_{TL} decreases (see the leftmost part of Fig. 7.1b). This growth is due to the increasing concentration of free metal in the bulk solution. The accumulation reaches a maximum value when there is no metal complexed in the bulk solution and all the metal transported to the resin is free. The maximum accumulation value in Fig. 7.1b is 75.7 nmol, a value that can be calculated as:

$$n_M\big|_{c_{TL}=0} = \left(J\big|_{c_{TL}=0}\right)At = \left(\frac{D_M c_M^*}{\delta^g}\right)At \qquad (7.9)$$

The results of this section indicate that under non ligand excess conditions, the concentrations used in the SLS to measure the lability degree can be very important when this lability degree has to be used in a system mixture. The dependence of the lability degree on the ligand concentration is especially important for weak complexes, see curve $K = 10^6$ m^3 mol^{-1} in Figure 7.1a, which tend to be labile in excess of ligand conditions and can drop to almost inert in non-excess of ligand conditions. Lability of strong ligands shows a more reduced dependence on the ligand concentration since they tend to be already inert or partially labile even in excess of ligand conditions (see curve $K = 10^8$ m^3 mol^{-1} in Figure 7.1a).

7.3 System with one metal and *h* ligands

Let us consider a solution containing one metal M and *h* ligands ${}^{1}\mathrm{L}$, ${}^{2}\mathrm{L}$,… ${}^{h}\mathrm{L}$, which react according to the general scheme:

$$\mathrm{M} + {}^{j}\mathrm{L} \underset{k_{\mathrm{d},j}}{\overset{k_{\mathrm{a},j}}{\rightleftharpoons}} \mathrm{M}\,{}^{j}\mathrm{L} \tag{7.10}$$

where:

$$K_j = \frac{k_{\mathrm{a},j}}{k_{\mathrm{d},j}} = \frac{c^{*}_{\mathrm{M}\,{}^{j}\mathrm{L}}}{c^{*}_{\mathrm{M}} c^{*}_{{}^{j}\mathrm{L}}} \tag{7.11}$$

is the stability constant of the above reaction and $k_{\mathrm{a},j}$ and $k_{\mathrm{d},j}$ stand for the association and the dissociation rate constants between M and ${}^{j}\mathrm{L}$, respectively.

As shown in references [4,5], the lability degree of a complex $\mathrm{M}\,{}^{j}\mathrm{L}$ under perfect-sink conditions can be written as:

$$\xi_j = 1 - \frac{c^{r}_{\mathrm{M}\,{}^{j}\mathrm{L}}}{c^{*}_{\mathrm{M}\,{}^{j}\mathrm{L}}} \tag{7.12}$$

where, $c^{r}_{\mathrm{M}\,{}^{j}\mathrm{L}}$ labels the concentration of $\mathrm{M}\,{}^{j}\mathrm{L}$ in the resin layer/diffusive gel interface. When the DGT device is deployed in the solution, the total metal flux can be computed as: [9]

$$J = \frac{D_{\mathrm{M}} c^{*}_{\mathrm{M}}}{\delta^{g}} + \sum_{j=1}^{h} \frac{D_{\mathrm{M}\,{}^{j}\mathrm{L}}\, c^{*}_{\mathrm{M}\,{}^{j}\mathrm{L}}}{\delta^{g}} \xi_j = \frac{D_{\mathrm{M}} c^{*}_{\mathrm{M}}}{\delta^{g}} + \sum_{j=1}^{h} \left(\frac{D_{\mathrm{M}\,{}^{j}\mathrm{L}}\, c^{*}_{\mathrm{M}\,{}^{j}\mathrm{L}}}{\delta^{g}} \left(1 - \frac{c^{r}_{\mathrm{M}\,{}^{j}\mathrm{L}}}{c^{*}_{\mathrm{M}\,{}^{j}\mathrm{L}}} \right) \right) \tag{7.13}$$

Eqns. (7.13) is a general expression that applies even without excess of ligand. However, the use of this expression requires the knowledge of the labilities of the complexes in the mixed system. Reference [5] suggests that the accumulation of the metal in the mixture can be assessed using the labilities of the complexes measured in the single ligand systems as:

$$n_{\mathrm{M}} \approx At\left(\frac{D_{\mathrm{M}}c^{*}_{\mathrm{M}}}{\delta^{g}} + \sum_{j=1}^{h}\frac{D_{\mathrm{M}^{j}\mathrm{L}}c^{*}_{\mathrm{M}^{j}\mathrm{L}}}{\delta^{g}}\xi_{j}^{h=1}\right) \tag{7.14}$$

where $\xi_{j}^{h=1}$ is the lability of $\mathrm{M}^{j}\mathrm{L}$ in the SLS.

The accuracy of Eqn. (7.14) in predicting the accumulation is also assessed in reference [5] concluding that Eqn. (7.14) is a good approximation for the DGT accumulation, with errors smaller than 10% which can even be reduced to less than 4% when DGT devices when a stack of two resin discs are used. However, there could be important differences between ξ_{j} and $\xi_{j}^{h=1}$. Despite, these differences are of opposite sign for different complexes and their influence on the total flux tends to cancel as explained below.

7.4 System with one metal and two ligands

Let us now study in detail a mixed system made by a metal (M) and two ligands ($^{1}\mathrm{L}$ and $^{2}\mathrm{L}$) that lead to simple complexes $\mathrm{M}^{1}\mathrm{L}$ and $\mathrm{M}^{2}\mathrm{L}$. All the results presented in this section have been obtained by simulation. Two different cases are studied, having in common that the strongest ligand is below the total metal concentration and differing in the affinity of the strongest ligand. Table 7.2 shows the parameters used in both cases.

Table 7.2. Concentrations, kinetic and stability constants used for simulations in the mixed system.

	c_{TM} (mol m^{-3})	$c_{\mathrm{T^1L}}$ (mol m^{-3})	$c_{\mathrm{T^2L}}$ (mol m^{-3})	$k_{a,1}$ (m^{3}mol^{-1}s^{-1})	$k_{a,2}$ (m^{3}mol^{-1}s^{-1})	K_1 (m^{3}mol^{-1})	K_2 (m^{3}mol^{-1})
Case 1	0.1	1.0	0.01 – 0.08	10^4	10^4	10^6	10^7
Case 2	0.1	1.0	0.01 – 0.08	10^2	10^4	10^4	10^8

Firstly, the systems with the metal and each one of the ligands were studied separately to compare the results with those of the mixed system. In the single ligand systems the ligand concentration was selected so that the resulting free ligand concentration in the bulk solution was equal to that of the mixture. Simulation results for the SLS and of the mixture allow to check how the lability degree in a single ligand system is influenced by the mixture.

7.4.1 Results for case 1

Fig. 7.3. shows the dependence of the lability degree of M^1L and M^2L in the mixture (continuous lines) on the concentration of the ligand (^2L), which is not in excess with respect to the metal ($c^*_{T,M} = 0.1\ mol\ m^{-3}$) while ^1L is in excess with respect to the metal concentration. The lability degrees in the SLS are also depicted in Figure 7.3 (markers). The lability degree in the mixture of the most inert complex increases with respect to the value in the SLS (orange markers and lines) while it slightly decreases for the most labile one (blue markers and lines). This pattern coincides with what was previously identified for the mixture effect in excess of ligand conditions. [5]

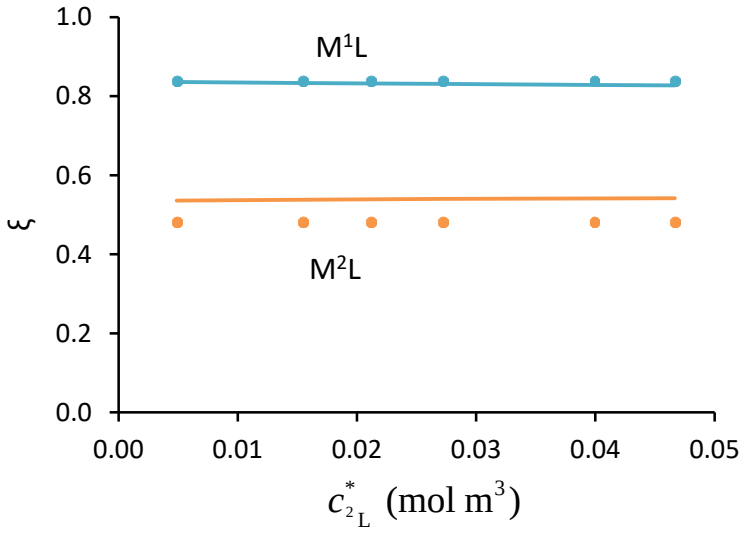

*Figure 7.3. Lability degree of the complexes (ξ) as functions of $c^*_{^2L}$ for **case 1**. Markers represent the labilities of complexes M^1L and M^2L in a SLS. Continuous lines denote the labilities of complexes M^1L and M^2L in the mixed system. Parameters used: D_M = 6.09 × 10⁻¹⁰ m² s⁻¹, D_L = 4.26 × 10⁻¹⁰ m² s⁻¹, D_{ML} = 4.26 × 10⁻¹⁰ m² s⁻¹, δ^r =4×10⁻⁴ m, δ^g =1.1×10⁻³ m, $c_{T,R}$ =28 mol m⁻³, t=5h. Other parameters are presented in table 7.2. There were used perfect-sink conditions between M and the resin sites.*

Equilibrium between M, ^jL and M^jL can be analysed using the relation:

$$\frac{Q_j}{K_j} = \frac{c_{M^jL} \Big/ \left(c_M c_{^jL}\right)}{c^*_{M^jL} \Big/ \left(c^*_M c^*_{^jL}\right)} \tag{7.15}$$

According to the second principle of the Thermodynamics, when $Q_j / K_j < 1$ the system is not in equilibrium but tends to increase the complex concentration, M^jL.

Analogously, when $Q_j/K_j > 1$ the complex tends to dissociate to reach equilibrium while $Q_j/K_j = 1$ means equilibrium situation. Fig.7.4a depicts the ratio Q_j/K_j for complexes M^1L and M^2L in the single ligand systems for case 1, when c_{T^2L} = 0.08 mol m^{-3}.

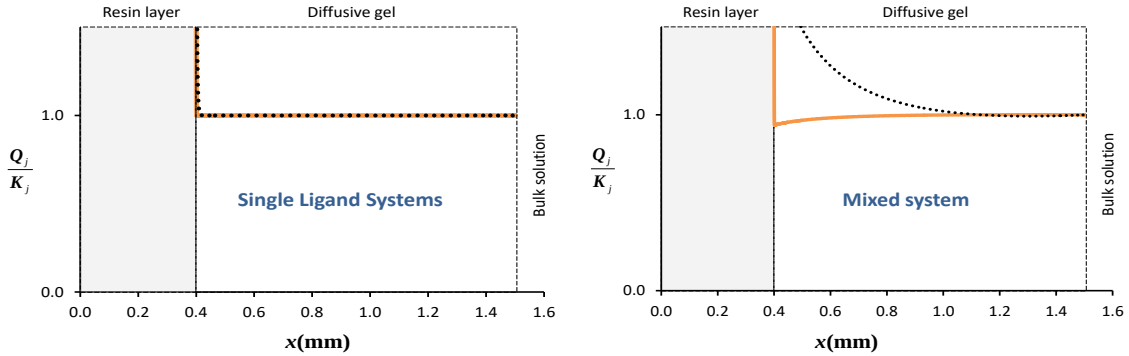

(a) (b)

*Figure 7.4. Ratios Q_j/K_j in (a) single ligand systems and (b) mixed system, for **case 1**. Continuous orange lines correspond to Q_1/K_1 and dotted black lines represent Q_2/K_2. c_{T^2L} =0.08 mol m^{-3}. Other parameters as in Table 7.2 and Fig 7.3.*

In the resin domain, none of the complexes are in equilibrium, since $Q_j/K_j \gg 1$, and they tend to dissociate because the concentration of free metal is almost zero. Dissociation is also the trend in the reaction layer located in the gel domain close to the resin-gel interface. M and M^1L are in equilibrium in the rest of the gel domain out of the reaction layer, as shown in Fig 7.4a. (continuous orange line). The same is true for the complex M^2L (see dotted black line in Fig 7.4a).

In the mixed system, both reactions are coupled by the free metal and the concentration profiles tend to evolve to a new steady-state. In the new state, the ratio Q_1/K_1 (Fig. 7.4b) is slightly below 1 in the gel domain, near the resin/gel interface, which means that M^1L tends to associate. Fig.7.4b also shows $Q_2/K_2 > 1$ in part of the diffusive gel, indicating dissociation of M^2L. This is corroborated in Fig. 7.5a, by comparing the profiles of the free metal and those of the complexes in the single ligand systems and in the mixture. Let us comment on this comparison with some more detail. We see, for instance in Fig. 7.5c that the concentration profile of free M in the single M^2L system is higher than in the single M^1L. In the mixture, the metal profile should accommodate

the tendencies of both complexes. Thus a profile in between those in the SLS will appear indicating that M^2L will tend to dissociate to increase the free metal profile up to the corresponding SLS system while an opposite behaviour will be exhibited by M^1L. Thus, M^1L slightly rises in the mixture (dotted and continuous red lines) and the profile of M^2L goes down (dotted and continuous green lines) in comparison to the respective profiles in the SLS. As the lability degree is defined in Equation (7.12), these changes in the profiles (at $x=\delta^r$) explain why the lability decreases for M^1L ($\xi_1 < \xi_1^{h=1}$) and increases for M^2L ($\xi_2 > \xi_2^{h=1}$). Notice that although M^2L is stronger than M^1L, M^2L tends to dissociate along the gel domain.

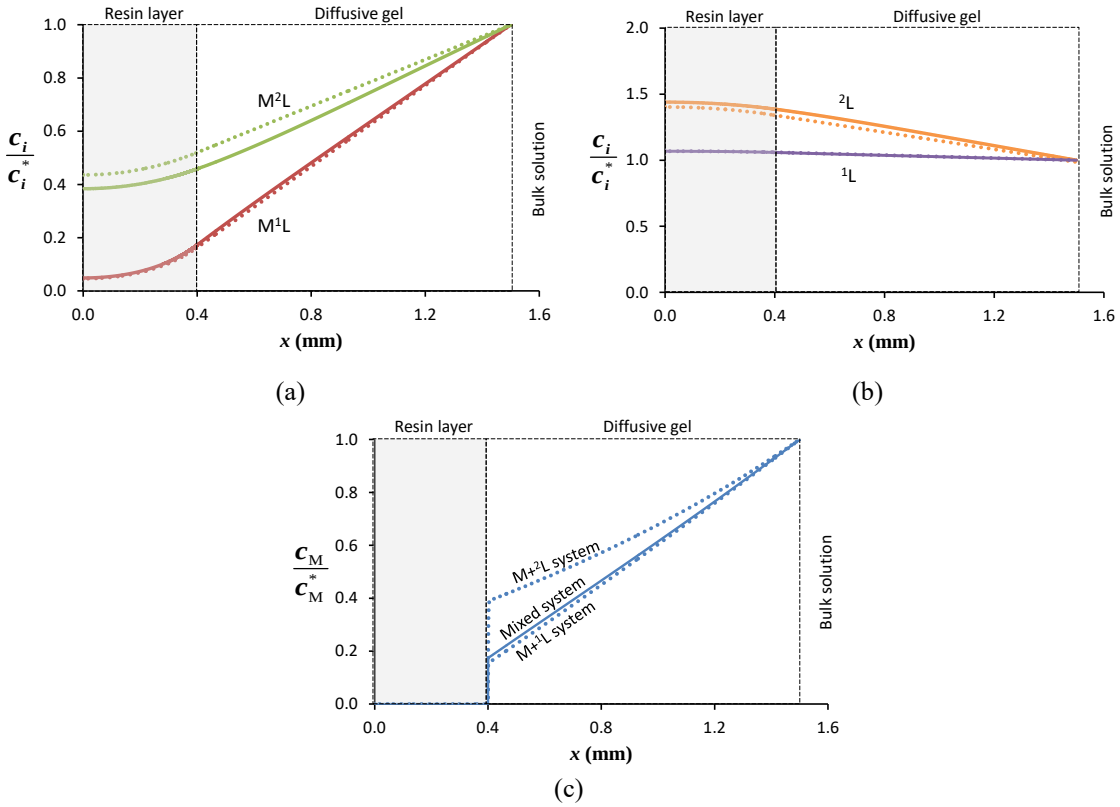

Figure 7.5. Normalized concentration profiles for (a) complexes, (b) ligands and (c) metal, in ***case 1****. Dotted lines stand for values in the single ligand systems and continuous lines denote values in the mixed system.* c_{T^2L} *=0.08 mol m*$^{-3}$*. The rest of parameters as in Table 7.2 and Fig 7.3.*

Finally, we have used Eqn. (7.14) to estimate the accumulation in the mixture, using the information of the single ligand systems. Results are shown in Table 7.3.

Table 7.3. Percentage of metal bounded to ^2L in the mixed system and total accumulation of metal for different values of $c^*_{^2L}$, obtained with simulation and using Eqn. (7.14) for case 1. Parameters used as in Table 7.2 and Fig 7.3.

$c^*_{^2L}$ (mol m^{-3})	0	4.9×10^{-3}	1.5×10^{-2}	2.1×10^{-2}	2.7×10^{-2}	4.0×10^{-2}	4.6×10^{-2}
% M^2L	0.0%	5.1%	14.5%	18.8%	22.8%	30.1%	33.3%
n_M (nmol) obtained with simulation	213	208	200	197	193	187	184
n_M (nmol) calculated with Eqn. (7.14)		217	208	204	200	193	190
Discrepancy (%)		4.3	4.0	3.6	3.7	3.4	3.4

Table 7.3 indicates that the error in the prediction of the accumulation using the lability degree in the single ligand system is smaller than 4% at any ratio c_{T^1L}/c_{T^2L} scanned in the Table 7.2, which covers the concentration range where both complexes are relevant in the mixture.

7.4.2 Results for case 2

Lability degrees for both complexes in the mixture and in the single ligand systems, for case 2, are depicted in Figure 7.6. In case 2, a pattern opposite to case 1 appears: the lability degree for the most labile complex slightly increases in the mixture with respect to the value in the SLS while it decreases for the most inert complex. Thus, results obtained for cases 1 and 2 (Figs. 7.3 and 7.6), indicate that, without excess of ligand, at least two different patterns in the mixture system can be identified.

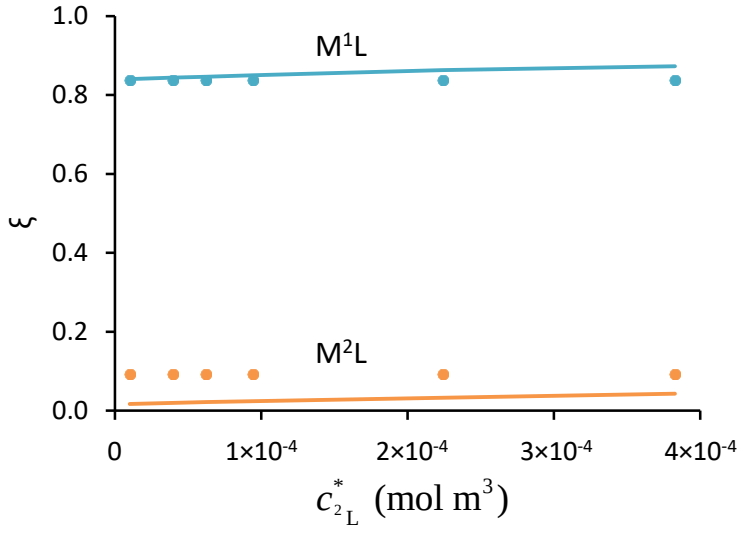

Figure 7.6. Lability degree of the complexes (ξ) as functions of $c^*_{2_L}$ *for* ***case 2****. Markers represent the labilities of complexes* M^1L *and* M^2L *in a single ligand system. Continuous lines denote the labilities of complexes* M^1L *and* M^2L *in the mixed system. Parameters used:* $D_M = 6.09 \times 10^{-10}$ *m² s⁻¹,* $D_L = 4.26 \times 10^{-10}$ *m² s⁻¹,* $D_{ML} = 4.26 \times 10^{-10}$ *m² s⁻¹,* $\delta^r = 4\times10^{-4}$ *m,* $\delta^g = 1.1\times10^{-3}$ *m,* $c_{T,R} = 28$ *mol m⁻³, t=5h. Other parameters are presented in table 7.2. There were used perfect-sink conditions between M and the resin sites.*

Let us comment on the results of case 2 with some more detail. Fig. 7.7 shows the ratio Q_j/K_j for complexes M^1L and M^2L in the single ligand systems, when $c_{T^2L} = 0.08$ mol m^{-3}. In the resin domain and the reaction layer the ratio $Q_j/K_j \gg 1$, indicating that then complexes tend to dissociate. In the rest of the gel domain, $M+^1L$ is in equilibrium in the SLS as show in Fig. 7.7a (continuous orange line). For the system $M+^2L$ there is a layer near the gel/bulk solution interface, where $Q_2/K_2 < 1$ and accordingly, there is association between M and ^2L. This result follows from the fact that ligand excess is not a good approximation for this system. Indeed, Fig. 7.8b shows an increasing concentration profile of the free ligand as the resin disc is approached indicating that the metal travelling to the resin disc will tend to associate with this increasing free ligand. Consequently, the free metal decreases steeply until there is almost no metal in the system and Q_2/K_2 recovers a value close to 1.

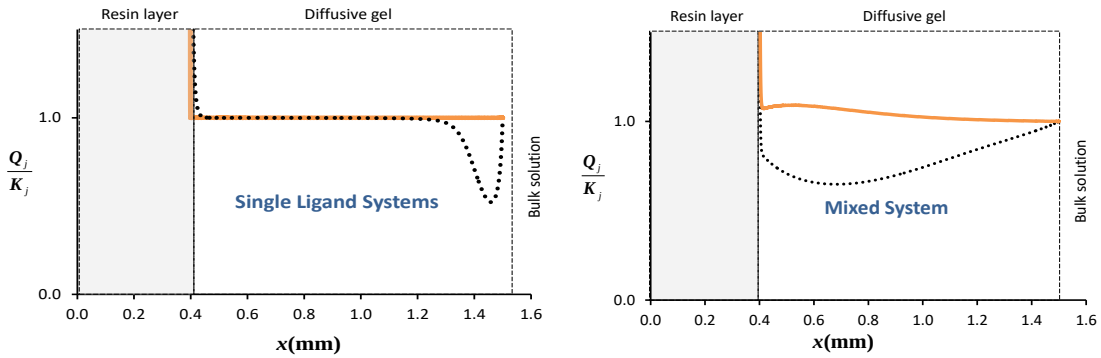

(a) (b)

*Figure 7.7. Ratios Q_j/K_j in (a) single ligand systems and (b) mixed system, for **case 2**. Continuous orange lines correspond to Q_1/K_1 and dotted black lines represent Q_2/K_2. c_{T^2L} =0.08 mol m^{-3}. Other parameters as in Table 7.2 and Fig 7.3.*

In the mixture, $Q_1/K_1 > 1$ and $Q_2/K_2 < 1$ in almost all the gel (see Fig. 7.7b) indicating that M^1L tends to dissociate while M^2L tends to associate. This trend is expected from the free metal profiles depicted in Fig. 7.8c. Notice that now, the metal profile in the single M^2L system is below that of M^1L (against what is depicted in case 1). Thus in the mixture, the metal will follow a compromise between both profiles in the SLS so that now, the more inert complex (M^2L) tends to be more inert as it tends to associate to reduce the profile of free metal. We could say that the affinity of the metal for ^2L is stronger than for ^1L so that M^1L acts as a source of metal to be bound to the increasing ^2L concentration found approaching the resin domain. If we compare the concentration profile for M^2L in the SLS (dotted green line in Fig.7.8a) with the profile in the mixture, we can see that it has increased, and for this reason $\xi_2 < \xi_2^{h=1}$. The concentration profile of M^1L slightly decreases (although it is hardly seen in the plot), and so there is a mild increment of the lability of M^1L ($\xi_1 > \xi_1^{h=1}$).

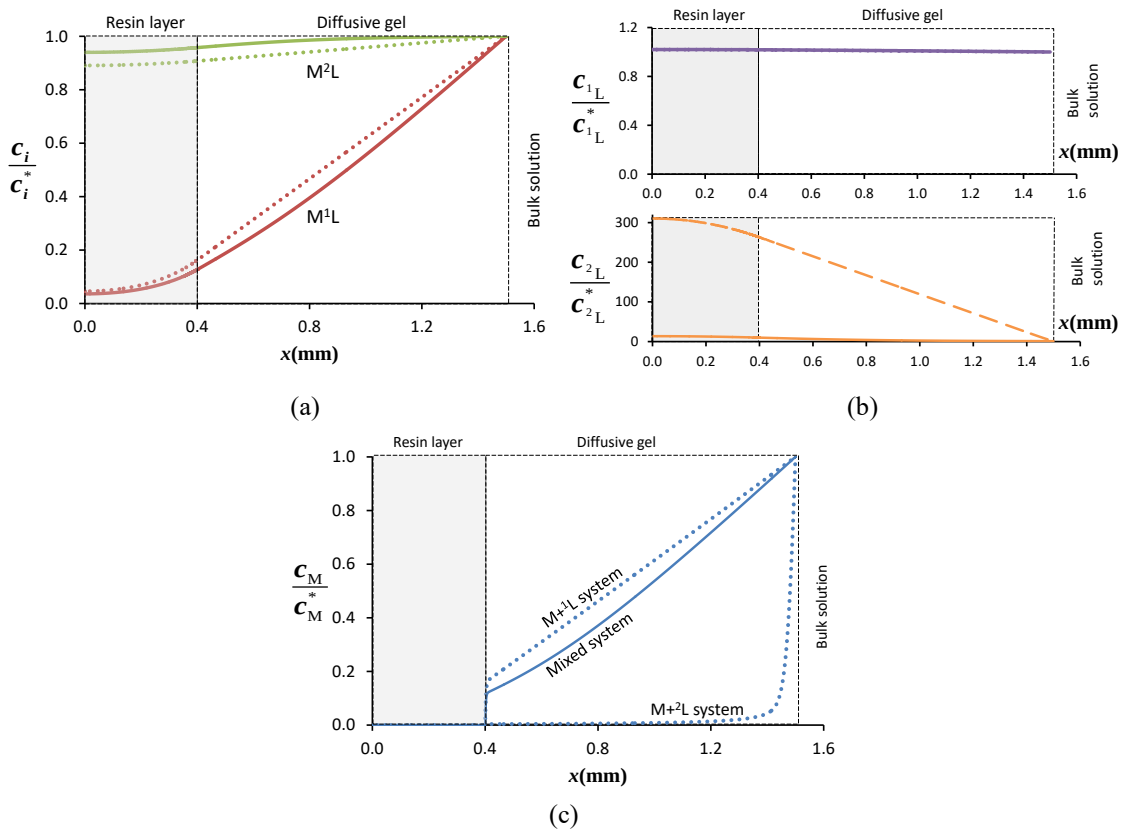

*Figure 7.8. Normalized concentration profiles for (a) complexes, (b) ligands and (c) metal, in **case 2**. Dotted lines stand for values in the single ligand system and continuous lines denote values in the mixed system. c_{T^2L} =0.08 mol m^{-3}. The rest of parameters as in Table 7.2 and Fig 7.3*

Eqn. (7.14) was used to estimate the accumulation in the mixture, using the information of the single ligand systems for case 2. Results are presented in table 7.4. It indicates that the mixture error can rise up to 24% when 80% of the metal in the mixture system corresponds to M^2L.

Table 7.4. Percentage of metal bounded to ^2L in the mixed system and total accumulation of metal for different values of $c^*_{^2L}$, obtained with simulation and using Eqn. (7.14), for case 2. Parameters used as in Table 7.2 and Fig 7.3

$c^*_{^2L}$ (mol m^{-3})	0	1.01×10^{-5}	3.98×10^{-5}	6.25×10^{-5}	9.46×10^{-5}	2.24×10^{-5}	3.83×10^{-5}
% M^2L	0	10.0%	30.0%	39.9%	49.9%	69.8%	79.6%
n (nmol) obtained with simulation	215	190	150	130	110	71	53
n (nmol) calculated with Eqn. (7.14)		202	163	143	123	84	65
Discrepancy		6.4%	8.6%	10.1%	12.3%	18.7%	22.4%

7.5 Study of a system with Ni, NTA and EtDiam

In this section, a system with Ni, Nitrilotriacetic acid (NTA) and Ethylenediamine (EtDiam), as a practical case of mixed systems, is studied. Experimental values for accumulations and %back are obtained for Ni-NTA and Ni-EtDiam in single ligand systems, in order to estimate labilities and kinetic constants. With these parameters, predictions for the accumulations in the mixed system are made. These predictions are compared with experimental values of accumulations and with values obtained by numerical simulation.

7.5.1 Ni-NTA system

DGT devices with two resin discs were deployed in a solution containing 9.2×10^{-3} mol m^{-3} of Ni and 10^{-2} mol m^{-3} of NTA. The Ionic strength of the solution was maintained constant at 51 mol m^{-3} and the pH at 8.0. Experimental results for total and %back accumulations of Ni in Ni-NTA system are presented in Table 7.5.

Table 7.5. Total accumulations of Ni (n_{Ni}), percentages of Ni accumulated on the back resin (%back) and labilities ($\xi^{h=1}_{Ni\text{-}NTA}$) in the Ni-NTA system for different times. pH=8.0, Ionic strength= 51 mol m^{-3}.

	Ni-NTA system		
t (h)	**%back**	**n_{Ni} (nmol)**	**$\xi^{h=1}_{Ni\text{-}NTA}$**
8	39.7%	24	0.51
16	40.8%	40	
24	50.0%	63	

The lability degree of the Ni-NTA complex is also presented in Table 7.5. It was calculated as:

$$\xi \approx \frac{J}{J_{\text{labile}}} = \frac{n_M/(At)}{\left(\frac{D_{ML}}{D_M}\right) n_M^{no-ligand}/(At)} = \frac{n_M/At}{D_{ML}\left(\frac{c^*_{ML}}{g}\right)} \tag{7.16}$$

where n_M and $n_M^{no-ligand}$ are the accumulations of metal in the same system, with and without ligand respectively. This expression can be used whenever the amount of free metal is very low, as shown previously.

The main reactions for this system are:

$$\text{Ni} + \text{NTA} \underset{k_{d,\text{Ni-NTA}}}{\overset{k_{a,\text{Ni-NTA}}}{\rightleftharpoons}} \text{Ni-NTA} \tag{7.17}$$

$$\text{H} + \text{NTA} \underset{k_{d,\text{H-NTA}}}{\overset{k_{a,\text{H-NTA}}}{\rightleftharpoons}} \text{H-NTA} \tag{7.18}$$

Reaction (7.17) is the complexation reaction between the metal and NTA to form the 1:1 stoichiometric complex Ni-NTA. Ni does not form complexes of higher stoichiometry with NTA within the range of concentrations analysed in this work. Reaction (7.18) is the protonation of NTA.

There is an additional reaction, because Ni can be accumulated in the resin domain according to:

$$\text{Ni} + \text{R} \underset{k_{d,\text{NiR}}}{\overset{k_{a,\text{NiR}}}{\rightleftharpoons}} \text{Ni-R} \tag{7.19}$$

Values for the kinetic constants were estimated using numerical simulation to predict the Ni accumulations presented in Table 7.5. Details of the fitting procedure are explained in the supporting information. Values for the estimated kinetic constants are presented in Table.7.9.

Assuming that protonation reactions are fast enough to be considered that reach equilibrium instantaneously at any spatial position and assuming that the diffusion of protons is so fast that there is an homogenous proton concentration profile, Ni- NTA system can be reduced to a system where Ni reacts with only one species that we can call as the effective ligand NTA^{eff} .[10] Thus,

$$\text{Ni} + \text{NTA}^{eff} \underset{k^{eff}_{d,\text{Ni-NTA}}}{\overset{k^{eff}_{a,\text{Ni-NTA}}}{\rightleftharpoons}} \text{Ni-NTA} \tag{7.20}$$

With:

$$c_{\mathrm{NTA}}^{eff} = c_{\mathrm{NTA}} + c_{\mathrm{H-NTA}} \tag{7.21}$$

Where:

$$c_{\mathrm{NTA}}^{eff} = c_{\mathrm{NTA}} + c_{\mathrm{H-NTA}} \tag{7.22}$$

$$k_{\mathrm{a,Ni\text{-}NTA}}^{eff} = \frac{k_{\mathrm{a,Ni\text{-}NTA}}}{1 + K_{\mathrm{H\text{-}NTA}} c_{\mathrm{H}}} \tag{7.23}$$

$$k_{\mathrm{d,Ni\text{-}NTA}}^{eff} = k_{\mathrm{d,Ni\text{-}NTA}} \tag{7.24}$$

$$K_{\mathrm{Ni\text{-}NTA}}^{eff} = \frac{k_{\mathrm{a,Ni\text{-}NTA}}^{eff}}{k_{\mathrm{d,Ni\text{-}NTA}}^{eff}} \tag{7.25}$$

7.5.2 Ni-EtDiam system

This system was studied using DGT devices with two resin discs deployed in a solution containing with 2.4×10^{-2} mol m^{-3} of Ni and 1.0 mol m^{-3} of EtDiam. The Ionic strength of the solution was maintained constant at 51 mol m^{-3} and the pH at 8.0. Table 7.6 shows the results for total and %back accumulations of Ni in this system.

Table 7.6. Total accumulations of Ni (n_{Ni}), percentages of Ni accumulated on the back resin (%back) and labilities in the Ni-EtDiam system for different times. pH=8.0, Ionic strength= 0.051 mol L^{-1}.

	Ni-EtDiam system		
t (h)	**%back**	**n_{Ni} (nmol)**	**$\xi^{h=1}_{\mathrm{Ni\text{-}EtDiam}}$**
8	4.9	116	1.0
16	7.3	243	
24	3.9	362	

In both the resin layer and diffusive gel, the species present in the Ni-EtDiam system are involved in the following set of reactions:

$$\mathrm{Ni} + \mathrm{EtDiam} \underset{k_{\mathrm{d,Ni\text{-}EtDiam}}}{\overset{k_{\mathrm{a,Ni\text{-}EtDiam}}}{\rightleftharpoons}} \mathrm{Ni\text{-}EtDiam} \tag{7.26}$$

$$\mathrm{Ni\text{-}EtDiam} + \mathrm{EtDiam} \underset{k_{\mathrm{d,Ni\text{-}EtDiam_2}}}{\overset{k_{\mathrm{a,Ni\text{-}EtDiam_2}}}{\rightleftharpoons}} \mathrm{Ni\text{-}EtDiam_2} \tag{7.27}$$

$$\text{Ni-EtDiam}_2 + \text{EtDiam} \underset{k_{\text{d,Ni-EtDiam}_3}}{\overset{k_{\text{a,Ni-EtDiam}_3}}{\rightleftharpoons}} \text{Ni-EtDiam}_3 \tag{7.28}$$

$$\text{H} + \text{EtDiam} \underset{k_{\text{d,H-EtDiam}}}{\overset{k_{\text{a,H-EtDiam}}}{\rightleftharpoons}} \text{H-EtDiam} \tag{7.29}$$

$$\text{H} + \text{H-EtDiam} \underset{k_{\text{d,H}_2\text{-EtDiam}}}{\overset{k_{\text{a,H}_2\text{-EtDiam}}}{\rightleftharpoons}} \text{H}_2\text{-EtDiam} \tag{7.30}$$

EtDiam is involved in two acid-base equilibria, Eqns. (7.29) and (7.30). Additionally, Ni can form Ni-EtDiam, Ni-EtDiam_2 and Ni-EtDiam_3 complexes. Eqn. (7.19), for the reaction of Ni with the resin sites, is also present in this system. Association and dissociation kinetic constants were estimated using numerical simulation to fit the experimental Ni accumulation data presented in Table 7.6. Details of the fitting procedure are reported in the supporting information. Values for the kinetic and stability constants used in simulations are presented in Table.7.9.

Since the experimental setup for this system uses excess of ligand conditions, assuming that protonation is a fast process that instantaneously reaches equilibrium, and assuming that Ni-EtDiam_i are in equilibrium (for i >1), Ni-EtDiam system can also be reduced to a simpler equivalent system: [10]

$$\text{Ni} + \text{EtDiam}^{eff} \underset{k^{eff}_{\text{d,Ni-EtDiam}}}{\overset{k^{eff}_{\text{a,Ni-EtDiam}}}{\rightleftharpoons}} \text{Ni-EtDiam}^{eff} \tag{7.31}$$

with:

$$c^{eff}_{\text{EtDiam}} = c_{\text{EtDiam}} + c_{\text{H-EtDiam}} + c_{\text{H}_2\text{-EtDiam}} \tag{7.32}$$

$$c^{eff}_{\text{Ni-EtDiam}} = c_{\text{Ni-EtDiam}} + c_{\text{Ni-EtDiam}_2} + c_{\text{Ni-EtDiam}_3} \tag{7.33}$$

$$k^{eff}_{\text{a,Ni-EtDiam}} = \frac{k_{\text{a,Ni-EtDiam}}}{B} \tag{7.34}$$

$$k^{eff}_{\text{d,Ni-EtDiam}} = \frac{k_{\text{d,Ni-EtDiam}}}{1 + \dfrac{K_{\text{Ni-EtDiam}_2} c^{eff}_{\text{EtDiam}}}{B}} \tag{7.35}$$

$$B = 1 + K_{\text{H-EtDiam}} c_{\text{H}} + K_{\text{H-EtDiam}} K_{\text{H}_2\text{-EtDiam}} c^2_{\text{H}} \tag{7.36}$$

$$K^{eff}_{\text{Ni-EtDiam}} = \frac{k^{eff}_{\text{a,Ni-EtDiam}}}{k^{eff}_{\text{d,Ni-EtDiam}}} \tag{7.37}$$

The experimental lability degree presented in Table 7.6 was calculated using Eqn. (7.16) and corresponds to Ni-EtDiam^{eff} complex.

7.5.3 Ni-NTA-EtDiam system

Values of the labilities obtained in the SLS and Eqn. (7.14) can be used to predict accumulations in a mixed system. In the case of mixed systems composed by Ni, NTA and EtDiam, Eqn. (7.14) turns into:

$$n_{\mathrm{Ni}} \approx At\left(\frac{D_{\text{Ni-NTA}}c^{*}_{\text{Ni-NTA}}}{\delta^{g}}\xi^{h=1}_{\text{Ni-NTA}} + \frac{D^{eff}_{\text{Ni-EtDiam}}c^{eff\ *}_{\text{Ni-EtDiam}}}{\delta^{g}}\xi^{h=1}_{\text{Ni-EtDiam}}\right) \tag{7.38}$$

where it was taking into account that the amount of free metal is negligible and effective species have been used.

Mixture and SLS experiments were made using total concentrations that lead to a common bulk concentration of each free ligand in both, the SLS and the mixture system. This procedure looks for an estimation of the lability of the complex measured in the SLS pertinent for the mixture. The accuracy of this procedure was studied using some examples in section 7.2. Accumulations obtained with Eqn. (7.38) can be compared with values obtained experimentally and with the values predicted by numerical simulation of the mixture using for the reactions (7.17), (7.18) and (7.26-7.30), the physicochemical parameters fitted from the data of the SLS and gathered in table 7.9. The resulting accumulations are reported in Table 7.7.

Table 7.7. Total accumulations of Ni for different times in the mixed system. Values obtained by simulation, with Eqn. (7.38) and experimentally. Parameters used: $c^{*}_{\text{Ni-NTA}}$ = 9.74×10^{-3} mol m^{-3}, $c^{eff\ *}_{\text{Ni-EtDiam}}$ = 1.32×10^{-2} mol m^{-3}, $\xi^{h=1}_{\text{Ni-NTA}}$ =0.50, $\xi^{h=1}_{\text{Ni-EtDiam}}$ =0.99, $D_{\text{Ni-NTA}}$ = 3.99 × 10^{-10} m^2 s^{-1}, $D^{eff}_{\text{Ni-EtDiam}}$ = 4.40 × 10^{-10} m^2 s^{-1}, pH=8.0, Π =2.0. Values for kinetic and stability constants used for simulations are presented in Table 7.9.

t (h)	%back	n_{Ni} (nmol) Experimental values	n_{Ni} (nmol) predicted with Eqn. (7.38)	n_{Ni} (nmol) Obtained by simulation	Discrepancy between predicted and simulated results	Discrepancy between predicted and experimental results
8	13.3%	72	89	80	10%	19%
16	15.4%	137	177	162	8%	23%
24	11.6%	232	266	243	9%	13%

Accumulations obtained with Eqn. (7.38) are close to the values obtained with simulation, with discrepancies below 10%. This discrepancy can be used as an assessment of the accuracy of Eqn. (7.38) in predicting the accumulation. In other words, this discrepancy can be interpreted as a measurement of the error due to replacing the lability degree in the mixture with the lability degree of the SLS computed as indicated above. The difference between the accumulations calculated with Eqn. (7.38) and the experimental values are bigger, in the order of 13% for 24h, since they include the experimental error in the determination of $\xi_i^{h=1}$.

Concentration profiles for effective species, in both single ligand and mixed systems, are presented in Figure 7.9. Concentration profiles show that this case is similar to the case 2 analysed in section 7.4.2, but there is a discontinuity of the concentration profile of charged species at the resin layer/diffusive gel interface, due to the Boltzmann factor.

For the Ni+EtDiam^{eff} system, there are excess of ligand conditions and the concentration profile of EtDiam^{eff} is flat (homogeneous) in the resin and diffusive gel domains both for the SLS and the mixture with the discontinuity associated to Π =2.0 at the interface. Additionally, Fig. 7.9a shows that the concentration of Ni-EtDiam^{eff} is higher in the SLS system (dotted red line) than in the mixed one (continuous red line) indicating that there is more dissociation of Ni-EtDiam^{eff} in the mixed system than in the SLS.

Concerning the Ni+NTA system, non-excess of ligand conditions are considered. The NTA^{eff} concentration profile shows that there is a flux of ligand from the resin to the bulk solution (orange lines in Fig. 7.9b). The concentration profile of Ni-NTA is higher when the complex change from SLS (dotted green line in Fig. 7.9a) to the mixed system (continuous green line in Fig. 7.9a) indicating that the rate of association increases when the complex changes from the SLS to the mixed system.

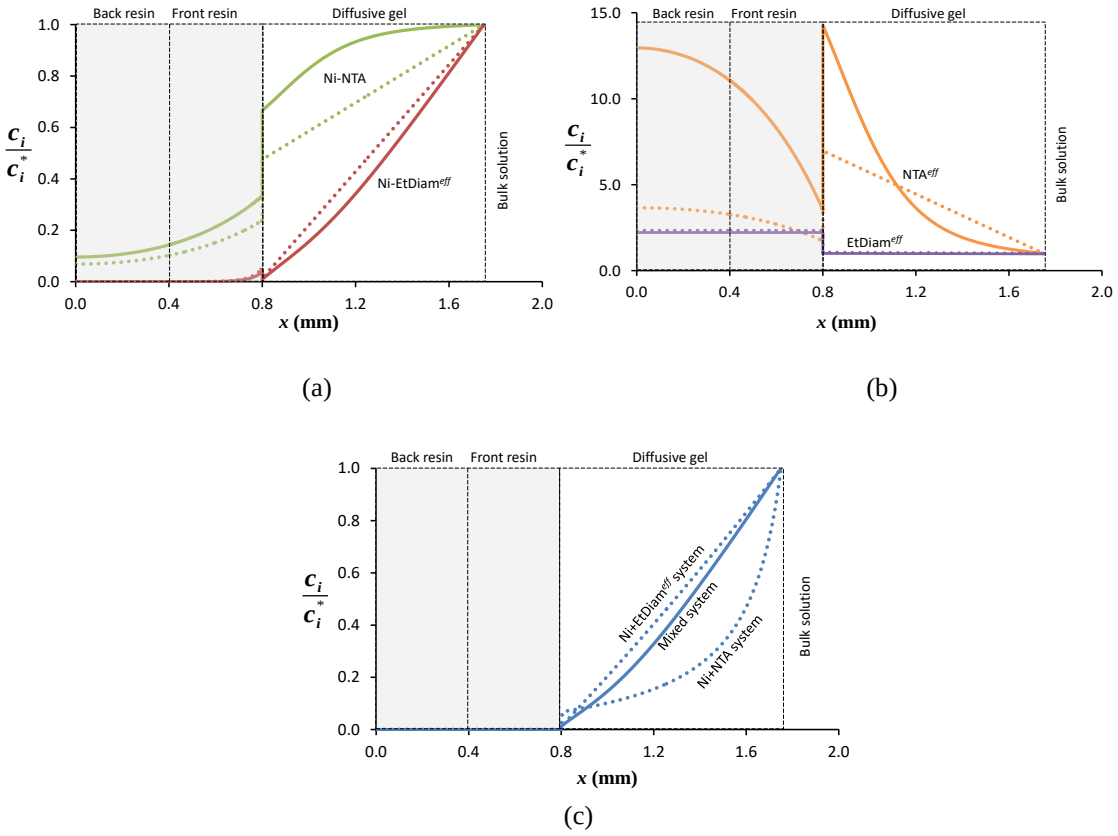

Figure 7.9. Normalized concentration profiles for (a) complexes, (b) ligands and (c) free Ni. Dotted lines stand for values in the SLS and continuous lines denote values in the mixed system. Parameters used: $c_{T,Ni}$ *= 2.5 ×10⁻³ mol m⁻³,* $c_{T,EtDiam}$ *= 1.0 mol m⁻³,* $c_{T,NTA}$ *= 10⁻² mol m⁻³,* D_{Ni} *= 6.08 × 10⁻¹⁰ m² s⁻¹,* $D_{Ni\text{-}NTA}$ *= 3.97 × 10⁻¹⁰ m² s⁻¹,* $D^{eff}_{Ni\text{-}EtDiam}$ *= 4.37 × 10⁻¹⁰ m² s⁻¹ , pH=8.0, Ionic strength= 0.051 mol L⁻¹.*

This behaviour can be easily understood considering the concentration profile of free Ni as shown in Fig. 7.9c. In the SLS, the free Ni in the $Ni+EtDiam^{eff}$ system is higher than in the single Ni+NTA system. In the mixture, the concentration profile of free Ni has to accommodate the effects of both complexes evolving to a new intermediate profile as seen in Fig. 7.9c. As in this new profile the free Ni is smaller than in the single $Ni+EtDiam^{eff}$, the complex $Ni\text{-}EtDiam^{eff}$ will tend to dissociate in the mixture to

increase the free metal profile up to the corresponding SLS system while Ni+NTA will tend to associate. It means that, in the mixture, the concentration of Ni-EtDiam^{eff} decreases, and the concentration of Ni-NTA increases in the gel with respect to the corresponding values in the SLS as seen in Fig. 7.9a. Consequently Ni-EtDiam^{eff} will be more labile and Ni-NTA will be more inert in the mixture than in the single ligand system. Labilities calculated with the simulation program for both single ligand and mixed system can be seen in Table 7.8.

Table 7.8. Labilities in SLS ($\xi^{h=1}$) and in the mixed system (ξ) of species Ni-NTA and Ni-EtDiam^{eff} .

	$\xi^{h=1}$	ξ
Ni-NTA	0.52	0.33
Ni-EtDiam^{eff}	0.99	0.99

Both effects are opposite and tend to compensate when the accumulation is considered. Notice that although the mixture influence in $\xi_{\text{Ni-NTA}}$ is higher than the influence on $\xi_{\text{Ni-Etdiam}}$, the main species in the mixture is Ni-EtDiam^{eff} due to the abundances of both ligands. This explains why the accumulation calculated with Eqn. (7.38) is higher than the value obtained by numerical simulation as reported in Table 7.7.

Finally, it is worthwhile to comment that the back accumulation (Tables 7.5 and 7.7) supports the results of Table 7.8. Due to the differences of lability shown by both complexes, the Ni accumulation on the back resin disc can be seen as coming from the Ni-NTA dissociation. In the single ligand Ni+NTA system, around 32 nmol of Ni are accumulated in the back resin. In the mixed system, only 27 nmol of Ni, coming from dissociation of Ni-NTA, are accumulated in the back resin. It implies that Ni-NTA is more inert in the mixed system than in the SLS.

7.6 Conclusions

The dependence of the lability degree of a complex on the ligand concentration was studied for any ligand to metal ratio. In excess of ligand conditions, the dependence is quite mild but the lability degree decreases when non ligand excess conditions are reached. The decrease is more important for weak complexes which tend to be labile in excess of ligand conditions.

Systems containing a mixture of ligands were studied with the aim of assessing the influence of the concentration of the ligands in the mixture on the lability degree of each complex. Different situations can arise: while in excess of ligand conditions the addition of a labile ligand tends to increase the lability degree of the more inert complexes, in non-excess of ligand conditions, an inert ligand can become more inert after the addition of a labile ligand. A physical explanation of this phenomenon is provided based on the metal profile in the single ligand systems.

A system with Ni, NTA and EtDiam was studied as a practical case. In the conditions here studied, the inert complex, Ni-NTA, decreases its lability in presence of a labile complex Ni-EtDiam.

Differences in labilities in the SLS and in the mixed systems are of opposite sign for different complexes and their influence on the accumulation tends to cancel. For the case 1 studied in section 7.4, when the concentrations of both ligands are quite constant along the device, discrepancies on the predictions of accumulations in a mixed system based on information about labilities in the SLS are below 5%. For the case 2 studied in section7.4 and for the system Ni, NTA and EtDiam studied in section 7.5, when there is a huge increase in the concentration of the strong ligand in the resin, discrepancies in predictions are below 23%.

7.7 Supporting information

7.7.1 Obtaining the kinetic constants by fitting the experimental accumulations

For the simulations it was assumed that diffusion coefficient of ligands, protonated ligands and complexes are equal. The diffusion coefficient of Ni was taken from [11]. Diffusion coefficients for Ni-NTA and Ni-EtDiam^{eff} used in simulations and in Eqn. (7.38) have been measured experimentally using a homemade diffusion cell device described elsewhere. [12,13]

Whenever the ionic strength is low, migration effects were considered using the partition model explained in Chapter 5. The Boltzmann factor was measured with Rb and Na for different ionic strengths. For I=50 mol m^{-3}, a value of $\Pi = 2.0$ was taken from Table 5.2 and used in simulations.

Values for the kinetic constants ($k_{a,\text{Ni-NTA}}$ and $k_{d,\text{Ni-NTA}}$) were estimated using numerical simulation to fit the experimental Ni accumulation presented in Table 7.5. Values of the stability constants for reactions (7.17), (7.18) were obtained from Visual MINTEQ 3.1. For reaction (7.19) it was used a high value of stability constant to assume perfect-sink conditions between Ni and the resin sites. The reaction of protonation, described for Eqn. (7.18), was assumed fast enough to reach always equilibrium. For this reason, high values for the kinetic constants were used in this reaction. Association and dissociation kinetic constants ($k_{a,\text{Ni-EtDiam}}$ and $k_{d,\text{Ni-EtDiam}}$) for Eqn. (7.26) were estimated using numerical simulation to fit the experimental data for Ni accumulation presented in Table 7.6. Stability constants for reactions (7.27) - (7.30) were obtained from Visual MINTEQ 3.1. Kinetic constant for these reactions were assumed high enough to reach always equilibrium. Values for kinetic and stability constants used in simulations are reported in Table.7.9.

Table 7.9. Kinetic and stability constants for reactions used in simulations for systems with Ni, NTA and EtDiam.

Reaction	k_a ($m^3 mol^{-1} s^{-1}$)	k_d (s^{-1})	K ($m^3\ mol^{-1}$)
$Ni + NTA \underset{k_{d,Ni\text{-}NTA}}{\overset{k_{a,Ni\text{-}NTA}}{\rightleftharpoons}} Ni\text{-}NTA$	1.32×10^{6}	2.29×10^{-3}	5.76×10^{8}
$H + NTA \underset{k_{d,H\text{-}NTA}}{\overset{k_{a,H\text{-}NTA}}{\rightleftharpoons}} H\text{-}NTA$	7.29×10^{6}	1.00	7.29×10^{6}
$Ni + EtDiam \underset{k_{d,Ni\text{-}EtDiam}}{\overset{k_{a,Ni\text{-}EtDiam}}{\rightleftharpoons}} Ni\text{-}EtDiam$	7.00×10^{4}	3.29	2.13×10^{4}
$Ni\text{-}EtDiam + EtDiam \underset{k_{d,Ni\text{-}EtDiam_2}}{\overset{k_{a,Ni\text{-}EtDiam_2}}{\rightleftharpoons}} Ni\text{-}EtDiam_2$	1.53×10^{3}	1.00	1.53×10^{3}
$Ni\text{-}EtDiam_2 + EtDiam \underset{k_{d,Ni\text{-}EtDiam_3}}{\overset{k_{a,Ni\text{-}EtDiam_3}}{\rightleftharpoons}} Ni\text{-}EtDiam_3$	12.74	1.00	12.74
$H + EtDiam \underset{k_{d,H\text{-}EtDiam}}{\overset{k_{a,H\text{-}EtDiam}}{\rightleftharpoons}} H\text{-}EtDiam$	1.05×10^{7}	1.00	1.05×10^{7}
$H + H\text{-}EtDiam \underset{k_{d,H_2\text{-}EtDiam}}{\overset{k_{a,H_2\text{-}EtDiam}}{\rightleftharpoons}} H_2\text{-}EtDiam$	1.28×10^{4}	1.00	1.28×10^{4}
$Ni + R \underset{k_{d,NiR}}{\overset{k_{a,NiR}}{\rightleftharpoons}} NiR$	10^{15}	1.00	10^{15}

7.8 Reference List

1. Puy, J.; Galceran, J.; Rey-Castro, C. Interpreting the DGT Measurement: Speciation and Dynamics. In *Diffusive Gradients in Thin-Films for Environmental Measurements*, Davison, W., Ed.; Cambridge University Press: Cambridge, 2016; pp 93-122.

2. Zhang, Z. S.; Buffle, J.; Town, R. M.; Puy, J.; van Leeuwen, H. P. Metal Flux in Ligand Mixtures. 2. Flux Enhancement Due to Kinetic Interplay: Comparison of the Reaction Layer Approximation with a Rigorous Approach. *J. Phys. Chem. A* **2009,** *113* (24), 6572-6580.

3. Pinheiro, J. P.; Salvador, J.; Companys, E.; Galceran, J.; Puy, J. Experimental verification of the metal flux enhancement in a mixture of two metal complexes: the Cd/NTA/glycine and Cd/NTA/citric acid systems. *Phys. Chem. Chem. Phys.* **2010,** *12* (5), 1131-1138.

4. Salvador, J.; Garcés, J. L.; Companys, E.; Cecilia, J.; Galceran, J.; Puy, J.; Town, R. M. Ligand mixture effects in metal complex lability. *J. Phys. Chem. A* **2007,** *111* (20), 4304-4311.

5. Uribe, R.; Puy, J.; Cecilia, J.; Galceran, J. Kinetic Mixture Effects in Diffusion Gradients in Thin Films (DGT). *Phys. Chem. Chem. Phys.* **2013,** *15* (27), 11349-11355.

6. Galceran, J.; Puy, J.; Salvador, J.; Cecília, J.; van Leeuwen, H. P. Voltammetric lability of metal complexes at spherical microelectrodes with various radii. *J. Electroanal. Chem.* **2001,** *505* (1-2), 85-94.

7. Alemani, D.; Buffle, J.; Zhang, Z.; Galceran, J.; Chopard, B. Metal flux and dynamic speciation at (bio)interfaces. Part III: MHEDYN, a general code for metal flux computation; application to simple and fulvic complexants. *Environ. Sci. Technol.* **2008,** *42*, 2021-2027.

8. Uribe, R.; Mongin, S.; Puy, J.; Cecilia, J.; Galceran, J.; Zhang, H.; Davison, W. Contribution of Partially Labile Complexes to the DGT Metal Flux. *Environ. Sci. Technol.* **2011,** *45* (12), 5317-5322.

9. Galceran, J.; Puy, J.; Salvador, J.; Cecília, J.; Mas, F.; Garcés, J. L. Lability and mobility effects on mixtures of ligands under steady-state conditions. *Phys. Chem. Chem. Phys.* **2003,** *5*, 5091-5100.

10. Mongin, S.; Uribe, R.; Rey-Castro, C.; Cecilia, J.; Galceran, J.; Puy, J. Limits of the Linear Accumulation Regime of DGT Sensors. *Environ. Sci. Technol.* **2013,** *47*, 10438-10445.

11. Shiva, A. H.; Teasdale, P. R.; Bennett, W. W.; Welsh, D. T. A systematic determination of diffusion coefficients of trace elements in open and restricted diffusive layers used by the diffusive gradients in a thin film technique. *Anal. Chim. Acta* **2015,** *888*, 146-154.

12. Zhang, H.; Davison, W. Diffusional characteristics of hydrogels used in DGT and DET techniques. *Anal. Chim. Acta* **1999,** *398* (2-3), 329-340.

13. Panther, J. G.; Stewart, R. R.; Teasdale, P. R.; Bennett, W. W.; Welsh, D. T.; Zhao, H. J. Titanium dioxide-based DGT for measuring dissolved As(V), V(V), Sb(V), Mo(VI) and W(VI) in water. *Talanta* **2013,** *105*, 80-86.

CHAPTER 8

CONCLUSIONS

(Bio)availability is a key issue to understand the toxicity or nutritional effects of chemicals in the environment. Diffusive Gradients in Thin films (DGT) technique provides an *in-situ* assessment of metal availability in waters. Many studies have been devoted to understand the theoretical basis of these samplers, but there are still many phenomena that need clarification for a proper interpretation of the DGT data. Computational tools and analytical methods for the interpretation of DGT measurements, have been developed in this work.

The main conclusions of this Thesis are:

- Numerical simulation tools based on iterative schemes and used in previous works, were here improved by incorporating the Finite Element Method to the spatial discretizations. The developed programs were used for the study of the spatio-temporal evolution of the concentrations of chemical species and other relevant state variables inside a DGT device considering diffusion, chemical reactions in volumic phases and migration of charged species at low salt background. The results obtained were accurate to the tolerance limits. In addition, the flexibility in the selection of meshes allowed: i) to simulate multiple domain problems with no greater difficulty than to specify boundaries between these domains and to input discrete expressions of boundary conditions. ii) to define meshes with a high density of points near the interfaces and with lower density in other regions, since the concentration profiles of some the species have abrupt changes in some regions of the device, especially near the resin / gel interfaces. iii) to work with meshes with a number of points lower than in simulators based on Finite Difference Method, increasing the computation speed and, consequently, decreasing the computational cost.

- The influence of the distribution of resin beads on the concentration profiles of the species, the total metal accumulation and the lability of the complexes in DGT devices has been studied. For very labile or inert complexes, this distribution does not show an influence on the concentration profiles, on the total accumulation of metal and on the lability degree of complexes. For partially labile complexes, the influence of this distribution increases with the value of the equilibrium constant K' and the diffusion coefficient of the complex. In these cases, the assumption of a homogeneous distribution of binding sites always leads to underestimate both c_{DGT} and the accumulation. However, the present results indicate that only a 13% decrease of accumulation arises when both i) inhomogeneous devices where resin beads are only dispersed in half of the resin volume and ii) complexes with stability constant K <100 m^3 mol^{-1} dominate the metal speciation.

- Analytical expressions for the concentration profiles in an inhomogeneous resin layer have been derived. Excess of ligand and perfect-sink conditions in the layer of the resin containing the binding agent, have been assumed. Predictions obtained with the analytical expresions agree with the rigorous numerical simulations.

- The dissociation rate constant of the complex, k_d, can be determined from the percentage of back accumulation in a DGT with a stack of two resin discs. The relative error values (due to inhomogeneity of the resin layer) found in recovering k_d from the %back are quite independent of K and k_d. In devices with binding agent only in half of the resin, there is a ratio of 2 between the real value and the recovered one assuming homogeneous distributions of binding resin beads.

- Differences in accumulations and lability degrees between devices with resins R and R/2 are very small when δ^r tends to zero or is so large that the complexes reach full dissociation in the layer $\delta^r/2 < x \leq \delta^r$. For intermediate thickness of the resin, differences in these magnitudes increase when δ^r increases.

- Two theoretical models for the interpretation of metal accumulations at different ionic strengths have been studied. The corresponding simulation tools have been used to analyse the accumulation of Mg. It has been found that, the main phenomenon that increases the Mg availability is the dependence of the kinetic association constant and the stability constant between the cation and the resin sites on the ionic strength. The accumulation of Mg at high ionic strength is thermodynamically limited by Mg binding to the resin at pH 7.5. However, as ionic strength decreases, the thermodynamic limitation is lower due to the increase of the stability and kinetic association constants.

- The electrostatic effects on DGT devices can be approximated using a partition factor at the resin-gel interface. This factor was here determined experimentally for different values of ionic strength by adding a small concentration of Rb to the system.

- The influence of the ionic strength on the stability constant of the Mg binding to the resin beads has a stronger influence on Mg accumulation than the Donnan partition at the resin-gel interface, in the range of ionic strength studied.

- There are some situations in which steady-state and perfect-sink conditions are not fulfilled in DGT deployments. It was found that equilibrium or competition effects can produce accumulations smaller than those predicted by the perfect-sink model and following a non-linear pattern with time.

- A set of analytical approximate expressions have been developed to reproduce the DGT accumulations when there are kinetic limitations in the metal binding to the resin, saturation or equilibrium influence or non-negligible competition effects. The binding of Mg or Mn have been used to exemplify the use of these expressions.

- Values of concentrations obtained with the simple approximate expressions reported in this work significantly improve the estimations based on perfect-sink conditions. Such an approach opens up the possibility of using DGT more widely in challenging systems and allows DGT data to be interpreted more fully.

- For the studied conditions, accumulations of Mg or Mn in single metal systems have provided examples of equilibrium effects.

- In a mixed system, the high accumulation of Mg reduces the accumulation rate of Mn, due to competition between Mg and Mn for the resin sites.

- The dependence of the lability degree of a complex on the ligand concentration was studied for any ligand to metal ratio. In excess of ligand conditions, the dependence is quite mild, but the lability degree decreases when non ligand excesss conditions are reached. The decrease is more important for weak complexes which tend to be labile in excess of ligand conditions.

- Systems containing a mixture of ligands were studied with the aim of assessing the influence of the concentration of the ligands in the mixture on the lability degree of each complex. Different situations can arise: While in excess of ligand conditions the addition of a labile ligand tends to increase the lability degree of the more inert complexes, in non-excess of ligand conditions, an inert ligand can become more inert after the addition of a labile ligand. A physical explanation of this phenomenon is provided based on the metal profile in the single ligand systems.

- A system with Ni, NTA and EtDiam was studied as a practical case. In the conditions here studied, the inert complex, Ni-NTA, decreases its lability in presence of a labile complex Ni-EtDiam.

- Differences in labilities in the singe ligand and in the mixed systems are of opposite sign for different complexes and their influence on the accumulation tends to cancel.

For the case 1 studied in section 7.4, when the concentrations of both ligands are quite constant along the device, discrepancies on the predictions of accumulations in a mixed system based on information about labilities in the SLS are below 5%. For the case 2 studied in section7.4 and for the system Ni, NTA and EtDiam studied in section 7.5, when there is a huge increase in the concentration of the strong ligand in the resin, discrepancies in predictions are below 23%.